This item was submitted to Loughborough's Institutional Repository (https://dspace.lboro.ac.uk/) by the author and is made available under the following Creative Commons Licence conditions.

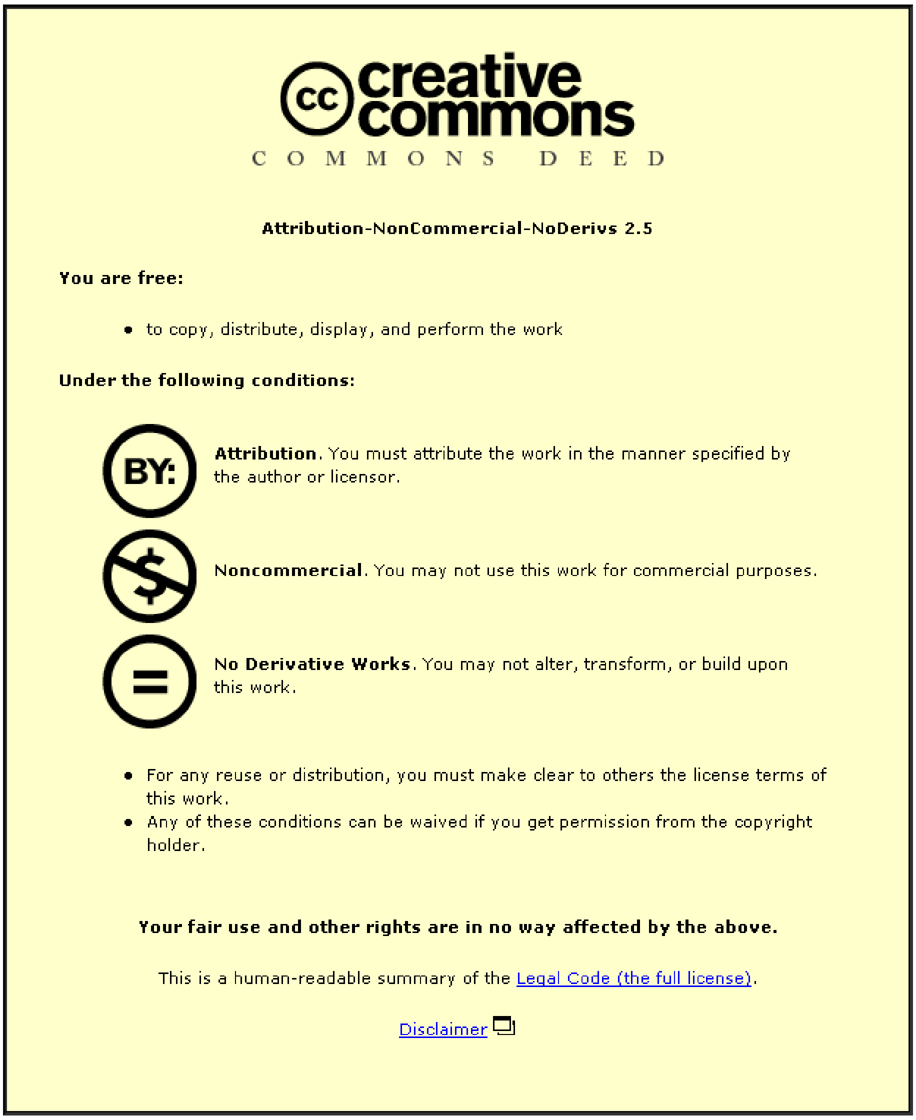

creative commons
COMMONS DEED

Attribution-NonCommercial-NoDerivs 2.5

You are free:

- to copy, distribute, display, and perform the work

Under the following conditions:

BY: **Attribution**. You must attribute the work in the manner specified by the author or licensor.

Noncommercial. You may not use this work for commercial purposes.

= **No Derivative Works**. You may not alter, transform, or build upon this work.

- For any reuse or distribution, you must make clear to others the license terms of this work.
- Any of these conditions can be waived if you get permission from the copyright holder.

Your fair use and other rights are in no way affected by the above.

This is a human-readable summary of the Legal Code (the full license).

Disclaimer

For the full text of this licence, please go to:
http://creativecommons.org/licenses/by-nc-nd/2.5/

Experimental investigation of air related tyre/road noise mechanisms

by

Jochen Eisenblaetter

Department of Aeronautical and Automotive Engineering
Loughborough University, United Kingdom

Doctoral Thesis

Submitted in partial fulfilment of the requirements for the award of Doctor of Philosophy (Ph.D.) of Loughborough University

December 2008

© Jochen Eisenblaetter 2008

Abstract

Exterior vehicle noise has a very big impact when it comes to environmental noise pollution. Due to the decrease of the other noise sources of a passenger car, like power-train and air turbulence noise in the last decade, the tyre/road noise has become a more important part in the overall noise generation of a vehicle nowadays. It is considered as the main noise source in nearly all driving conditions, especially with increasing vehicle speed. The easiest idea to tackle this pollution is to introduce rules like speed-limits to control the noise at a certain area or time. More interesting, however, is to approach the problem of unwanted noise directly at the source.

This Thesis, carried out at Loughborough University, aims to give a better understanding about the basic noise generation mechanisms at the tyre/road interface. Especially, the air related mechanisms of closed cavities are analysed. With the usage of a solid rubber tyre, unique measurements have been carried out and the results are compared to the theories already existing in the literature. These measurements reveal some of the strengths and weaknesses of the current understanding of air related noise generation.

KEYWORDS: Tyre noise, tyre/road noise, tyre noise generation, air pumping, Helmholtz resonance, air resonance radiation, groove resonance.

Acknowledgements

This Thesis was financially supported by the Department of Aeronautical and Automotive Engineering at Loughborough University.

First of all I would like to thank my supervisors Dr. Stephen J. Walsh and Prof. Dr. Victor V. Krylov for their support and encouragement throughout my time at Loughborough University. They were always on hand to guide me in the right direction. I really enjoyed the fruitful conversations with them about this research and other work related issues.

Further acknowledgement also has to be given to my friends in the United Kingdom and back in Germany. For instance Mr. Mohsan Hussain was always available for discussions about work or life in particular.

My friends back in Cologne gave me a place where I was always welcome, which has been very much appreciated. Thank you: Mr. Falko Hundrup, Mr. David Lichtenberg, Mr. Martin Lichtenberg and Mr. Dennis Tack.

Contents

Abstract i

Acknowledgements ii

Contents iii

Nomenclature vii

List of Figures xi

List of Tables xxiv

1. Introduction 1
- 1.1 Noise and traffic noise 1
- 1.2 Tyre/road interaction noise 3
- 1.3 Thesis objectives 5
- 1.4 Thesis structure 6

2. Literature survey and project definition 8
- 2.1 History of tyre development 8
- 2.2 History of road design 10
- 2.3 Tyre/road noise generation 11
  - 2.3.1 Introduction 11
  - 2.3.2 Noise generation mechanisms 12
    - 2.3.2.1 Impact mechanism 12
    - 2.3.2.2 Adhesion mechanism 14
    - 2.3.2.3 Air displacement mechanism 16
  - 2.3.3 Noise amplification and reduction mechanisms 19
    - 2.3.3.1 The horn effect 19

2.3.3.2 Acoustical impedance effect 20
2.3.3.3 Mechanical impedance effect 20
2.3.3.4 Tyre resonance 20
2.4 Summary and thesis orientation 22

3. Theoretical models of air related noise generation mechanisms 25
3.1 Leading edge: Hayden model 26
3.1.1 Monopole theory 26
3.1.2 Literature validation 28
3.2 Leading edge: Gagen model 31
3.2.1 Kinetic energy of expelled jet 32
3.3 Contact patch: groove resonance model 33
3.4 Trailing edge: air resonant radiation 34
3.4.1 Geometric explanations 35
3.4.2 Mass-spring-damper system 37
3.5 Discussion and Summary 39

4 Experimental apparatus and measurement methods 41
4.1 Experimental apparatus 42
4.1.1 Chassis dynamometer 42
4.1.2 The solid rubber tyres 46
4.1.3 Experimental rig 51
4.1.4 Microphone location: directivity pattern measurement 53
4.1.5 Microphone location: leading and trailing edge recordings 54
4.2 Measurement method 57
4.2.1 Data acquisition 57
4.2.2 Bandpass filters 58
4.2.3 Spline interpolation 60
4.2.4 Hilbert Transform 61
4.3 Discussion and Summary 62

5 Results and discussions: leading edge 64
5.1 Directivity pattern measurements 64
5.2 Circular cylindrical cavities 68

5.2.1 Large cavity 69
5.2.2 Small cavity 79
5.3 Rectangular cavities 87
5.3.1 Square cavity 87
5.3.2 Long cavity 95
5.3.3 Wide cavity 102
5.4 Comparison of the effect of cavity geometry 110
5.5 Frequency analysis 112
5.6 Comparison with theoretical models 115
5.6.1 Monopole theory 115
5.6.2 Gagen model 121
5.6.3 Inverse air-resonant radiation 122
5.7 Conclusions 125

6 Results and discussions: contact patch 128
6.1 Grooves 128
6.1.1 Square Groove 129
6.1.2 Small groove 137
6.1.3 Chevron 143
6.2 Conclusions 149

7 Results and discussions: trailing edge 151
7.1 Circular cylindrical cavities 151
7.1.1 Large cavity 152
7.1.2 Small cavity 160
7.2 Rectangular cavities 163
7.2.1 Square cavity 164
7.2.2 Long cavity 167
7.2.3 Wide cavity 170
7.3 Comparison of the effect of cavity geometry 174
7.4 Frequency analysis 176
7.5 Conclusions 178

8 Conclusions and future work 180

8.1 Conclusion and summary of results 180
8.2 Future work suggestions 184

References 185

Appendices 192
A1 Hayden model 192
A2 Gagen model (wave equations) 194
A3 Nilsson model (wave equations) 196
A4 Sound radiation: anechoic chamber 199
A5 Sound radiation: chassis dynamometer 205
A6 Displaced volume estimation 209
A7 Unloaded tyre 212
A8 Air resonant radiation amplitude 215

Nomenclature

Arabic Letters

A	Length the groove/cavity is shortened due to compression
B	Constant
C	Contact patch length
c	Sound speed in the ambient medium (e.g. air = 340.29 m/s)
d	Pipe/groove diameter
D	Depth of groove/cavity in the tyre
E	Energy
E_p	Kinetic energy
F_t	Force at tyre position
F_m	Force at mounting point
F_r	Force at the centre of gravity of rig
F_w	Force at the position of the additional weights
f	Frequency
fc	Fractional change of groove/cavity volume
f_L	Function of cavity size
h	Height
$I(r_{mic},t)$	Function of acoustic intensity

j	Imaginary unit,
$K(\omega,x)$	Function of compliance (spring reactive component of radiation impedance)
k	Wavenumber
L	Circumferential length of groove/cavity in the tyre
L_f	Circumferential length change of groove/cavity dependent on cavity size function
L_p	Sound pressure level (SPL)
L_R	Length of tyre rig section
$M(\omega,x)$	Function of inertance (mass-reactive component of radiation impedance)
$m(t)$	Function of fluid mass change
m_0	Initial fluid mass
n	Number of cavities per tyre width
p	Acoustic pressure
$p(\omega,x)$	Function of acoustic pressure
p_{mag}	Magnitude of spectral peak at harmonic frequency
p_{ref}	Reference sound pressure
$\overline{p}$	Mean squared acoustic pressure
Q	Volumetric flow rate
$\overline{Q}$	Mean volumetric flow rate
r	Tyre diameter
$R(\omega,x)$	Function of resistive component of radiation impedance
r_{mic}	Radial distance from source
$S(x)$	Function of Area of opening between road and edge of the cavity
$S_{acc}(x)$	Function of exact area of opening between road and edge

	of the cavity
t	Time
T	Closure time of groove/cavity
u	Volume velocity
$u(\omega,x)$	Function of volume velocity
V	Displaced volume of cavity
V_0	Initial cavity volume
v	Tyre/vehicle speed
v_0	Tyre reference speed
v_{exp}	Speed exponent
v_p	Particle velocity
W	Width of groove/cavity in the tyre (transversal direction)
X	Constant for pipe resonance calculation between 0.3 and 0.4
x	Distance from trailing edge
x_1	Distance from trailing edge to middle of cavity
x_{circ}	Circumferential distance of grooves/cavities
y	Distance inside the groove
$Z(\omega,x)$	Function of impedance of travelling wave out of the horn
$Z_2(\omega,x)$	Function of impedance of standing wave out of the cavity
$Z_3(\omega,x)$	Function of impedance of standing wave inside the cavity

Greek Letters

β	Coefficient to be multiplied by mass-reactive component to

	compensate for the leakage due to sound energy spreading side-ways
γ	Coefficient to be multiplied by radiation-resistance component to compensate for the leakage due to sound energy spreading side-ways
ϕ	Velocity potential
λ	Wavelength
π	Pi, mathematical constant: 3.14159….
ρ	Density of medium e.g. air
ω	Circular frequency

List of Figures

Figure 1.1	Noise emission comparison from 1974 and 1999 [de Graff, 2000]	5
Figure 2.1	Comparison of a) first pneumatic tyre [Blackcircles.com Ltd, 2008]; and b) a recent tyre design [Yokohama Tire Corporation, 2008]	9
Figure 2.2	Drawing of road design by: a) Telford's; and b) MacAdam	10
Figure 2.3	Illustration of impact mechanisms and resulting tyre vibration due to: a) leading edge road texture impact; and b) inverse impact mechanism at trailing edge	13
Figure 2.4	Illustration of sidewall vibrations due to the impact in between the tyre and the road	14
Figure 2.5	Illustration of vibrations due to adhesion: a) Stick/slip at the contact patch; b) resulting tangential tread element vibrations at the trailing edge	15
Figure 2.6	Air displacement illustration at the leading and trailing edge	17
Figure 2.7	Illustration of air related mechanism at the contact patch: a) groove resonance; and at the trailing edge: b) air resonant radiation	18
Figure 2.8	Illustration of the horn built between the tyre tread	19

	and the road surface	
Figure 2.9	Illustration of tyre carcass/belt vibrations	21
Figure 3.1	Illustration of Groove/cavity dimensions	26
Figure 3.2	Illustration of monopole source sound radiation at the tyre/road interface	27
Figure 3.3	Schematic view of tread volume and related area *S* underneath it, after [Nilsson, 1979]	35
Figure 3.4	Comparison of Nilsson simplifications and accurate geometry	36
Figure 4.1	Photograph of the chassis dynamometer facility at Loughborough University	42
Figure 4.2	Comparison of the effect of different noise reduction mechanisms for a dynamometer speed of 19km/h, with a smooth tyre running on the drum	43
Figure 4.3	Comparison of noise emitted by the chassis dynamometer at three different dynamometer speeds	45
Figure 4.4	Drawing of a solid rubber tyre with examples of tread cut into the smooth surface	46
Figure 4.5	Photograph of the experimental solid rubber tyre: a) original; and b) modified tyre with enlarged shaft accommodation and smooth rolling surface	47
Figure 4.6	Photographs of two experimental tyres with cylindrical cavities: a) ‘large, 9 mm diameter, cavity’; and b) ‘small, 2.5 mm diameter, cavity’	49
Figure 4.7	Photographs of the tyres with rectangular cavities: a) ‘square cavity’; b) ‘long cavity’; and c) ‘wide cavity’	50
Figure 4.8	Photographs of the tyres equipped with grooves: a) ‘square groove’; b) ‘small groove’; and c) ‘chevron’	51

	type of groove	
Figure 4.9	Diagram of the experimental rig design with tyre mounted onto the chassis dynamometer drum	52
Figure 4.10	Photograph of the original rig layout with tyre, wooden cover and weights in place	53
Figure 4.11	Photograph of the sound radiation measurement setup, the wooden microphone support faces the trailing edge	54
Figure 4.12	Photograph of microphone support isolated from ground vibrations excited by the driving mechanism of the chassis dynamometer	55
Figure 4.13	Photograph of the experimental rig with the two microphones in place facing the leading and the trailing edges	56
Figure 4.14	FFT of the two seconds time history signal from the 'smooth tyre' (red) running on the chassis dynamometer in comparison with the signal generated by the tyre with the: a) 'small cavity; and b) 'large cavity'	59
Figure 4.15	Spline interpolation applied in between measured points of an example signal, to produce more accurate peaks and troughs	60
Figure 4.16	Hilbert transform of the example signal from Figure (4.15)	62
Figure 5.1	Circular diagram of the frequency content of the sound radiation measurements at 36 locations around the spinning tyre equipped with the 'large cavity' running at 41 km/h	65
Figure 5.2	Sound radiation, at a frequency of 6256 Hertz, of tyre equipped with the 'large cavity' running on the	66

chassis dynamometer

Figure 5.3 Sound radiation, at a frequency of 4993 Hertz, of tyre equipped with the 'large cavity' running on the chassis dynamometer 67

Figure 5.4 Sound radiation, at a frequency of 3642 Hertz, of tyre equipped with the 'large cavity' running on the chassis dynamometer 68

Figure 5.5 Photograph of top view of the tyre equipped with the 'large cavity' 69

Figure 5.6 Time history of the leading edge signal from the tyre with the 'large cavity' at 41km/h: (a) unfiltered signal; and (b) bandpass filtered signal 70

Figure 5.7 Time history of the leading edge signal from the tyre with the 'large cavity' for different speeds including average peak level: (a) 19 km/h; (b) 31 km/h; and (c) 41 km/h 71

Figure 5.8 Example leading edge signal event of the 'large cavity' contacting the chassis dynamometer drum at 41 km/h, with assumed contact patch area 72

Figure 5.9 Four different example peaks of the leading edge signal at a tyre speed of 41 km/h generated by the 'large cavity' 74

Figure 5.10 Four different example peaks of the leading edge signal at a tyre speed of 31 km/h generated by the 'large cavity' 75

Figure 5.11 Four different example peaks of the leading edge signal at a tyre speed of 19 km/h generated by the 'large cavity' 76

Figure 5.12 Average peak of the leading edge signal from the tyre with the 'large cavity' for the three different 79 speeds: (a) normal recordings; and (b) slower velocity signals multiplied by the speed factor

Figure 5.13 Photograph of top view of the tyre equipped with the ‘small cavity’ 80

Figure 5.14 Time history of the leading edge signal from the tyre with the ‘small cavity’ at 41km/h: (a) unfiltered signal; (b) normal bandpass filtered signal; and (c) 3rd order bandpass Butterworth filter used 80

Figure 5.15 Four different example peaks of the leading edge signal at a tyre speed of 41 km/h generated by the ‘small cavity’ 81

Figure 5.16 Four different example peaks of the leading edge signal at a tyre speed of 31 km/h generated by the ‘small cavity’ 83

Figure 5.17 Four different example peaks of the leading edge signal at a tyre speed of 19 km/h generated by the ‘small cavity’ 84

Figure 5.18 Average peak of the leading edge signal from the tyre with the ‘small cavity’ for four different speeds: (a) normal recordings; and (b) slower velocity signals multiplied by the speed factor 86

Figure 5.19 Photograph of top view of the tyre equipped with the ‘square cavity’ 88

Figure 5.20 Time history of the leading edge signal from tyre with the ‘square cavity’ at 41km/h: (a) unfiltered signal; and (b) bandpass filtered signal 88

Figure 5.21 Time history of the leading edge signal from the tyre with the ‘square cavity’ for different speeds including average peak level: (a) 19 km/h; (b) 31 km/h; and (c) 41 km/h 89

Figure 5.22	Four different example peaks of the leading edge signal at a tyre speed of 41 km/h generated by the 'square cavity'	90
Figure 5.23	Four different example peaks of the leading edge signal at a tyre speed of 31 km/h generated by the 'square cavity'	91
Figure 5.24	Four different example peaks of the leading edge signal at a tyre speed of 19 km/h generated by the 'square cavity'	93
Figure 5.25	Average peak of the leading edge signal from the tyre with the 'square cavity' for the three different speeds: (a) normal recordings; and (b) slower velocity signals multiplied by the speed factor	94
Figure 5.26	Photograph of top view of the tyre equipped with the 'long cavity'	96
Figure 5.27	Time history of the leading edge signal from the tyre with the 'long cavity' for different speeds including average peak level: (a) 19 km/h; (b) 31 km/h; and (c) 41 km/h	96
Figure 5.28	Four different example peaks of the leading edge signal at a tyre speed of 41 km/h generated by the 'long cavity'	97
Figure 5.29	Four different example peaks of the leading edge signal at a tyre speed of 31 km/h generated by the 'long cavity'	99
Figure 5.30	Four different example peaks of the leading edge signal at a tyre speed of 19 km/h generated by the 'long cavity'	100
Figure 5.31	Average peak of the leading edge signal from the tyre with the 'long cavity' for the three different speeds: (a) normal recordings; and (b) slower	102

velocity signals multiplied by the speed factor

Figure 5.32 Photograph of top view of the tyre equipped with the ‘wide cavity’ 103

Figure 5.33 Time history of the leading edge signal from the tyre with the ‘wide cavity’ for different speeds including average peak level: (a) 19 km/h; (b) 31 km/h; and (c) 41 km/h 103

Figure 5.34 Four different example peaks of the leading edge signal at a tyre speed of 41 km/h generated by the ‘wide cavity’ 105

Figure 5.35 Four different example peaks of the leading edge signal at a tyre speed of 31 km/h generated by the ‘wide cavity’ 106

Figure 5.36 Four different example peaks of the leading edge signal at a tyre speed of 19 km/h generated by the ‘wide cavity’ 107

Figure 5.37 Average peak of the leading edge signal from the tyre with the ‘wide cavity’ for the three different speeds: (a) normal recordings; and (b) slower velocity signals multiplied by the speed factor 109

Figure 5.38 Leading edge signal example events of the different cavities at the same tyre velocity of 41 km/h: (a) circular cavities; (b) rectangular cavities 111

Figure 5.39 Leading edge signal of the different cavities at the same tyre velocity of 31 km/h: (a) circular cavities; (b) rectangular cavities 112

Figure 5.40 Fast Fourier Transform of leading edge signal of the tyre with the ‘large cavity’: (a) 19 km/h; (b) 31 km/h; and (c) 41 km/h 113

Figure 5.41 Magnified Fast Fourier Transform of leading edge 115 signal of the tyre with the ‘large cavity’: a) 19 km/h; b) 31 km/h; and c) 41 km/h

Figure 5.42 Zoomed example event at the leading edge of the tyre equipped with the ‘large cavity’ for the three different speeds, the time when the cavity edge touches the road is marked 116

Figure 5.43 Zoomed example event at the leading edge of the tyre equipped with the ‘wide cavity’ for two different speeds, the time when the cavity edge touches the road is marked 117

Figure 5.44 Sound pressure pulses recorded at the leading edge for the tyre with the ‘wide cavity at 41 (dotted green) and 31 km/h (dashed blue) over: (a) time; and (b) distance; and prediction of the displaced cavity volume over: (c) time; and (d) distance 120

Figure 5.45 Overlaid leading and trailing edge signal for the tyres equipped with the circular cavities: (a) ‘large cavity’ at 41 km/h; (b) ‘large cavity’ at 31 km/h; (c) ‘small cavity’ at 41 km/h and (d) ‘small cavity’ at 31 km/h 123

Figure 5.46 Overlaid leading and trailing edge signal for the tyres equipped with the rectangular cavities: (a) ‘square cavity’ at 41 km/h; (b) ‘square cavity’ at 31 km/h; (c) ‘long cavity’ at 41 km/h; (d) ‘long cavity’ at 31 km/h; (e) ‘wide cavity’ at 41 km/h and (f) ‘wide cavity’ at 31 km/h 124

Figure 6.1 Photograph of top view of the tyre equipped with the ‘square groove’ 129

Figure 6.2 Recorded signals of the trailing edge of the tyre equipped with the ‘square groove’ at 41km/h: (a) unfiltered signal; and (b) bandpass filtered signal 130

Figure 6.3 Leading and trailing edge signal of the tyre with the ‘square groove’ at 41 km/h and assumed contact patch area 131

Figure 6.4 Leading and trailing edge signal of the tyre with the ‘square groove’ at 31 km/h and assumed contact patch area 132

Figure 6.5 Instantaneous frequency at the leading edge for the tyre with the ‘square groove’ at 41 km/h and 31 km/h 133

Figure 6.6 Instantaneous frequency at the trailing edge for the tyre with the ‘square groove’ at 41 km/h and 31 km/h 134

Figure 6.7 Example of the leading edge signal from the tyre with the ‘square groove’ for two different speeds: (a) normal recordings; and (b) slower velocity signal multiplied by speed factor 135

Figure 6.8 Example peak of the trailing edge signal from the tyre with the ‘square groove’ for two different speeds: (a) normal recordings; and (b) slower velocity signal multiplied by speed factor 136

Figure 6.9 Photograph of top view of the tyre equipped with the ‘small groove’ 137

Figure 6.10 Leading and trailing edge signal of the tyre with the ‘small groove’ at 41 km/h and assumed contact patch area 138

Figure 6.11 Leading and trailing edge signal of the tyre with the ‘small groove’ at 31 km/h 139

Figure 6.12 Instantaneous frequency at the leading edge for the tyre with the ‘small groove’ at 41 km/h and 31 km/h and assumed contact patch area 140

Figure 6.13 Instantaneous frequency at the trailing edge for the tyre with the ‘small groove’ at 41 km/h and 31 km/h 141

Figure 6.14 Example of the leading edge signal from the tyre with the ‘small groove’ for two different speeds: (a) normal recordings; and (b) slower velocity signal multiplied by speed factor 142

Figure 6.15 Example peak of the trailing edge signal from the tyre with the ‘small groove’ for two different speeds: (a) normal recordings; and (b) slower velocity signal multiplied by speed factor 143

Figure 6.16 Photograph of top view of the tyre equipped with the ‘chevron’ shape of groove 144

Figure 6.17 Recorded signals of the trailing edge of the tyre equipped with the ‘chevron’ shape of groove at 41km/h: (a) unfiltered signal; and (b) bandpass filtered signal. The chevron points in the direction of rotation 144

Figure 6.18 Recorded signals of the trailing edge of the tyre equipped with the ‘chevron’ shape of groove at 41km/h: (a) unfiltered signal; and (b) bandpass filtered signal. The chevron points against the direction of rotation 145

Figure 6.19 Leading and trailing edge signal of the tyre with the ‘chevron’ shaped groove at 41 km/h, the chevron points against the direction of rotation 146

Figure 6.20 Instantaneous frequency at the trailing edge for the tyre with the ‘chevron’ shaped groove, pointing against the direction of rotation, at 41 km/h and 31 km/h 147

Figure 6.21 Example peak of the trailing edge signal from the tyre with the ‘chevron groove’ for two different speeds: (a) normal recordings; and (b) slower velocity signal multiplied by speed factor 148

Figure 7.1 Photograph of top view of the tyre equipped with the ‘large cavity’ 152

Figure 7.2 Time history of the trailing edge signal generated by the tyre with the ‘large cavity’ at 41 km/h: (a) unfiltered; and (b) bandpass filtered signal 152

Figure 7.3 Magnified example event of the trailing signal generated by the tyre with the ‘large cavity’ at 41 km/h, including marked position “cavity fully open” (red dotted line) 153

Figure 7.4 Instantaneous frequency in comparison to the frequency calculation via the maxima and minima of the oscillation found at an example event at the trailing edge of the tyre with the ‘large cavity’ at 41 km/h 154

Figure 7.5 Example events of trailing edge signal from the tyre with the ‘large cavity’ at: (a) 41 km/h; (b) 31 km/h; and (c) 19 km/h 156

Figure 7.6 Instantaneous frequency of the oscillations at the trailing edge produced by the tyre with the ‘large cavity’ in comparison to the frequency change predicted by Nilsson [Nilsson et al., 1979 158

Figure 7.7 Trailing edge signal comparison of an example event of the tyre with the ‘large cavity’ in reference to the speed of 41 km/h, the other signals are multiplied by the speed factor 159

Figure 7.8 Photograph of top view of the tyre equipped with the ‘small cavity’ 160

Figure 7.9 Example events of trailing edge signal from the tyre with the ‘small cavity’ at: (a) 41 km/h; (b) 31 km/h; and (c) 19 km/h 161

Figure 7.10 Instantaneous frequency of the oscillations at the trailing edge produced by the tyre with the ‘small cavity’ in comparison to the frequency change predicted by Nilsson [Nilsson et al., 1979] 162

Figure 7.11 Trailing edge signal comparison of an example event of the tyre with the ‘small cavity’ in reference to the speed of 41 km/h, the other oscillations are multiplied by the speed factor 163

Figure 7.12 Photograph of top view of the tyre equipped with the ‘square cavity’ 164

Figure 7.13 Example events of trailing edge signal from the tyre with the ‘square cavity’ at: (a) 41 km/h; (b) 31 km/h; and (c) 19 km/h 164

Figure 7.14 Instantaneous frequency of the oscillations at the trailing edge produced by the tyre with the ‘square cavity’ in comparison to the frequency change predicted by Nilsson [Nilsson et al., 1979] 165

Figure 7.15 Trailing edge signal comparison of an example event of the tyre with the ‘square cavity’ in reference to the speed of 41 km/h, the other oscillations are multiplied by the speed factor 166

Figure 7.16 Photograph of top view of the tyre equipped with the ‘long cavity’ 167

Figure 7.17 Example events of trailing edge signal from the tyre with the ‘long cavity’ at: (a) 41 km/h; (b) 31 km/h; and (c) 19 km/h 168

Figure 7.18 Instantaneous frequency of the oscillations at the trailing edge produced by the tyre with the ‘long cavity’ in comparison to the frequency change predicted by Nilsson [Nilsson et al., 1979] 169

Figure 7.19 Trailing edge signal comparison of an example event of the tyre with the ‘long cavity’ in reference to the speed of 41 km/h, the other oscillations are multiplied by the speed factor 170

Figure 7.20 Photograph of top view of the tyre equipped with the ‘wide cavity’ 171

Figure 7.21 Example events of trailing edge signal from the tyre with the ‘wide cavity’ at: (a) 41 km/h; (b) 31 km/h; and (c) 19 km/h 171

Figure 7.22 Instantaneous frequency of the oscillations at the trailing edge produced by the tyre with the ‘wide cavity’ in comparison to the frequency change predicted by [Nilsson et al., 1979] 172

Figure 7.23 Trailing edge signal comparison of an example event of the tyre with the ‘wide cavity’ in reference to the speed of 41 km/h, the other oscillations are multiplied by the speed factor 173

Figure 7.24 Trailing edge signal example events of the different cavities at the same tyre velocity of 41 km/h: (a) circular cavities; (b) rectangular cavities 174

Figure 7.25 Trailing edge signal of the different cavities at the same tyre velocity of 31 km/h: (a) circular cavities; (b) rectangular cavities 175

Figure 7.26 Fast Fourier Transform of trailing edge signal generated by the tyre with the ‘large cavity’: (a) 19 km/h; (b) 31 km/h; and (c) 41 km/h 176

Figure 7.27 Zoomed Fast Fourier Transform of the trailing edge signal generated by the tyre with the ‘large cavity’: (a) 19 km/h; (b) 31 km/h; and (c) 41 km/h 178

List of Tables

Table 1.1 Sound pressure levels of different sounds 2

Table 2.1 Overview of frequency range for tyre/road noise generation mechanisms with speed exponents, used to predict the change of sound radiation when the tyre velocity is changed [Kuipers and van Blokland, 2001] 22

Table 4.1 Geometry of the experimental tyre after modification 48

Table 4.2 Cylindrical cavity dimensions for two experimental tyres 48

Table 4.3 Rectangular cavity dimensions for three experimental tyres 50

Table 4.4 Groove dimensions for three experimental tyres 51

Table 4.5 Bandpass filter options 60

Table 5.1 Number and average amplitude values of peaks taken from Figure 5.7 of the leading edge signal of the tyre with the ‘large cavity’ 71

Table 5.2 Peak value calculation for the leading edge signal of the tyre with the ‘large cavity’ at 41 km/h 74

Table 5.3 Peak value calculation for the leading edge signal of the tyre with the ‘large cavity’ at 31 km/h 75

Table 5.4 Peak value calculation for the leading edge signal of the tyre with the ‘large cavity’ at 19 km/h 76

Table 5.5 Calculated peak amplitudes for the two lower speeds in comparison to the high speed of 41 km/h for the tyre with the ‘large cavity’ 78

Table 5.6 Peak value calculation for the leading edge signal of the tyre with the ‘small cavity’ at 41 km/h 82

Table 5.7 Peak value calculation for the leading edge signal of the tyre with the ‘small cavity’ at 31 km/h 82

Table 5.8 Peak value calculation for the leading edge signal of the tyre with the ‘small cavity’ at 19 km/h 84

Table 5.9 Calculated peak amplitudes for the two lower speeds in comparison to the reference speed of 41 km/h for the tyre with the ‘small cavity’ 85

Table 5.10 Speed unit conversion for the tyre with the ‘small cavity’ 86

Table 5.11 Number and average amplitude values of peaks taken from Figure (5.21) of the leading edge signal of the tyre with the ‘square cavity’ 89

Table 5.12 Peak value calculation for the leading edge signal of the tyre with the ‘square cavity’ at 41 km/h 90

Table 5.13 Peak value calculation for the leading edge signal of the tyre with the ‘square cavity’ at 31 km/h 92

Table 5.14 Peak value calculation for the leading edge signal of the tyre with the ‘square cavity’ at 19 km/h 92

Table 5.15 Calculated peak amplitudes for the two lower speeds in comparison to the reference speed of 41 km/h for the tyre with the ‘square cavity’ 94

Table 5.16 Number and average amplitude values of peaks taken from Figure 5.27 of the leading edge signal of the tyre with the ‘long cavity’ 97

Table 5.17 Peak value calculation for the leading edge signal of 98 the tyre with the ‘long cavity’ at 41 km/h

Table 5.18 Peak value calculation for the leading edge signal of the tyre with the ‘long cavity’ at 31 km/h 99

Table 5.19 Peak value calculation for the leading edge signal of the tyre with the ‘long cavity’ at 19 km/h 100

Table 5.20 Calculated peak amplitudes for the two lower speeds in comparison to the reference speed of 41 km/h for the tyre with the ‘long cavity’ 101

Table 5.21 Number and average amplitude values of peaks taken from Figure 5.33 of the leading edge signal of the tyre with the ‘wide cavity’ 104

Table 5.22 Peak value calculation for the leading edge signal of the tyre with the ‘wide cavity’ at 41 km/h 105

Table 5.23 Peak value calculation for the leading edge signal of the tyre with the ‘wide cavity’ at 31 km/h 106

Table 5.24 Peak value calculation for the leading edge signal of the tyre with the ‘wide cavity’ at 19 km/h 108

Table 5.25 Calculated peak amplitudes for the two lower speeds in comparison to the reference speed of 41 km/h for the tyre with the ‘wide cavity’ 108

Table 5.26 Repetition frequencies of the cavity and the chassis dynamometer in dependence of tyre speed 113

Table 5.27 Duration for the cavity to be completely closed in dependence of cavity length and rotational speed of the tyre 116

Table 5.28 Comparison of maximum pressure amplitudes to the energy model presented by Gagen for the different types of cavities 122

Table 6.1 Groove resonance frequency calculation for the tyre with the ‘square groove’ 133

Table 6.2 Groove resonance frequency calculation for the tyre with the ‘small groove’ 138

Table 6.3 Groove resonance frequency calculation for the tyre with the ‘chevron’ shaped groove 147

Table 7.1 Chosen variables for best fit of predicted frequency (by Nilsson) to results 157

Chapter 1

Introduction

In this chapter a general introduction to environmental noise is given. Also a historic overview of tyre/road noise that is playing a big role in environmental noise is presented. Finally the objectives of the research and the structure of the Thesis are explained.

1.1. Noise and traffic noise

Noise can generally be defined as unwanted sound. With the industrialisation hence the development of large industries and transportation the human ear was exposed to a lot more sound or noise than it used to be in the times before.

The healthy human ear can recognise sounds in the frequency range from 20 Hz to 20 kHz. The weakest sound a human ear can detect has an amplitude of 20 millionths of a Pascal (20 µPa). On the other hand it is even capable of sound pressures more than a million times higher. As a result of this broad range of nearly unmanageable numbers another scale is normally introduced: the decibel [dB] scale. Therefore the linear sound pressure p is converted into a logarithmic sound pressure level L_p (with the acronym SPL). The mathematical definition is

$$L_p = 10 \cdot \log_{10}\left(\frac{p}{p_{ref}}\right)^2 , \qquad (1.1)$$

where:

$$p_{ref} = 20 \cdot 10^{-6} Pa \qquad (1.2)$$

is the previously mentioned internationally standardised reference sound pressure that makes the sound pressure level to 0 dB at the threshold of hearing. Table 1.1 shows a brief composition of different sounds and their resulting sound pressure levels. Here the A-weighted sound pressure level is used: dB(A); it is widely accepted for noise-assessed purposes regarding the human ear at normal noise levels. For this A-weighting the measured levels on a decibel scale of noise are converted using a frequency dependent weighting that approximates the characteristics of human hearing.

Effects	Sound intensity ratio	SPL in dB(A)		example sound source
Serious hearing damage	100 000 000 000 000	140 dB		Space rocket launch (in vicinity of lauch pad)
Threshold of hearing damage				
Serious hearing damage hazard	100 000 000 000	110 dB		Rock music concert near the stage
Health effects	100 000 000	80 dB		Heavy truck, 70 km/h (10 m distance)
Good environment	10 000	40 dB		Subdued radio music
Uncomfortably quiet	p_{ref}	0 dB		Anechoic chamber
Threshold of hearing				

Table 1.1 Sound pressure levels of different sounds

The red zone in Table 1.1 illustrates the damaging region for human hearing with sound pressure levels above 110 dB. The yellow zone is the hazardous area that contains sound pressure levels above 80 dB and goes up to 110 dB, and the green zone is assumed to be the healthy area with respect to the human ear. As can be seen in Table 1.1, the traffic noise generated by lorries and cars already may have adverse health effects. Road traffic noise, as reported by the EU [EU, 1996] is supposed to create about 90% of the noise imposed upon the European population. With nearly a quarter of the population actually suffering from high noise levels.

This environmental noise causes a variety of adverse health effects and the evidence is strong for annoyance and severe sleep disturbances [Institute of Environment and Health, 1997]. An example for the resulting benefit of noise reduction is given by Öhrström [Öhrström, 2004], who presented results of a sleep log for a period of 3 nights. People living at a very busy road, were questioned before and after the opening of a new tunnel for diverting the traffic that introduced a reduction of road traffic of about 90% during 24 hours. According to Öhrström exposure to high levels of road traffic noise introduces bad effects on sleep, and sleep quality is remarkably improved when the noise is reduced considerably.

1.2. Tyre/road interaction noise

In 1979 Nilsson [Nilsson, 1979] predicted that in the future tyre noise will be the main source for noise pollution of a vehicle. It is said that the exterior tyre/road interaction noise has become a concern only during the last few decades, as evidenced by the fact that there are rarely papers existing before the 1970’s regarding this topic. However, it is interesting to consider that even in the Roman Empire there were complaints about traffic noise due to the interaction of metal (wheel rim as well as horse shoes) upon stone (pavement) [Sandberg, 2001]. Today it is commonly accepted that at low vehicle speeds, the power unit noise dominates, whereas at high speeds the tyre/road noise dominates. Between high and low speeds, there is a certain “crossover speed” where the contributions are about the same.

Tyre/road noise was already dominant in the mid 20th century along the highways but only at high speeds. During this time the crossover speed was in the range of 50 to 70 km/h for cars and from 70 to 90 km/h for lorries. In the 1980’s and 1990’s, the crossover speed for constant driving conditions was said to be from 50 to 60km/h for cars and from 60 to 70 km/h for lorries [Sandberg, 1982]. This decrease indicates that tyre/road noise dominated motorway based driving conditions, whereas power unit and transmission noise dominated urban based driving conditions.

According to Sandberg [Sandberg, 2001] the crossover speed since the 1990’s is even lower. This further decrease leads to the conclusion that tyre/road noise dominates over power unit noise for all speeds and gears except first gear. So in practice at constant speed, driving tyre/road noise almost certainly dominates, even in a “30km/h” zone or a congested urban situation. The only exception may be an accelerating vehicle. In this case tyre/road, power and transmission unit noise levels increase in a certain proportion, dependent on various variables as engine size or gearbox model. In the case of an accelerating vehicle, the power unit noise dominates.

The noise inside of the vehicle cabin was and still is a significant area for commercial product development in comparison to the outside noise. This quantification means vehicles that are quiet on the inside, are assumed to be comfortable and lead to a luxurious feeling for the driver. However, the outside noise of the vehicle is now the concern for environmental noise pollution legislative requirements. This requirement however, may not be highly demanded from a customer point of view. An example development of environmental noise pollution generated by vehicles can be seen in Figure 1.1. Three different plots are presented showing the trends between the vehicle speed (x-axis) and noise emission (y-axis). The first plot on the left displays the development regarding passenger cars, the middle one represents the light trucks and the final plot shows the tendency for heavy lorries. On all three plots the dashed blue line indicates a test in 1974 and the solid red line displays a recent inspection from 1999. By taking a closer look at Figure 1.1, it can be seen that the noise level increases with speed in 1974 were nearly linear, whereas today the tendency is rather digressive. More significantly for passenger cars the noise level has actually increased for speeds from 30 to 100km/h, which is the most important speed section for urban and rural traffic. This dilemma could be the result of traffic today; it may also be due to some kind of inertia effect as there are many old vehicles still on the road, for which the new legislative requirements do not apply. Nevertheless, it is clear that action must be taken to reduce the noise pollution by road traffic.

http://www.unece.org/trans/doc/2000/wp29grb/TRANS-WP29-GRB-33-inf08e.pdf

Page 2

Figure 1.1 Noise emission comparison from 1974 and 1999 [de Graff, 2000]

1.3. Thesis objectives

The aim of this Thesis is to investigate, experimentally, into the air related effects of tyre/road noise. Those effects are still not completely understood and contradictory theories have been presented in the literature to explain the air movements occurring when a tyre is in contact with the road. The main idea in this Thesis is to avoid the complex structure of a modern vehicle tyre and conduct measurements that can be easier to analyse and could lead to a more fundamental understanding of the air effects in tyre/road noise. In order to achieve this aim, the following points will be considered:

- A literature survey encompassing explanation and identification of the tyre/road noise mechanisms of interest.
- An appropriate simple tyre design will be presented that will be used to conduct tyre/road noise measurements.
- A test rig will be built and a measurement routine chosen by utilising the facilities available at Loughborough University.
- The obtained results will be compared to air related models from the literature and further findings will be explained.

1.4. Thesis structure

Initially this Thesis gives a short introduction to tyre and road history as well as the tyre function. The complex structure of a modern tyre can lead to manifold generating mechanisms of the noise produced during tyre/road interaction. The literature survey in Chapter 2 deals with all the mechanisms of tyre/road noise that exist to date. In Chapter 3, the theories of the air related models are explained in detail. These theories are then divided into models for the leading edge, contact patch and trailing edge of a tyre. The measurement results are also divided into these three stages. Chapter 4 presents details about the measurement setup and the uniquely designed tyre-noise rig. Chapter 4 also contains an explanation of the methods applied to condition the data.

The results are presented in Chapters 5 to 7. Where Chapter 5 presents an extensive analysis of the leading edge signal generated by tyres with cavities. An assessment of the models introduced in Chapter 3 are given, as well as a comparison between leading edge and trailing edge signals. In Chapter 6, data recorded for tyres with grooves are explained. Only for grooved tyres, can air movement be measured at the outside of the tyre, when the groove is completely covered by the road. Chapter 7, the last measurement chapter, presents the findings at the trailing edge of a tyre for the tyres with cavities only.

Finally Chapter 8 gives the conclusions obtained within this Thesis. In addition, future work is proposed that could be undertaken to collect more information about the air related mechanisms at the tyre/road interface.

Chapter 2

Literature survey and project definition

In this chapter a short introduction to the history of tyre/road noise is given. Mechanisms related to tyre/road noise are then explained in detail. These are divided into generation and amplification mechanisms. Finally the findings are summarised and a resulting orientation of the Thesis is presented.

2.1. History of tyre development

The wheel could arguably be one of the most significant inventions of all time. More often than not a new invention is likely to be compared to it. The first wheel was supposedly invented between 5500 and 3000 BC [Anthony, 2007]. The need for this invention could have either been pottery or transportation use. Wood was the main material used to build wheels by the Egyptians, Romans and Syrians. Even now if the performance is adequate, basic wheel constructions are still installed all over the world.

By definition, the tyre itself is a combination of the extremities of a wheel. In the early days this outer layer used to be a wooden cover that suffered from the wearing of the road. Later, wheels were also developed that had a leather cover, for instance in Egypt. The Romans are supposed to have used iron-covered wheels.

a)
http://www.blackcircles.com/general/history

b)
http://www.yokohamatire.com/customer_service/construction.aspx

Figure 2.1 Comparison of: a) first pneumatic tyre [Blackcircles.com Ltd, 2008]; and b) a recent tyre design [Yokohama Tire Corporation, 2008]

The first rubber tyres are comparatively different to those developed today, as illustrated in Figure 2.1. Back in 1844 Charles Goodyear's invention of vulcanized rubber initiated the rubber tyre development [The Goodyear Tire and Rubber Company, 2008]. Shortly after that the Scotsman Robert William Thomson (1822-1873) invented and patented the first pneumatic rubber tyre in 1845 [Blackcircles.com Ltd, 2008]. This first design used a number of thin inflated tubes inside a leather cover as shown in Figure 2.1a that yield to a number of advantages over later designs. For instance, it would need more than just one puncture to deflate the whole tyre, and also varying the pressures in the different tubes could alter the ride conditions significantly. Nevertheless, it is a complex design and therefore costly to produce. Despite these developments the solid rubber tyre (patented by Robert William Thomson in 1867) was the main tyre to be found on the roads until the late 18th Century. John Boyd Dunlop (1840-1921) invented the first practical pneumatic or inflatable rubber tyre for a bicycle. As a result Dunlop's tyre patented in 1888 is known as the base of today's tyre development [Dunlop Tires, 2008], and so he received the most recognition. The main objective of the air-inflated tyre was to give smooth riding comfort by allowing the vehicle to run on a cushion of air. This tyre introduced a spring like mechanism under the un-sprung axle that was also capable of clasping around small obstacles on the road.

Over the years the tyre has been further developed resulting in the highly technological designs used today as shown in Figure 2.1b. Two of the milestones in technical tyre development are: creating a radial tyre that improved grip in 1948 (Michelin) and designing a tyre without an inner tube for cars in 1972 (Dunlop). Today, it is essential for a tyre to deliver a good performance. This means structural integrity, longevity, comfort and grip.

2.2. *History of road design*

Road design began with a surface of beaten earth initiated by the movement of animals [Lay, 1992]. This compacted soil was sometimes reinforced with gravel or stones. The first indications of roads constructed by humans date back to about 4000 B.C. However, modern road development started in the 18th Century. Pioneers such as John Metcalfe, Thomas Telford and John Loudon MacAdam put forward the idea of building raised, cambered roads that allowed water to drain off them as fast as possible.

a) and b)
http://www.saburchill.com/history/chapters/IR/024.html

Figure 2.2 Drawing of road design by: a) Telford’s; and b) MacAdam [Saburchill.com, 2008].

Thomas Telford (born 1757) improved the method of building roads with broken stones. Eventually his design became the norm of praxis for all road constructions. Telford’s usage of solid earth as a base topped with a layer of small broken stones is shown in Figure 2.2a [Neath Port Talbot County Borough, 2008]. To guarantee a smooth finish a thin layer of mud was introduced on the top and ditches on both sides of the road for drainage.

John Loudon McAdam (born 1756) designed roads using broken stones laid in symmetrical, tight patterns. This base was covered with small stones to create a hard surface. Eventually he used a third layer of gravel for a smooth surface, as illustrated in Figure 2.2b [Neath Port Talbot County Borough, 2008].

Later the basic road toppings were enhanced with tar that was eventually replaced by asphalt, or concrete. In general road designs have not changed dramatically over the years. However, the surface of a road is a very significant factor when it comes to tyre/road noise. Substantial research is being undertaken in this area with different materials used to minimise noise. Unfortunately the durability of the road is often sacrificed for improved acoustics.

2.3. Tyre/road noise generation

2.3.1. Introduction

Tyre/road noise has been researched extensively since the 1970s, but it could have been a concern much earlier. According to Sandberg [Sandberg, 2001] tyre/road noise was an issue when the iron-supported wheels were driven over a stone pavement back in the 19th Century.

Today roads are much smoother than in former times and tyres have changed from wood (covered with iron or leather) to steel/alloy rims surrounded by a rubber, air-inflated tyre. Unfortunately this design makes it more challenging to tackle tyre/road interaction noise. The complexity of the modern tyre/road system results in many tyre/road noise generating mechanisms. In addition, those mechanisms are also interacting to generate the whole tyre/road noise phenomenon. According to Sandberg and Ejsmont [Sandberg and Ejsmont, 2002] there are currently seven different mechanisms (or groupings) responsible for the occurrence of tyre/road noise. However, opinion is divided about the relative portion that each of these mechanisms contributes to the whole tyre/road noise event.

These seven phenomena of tyre/road noise can be categorised into two groups: the generating mechanisms and the amplification or reduction mechanisms. The generating mechanisms can be split into two further groups of aerodynamically generated noise and the noise generated due to vibration. The generating mechanisms therefore include the air displacement mechanism and the so-called impact mechanism (mostly radial vibration) and the adhesion mechanism (mostly tangential vibration). The other four remaining mechanisms, responsible for amplification or reduction of the tyre/road noise are the horn effect, the acoustical impedance effect, the mechanical impedance effect and the tyre resonance effect. The following sections give a short explanation about each of these seven mechanisms.

2.3.2. Noise generation mechanisms

2.3.2.1 Impact mechanism

The impact mechanism is thought to be mainly a radial excitation mechanism [Sandberg and Ejsmont, 2002]. Due to a sudden displacement of the tread elements, vibrations are generated. Those displacements can be caused by a collision between the tyre tread and an object on the road surface, as illustrated in Figure 2.3a. Another impact can be a result of normal contact of the tread and road surface. When an element at the leading edge enters the contact patch it also gets displaced, depending on the load of the tyre. Furthermore, a similar process happens at the trailing edge when the radial compression of the tread, because of the tyre load, is released. This mechanism is illustrated in Figure 2.3b. It is often referred to as the “inverse impact” mechanism at the trailing edge. One problem when analysing this mechanism is the complex relationship between tread depth and the impact displacement, depending on the rubber stiffness, groove width and other variables. In the frequency range between 500 and 1000 Hertz bending waves are the most common wave types in a tyre. Therefore, whatever the nature of this impact mechanism, it generates these bending waves, the sound from which can also be amplified by resonances in the tyre. Thus, it could be assumed that a tread-less smooth tyre would generate no sound whilst rolling over a smooth surface. However, this is not the case as a slick tyre can also produce sound. Depending on the surface it is running on it might even generate more sound than a tyre equipped with a tread [Iwao and Yamazaki, 1996].

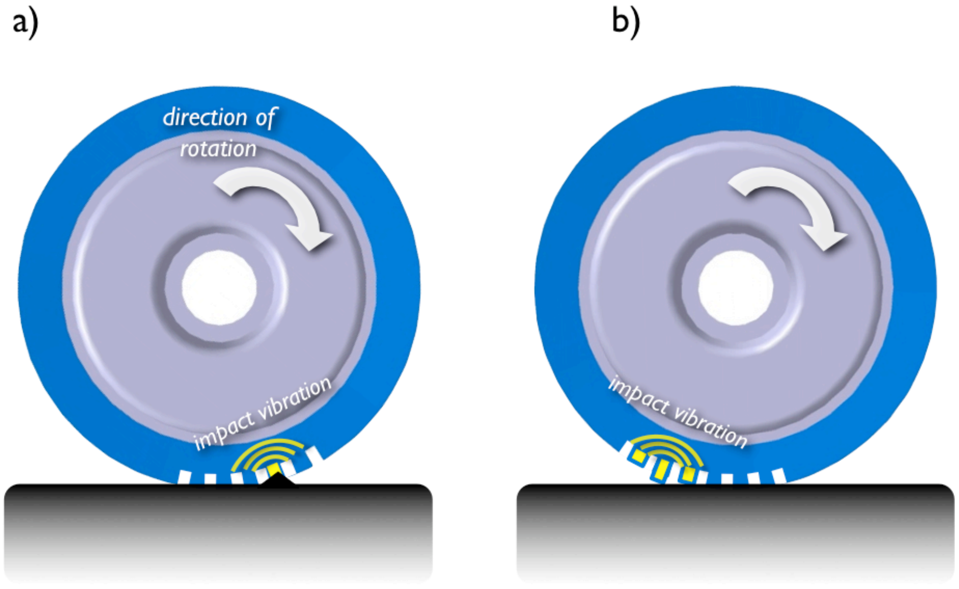

Figure 2.3 Illustration of impact mechanisms and resulting tyre vibration due to: a) leading edge road texture impact; and b) inverse impact mechanism at trailing edge

Another vibration initiated by the impact mechanism is sidewall vibrations. Figure 2.4 displays this phenomenon in which the height of the sidewall and inflation pressure are also important factors. The sidewall can act as a ‘sound board’ and therefore radiate sound into the environment [Kuijpers and van Blokland, 2001]. Resonance frequencies of sidewall vibrations are in the region of 400 to 800 Hertz [Virmalwar et al., 1999].

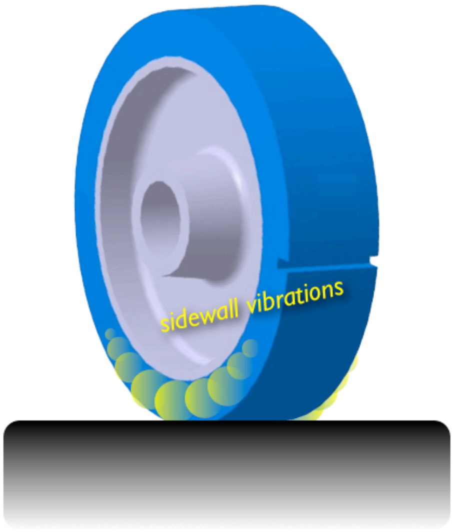

Figure 2.4 Illustration of sidewall vibrations due to the impact in between the tyre and the road

2.3.2.2 Adhesion mechanism

When all forces - that should exist on a tyre - are taken into account, there must also exist some lateral and longitudinal stresses. These stresses result in tangential displacements from the tyre circumference point of view. In the footprint as shown in Figure 2.5a tangential displacements occur, whether the tyre is in a free rolling or driving stage. Whilst passing through the contact patch a tread element accumulates a potential energy until the friction forces from the interaction with the road are lower than the forces in the tread element. Suddenly, the tread element slips back into its initial position. There it sticks or locks again. This process may be repeated even whilst the element is in the contact area between the tyre and road, it is called scrubbing or simply stick/slip as in Figure 2.5a. Stick/slip will give increased noise when friction is increased, typically at high frequencies [Sandberg and Ejsmont, 2002].

Another similar adhesion mechanism is called stick/snap. Stick/snap occurs at the trailing edge and can either result in tangential or radial vibrations. The latter can be initiated when a very warm winter tyre tread contacts a dry clean surface, it can also occure for a racing car tyre in normal test conditions as the tyres are mostly softer and prone to significant heating up. In this case the rubber element sticks to the road surface and before it is released again at the trailing edge of the tyre, it will be stretched slightly. When the tread block is finally released it continues vibrating until it reaches its initial, uncompressed condition. However, the main vibration direction for stick/snap is supposed to be the tangential one, as illustrated in Figure 2.5b. This vibration is significantly increased with load [Taylor and Bridgewater, 1998].

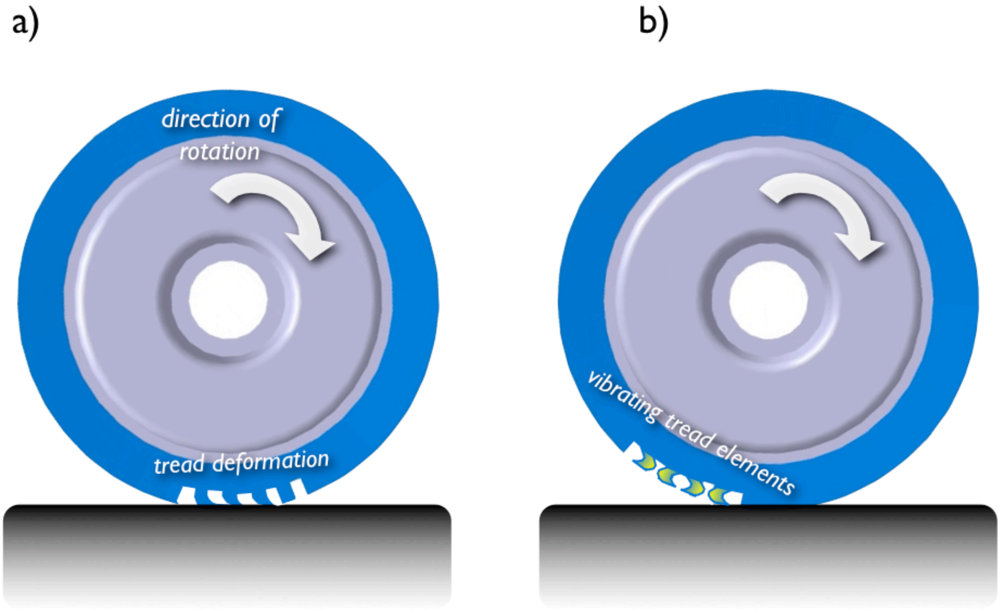

Figure 2.5 Illustration of vibrations due to adhesion: a) Stick/slip at the contact patch; b) resulting tangential tread element vibrations at the trailing edge

Most roads will be covered with a layer of dirt that reduces the adhesion between tyre and road considerably. Thus, the stick/snap mechanism resulting in radial vibration of the tread element is not that relevant with regards to tyre/road noise in normal traffic conditions. The only condition where it can change the noise behaviour of a tyre will be in the laboratory when a tyre is driven on a chassis dynamometer drum. The adhesion effects in general are very difficult to simulate and measure because of changing material properties during wear [Kroeger et al., 2004].

2.3.2.3 Air displacement mechanism

Air displacement mechanisms are “air-borne based phenomena”. One of these is the air turbulence effect that can be further divided into two different categories. The first is called displacement turbulence noise. In this case air turbulence is caused by the tyre moving along in a longitudinal direction, thus displacing the air at the leading edge of the tyre. The second category is named rotational turbulence noise. Here the tread pattern and to some extent even the smooth tyre can drag air around it as it rotates, like a fan. This could also be called spinning disc noise because only the rotation of the wheel is the cause for this noise not the longitudinal movement along the road. Chanaud [Chanaud, 1969] carried out investigations regarding spinning disc noise and concluded that this was only important at very high speeds. Ruhala and Burroughs [Ruhala and Burroughs, 1998] investigated the turbulence noise generated by the spinning rim only, but found this was less significant then expected. Therefore, Sandberg and Ejsmont [Sandberg and Ejsmont, 2002] concluded that it is not very likely for rotational turbulence noise to have an affect on overall sound levels, but it may be a factor to consider at higher speeds on low noise road surfaces, where other higher frequency tyre/road noise radiation is low.

A further air displacement mechanism is the air pumping effect named by Hayden [Hayden, 1971] in 1971. Hayden proposed a theory based on the deformation of a cavity between the tread elements when they enter the contact patch. The cavity is compressed and thus air is pressed away at the leading edge of a tyre as shown in Figure 2.6. At the trailing edge there can be a corresponding air displacement, due to tread and cavity expansion that should generate a sucking effect as it is shown on the left hand side of Figure 2.6. In volumetric flow rate terms, this characterises the driving mechanism as an acoustic monopole. As a result of this idea, Hayden modelled a prediction of the sound pressure level of a tyre at an observation point 50 ft away from the roadway.

The air pumping mechanism can occur as a result of air pockets in a tyre tread pattern, but also for pockets in the road surface as identified by

Schaaf [Schaaf et al., 1990] and Hamet [Hamet et al., 1990]. However, the effect of the road surface seems to decay very quickly and therefore might not have such a significant influence.

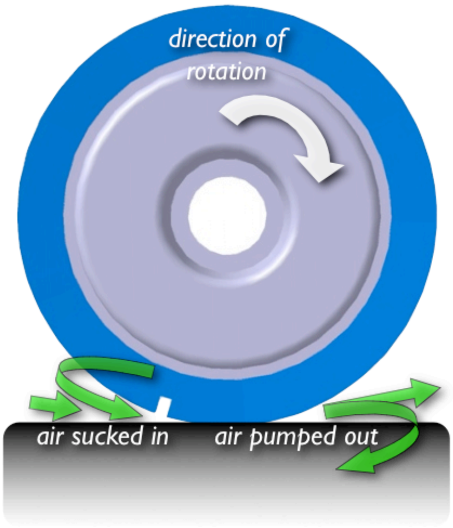

Figure 2.6 Air displacement illustration at the leading and trailing edge

According to Sandberg and Ejsmont [Sandberg and Ejsmont, 2002] air pumping occurs in a frequency range from 1 to 10 kHz. A more recent theory of the air pumping mechanism has been developed by Gagen [Gagen, 1999, 2000] and also by Kim et al. [Kim et al., 2006]. Both models are based on computational fluid dynamics simulations, where Kim et al. additionally apply a Kirchoff integral method. Gagen also delivers a prediction for the energy emitted at the leading edge of a tyre equipped with a groove with one open end. However, so far there has not been any experimental confirmation for either model. Also Gagen's model is not mentioned in a recent publication by Kropp [Kropp et al., 2004], where some ideas about air pumping are discussed. According to Kropp air pumping is a very complex process, thus, some models only fit for certain cases but cannot be generalised.

Even within the contact patch there are thought to be significant air displacements. So-called pipe resonances occur in channels of the footprint of a tyre because the tread grooves convert into pipes when they are covered by the road surface, as illustrated in Figure 2.7a. In fact when in contact with the road, every tread pattern design is a system of pipe resonators. The resonance frequency of the pipes is only dependent on their geometry, not on the driven speed of the vehicle. So inflation pressure and load might be the only two variables that can slightly change the resonant frequencies of the grooves because the contact patch length depends on both variables. As a result it can be said that, in general, the resonance frequency is only a function of groove length.

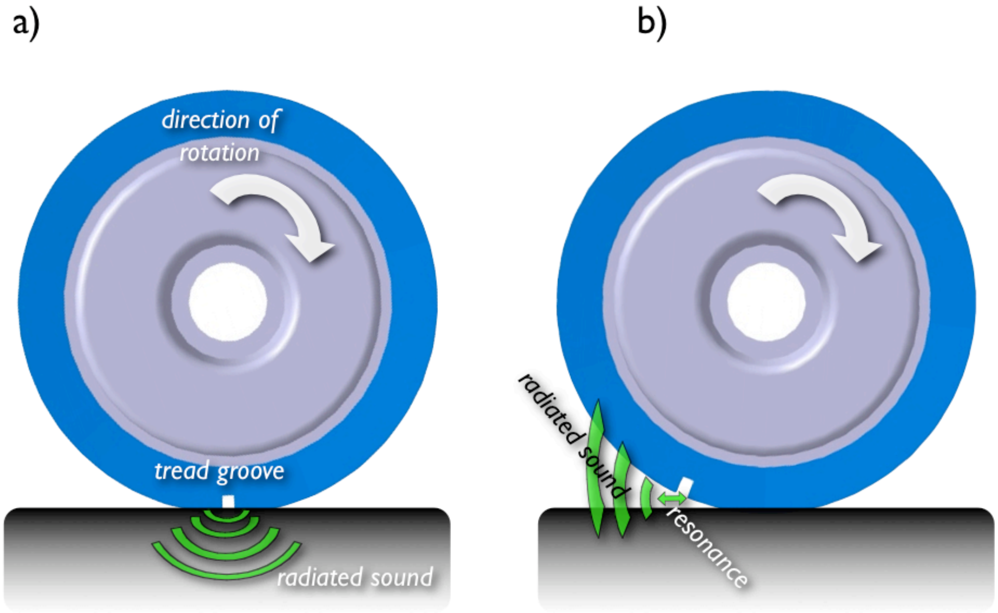

Figure 2.7 Illustration of air related mechanism at the contact patch: a) groove resonance; and at the trailing edge: b) air resonant radiation

The last air related noise phenomenon of a tyre is the air resonant radiation, or Helmholtz resonance. This effect is modelled as a simple mass-spring vibration system. For this application the air in front of the cavity acts as the mass and the volume of the cavity is the spring as indicated in Figure 2.7b. In some special cases this phenomenon can be the main mechanism for tyre/road interaction noise according to Nilsson [Nilsson et al., 1979]. The acoustical result of a Helmholtz resonance for a tyre is assumed to be a tone blast. This means that as soon as the cavity leaves the ground at the trailing edge there will be a high amplitude medium frequency signal that is decaying with increasing frequency. To avoid the occurrence of the Helmholtz resonance effect efficient ventilation of all grooves is recommended, either by designing an appropriate tread pattern or by using a porous road surface [Sandberg and Ejsmont, 2002].

2.3.3. Noise amplification and reduction mechanisms

2.3.3.1 The horn effect

One significant tyre noise amplification mechanism is the so-called horn effect. When noise is generated just at the leading or trailing edge it is typically amplified by the horn effect. The name horn effect is chosen, because from the side view of a tyre, the tyre tread and the road surface create a horn shape, as is illustrated in Figure 2.8 marked by the red area. The first elaboration of this effect was by Schaaf and Ronneberger [Schaaf and Ronneberger, 1982]. They invoked the reciprocity principle for quantification of the horn effect. Thus, comparison measurements were made with and without the tyre, with the source directly at the contact patch and the receiver in the far field and vice versa.

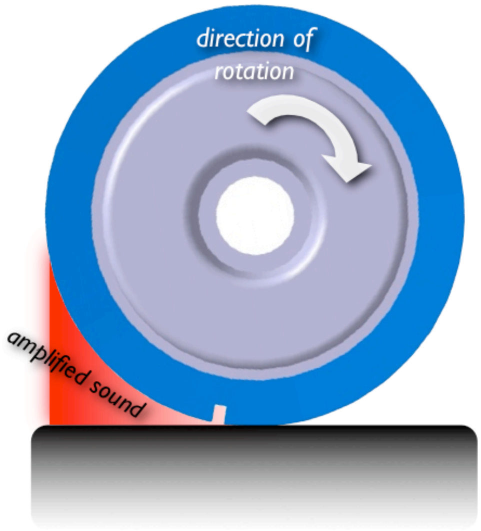

Figure 2.8 Illustration of the horn built between the tyre tread and the road surface

Due to the horn effect, Schaaf and Ronneberger measured amplifications of up to 25 dB at certain receiving positions for frequencies up to approximately 1000 Hertz. Further, it can be said that the efficiency of the horn built by tyre and road surface is higher the wider the tyre, as is reported in experimental investigations by Graf [Graf et al., 2002] and suggested by a theoretical model by Kuo [Kuo et al., 2002]. However, the efficiency of the horn effect can drop when at least one of the surfaces, either tyre (tread) or road, are porous [Kropp et al., 2002].

2.3.3.2 Acoustical impedance effect

The acoustical impedance effect in tyre/road noise is defined as the acoustical behaviour of the road structure regarding amplification or attenuation of radiated sound. For example, porous surfaces should act like sound absorbing material, thus affecting sound propagation into the far field. The influence of the horn effect can, for instance, be reduced dramatically by these road surfaces according to [Beckenbauer, 2003]. Results of a computational model developed by Duhamel et al. [Duhamel et al., 2006] show that an absorbing road can reduce the sound propagation by 2 to 5 dB in comparison to a rigid road.

2.3.3.3 Mechanical impedance effect

Mechanical impedance is defined as a measure of how much a structure resists motion when subjected to a given force. The mechanical impedance effect in tyre/road noise describes the vibrational behaviour of road when a tyre impact takes place. Beckenbauer [Beckenbauer, 2003] found that a tyre could have a local mechanical impedance effect onto the road surface. In his publication, Beckenbauer proves that the elasticity and damping characteristics of the top layer of a road can have a significant influence on the noise contribution into the far field.

2.3.3.4 Tyre resonance

The literature defines two different categories of whole tyre resonances. One is belt vibration, as is illustrated in Figure 2.9 and the other one is air cavity resonance in the tyre tube. Both can be initiated by an impact from the road surface, for instance, impact mechanisms such as texture impact or inverse impact. Due to this, four different types of impact waves can be initiated [Larsson et al., 2002]. First of all membrane waves occur at low frequencies. At higher frequencies these waves change in nature into bending-type waves. A Longitudinal wave is the third wave type that can be generated in a vibrating tyre and the fourth wave type is a shear wave. The shear wave takes place between the parallel movement of the reinforced belt and the tyre tread. In general tyre belt/carcass vibrations are likely to be in a region in between 700 to 1300 Hertz [Sandberg and Ejsmont, 2002]. The design and construction of the belt would have a significant influence towards the frequency range of the vibrations.

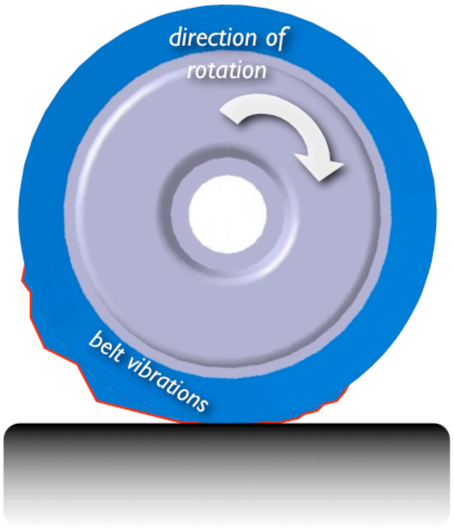

Figure 2.9 Illustration of tyre carcass/belt vibrations

The frequency of the cavity resonance is dependent on the tyre and rim size and on the fluid medium the tyre is filled with. The noise due to cavity resonance in a tyre is assumed to be more important for interior vehicle noise than exterior noise. The reason for that is the low resonance frequency of approximately 200 to 300 Hertz that generates a structural noise [Periyathamby, 2004] and [Torra i Fernandez and Nilsson, 2004] (for an air filled tube). According to Nilsson [Nilsson, 1979], for instance, a tyre filled with rubber exhibits a lower resonance frequency and also increased damping.

2.4. Summary and thesis orientation

The various mechanisms of tyre/road noise are summarised in Table 2.1 [Kuijpers and van Blokland, 2001]. The mechanisms are explained in terms of frequency range and a speed exponent, v_{exp}. By using a given speed exponent the variation of sound pressure level amplitude, L_p, in dependence of tyre velocity can be calculated for a specific tyre/road noise generation mechanism by the following equation:

$$L_p \sim 10 \cdot \log\left(\frac{v}{v_0}\right)^{v_{\exp}} = v_{\exp} \cdot 10 \cdot \log\left(\frac{v}{v_0}\right), \tag{2.1}$$

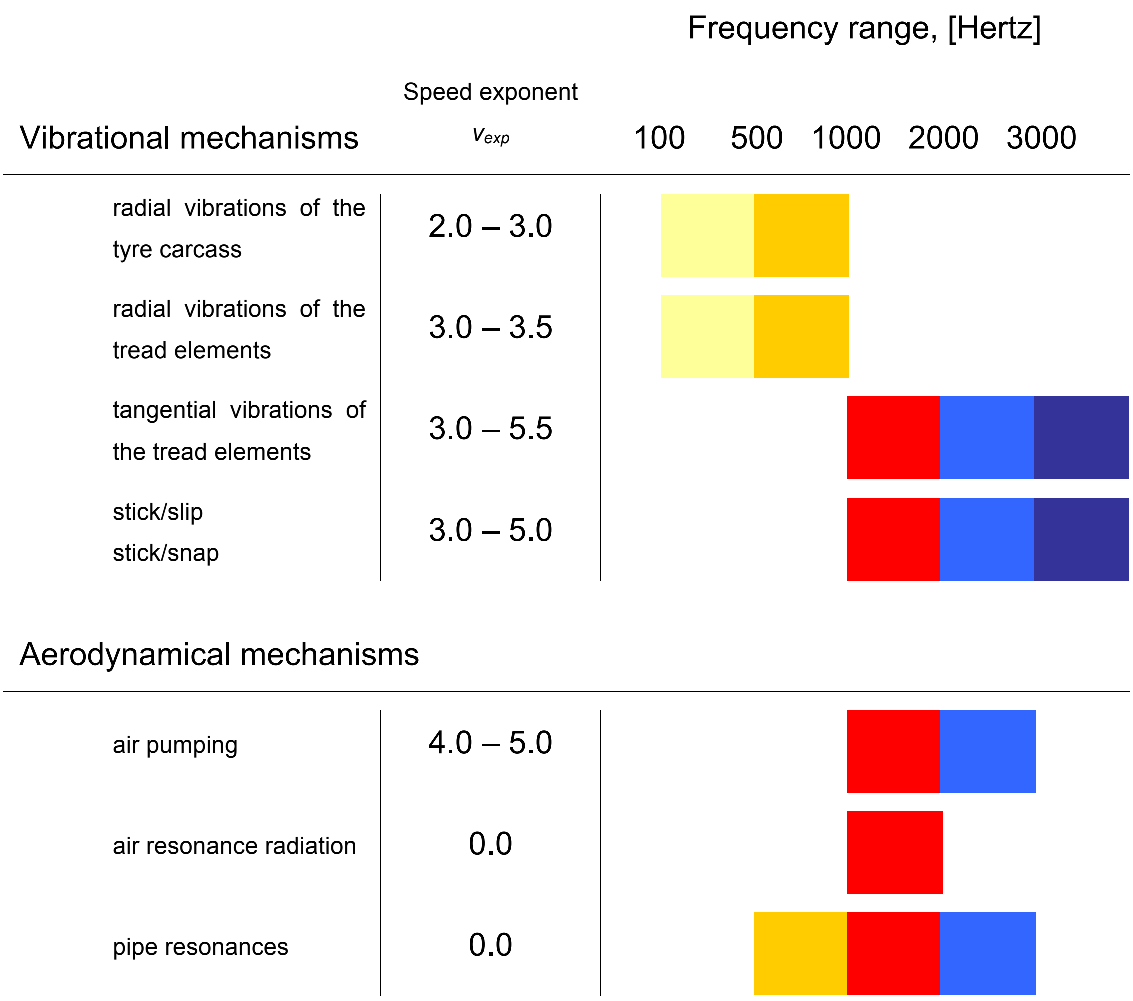

	Speed exponent	Frequency range, [Hertz]				
Vibrational mechanisms	v_{exp}	100	500	1000	2000	3000
radial vibrations of the tyre carcass	2.0 – 3.0	🟨	🟧			
radial vibrations of the tread elements	3.0 – 3.5	🟨	🟧			
tangential vibrations of the tread elements	3.0 – 5.5			🟥	🟦	🟪
stick/slip stick/snap	3.0 – 5.0			🟥	🟦	🟪
Aerodynamical mechanisms						
air pumping	4.0 – 5.0			🟥	🟦	
air resonance radiation	0.0			🟥		
pipe resonances	0.0		🟧	🟥	🟦	

Table 2.1 Overview of frequency range for tyre/road noise generation mechanisms with speed exponents, used to predict the change of sound radiation when the tyre velocity is changed [Kuipers and van Blokland, 2001]

The speed exponent v_{exp} taken from Table 2.1, and the actual rolling speed v are needed to predict the change in sound pressure amplitude in comparison to a reference speed v_0.

In Table 2.1 the radial vibrations clearly dominate the low frequency noise of less than 1000 Hertz. Unfortunately, a dominating mechanism for the high frequency noise cannot be identified. This noise is caused by a combination of many different noise-generating mechanisms that makes the understanding of high frequency tyre noise a complex process.

It is clear from earlier sections of this chapter that significant work has already been undertaken into the area of tyre/road noise. The amplification mechanisms such as acoustical impedance and mechanical impedance and the tyre resonance effects will not be of interest because in this Thesis the actual source of the noise phenomena will be identified. The same rationale applies to the horn effect that is now rather extensively explored in references [Schaaf and Ronneberger, 1982], [Graf et al., 2002] and [Kuo et al., 2002].

When considering the generation mechanisms, the tyre carcass and radial vibrations of the tread elements occur generally in the lower frequency region, as shown in Table 2.1. These mechanisms are not that important in the frequency region for exterior noise, as explained earlier. Sandberg [Sandberg, 2003] describes the main problematic area of tyre/road noise as the frequency region around 1000 Hertz. Thus, the aim of this Thesis is to focus on the noise generating mechanisms that are assumed to be responsible in that frequency region.

General rules of tyre tread design are already formulated [Saemann, 2006]. Saemann noted in 2006 that a tyre with an intelligent pattern produces only up to 3 dB(A) more noise than a slick tyre, but according to Kropp [Kropp, 1989] there is still a lack of quantitative knowledge about the influence of the different tyre noise mechanisms. At the Euronoise 2006 Conference [Kropp, 2006] Kropp noted again a lack of models specifically for the air related effects. This area is also supported by Sandberg and Ejsmont [Sandberg and Ejsmont, 2002], who suggest that the air pumping effect “is believed to be one of the most important in tyre/road noise generation, if not the most important at least for several tyre/road combinations”.

Therefore, this Thesis extends research into the air related effects of tyre/road noise, where Hayden [Hayden, 1971] is a pioneer with his model of “air pumping”. Hayden’s theory was supported in former times [Plotkin et al., 1979 and Samuels, 1979], however, has recently been questioned by Gagen [Gagen, 2000] without a satisfactory experimental validation. Thus the aim of this Thesis is to provide further experimental insight into the basics of air related displacement mechanisms at the tyre/road interface.

Chapter 3

Theoretical models of air-related noise generation mechanisms

This chapter deals with an explanation of four different air related models of tyre/road noise presented in the literature. Those models are assessed by the measurements conducted for this Thesis. Results of the comparison between the models and measurements are presented in Chapter 5 through to Chapter 7.

A pioneer in the field of air related noise generated by a tyre rolling over a road is Hayden [Hayden, 1971], who introduced the expression ‘air pumping’ and proposed a theoretical model to describe the phenomena. Air pumping is the main expression used for air related mechanisms at the tyre road interface [Sandberg and Ejsmont, 2002]. However, there are other mechanisms as well, which have been presented throughout the years. This chapter lists all the important processes in analogy to their time of occurrence regarding the tyre tread position. At first, when the tyre tread touches the road surface an air movement out of the tread is initiated. Two theoretical approaches explain a possible solution for the process at the leading edge, introduced by Hayden and Gagen [Gagen, 1999, 2000]. When the tyre processes further and the tread is covered by the road, the groove resonance is the active noise generating mechanism. Finally at the trailing edge of a tyre when the tread lifts off the road again another mechanism is found to be active, which is the air resonant radiation introduced by Nilsson [Nilsson et al., 1979]. Those four theoretical approaches are explained in detail in the following section.

The notations of groove/cavity dimensions used throughout the remainder of this thesis are illustrated in Figure 3.1. The groove width in direction of the tyre width is labelled *W,* the depth of the groove is written as *D,* and the length of the groove, *L,* is in the direction of the tyre rotation.

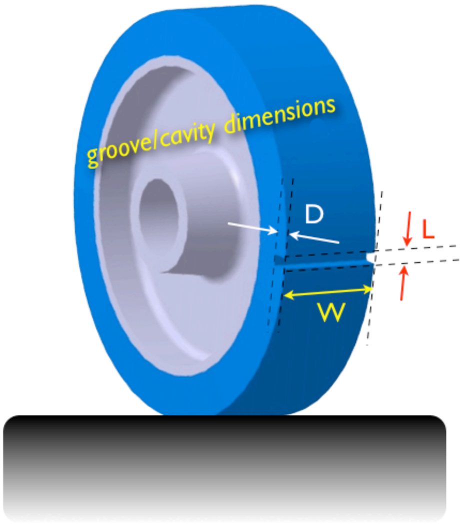

Figure 3.1 Illustration of groove/cavity dimensions

3.1. Leading edge: Hayden model

3.1.1. Monopole theory

In 1971 Hayden [Hayden, 1971] introduced a theory for tyre/road noise that describes the process of a tyre tread cavity hitting the road surface. Hayden's model is based on the monopole theory. In the monopole theory the sound source is assumed to be acting at one point in space and the sound is radiated in spherical waves away from the source into the space, as shown for an example of a tyre in Figure 3.2.

During the process of air pumping a transient volumetric flow is created when air is squeezed out of the cavity at the leading edge or sucked into it at the trailing edge of a tyre contact patch. Over time these fluctuations of the volumetric flow are assumed to be the driving mechanisms of the acoustic monopole or simple source theory. From the definition of sound intensity $I(r_{mic},t)$ that is the time average of pressure p and particle velocity v_p

$$I(r_{mic},t) = \overline{p \cdot v_p}\,, \tag{3.1}$$

in combination with the relationship between pressure and particle velocity in a free field where the ambient density is ρ and c the speed of sound

$$v_p = \frac{p}{\rho \cdot c}, \tag{3.2}$$

the following general expression for sound intensities for a simple monopole in free space is formulated

$$I(r_{mic},t) = \frac{\left(\overline{p \cdot p}\right)}{\rho \cdot c} = \frac{\rho}{16 \cdot \pi^2 \cdot r_{mic}^2 \cdot c} \cdot \overline{\left(\frac{\partial Q}{\partial t}\right)^2}\,. \tag{3.3}$$

Where Q is the volumetric flow rate and r_{mic} the recording distance of the source.

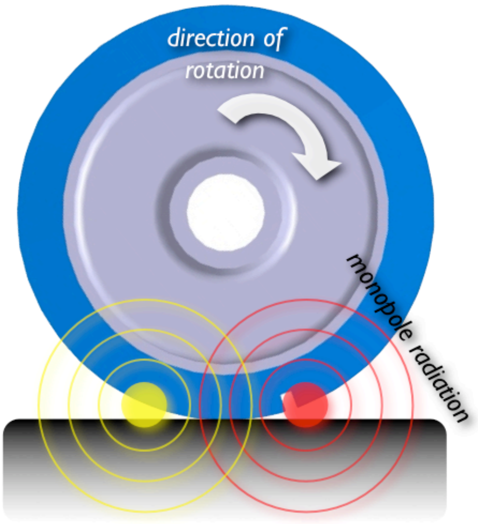

Figure 3.2 Illustration of monopole source sound radiation at the tyre/road interface

A monopole is defined as a source that radiates sound equally in all directions in space. A simple example of a monopole source is a sphere with a radius that alternately expands and contracts in a sinusoidal behaviour. The monopole source creates a sound wave by alternately introducing and removing fluid into the surrounding area. A tyre would be expected to have two separate monopoles one at the leading and one at the trailing edge, as is illustrated in Figure 3.2. This indicates that the monopole assumption is clearly an approximation.

Eventually Hayden presents a mathematical prediction of the sound pressure level $L_p(r_{mic},v)$ from Equation (1.1) in combination with Equation (A1.6) generated by a cavity at the circular frequency of reoccurrence ω (A1.5) of the cavity

$$L_p(r_{mic},v) = 20\log\left(\frac{\rho \cdot v^2 \cdot (fc) \cdot D \cdot W}{p_{ref} \cdot 2 \cdot x_{circ} \cdot r_{mic}} \cdot \sqrt{n}\right). \tag{3.4}$$

This is dependent on the cavity width W and depth D, the circumferential distance to the next cavity x_{circ}, the distance of the microphone to the source r_{mic}, the reference sound pressure level p_{ref} and the squared tyre speed v. Hayden also adds a factor for the number of cavities (sources) per tyre width, n. However, the difficulty with this model is how to accurately estimate the fractional change in the cavity volume (fc) when the load of the tyre compresses the cavity. Hayden assumed this change to be 0.1 or 10 % of the cavity volume.

3.1.2. Literature validation

To get an accurate idea of the volume change it should be measured not assumed. This was carried out by Samuels [Samuels, 1979] and Plotkin [Plotkin et al., 1979] and presented at the International Tyre Noise Conference in 1979. Both introduced a practical validation of the application of the monopole theory based on Equation (3.3). However, neither of them used Hayden's sound pressure level prediction at a certain frequency from Equation (3.4).

Samuels [Samuels, 1979] used a photographic technique to record the deformation of the tyre tread in the contact patch. By mounting a camera underneath a transparent road surface, photographs were taken that showed the changing surface dimensions of a tread cavity. With this information and a “constant tread depth approach accepted by the industry” the volume was calculated. This means that the volume change is still assumed, because the actual volume change is not measured, only the surface deformation. Unfortunately Samuels failed to provide reference details for the tread depth approach, in addition many of the initial values used in his calculations are not provided. Based on the monopole theory, Samuels [Samuels, 1979] proposed the following equation

$$L_p(r_{mic}) = 20\log\left(\frac{\rho \cdot p_{mag} \cdot c \cdot k}{p_{ref} \cdot 4\pi \cdot r_{mic}}\right). \tag{3.5}$$

Samuels introduced additional variables: k as the wavenumber, and p_{mag} as the magnitude of the spectral peak at the tread element passing frequency. This magnitude value was found by conducting a Fourier analysis of the differentiated cavity volume change. Samuels claims to have found good agreement between the values calculated by Equation (3.5) and the measured values of source strength, at least for the fundamental tread element passing frequency.

Another approach was presented by Plotkin et al. [Plotkin et al., 1979], where the volume change of the cavity was measured using a complex experimental procedure. At first it was checked by high-speed photographs that cavity compression of a tyre tread only depends on the pressure between the road and the tyre. Hence it was concluded that the volume change is independent of tyre speed. Then Plotkin et. al placed a latex bladder filled with water into a groove (with one open end) of a heavy truck crossbar tyre. The tyre was then advanced in 1 mm increments on the rotating drum and the displaced water volume was recorded. It was found that the volume in the cavity first slightly increased and then decreased until reaching a minimum value. To predict a sound pressure due to this measured volume change the monopole theory from Equation (A1.2) was used. The volumetric flow rate Q was written in terms of volume, hence, the second time derivative of volume displaced $\ddot{V}$ (A1.1) was used giving an estimate of the pressure as [Plotkin et al., 1979]

$$p(t) = \frac{\rho \cdot \ddot{V}}{4\pi \cdot r_{mic}}. \tag{3.6}$$

This solution is only valid for small values of radius r in comparison to the wavelength from the emitted sound, with low fluid velocities in comparison to the speed of sound [Gagen, 2000]. Due to the fact that the experimental measurement from Plotkin was conducted at low speed, the volume displaced was measured independent of distance, hence, the time derivative can be substituted with

$$\ddot{V} = \frac{\partial^2 V}{\partial t^2} = \frac{\partial^2 V}{\partial x^2} \cdot v^2 = V'' \cdot v^2. \tag{3.7}$$

Substituting into Equation (3.6) this eventually leads to

$$p(x) = \frac{\rho \cdot V'' \cdot v^2}{4\pi \cdot r_{mic}}. \tag{3.8}$$

where the pressure generated at the leading edge of a tyre is dependent on the volume that is squeezed out and on the speed of the tyre. Note that the tyre speed has significant influence because it is a squared quantity. Plotkin considered the sound radiation into a quarter space. As a result the corresponding Equation (3.8) was multiplied by a factor of 4. This was done because the microphone was positioned at the side of the tyre so the road surface and the tyre sidewall were building mirror sources. Two mirror sources in total lead to an increase in source strength by the factor 4. Plotkin then compared the predicted pressure calculated by Equation (3.8) with measured pressure against time. The results showed a good agreement. However, Hayden initially assumed pockets in the tyre, whereas Plotkin et al.

used a groove that is open at one end. This will probably mean that the groove resonance effect also occurred in the recordings conducted by Plotkin. Whereas, for pockets there would be a defined end of the squeezing process due to the fact that the cavity is closed completely by the road at some stage of the process.

As indicated by Plotkin, the common assumption is that the volume change of cavities contacting the road reaches a constant value (independent of tyre speed). So the second derivative of this volume change when used in Equation (3.8) results in the pressure that is generated. Consequently, for higher tyre speeds, a higher amplitude and higher frequency pressure peak is generated when recorded against time. Thus, tyre deformation is directly linked to volume fluctuations, which result in sound propagation. Hamet et al. [Hamet et al., 1990] however, claim with their investigation of cavities in the road that air pumping can also be found without volume deformation.

3.2. Leading edge: Gagen model

Another approach for air pumping was introduced by Gagen [Gagen, 1999, 2000]. Gagen was the first to use computational fluid dynamics modelling to simulate the aerodynamically related processes occurring at the leading edge of the tyre with a groove open at one end. He also used volume change as the initiation of the air movements. Conte and Jean [Conte and Jean, 2006] in contrast used computational fluid dynamics to simulate air fluctuations without volume change from cavities in the road surface.

Gagen [Gagen, 2000] argues that the Hayden model cannot be used to model the effect of air being pumped out at the leading edge of the tyre. Due to the simplicity of the monopole theory the model might not be suitable for the complex air squeezing process at the tyre/road interface. His main argument is that air actually responds sluggishly to local volume changes, while the monopole theory equates local air movements exactly with the volume changes of the system. (This “sluggishness” in terms of fluid dynamics is additional to the usual propagation delay of wave motion at finite speed).

3.2.1. Kinetic energy of expelled yet

Gagen derives a formula for the kinetic energy (based on acoustic wave equations, explained in Appendix A2) that is generated by the air when squeezed out of a groove due to the volume change. According to Gagen the energy, *E,* of air expelled from a linearly squeezed groove with one open end is

$$E = \frac{A}{L-A} E_p . \tag{3.9}$$

with *A* being the amount of volume change and *L* the length of the groove in circumferential dimensions. The kinetic energy E_p is dependent on the mass of air, m_0, moving at a certain speed across the groove that in accordance to the notation is defined by groove width *W* (perpendicular to circumferential tyre dimension) and closure time *T:*

$$E_p = \frac{1}{2} m_0 \left(\frac{W}{T}\right)^2 . \tag{3.10}$$

The initial fluid mass m_0 being dependent on the density ρ and the cavity dimensions (Figure 3.1) defined as

$$m_0 = \rho \cdot D \cdot W \cdot L . \tag{3.11}$$

By combining Equations (3.9), (3.10) and (3.11), the kinetic energy of an expelled jet according to Gagen finally becomes

$$E = \frac{\rho \cdot D \cdot A^3 \cdot W^3 \cdot v^2}{2\left(1 - \frac{A}{L}\right) \cdot L^4}. \tag{3.12}$$

Given by Equation (3.12) the energy of the expelled air is dependent on the geometry of the cavity, the volume reduction of the cavity in the contact patch and the squared speed of the tyre/vehicle. This derived model is investigated by the use of computational fluid dynamics but has not been experimentally confirmed.

3.3. Contact patch: groove resonance model

Sections 3.1 and 3.2 described mechanisms that are assumed to occur at the leading edge of the tyre. Another possible mechanism is focused on, in the contact patch area. This is the pipe resonance effect for grooves, also well known from other areas of acoustics. As introduced for tyres by Favre [Favre, 1979] in considerable detail and later updated by Sandberg [Sandberg, 2004] the groove resonance effect is developed from the basic acoustical application of a pipe resonance. This resonance frequency, f, is dependent on the length W (according to Figure 3.1) of the groove and the fluid medium, contained within the groove. Thus, for an open pipe assuming the wavelength $\lambda=2W$, then

$$f = \frac{c}{2W}. \tag{3.13}$$

In addition it is quite common to introduce a correction factor to consider the diameter d of a pipe [Sandberg and Ejsmont, 2002]. The equation for calculating the resonance of a pipe with a certain length W and two open ends is then approximated by

$$f_n = \frac{n \cdot c}{2 \cdot (W + 2 \cdot X \cdot d)}. \tag{3.14}$$

The integer *n* describes the order of given harmonics of the fundamental frequency, *f*. The factor *X* is a constant, which according to Sandberg is generally considered to be in a range between 0.3 and 0.4.

There are usually grooves in a tyre with one open end and the other closed. In this case [Sandberg and Ejsmont, 2002] the corresponding equation is:

$$f_n = \frac{(n - 0.5) \cdot c}{2 \cdot (W + X \cdot d)}. \tag{3.15}$$

For this type of groove the fundamental frequency is approximately a quarter of the wavelength (called λ/4 resonator).

Certain guidelines have been formulated by experts to prevent groove resonances from dominating the noise generation in the contact patch. The main idea is that all grooves should be well ventilated. Unfortunately, in that case a high number of tread blocks is introduced that are effected by vibrational excitation [Sandberg, 2004]. Gagen [Gagen, 1999] does not recommend the usage of medium wide grooves because they produce a significantly higher noise level in comparison to thin and very wide grooves. A further idea is to change the width within a groove. According to Sandberg this should be narrow at the closed end. However, this might lead to more noise radiation at the trailing edge because the groove might behave more like a cavity.

3.4. Trailing edge: air resonant radiation

There is one widely accepted model that describes the trailing edge noise generation process of a tyre equipped with a groove, derived by Nilsson

[Nilsson, 1979] and based on a Helmholtz type of resonance. This resonance effect is created by the volume of air in a groove of a tyre and a mass reactance in the area between the tyre tread and the road surface at the trailing edge. Nilsson builds a damped mass and spring system to describe the resonance occurring at the trailing edge. The area in the cavity is seen as the spring and the changing area underneath the cavity is the vibrating mass with a connected damper. This changing mass and damper yields to a frequency modulation at the trailing edge with changing amplitude.

3.4.1. Geometric explanations

The initial volume, V_0, of the groove or cavity can be measured or calculated. The area, *S(x),* of the air in between the groove and road surface has to be approximated. As shown in Figure 3.3, the height *h* is needed to get an idea about the area *S(x)*, that lies underneath the cavity at the trailing edge. Nilsson calculates this assuming of the area *S(x)* is only dependent on the distance *x* of the centre of the hole from the point of contact of the tyre.

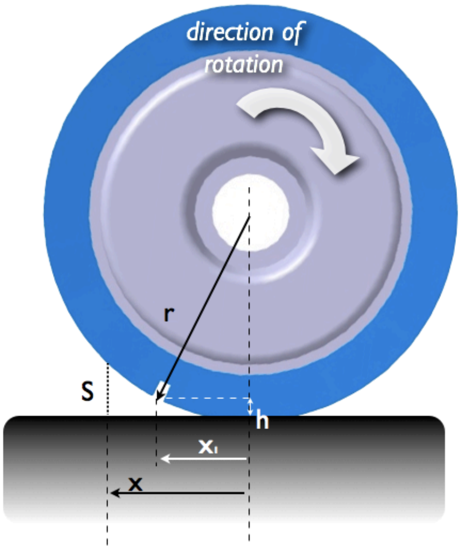

Figure 3.3 Schematic view of tread volume and related area *S(x)* underneath it, after [Nilsson, 1979]

Basic trigonometry is used to calculate the height *h* in. Thus,

$$x_1^2 = 2rh - h^2. \tag{3.16}$$

Nilsson [Nilsson, 1979] assumes for small values of the height, *h,* the squared term, h^2, to be negligible. Therefore, the height, *h*, can be expressed as

$$h \approx \frac{x_1^2}{2r}. \tag{3.17}$$

Thus, the area *S(x)* underneath the cavity, with respect to the cavity width, *W,* can be approximated to

$$S(x) = \frac{x_1^2}{2r} \cdot W. \tag{3.18}$$

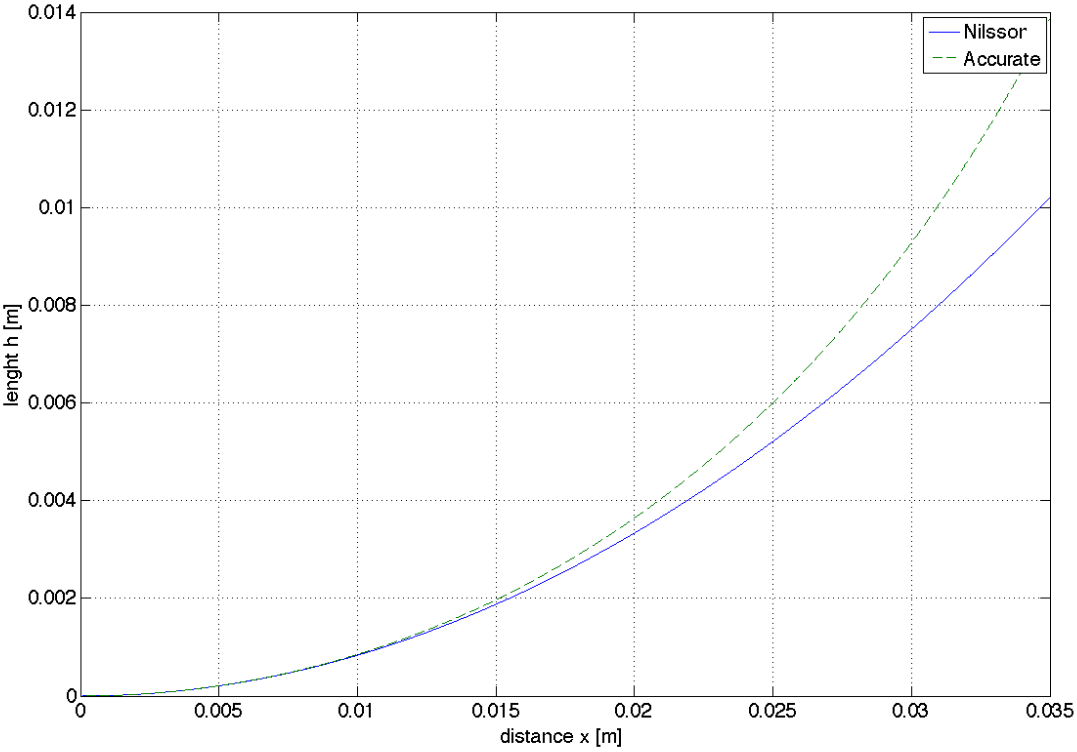

Figure 3.4 Comparison of Nilsson simplifications and accurate geometry

The mathematically correct value of the area *$S_{acc}(x)$*, where exact geometric calculations are used, would however be

$$S_{acc}(x) = \left(\frac{r^2}{\sqrt{r^2 - x_1^2}} - r \right) \cdot W . \tag{3.19}$$

The difference between Equation (3.18) and (3.19) is shown in Figure 3.4 for a given tyre radius $r = 0.06$ m without taking the width W of the cavity into account. The difference in height h is not significant, especially for significantly small values of x up to 0.015 m; thus, as mentioned by Nilsson the difference is negligible. This statement will be compared later on to the results obtained by the measurement.

3.4.2. Mass-spring-damper system

As previously mentioned Nilsson [Nilsson, 1979] applied a Helmholtz type of resonator to explain the trailing edge signal recorded from tyres with grooves. In that case the cavity volume would be the compliance (spring) and the expanding area between tyre and road would be the inertance (mass-reactance). The basics of this resonance circuit are explained in Appendix A3. According to Nilsson the resistance part of the mass, spring and damper system, *$R(\omega,x)$*, can be is defined, as

$$R(\omega,x) = \frac{\gamma \cdot \rho \cdot c(kx_1)^2}{S(x)\left[1 + (kx_1)^2\right]}. \tag{3.20}$$

Here a coefficient, γ, is implemented to compensate for the approximation that is introduced by assuming the travelling wave will only move in one direction away from the tyre. Due to the fact that energy can also spread sideways, which leads to losses, the coefficient must be smaller than unity.

The variable, *k*, is the wavenumber used to calculate the resonance frequency of the system.

The mass reactance, *M(ω,x)*, according to Nilsson, is

$$M(\omega,x)=\frac{\beta\cdot\rho\cdot c\cdot kx_1}{\omega\cdot S(x)\left[1+\left(kx_1\right)^2\right]},\tag{3.21}$$

where a coefficient, β, is introduced, because of the same reason as for coefficient γ. Nilsson evaluates those two coefficients γ and β experimentally for the best fit of his model to the measured data.

Nilsson also defines a spring constant by the following equation that is derived from a combination of impedance from a standing wave generated at the contact zone and one initiated by a wave in the actual cavity. This spring constant *K(ω,x)* is defined as

$$K(\omega,x)=\left[\frac{V_0}{\rho\cdot c^2}+\frac{S(x)}{\omega^2\cdot\rho\cdot x_1}\left(1-\frac{kx_1}{\tan\left(kx_1\right)}\right)\right]^{-1}.\tag{3.22}$$

In accordance to the literature, for a free movement vibration of a damped mass and spring system (Equation (A3.15)), the undamped oscillating part is described by the real part only. The circular frequency *ω(x)* is in this case equal to

$$\omega(x)=\sqrt{\frac{K(\omega,x)}{M(\omega,x)}-\left(\frac{R(\omega,x)}{2M(\omega,x)}\right)^2}.\tag{3.23}$$

As Nilsson was only interested in the frequency content of the signal not in the actual shape in the time history, he only used the undamped part to build his final model. By combining Equations (3.20), (3.21) and (3.22) with Equation (3.23)

$$\frac{V_0}{S(x)x_1} = \frac{1+(kx_1)^2}{\beta\cdot(kx_1)^2\cdot\left[1+\left(\frac{\gamma\cdot kx_1}{2\beta}\right)^2\right]} - \frac{1-\frac{kx_1}{\tan(kx_1)}}{(kx_1)^2}. \tag{3.24}$$

Nilsson ends up with this final result where the frequency, via wavenumber, *k,* of the oscillating volume can be calculated in dependence of the cavity position *x.* When the tyre is moving, the position of the cavity, relative to the road, *x*, increases and so does the Area *S(x)*. Therefore, Nilsson predicts a frequency change generated by the oscillating air. This is only valid for small changes of frequency, however.

In the literature Nilsson’s theory has been confirmed by Jennewein and Bergmann [Jennewein and Bergmann, 1984], and Ronneberger [Ronneberger, 1989]. Both authors also confirm a Helmholtz resonance at the trailing edge of the tyre with transverse tread grooves. The Helmholtz resonance can also be found for a cavity in the road surface, as investigated by Deffayet [Deffayet, 1989], However, Nilsson’s model only explains the frequency content of the signal and not the amplitude. This is due to the fact that Nilsson only takes the real part of Equation (A3.11) for his model, so there is no damping included. Therefore, the amplitude stays constant.

3.5. Discussion and summary

For each section: leading edge, contact patch and trailing edge, of a tyre in contact with the road, a mathematic explanation is presented. At the leading edge a model introduced by Hayden [Hayden, 1971] is normally referred to, namely air pumping. The expression is used in the literature for the whole air related effect at the contact patch of a tyre. Hayden developed a relationship between the volume squeezed out of a cavity at the leading edge and the resulting sound pressure level. This relationship is based on the Monopole Theory. Recently another approach for an explanation of the process, happening at the leading edge, was introduced by Gagen [Gagen, 1999, 2000]. Gagen doubts the applicability of the monopole theory used by Hayden. Instead Gagen presents an equation for the energy generated by the airflow out of the groove at the leading edge. This thesis aims to clarify the process happening at the leading edge of the tyre by conducting a series of experiments with tyres equipped with different types of cavities.

The noise generation at the contact patch of a tyre equipped with a groove is generally explained by the pipe resonance theory. This theory only predicts the resonance frequency but not the amplitude of the sound radiated. However, it is stated that medium sized grooves emit the highest sound in comparison to very wide or very small grooves [Gagen, 2000]. Tyres equipped with grooves are used to investigate if this resonance is also found in the experimental work of this project.

At the trailing edge of a tyre equipped with a groove the air resonance radiation explained by Nilsson [Nilsson, 1979] is an accepted approach to understand the process occurring. However, this only explains the frequencies of the resonance but not the amplitude. The sound radiation at the trailing edge is measured and analysed regarding the cavity dimension with different cavities in a tyre. Nilsson uses a mathematical simplification to calculate the area, *S*, underneath a tyre groove by Equation (3.18). The results for the trailing edge found in Chapter 7 will be investigated to determine if there is a better fit when the exact mathematical expression from Equation (3.19) is used.

Chapter 4

Experimental apparatus and measurement methods

In this chapter the experimental testing conducted is introduced. The first section describes the chassis dynamometer laboratories at Loughborough University. All measurements for this Thesis were carried out in these facilities. Details of slight modifications implemented to lower the noise radiation of the chassis dynamometer driving mechanism are explained. A special tyre presented in this chapter was chosen to investigate the air effects of tyre/road noise, along with different treads used. A rig was constructed to run the tyre on the chassis dynamometer. This rig is illustrated and explained.

Two different types of measurements to record tyre/road noise were conducted. In the first stage the sound radiation of a tyre was measured with a high number of microphones. In the second stage only two microphones were used however they were located in close proximity of the source: pointing to the leading and trailing edge of the tyre. The facilities where the measurements were conducted are not anechoic, thus, signal condition techniques needed to be applied to the measurement results. This conditioning was carried out using bandpass filter and interpolation techniques explained in the last section of this chapter.

4.1. Experimental apparatus

4.1.1. Chassis dynamometer

The dynamometer is designed for vehicle performance and emission testing so it does not take noise reduction into account. During data collection the chassis dynamometer available at Loughborough University produced high levels of noise, whilst running. Therefore, initially noise reduction needed to be applied to the driving mechanism of the dynamometer. The dynamometer consists of two double drum sections to accommodate a car with one driven axle. For the experiments reported in this Thesis just one single drum, to place the tyre on, was needed. It was chosen to place the rig onto the drum that is the furthest away from the driving engine of the dynamometer. This position is also in the centre of the room, which is a further advantage, because the influence from reflections of the wall is minimized.

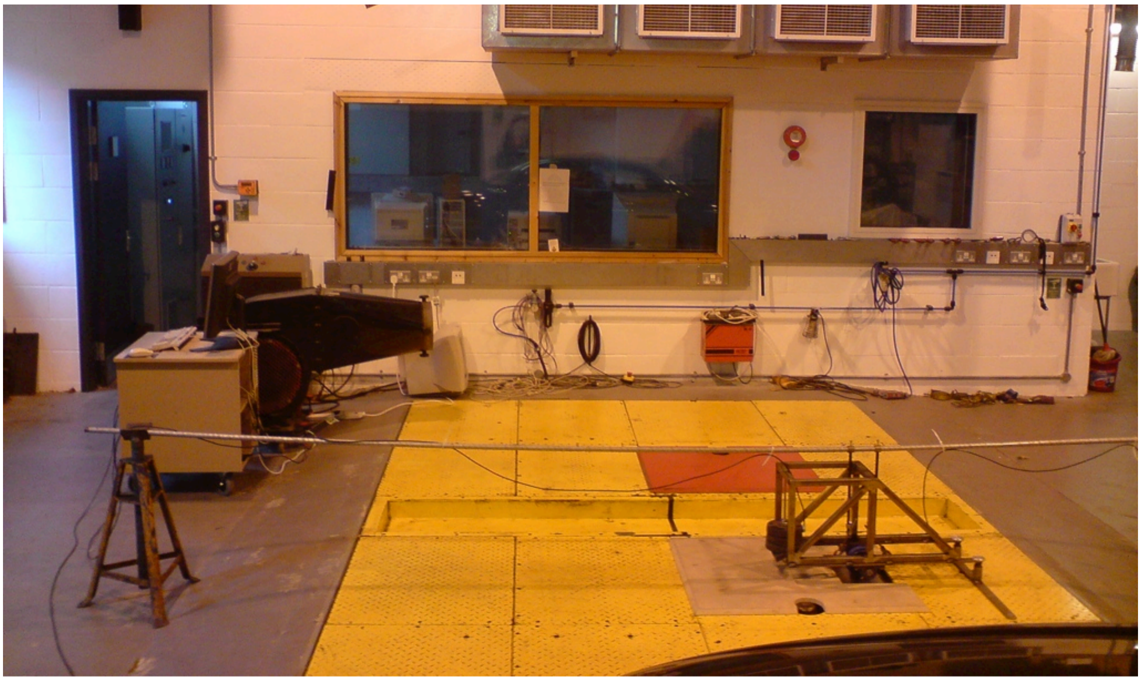

Figure 4.1 Photograph of the chassis dynamometer facility at Loughborough University

Figure 4.1 shows the arrangement of the rig that is located on top of the chassis dynamometer drum in the bottom right corner. The driving mechanism of the chassis dynamometer is located on the left hand side underneath the yellow steel covers. The other double section of drums that is not in use is covered by a red wooden plate to minimize sound radiation from the drums and the driving mechanisms underneath. Also for the drum section that is in use a brown wooden plate is implemented for shielding, as can be seen in Figure 4.1. Only a small section of that plate is left open to allow the tyre to run on the drum. Further insulation at the base of the chassis dynamometer could not be introduced due to safety reasons.

When the chassis dynamometer drums are rotating unwanted noise is generated by the driving mechanism and the fans that provide cooling for the driving mechanism. In order to reduce the unwanted noise the cooling fans were switched off during the measurement period as it was of short duration. Therefore, an override option was implemented into the software of the control unit of the dynamometer. This significantly reduces the background noise radiation, at least for low dynamometer speeds.

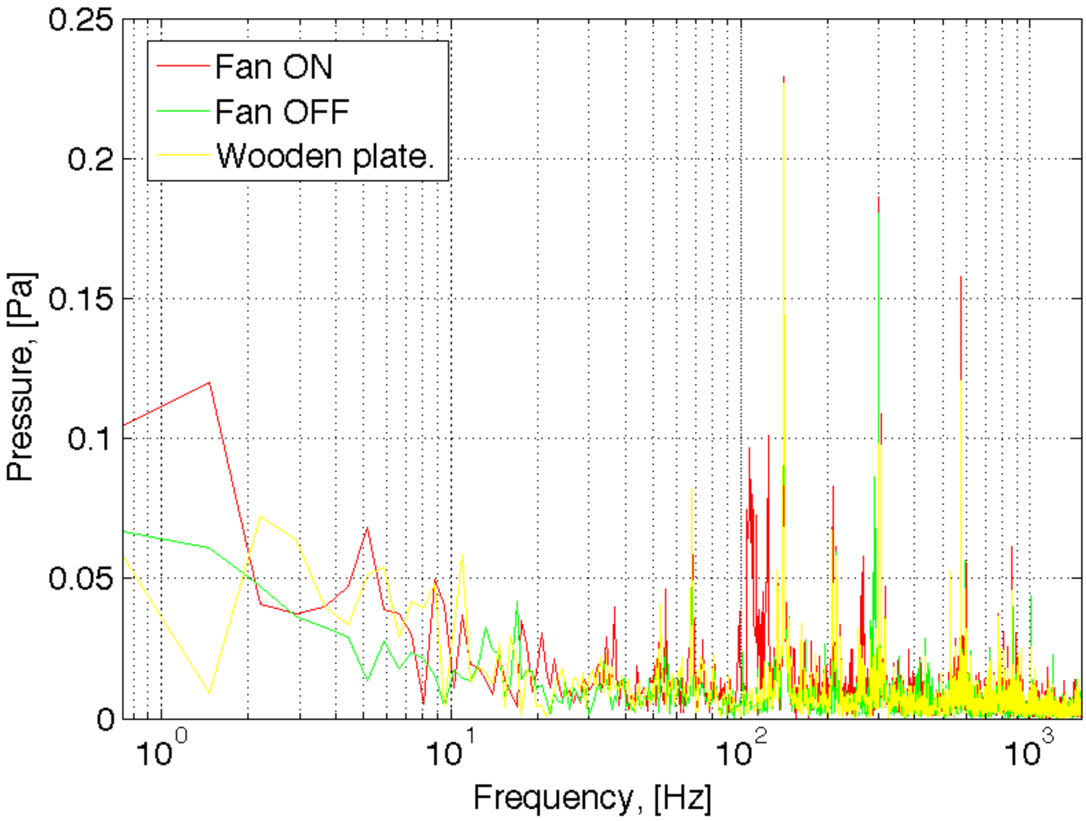

Figure 4.2 Comparison of the effect of different noise reduction mechanisms for a dynamometer speed of 19km/h, with a smooth tyre running on the drum

Figure 4.2 shows the frequency content of the measurement results of the three different noise reduction stages. The first measurement was taken with the dynamometer running at 19 km/h, shown by the red line, with no reduction mechanisms in place. The next stage was recorded when the cooling fans were switched off, as shown by the green line. The third stage was carried out with all reduction mechanisms in place, so the cooling fans were switched off and wooden plates introduced to cover the rollers of the chassis dynamometer, as shown by the yellow line. A microphone facing the trailing edge of the tyre recorded the noise level at the three stages.

Figure 4.2 shows that mainly the low frequency areas below 300 Hertz are influenced by the noise generated by the chassis dynamometer. The red line, where no noise reduction is in place, clearly dominates at all frequencies, especially between 100 Hertz and 300 Hertz. Thus, the possibility of switching off the cooling fans significantly reduces the unwanted noise at low frequencies. By introducing the wooden plates, further noise reduction is achieved but it is not as effective as the previous step. As only a slight difference in the frequency region of around 300 Hertz and 1000 Hertz is achieved. This potentially is due to the microphones being located very close to the tyre (and dynamometer), thus, the wooden plates do not provide such effective shielding. However, for the whole chassis dynamometer chamber it would probably have a more significant effect because less noise would be emitted to the surroundings, hence fewer reflections occur from the walls.

Another problem identified was that with increased speed the noise of the driving mechanism reaches high levels. Even with the reduction mechanisms in place a considerable amount of unwanted noise was recorded. Figure 4.3 overleaf shows a comparison of the sound pressure generated at different driving speeds of the chassis dynamometer plotted over frequency. The red line displays the high speed of 41 km/h, the green line the medium speed of 31 km/h and the yellow line shows the low speed case of 19 km/h. These three dynamometer speeds were chosen from a number tested and represent the best trade off regarding speed and acceptable unwanted noise generation. Figure 4.3 illustrates that the low speed case shows a moderate low-level noise influence, whereas the high speed case of 41 km/h shows high levels of noise generated by the chassis dynamometer at certain frequencies. This is especially apparent in the frequency region below 100 Hertz. In addition the high speed case generates a lot of noise at the frequency of 650 Hertz and at 1300 Hertz, the latter one is probably a harmonic. Therefore it was found that keeping the speed of the chassis dynamometer as low as possible reduced the dynamometer noise. The only roller surface available is smooth metal. Thus, it is of good use for basic investigations into the tyre noise generation mechanisms, however influences of the road surface cannot be considered.

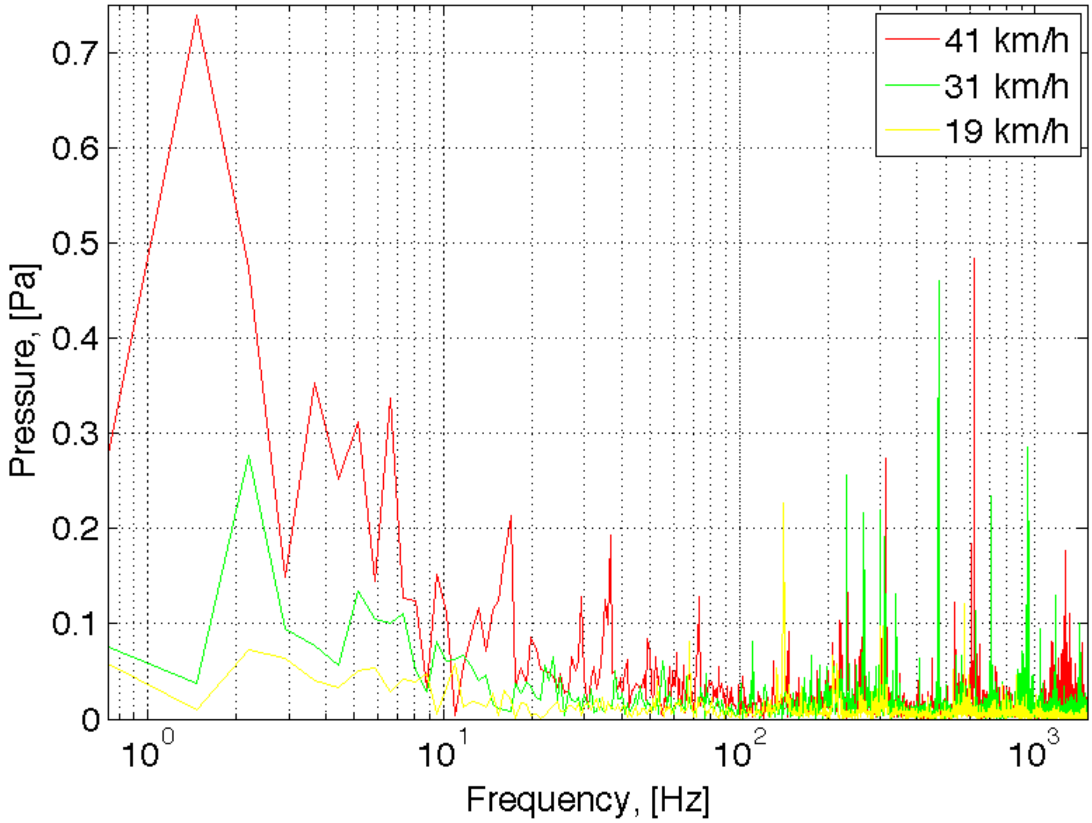

Figure 4.3 Comparison of noise emitted by the chassis dynamometer at three different dynamometer speeds

4.1.2. The solid rubber tyres

The experiments in this Thesis are meant to be as “simple” as possible. To eliminate the complex geometry and the influence of numerous different materials used in a modern tyre, a simple castor was used for the measurements of tyre/road noise. This solid tyre should result in increased damping of the tyre body according to experiments done with a real tyre filled with rubber by Nilsson [Nilsson, 1979] and also Richards [Richards, 1974]. Thus, it would help to reduce other unwanted vibrational noise generated by the rolling tyre. The Author of this dissertation is not aware of any work done with solid rubber tyres concerning aerodynamical tyre road noise. The main reasons for the chosen tyre for this project are low cost and constant material properties. Furthermore it should be rather small in comparison to the drum of the chassis dynamometer, thus, the curvature of the drum would not affect the measurements. The tyre material should not be too stiff so that the contact patch is still affected by the load of the tyre. However, it should not be too soft either so holes or grooves can be accurately machined into the tyre structure as shown in Figure 4.4.

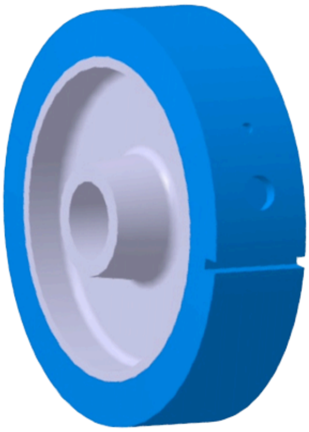

Figure 4.4 Drawing of a solid rubber tyre with examples of tread cut into the smooth surface

Figure 4.5a overleaf shows a photograph of the chosen unmodified tyre. The tyre itself is low cost because it is a mass produced castor with a firm rubber surface. The tyre geometry is ideal; the rubber surface is thick enough to allow a thread depth of up to 10 mm as shown in Table 4.1. Also the diameter of 121 mm of the tyre in combination with the chassis dynamometer drum (diameter: 500 mm) results in a good drum/tyre ratio of 4.23. This guarantees that the contact patch of the solid rubber tyre on the curved drum is similar to that of an actual car tyre on a flat road surface.

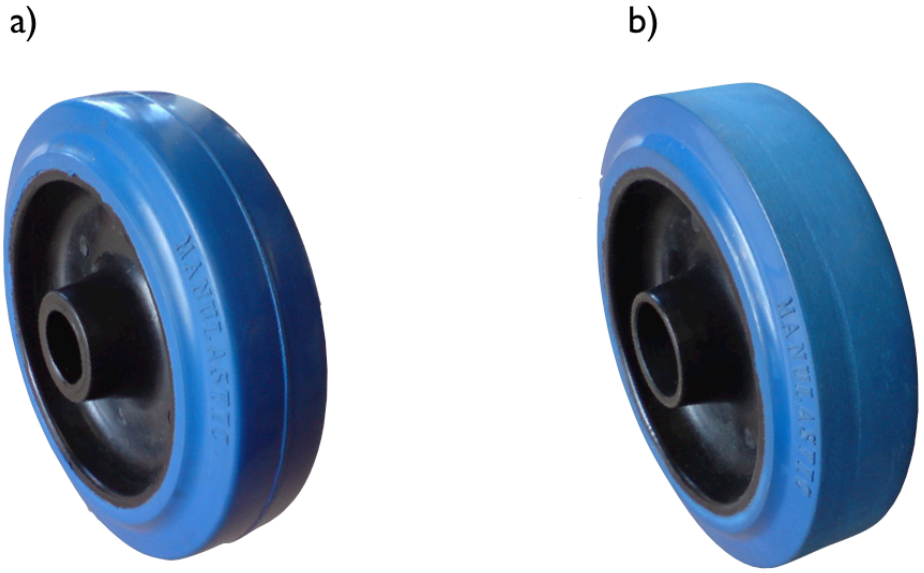

Figure 4.5 Photograph of the experimental solid rubber tyre: a) original; and b) modified tyre with enlarged shaft accommodation and smooth rolling surface

However, the black rim, constructed from plastic, needed to be modified to make sure that the tyre ran smoothly even at high speed. The inner diameter was therefore enlarged as shown in Figure 4.5b (in comparison to the original tyre, Figure 4.5a). This enabled a shaft to be accommodated that was supported by ball bearings, and guaranteed a tight and perpendicular fit to the tyre. As a result of the manufacturing process the middle of the tyre tread contains a circumferential line. Thus, the blue rolling surface was modified to get a smooth and even contact to the chassis dynamometer drum. This modification could introduce a slight variation between different tyres due to the adjustments that were needed to initialise the roller for the measurements. The modified tyre in Figure 4.5b shall be referred to as 'smooth tyre', sometimes it is also called 'plain tyre'.

Width [mm]	Diameter [mm]	Rubber thickness [mm]
26	121	15

Table 4.1 Geometry of the experimental tyre after modification

The next step considered was the tread design. In this Thesis the air related effects of tyre road noise were analysed. Sandberg and Ejsmont [Sandberg and Ejsmont, 2002] recommended a good ventilation of the tyre tread for low air related noise generation, as stated in Chapter 3. In contradiction to this statement the most effective tread for noise generation is a tread with cavities, because the air can only escape suddenly in one direction. Thus initially it was decided to equip tyres with cavities. From a manufacturing point of view a circular cavity is the easiest to produce so this was the first one to be made and experimentally tested. Two different tyres were produced, one with a large cavity and another with a small cylindrical cavity with the geometrical dimensions as displayed in Table 4.2.

	Large cavity	Small cavity
Diameter, [mm]	9	2.5
Depth D, [mm]	5.5	2
Volume V_0, [mm^3]	350	9.8

Table 4.2 Cylindrical cavity dimensions for two experimental tyres

Photographs of the two tyres are shown in Figure 4.6, in which the difference of cavity size is noticeable. The tyre with the large (9 mm diameter) cavity shall be referred to as the ‘large cavity’ tyre and the tyre with the small (2.5 mm diameter) cavity as ‘small cavity’ tyre respectively. The ‘large cavity’ is of a size similar in dimension to a normal tyre tread for an ordinary vehicle tyre. The ‘small cavity’ however scales to the small tyre when it is compared to the proportions of the tread of a realistic tyre. The noise generated by both of these designs was compared to other tread designs including the plain tyre shown in Figure 4.5b.

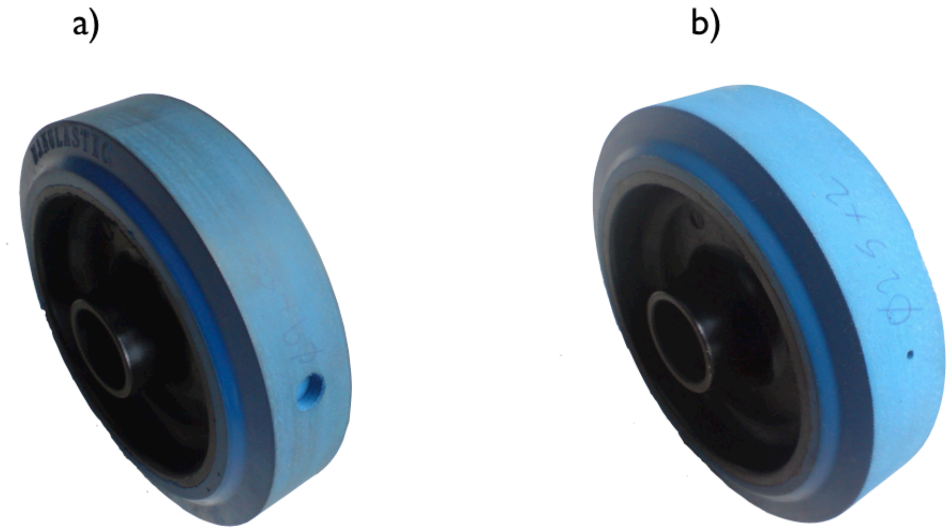

Figure 4.6 Photographs of two experimental tyres with cylindrical cavities: a) 'large, 9 mm diameter, cavity'; and b) 'small, 2.5 mm diameter, cavity'

The next tread designs were rectangular cavities, which are intended to give a more realistic approach when compared to a real tyre tread. The dimensions are similar to the tyre with the 'large cavity'.

Figure 4.7 shows photographs of the three different rectangular cavities constructed. The cavities were cut with a milling machine. In Figure 4.7a the large square cavity is shown with the same depth and length as the large cylindrical cavity described earlier, however, the volume is about 27 % larger because of the squared area instead of a circular area. This tyre shall be referred to as the 'square cavity' tyre.

In addition tyres with two further cavity dimensions were engineered. Both have the same volume, which is half the volume of the 'square cavity'. The only difference is the alignment of the cavity itself, one has the longer side in the longitudinal direction of tyre rotation, see Figure 4.7b. This cavity shall be referred to as the 'long cavity'. The other cavity has the longer side in the lateral direction of the tyre circumference as shown in Figure 4.7c, this shall be referred to as the 'wide cavity'. Thus, all three types of cavity are linked together volume wise: either half the volume or the same volume with different orientation. This is done to see if the measurement shows any connection between cavity volume and noise generation. Table 4.3 summarises the geometries of the three different rectangular cavities.

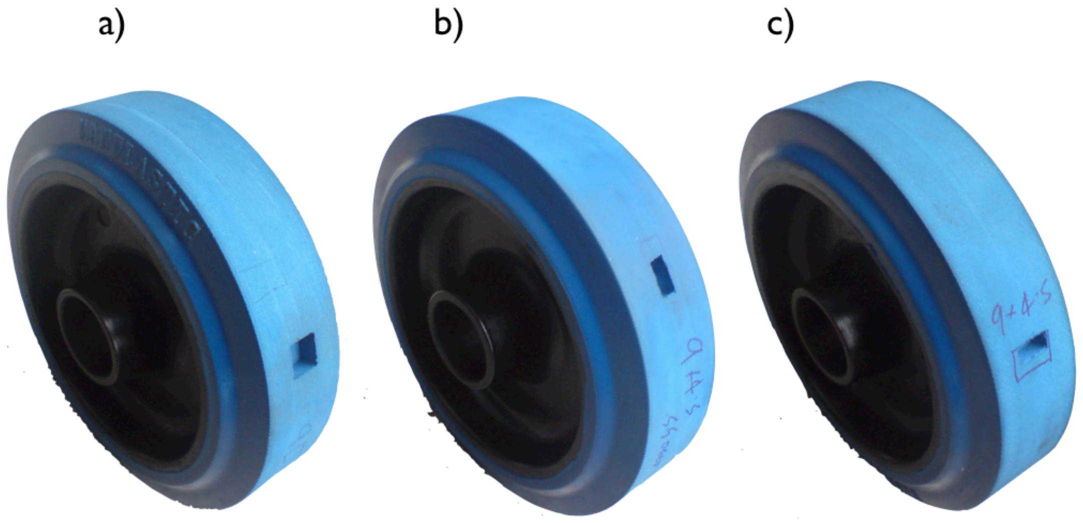

Figure 4.7 Photographs of the tyres with rectangular cavities: a) 'square cavity'; b) 'long cavity'; and c) 'wide cavity'

	Square cavity	Long cavity	Wide cavity
Width W, [mm]	9	4.5	9
Depth D, [mm]	5.5	5.5	5.5
Length L, [mm]	9	9	4.5
Volume V_0, [mm^3]	445.5	222.75	222.75

Table 4.3 Rectangular cavity dimensions for three experimental tyres

The last set of tyres that were used are equipped with a groove in the tread. They are expected to be not that efficient in overall noise radiation but will result in a more realistic acoustical experience in comparison to a real tyre. Figure 4.8 shows photographs of the three tyres with grooves used during the experimental testing. All grooves were cut using a milling machine. Figure 4.8a shows the tyre, which shall be referred to as tyre with the 'square groove'. The second tyre in Figure 4.8b, shall be named the tyre with the 'small groove'. And finally in Figure 4.8c a special kind of groove is introduced, which is chosen to give an idea about the directional behaviour of a tyre tread. This tyre shall be referred to as the tyre with the 'chevron'. Table 4.4 shows the details of the dimensions of the grooves cut into the tyres.

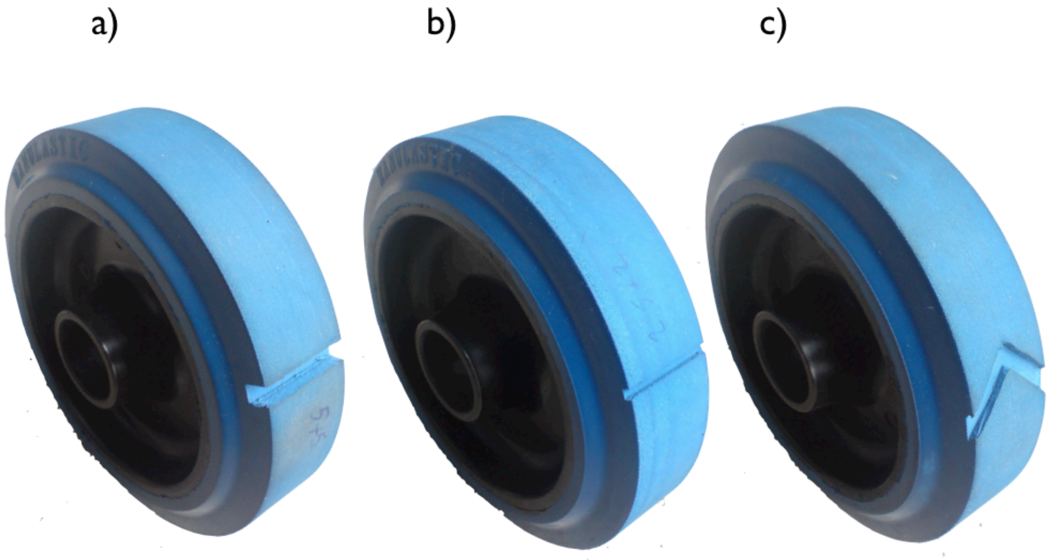

Figure 4.8 Photographs of the tyres equipped with grooves: a) 'square groove'; b) 'small groove'; and c) 'chevron' type of groove

	Square groove	Small groove	Chevron
Width *W*, [mm]	26	26	30
Depth *D*, [mm]	5	2	2
Length *L*, [mm]	5	2.5	5
Volume V_0, [mm^3]	650	130	300

Table 4.4 Groove dimensions for three experimental tyres

4.1.3. Experimental rig

The design of the experimental rig was suggested by an example presented by Graf [Graf, 2002]. However, the load of the tyre for this rig is provided by weights instead of a bolting mechanism. Thus, the real load on the tyre can be estimated via calculation. Figure 4.9 shows a diagram of the rig design. The supporting frame that holds everything in place is drawn in green. The tyre (blue) is mounted In the middle of the rig. It is held in place by the yellow shaft that is running in ball bearings to be as silent as possible. The shaft is designed to accommodate the tyre with a tight fit but still allows a quick and easy exchange of the tyre. To put additional (apart from the frame) load on the tyre, weights can be placed onto the frame at the right hand side, as indicated by the purple disc. The orange plates are the acoustical shielding plates of the chassis dynamometer. To help simulation of an even road surface, the plates should be placed as close as possible to the chassis dynamometer and to the tyre. Rubber bushes at the front fixture of the rig introduce insulation to the plates from the vibrational excitation of the rig and vice versa.

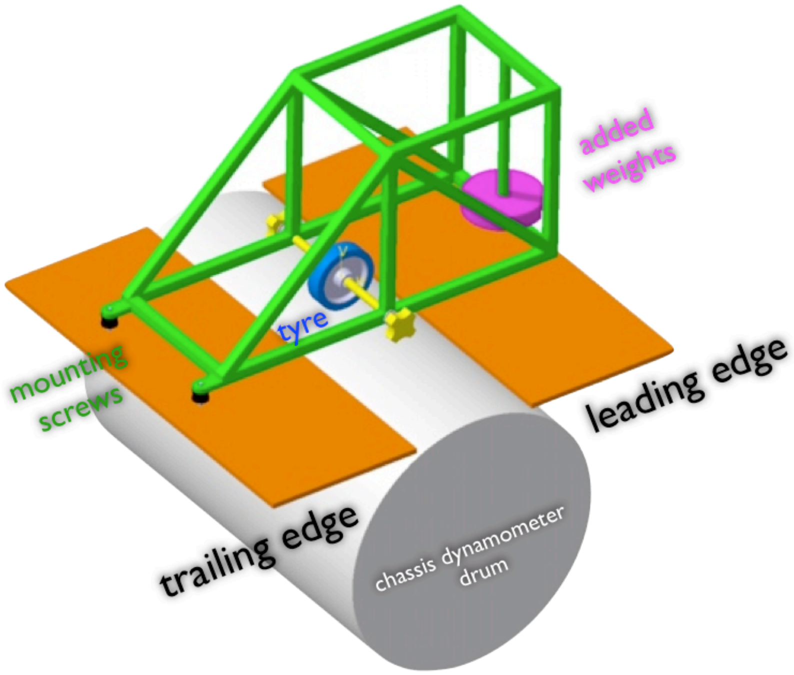

Figure 4.9 Diagram of the experimental rig design with tyre mounted onto the chassis dynamometer drum

A photograph of the rig is displayed in Figure 4.10, including the blue tyre in the centre mounted to the metal frame. The frame itself is about 13.5 kg in weight, additionally there can be extra load applied to the tyre by the weights (up to 20 kg) at the right hand side of the rig. Altogether this leads to a load of approximately 57.6 kg at the roller itself (see Appendix A7). The maximum load the tyre is capable of is 150 kg. The roller turns clockwise from this point of view. Thus, the leading edge of the tyre is at the right hand side and the trailing edge at the left hand side. On the left hand side are the mounting points of the rig that are insulated from the metal plates by two rubber bushes. Furthermore the wooden plate covering the chassis dynamometer drums by leaving only a small section for the roller to run on is shown. This plate is installed to prevent noise radiation generated from the driving mechanism of the chassis dynamometer.

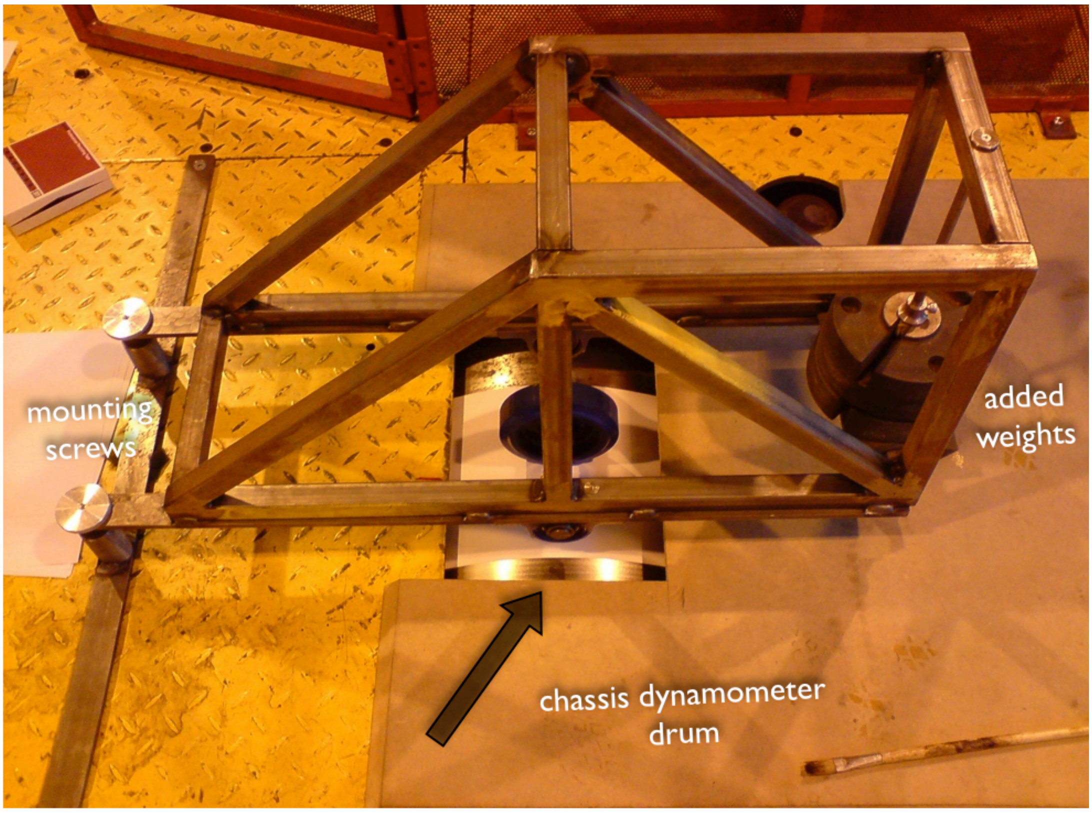

Figure 4.10 Photograph of the original rig layout with tyre, wooden cover and weights in place

4.1.4. Microphone location: directivity pattern measurements

At first directivity pattern measurements of the radial sound radiation around the tyre with the 'large cavity' were conducted in the chassis dynamometer lab. While the tyre was spinning on the chassis dynamometer drum a circular array of seven microphones was placed next to it at a distance of 1000 mm and a height of 200 mm.

The microphones themselves were mounted accurately in a 10 degrees interval onto a wooden support, whose dimension is a quarter circle of a radius of 1000 mm, as shown in Figure 4.11. To capture the whole sound field around the tyre the microphone support needed to be moved and the measurements were repeated at different positions. This movement was done six times to cover a whole circle of 360 degrees around the tyre (with the outer microphones overlapping each time). Sound radiation plots with a resolution of 10 degrees around the whole tyre could be produced with this setup. These plots give an idea about the noise distribution around the tyre. It is expected that the recorded result, however, is contaminated by unwanted noise, generated by the chassis dynamometer and reflections off the walls and ceiling.

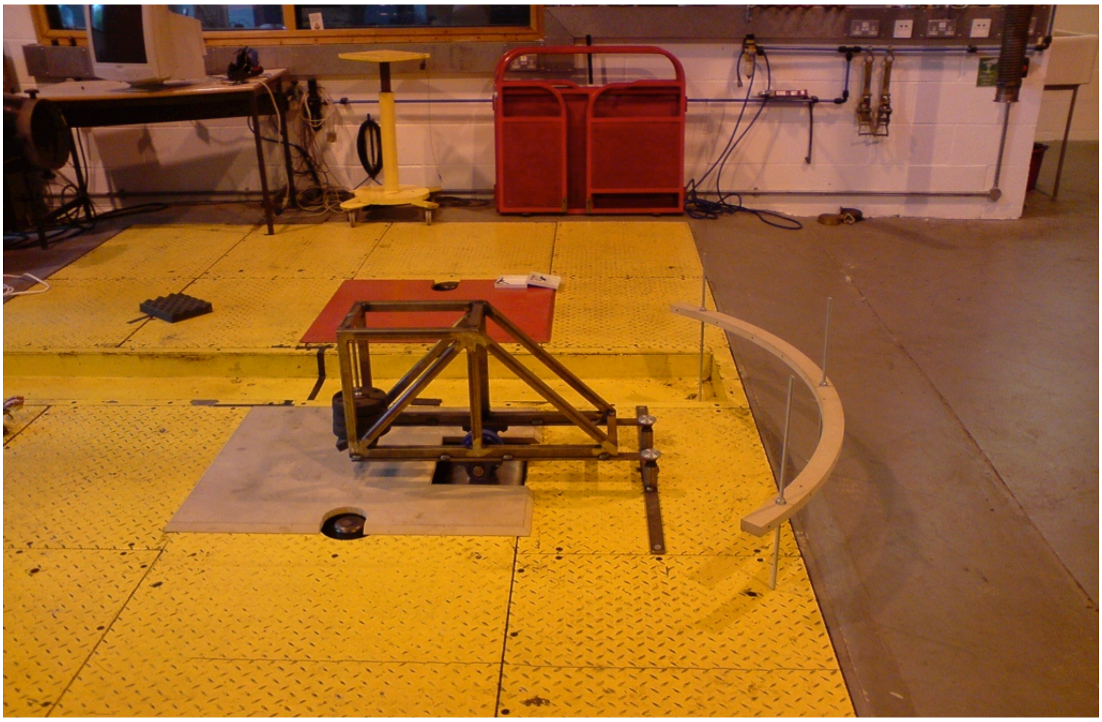

Figure 4.11 Photograph of the sound radiation measurement setup, the wooden microphone support faces the trailing edge

4.1.5. Microphone location: leading and trailing edge recordings

This time only two microphones were used to measure the sound produced by the tyre. They were placed closer to the actual source, the leading and trailing edge of the tyre. Thus, a better signal strength can be obtained and less reflection influences the measurements. To prevent any structural vibration affecting the microphone recordings the microphones should have no physical connection to the vibrating rig that holds the tyre. For the same reason the microphones should not be based on the metal plates covering the chassis dynamometer with its driving mechanism, as it was done at the sound radiation measurements mentioned previously. Thus, it was chosen to configure a microphone support based on the concrete floor. The arrangement of the microphone support is shown in Figure 4.12. A long metal rod was used to bridge the chassis dynamometer. This rod was placed onto metal stands so it could be adjusted to the right height. With this design it was possible to place the microphones very close to the spinning tyre but isolated from ground vibrations. In addition to that the connection cable from the microphones could be guided away from the chassis dynamometer to lower the noise influence due to electric induction.

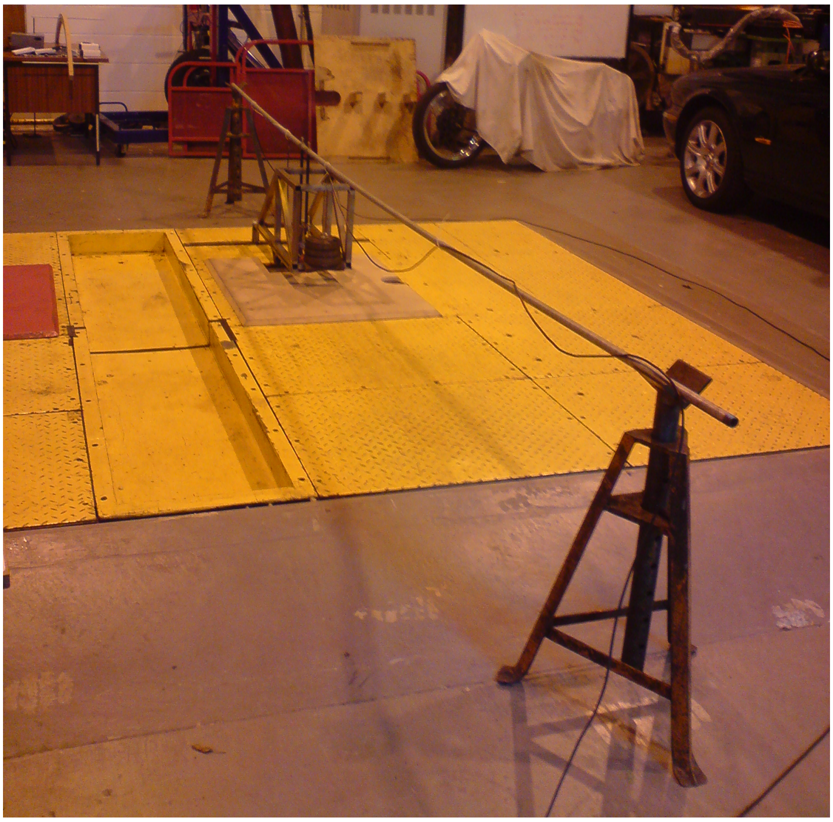

Figure 4.12 Photograph of microphone support isolated from ground vibrations excited by the driving mechanism of the chassis dynamometer

Figure 4.13 shows the freely attached microphones located in close proximity to the tyre, without contacting the frame the tyre is mounted to. So the data could be recorded not more than 40 mm away from the source, in this case the contact patch. This close position guaranteed good signal strength and less influence from reflections of the walls of the reverberant room. However, the microphones were close to the chassis dynamometer as well, so the noise, generated by the rotation of the drum, was recorded as well. In addition to that extra care needed to be taken when the tyre was running, so that the microphones do not contact the tyre or the vibrating metal frame of the tyre support. To make sure that the microphones show the right sign for an analysis a short tap on the microphone was recorded. This tap initiated a positive peak in the recordings. Due to this fact it is assumed that a pressure pulse moving towards the microphone is recorded with a positive sign.

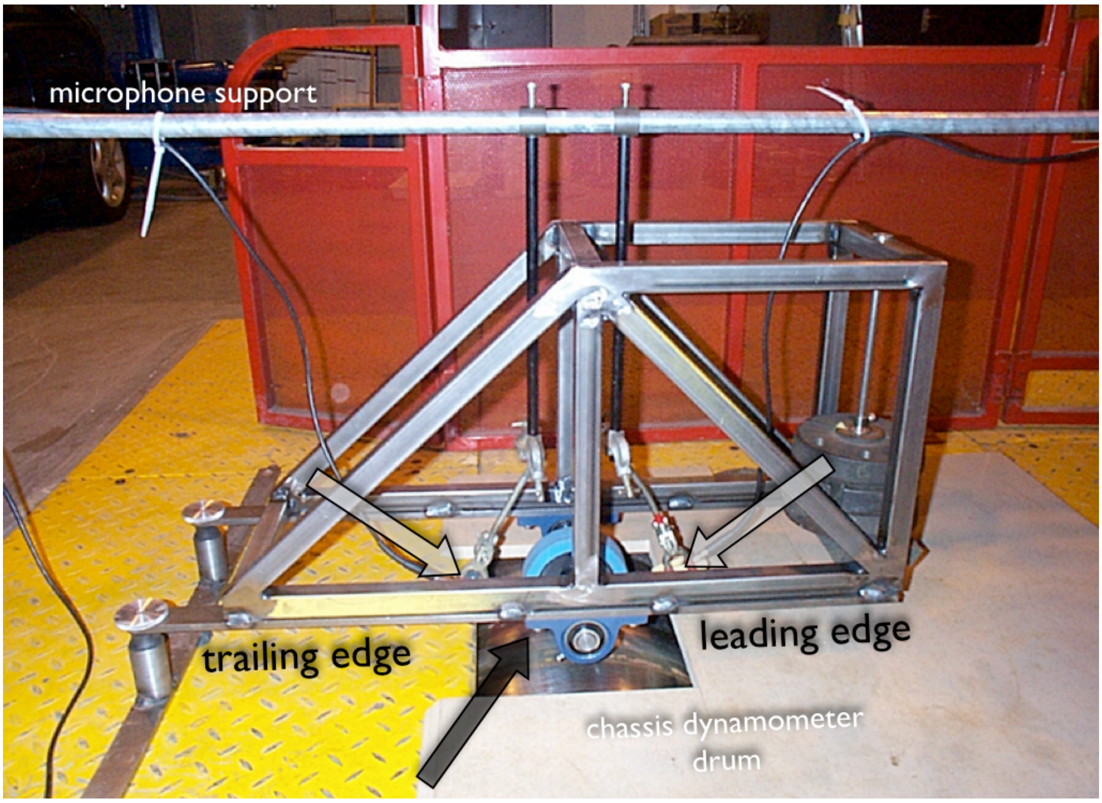

Figure 4.13 Photograph of the experimental rig with the two microphones in place facing the leading and the trailing edges

4.2. Measurement method

4.2.1. Data acquisition

The measured sound was recorded with a real time analyser, called Focus from the company LDS Systems. With this mobile solution it is possible to record up to eight channels in the time domain while doing a simultaneous frequency analysis. However, after some initial investigations it was decided to record the time history only and post process it later in MATLAB. Thus, the maximum sampling frequency of the system of 96000 Hertz could be utilised. This high sampling rate gave sufficient time resolution to analyse the data recorded at the leading and trailing edge of the tyre in detail. According to Gagen [Gagen, 2000], the air effects occurring around a tyre are considered to be of a very quick nature, this makes a high sampling rate a necessity.

The duration of the recording time of each signal is two seconds. This short interval was chosen to keep the recorded file within a reasonable size to make it possible to post process in MATLAB. Despite the short interval of two seconds the recording still gives a sufficient time history for interpretation. In combination with the high sampling rate used 192000 data points for each signal were created. With the chosen dynamometer speeds of 19, 31 and 41 km/h the signal contains from 27 cavity repetition events, for the lowest speed up to 60 cavity repetition events for the high. This gives a sufficient number of events, for all speeds, to take satisfactory average values, for all the different tyres. For the tyre equipped with the ‘small cavity’ the dynamometer speed was even increased to 91 km/h to investigate into a possible difference in the process happening. For real traffic conditions, 41 km/h is a low speed. However for these experiments a trade off had to be made between the background noise (generated by the chassis dynamometer) and tyre noise of interest. Whilst running at high speeds the chassis dynamometer produces too much noise.

4.2.2. Bandpass filters

In the previous section it is mentioned and shown that the chassis dynamometer driving mechanisms generates a lot of unwanted noise. This noise was recorded by the microphones as well as the sound generated by the spinning tyre. As shown the low frequency region is dominated by the chassis dynamometer noise. To get an idea of the magnitude of influence and to find a solution, measurements were conducted at first with the 'smooth tyre' running on the chassis dynamometer. The results were then compared to the signal produced by the other tyres. With this comparison the pure signal generated by the altered tyre could be identified and so a filtering process could be introduced to the whole signal. The filtering is applied to the time recording because the emphasis is on the shape of the signal in the time domain generated at the leading and trailing edge of the tyre.

To find out the frequencies involved in the process, the signal is converted into the frequency domain after recording. Figure 4.14 shows the Fast Fourier Transform (FFT) of two recorded time histories at the trailing edge of the tyre in comparison to the time history of the 'smooth tyre'. In Figure 4.14a the 'smooth tyre' and the tyre with the 'small cavity' are compared. In Figure 4.14b the 'smooth tyre' is compared to the tyre with the 'large cavity'. The dynamometer speed for both measurements was 41 km/h. The low dominant frequencies are similar for all types of tyres; Especially the frequencies below 4000 Hertz for the tyre with the 'small cavity' and below 2000 Hertz for the tyre with the 'large cavity'. Frequencies above 20000 Hertz are also similar for the 'smooth tyre' and the tyres with a cavity. Thus, a bandpass filter was applied to the signal.

With a second order Butterworth bandpass filter the time history could be changed and the unwanted frequencies that influenced the identification process could be minimized. The higher the order of the Butterworth filter the sharper the filter behaviour [Kuo, 1966]. For the measurements recorded the phase of the filter should still show a linear behaviour, because the frequencies of the time history should not be changed. Therefore, the low filter order of two is a good compromise. The chosen options for the filter in accordance to Figure 4.14 are shown in Table 4.5 overleaf. Two different filters were applied to the signals of the two different types of cavities. However, the only difference was the lower frequency boundary, where 1440 Hertz was used for the 'large cavity'. This lower frequency limit was also used for the other tyres. Only for the tyre equipped with the 'small cavity' the lower frequency boundary was chosen slightly higher, with 2400 Hertz. Those filters were applied to all the measured signals and resulted in a satisfactory time signal of the processed data. The implementation of the filter was done with the software MATLAB after the measurements have been conducted.

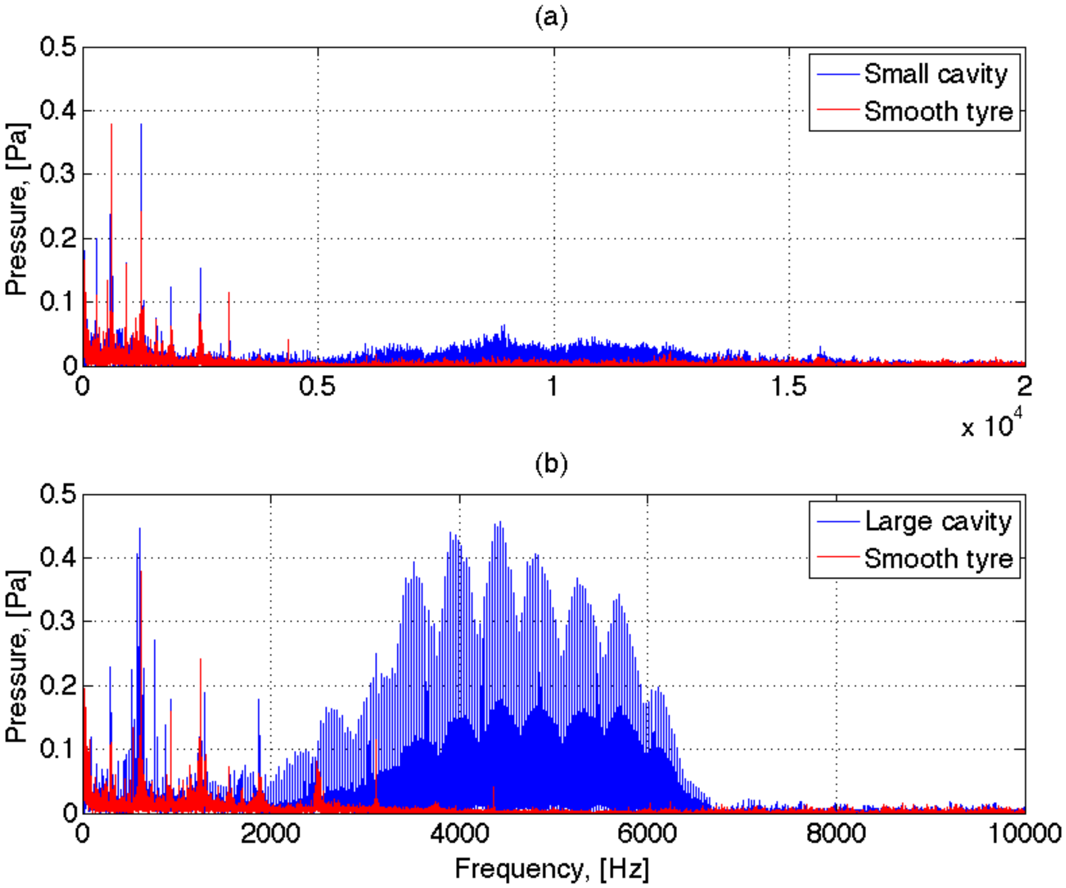

Figure 4.14 FFT of the two seconds time history signal from the 'smooth tyre' (red) running on the chassis dynamometer in comparison with the signal generated by the tyre with the: a) 'small cavity; and b) 'large cavity'

Tyre tread	Bandpass filter type	Order	Lower cut-off frequency [Hertz]	Higher cut-off frequency [Hertz]
Large cavity	Butterworth	2nd	1440	24000
Small cavity	Butterworth	2nd	2400	24000

Table 4.5 Bandpass filter options

4.2.3. Spline interpolation

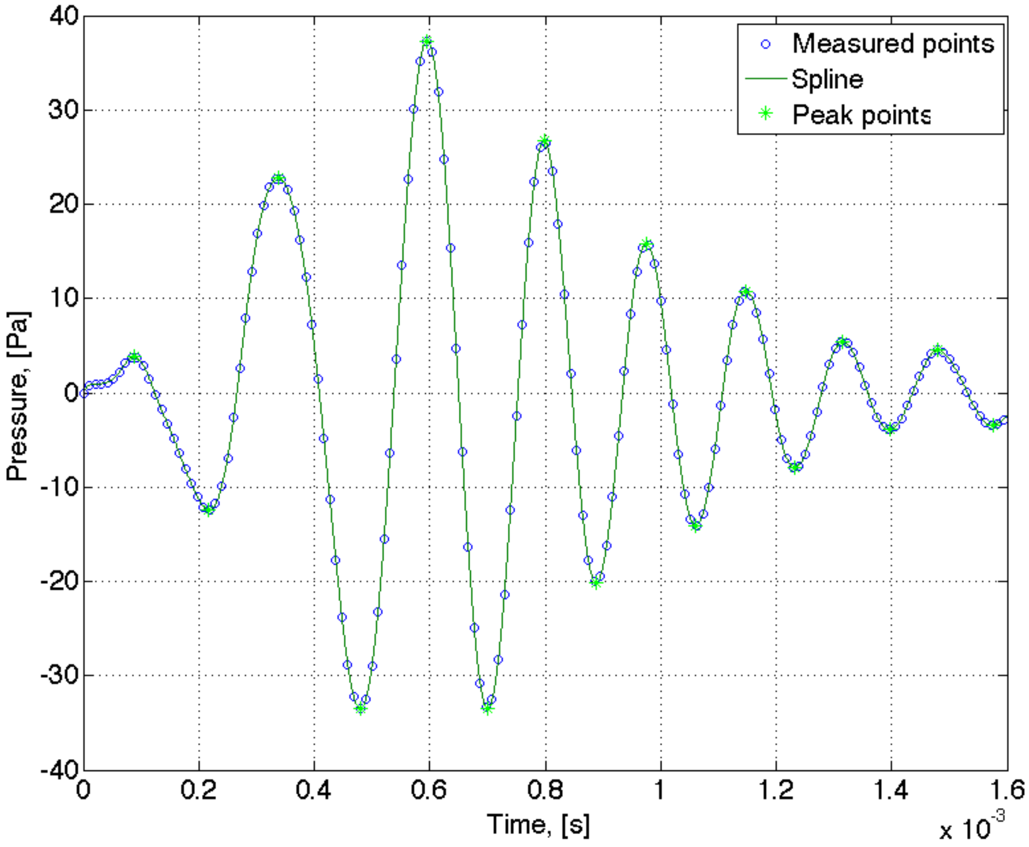

Figure 4.15 Spline interpolation applied in between measured points of an example signal, to produce more accurate peaks and troughs

In addition to the bandpass filtering a second data conditioning process is introduced. The frequency resolution of a signal can be improved by a mathematical approximation in between the measured data points. This yields an even smoother shape of the signal. It is found that by applying a spline interpolation to the signal these demands effects are best met. The spline interpolation is a piecewise polynomial interpolation, which is very flexible and quick to use. With the processing software MATLAB the spline interpolation can be applied to the measurement recordings after the bandpass filter is implemented. Figure 4.15 shows an example of the application of a spline function to the time history recoding of an event at the trailing edge of the tyre. The blue circles demonstrate the points actually measured. The spline function is shown as the green solid line connecting the points in a smooth way. Thus, to estimate the maximum amplitude of the peaks and troughs in the measured signal the maxima of the spline interpolated signal are used instead. As can be seen in Figure 4.15 those points marked with stars give slight different amplitudes in comparison to the blue circular markings from the measurement.

4.2.4. Hilbert transform

The signal shown in Figure 4.15 shows a frequency modulation and changing amplitude behaviour at the same time. Shown before is the Fast Fourier Transform to get the frequencies occurring in the whole signal. When the frequency that occurs at a certain point in time is wanted, the Fast Fourier Transform is of no use. Therefore another transform is used: the Hilbert transform. The main difference between the Fast Fourier Transform and the Hilbert Transform is that the latter is a local descriptor of the signal, instead of a global one [Sun, Sclabassi, 1993]. Thus, the Hilbert transform gives an idea of the instantaneous frequency of the signal at a given time. This is used in this Thesis to identify the frequencies in a signal. Figure 4.16 shows the Hilbert transform of the example signal introduced in Figure 4.15. It can be seen that it is the same time span as on the figure before but the y-axis is now frequency instead of amplitude.

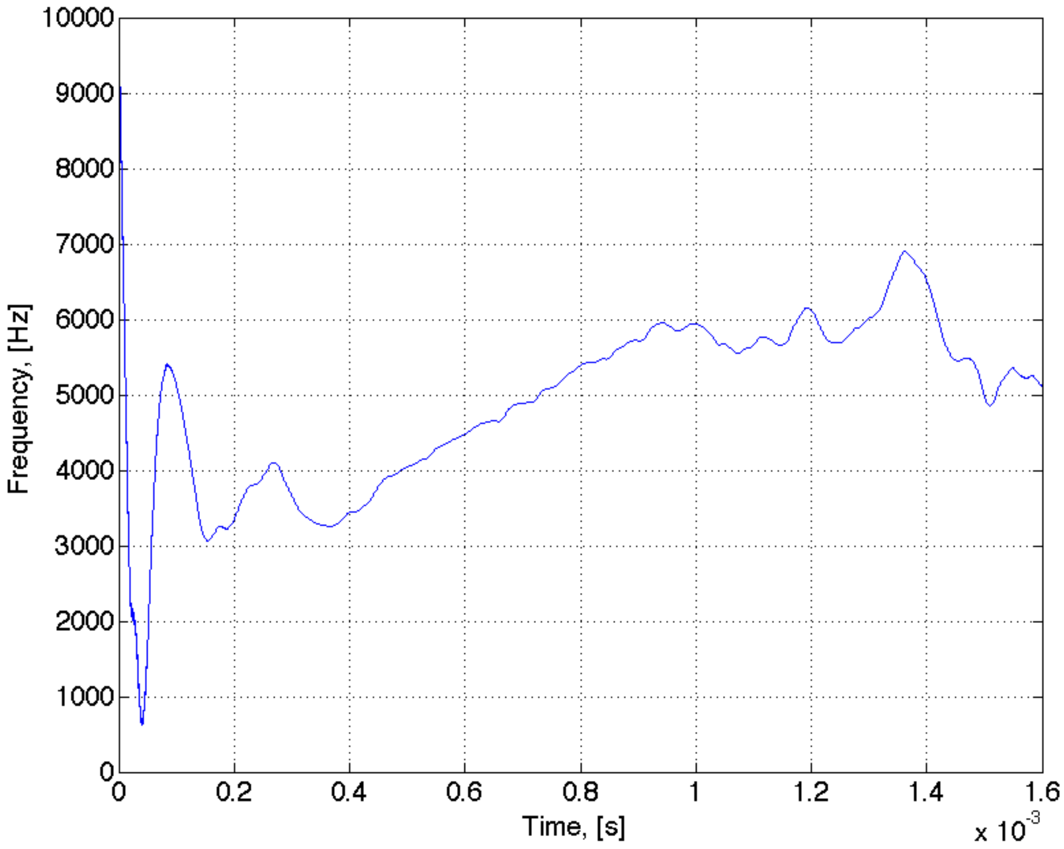

Figure 4.16 Hilbert transform of the example signal from Figure 4.15

4.3. Discussion and summary

The measurement setup is introduced and explained in this section of the Thesis. The room where the chassis dynamometer is located at Loughborough University is not equipped with anechoic termination. Thus, the acoustic measurements conducted are influenced by reflections of the walls and ceiling in this room. Especially the sound radiation measurements suffer from these reflections as shown later on. Moving the microphones closer to the source, the leading and trailing edge of the tyre, can reduce the influence of the reflections.

Another problem is the unwanted noise generated by the chassis dynamometer that is also recorded by the microphones close to the tyre. Applying a second order Butterworth bandpass filter to the time history of the recordings reduces the effects of background noise on the measurements. This however does not completely remove the noise without having an influence on the signal of interest. The measured data is further conditioned by a mathematical spline interpolation to improve the resolution and so the shape of the signal. It needs to be mentioned that the used filter did not change the characteristics of the signal. Hence, interpretation of the filtered signal is still related to the recorded unfiltered signal.

The tyres needed modification before they could be used for the experiments. This can introduce some inaccuracy in geometry between the different tyres. In addition to that, there were slight problems with cutting the holes and grooves into the tyre due to the soft rubber material of the tyre tread. Those two issues can be an indication for variations between the models and measurements described later on in this Thesis.

Chapter 5

Results and discussion: leading edge

The measurement results shown in the next chapters are divided into the different tyre types used and split regarding the microphone position. First of all the results of the sound radiation measurements are presented. They were conducted with the tyre equipped with the ‘large cavity’ to give a general idea of the sound field around a tyre with a cavity.

In the following section the emphasis is on the sound generation of the leading edge of the rotating tyre. The results of the circular cavities and of the tyres with the rectangular cavities, introduced in Chapter 4, are presented. It is aimed to get a better understanding of the process happening at the leading edge when the cavity hits the road surface. In addition to that the measured results are compared against the before introduced models from Chapter 3 for the leading edge signal of a tyre.

5.1. Directivity pattern measurements

For the directivity pattern measurements seven microphones were used at a time to measure the sound field around the tyre with the ‘large cavity’, running on the chassis dynamometer at 41 km/h. The measured time history data is post processed within MATLAB, this means it is filtered and transformed into the frequency domain. This transformation is done to get an idea where in respect to the tyre and at what frequencies the highest noise levels occurred. Figure 5.1 shows a three-dimensional plot of the Fast Fourier Transform of the time signals 360 degrees around the tyre. Only the frequencies in between 2000 Hertz and 10000 Hertz are shown because the lower frequencies are generated by the chassis dynamometer and so not of interest for the noise source: tyre. There are no dominant components in the frequencies higher than 10000 Hertz so these are cut off as well.

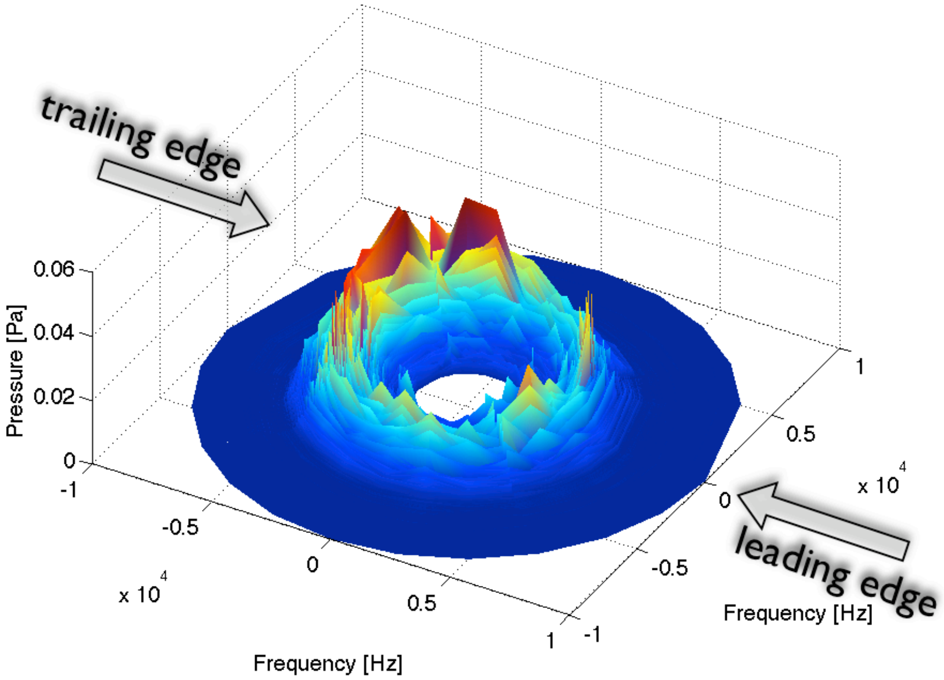

Figure 5.1 Circular diagram of the frequency content of the sound radiation measurements at 36 locations around the spinning tyre equipped with the ‘large cavity’ running at 41 km/h

On the left hand side of Figure 5.1 indicated by the arrow is the trailing edge of the tyre and on the right hand side the leading edge, respectively. There is one Fast Fourier Transform plotted for every 10 degrees of the 360 degrees circle around the tyre. The plot starts at 2000 Hertz in the centre of the circle, the frequency increases with larger radius. The data in between the measured lines of 10 degrees is interpolated by the software MATLAB. As shown: the main sound is generated at the trailing edge of the tyre. In this direction there are significant red peaks. However, there is also sound generated at the side and at the leading edge of the tyre. The main problem of the measurement was that there were reflections from the walls, floor and ceiling that influenced the recordings. This noise explains the high peak at the top of Figure 5.1 that is at the side of the tyre, where the closest wall was located.

The next figures show more detailed sound radiation profiles. In Figure 5.1 all the frequencies and amplitudes are displayed in a three-dimensional plot, whereas in the next figures the sound radiation at just one frequency is shown with its amplitude around the tyre, generating a two-dimensional plot. This layout makes it easier to identify the actual directivity but it is for one certain frequency only. In the first example the frequency 6256 Hertz is chosen. The plot is a top view of the rig where the trailing edge of the tyre is pointing to the left hand side from the centre of Figure 5.2, and the leading edge points to the right hand side from the centre of the figure. For this rather high frequency in respect to tyre noise the sound radiation to the sides are dominant. However, as shown there is only little sound radiation at the leading edge, as already indicated by Figure 5.1.

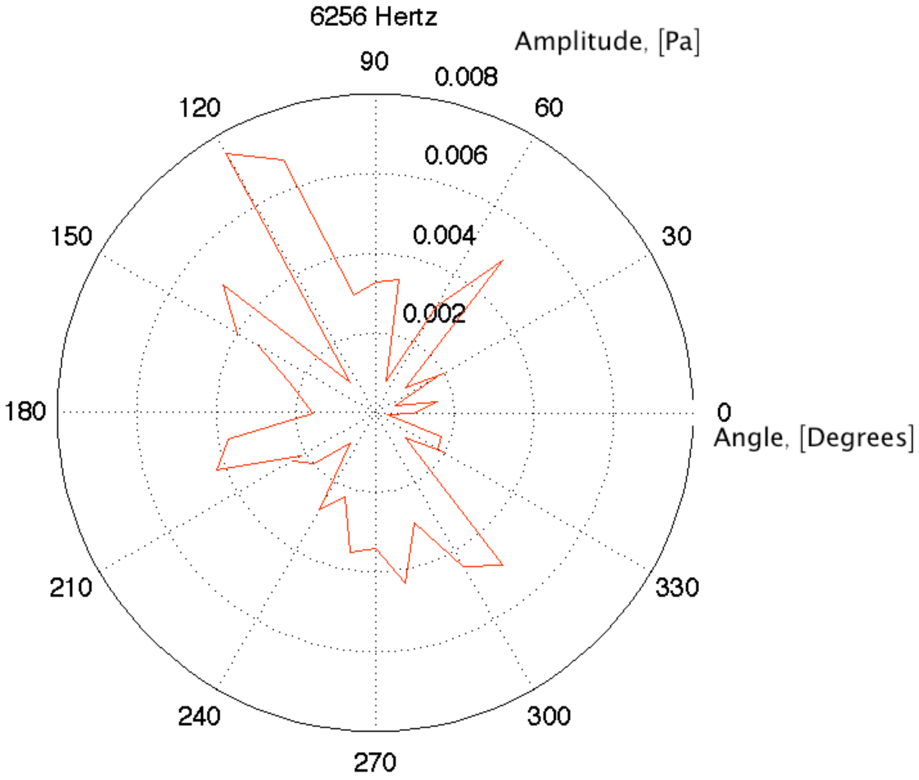

Figure 5.2 Sound radiation, at a frequency of 6256 Hertz, of tyre equipped with the 'large cavity' running on the chassis dynamometer

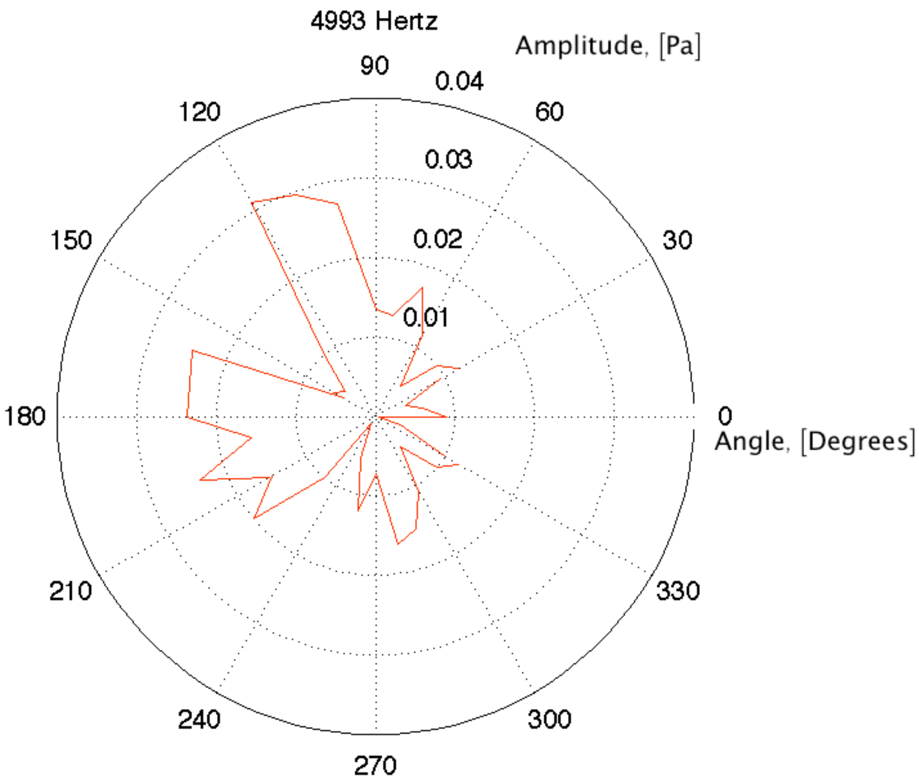

Figure 5.3 Sound radiation, at a frequency of 4993 Hertz, of tyre equipped with the 'large cavity' running on the chassis dynamometer

The next plots show a similar behaviour. Both have a rather weak signal at the right hand side of the plot, the leading edge, and both have noise influence. Especially in Figure 5.3 at the top, a very high peak is shown at one side of the tyre that cannot be found at the other side. Ideally a mirror effect with both sides showing equal amplitudes would be expected. This mirror effect is apparent in Figure 5.4, where the top and bottom of the plot are identical. Again the signal at the leading edge is rather low.

It has been clearly shown that the main noise source was the rear of the tyre. However, there were big noise influences caused by the reflections within the room. The microphones were tested beforehand with a speaker in an anechoic environment; this provided much better results of the recorded sound field, the results of that can be found in the Appendices in section A4. In the room where the chassis dynamometer is located that has no anechoic termination the signals in the far field are significantly influenced by noise, results of an experiment in there with the same microphones located around a speaker are embedded in the appendices in section A5.

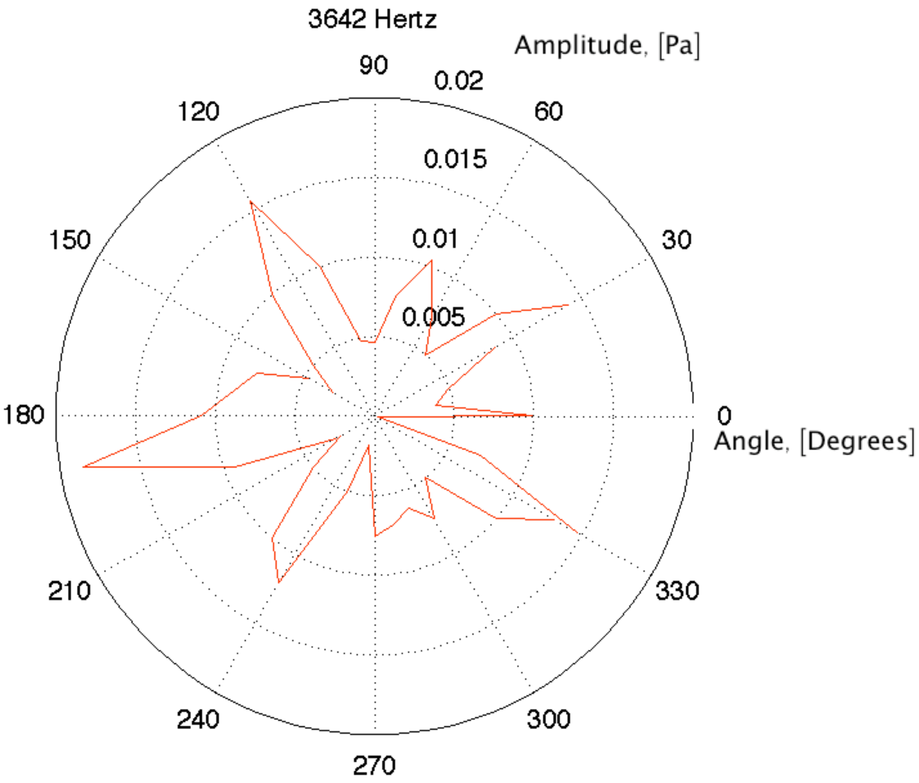

Figure 5.4 Sound radiation, at a frequency of 3642 Hertz, of tyre equipped with the ‘large cavity’ running on the chassis dynamometer

To analyse the pure signal, generated by the tyre, the microphones were located in the vicinity of the contact patch very near to the actual source. Only two microphones of better quality were used to record the process at the leading and at the trailing edge simultaneously. This would give further clarification about the signal structure at both sides of the tyre that is described in detail in the next chapters.

5.2. Circular cylindrical cavities

In Chapter 4 two different types of cylindrical cavities used in a tyre during this project, are introduced: the ‘large cavity’ and the ‘small cavity’. The size difference of both of them is significant. Thus, it is expected to get a difference in noise generation between the tyre with the ‘large cavity’ and the one with the ‘small cavity’ at the leading edge. First of all the ‘large cavity’ is analysed regarding the noise generation at the leading edge.

5.2.1. Large cavity

Figure 5.5 shows a top view of the tyre with the ‘large cavity’. The cylindrical hole is large in comparison to the tyre itself and with a volume of 350 mm^3 similar from the size point of view, to a real tyre tread. The first signal to be inspected is the leading edge signal of the tyre with the ‘large cavity’. The time history was recorded at three different speeds and afterwards filtered in MATLAB with a Butterworth bandpass filter as explained in Chapter 4.

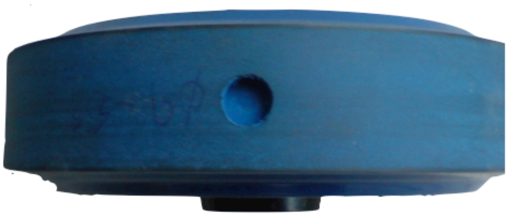

Figure 5.5 Photograph of top view of the tyre equipped with the ‘large cavity’

In Figure 5.6 the recorded leading edge time history of this tyre running at a speed of 41 km/h is shown. At the top (Figure 5.6a) the pure unfiltered signal is presented over the interval of two seconds. Some peaks related to the event at the leading edge when the cavity contacts the chassis dynamometer drum can already be identified. However, there is a lot of noise as indicated by the oscillations around the centreline of the plot. To minimize this noise the 2nd order bandpass Butterworth filter is applied to the signal, with the details according to Table 4.5. The bandpass filtered signal is shown in Figure 5.6b. The noise around the centreline is clearly reduced and the reoccurring events at the leading edge are clearly dominant now. The distance of the events is depended on the rotational speed of the tyre and is referred to frequency of reoccurrence. The maximum amplitude of the peaks is slightly different in comparison to the ones of the unfiltered signal. It has to be mentioned though that the amplitudes of the peaks, when compared to each other, show a large fluctuation over the short recording duration of two seconds. This behaviour is analysed later on, it was already mentioned by Ronneberger [Ronneberger, 1984] that the peak at the leading edge is more inconsistent than the one generated at the trailing edge of the tyre. Therefore, an average value of the amplitude will be taken for which the number of peaks available should be sufficient.

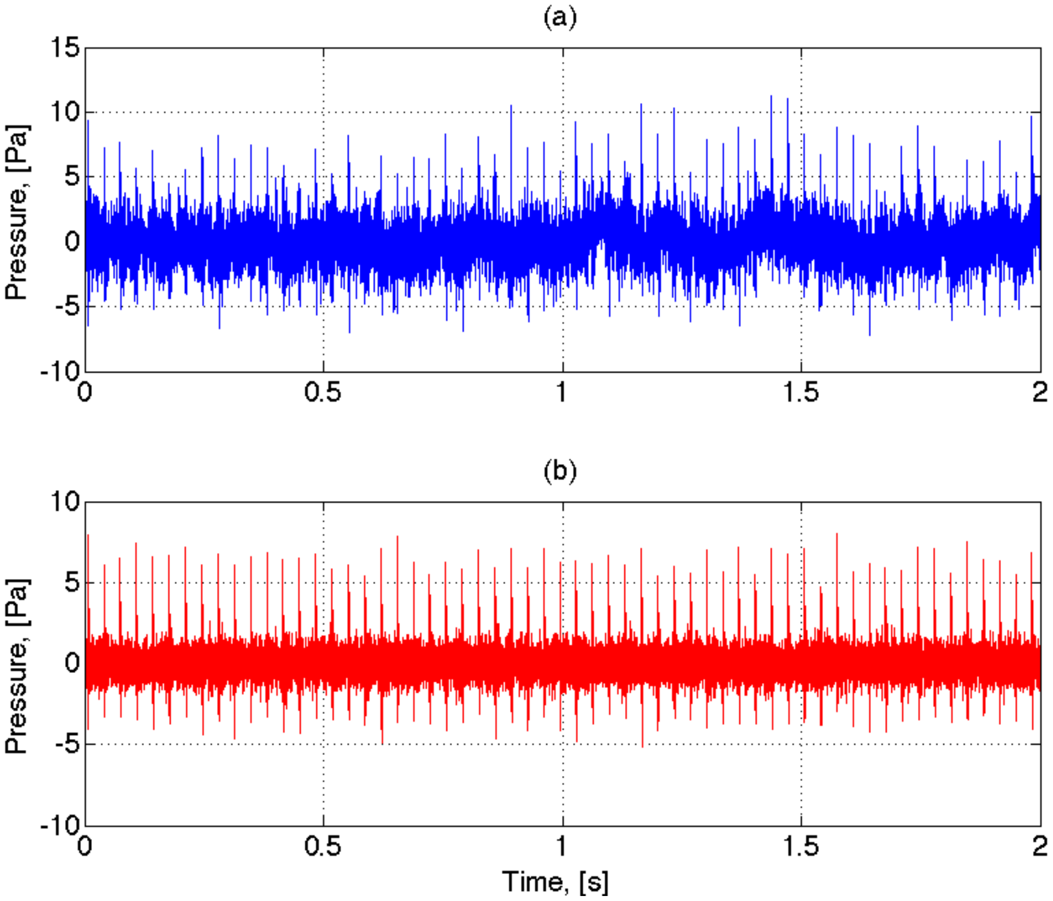

Figure 5.6 Time history of the leading edge signal from the tyre with the 'large cavity' at 41km/h: (a) unfiltered signal; and (b) bandpass filtered signal

At next, the time histories of the different rotational speeds are compared to each other. A lower overall sound radiation, hence lower peak amplitudes are expected with lower tyre speed. In Figure 5.7 the signals of the three different speeds are shown. The lowest speed of 19 km/h is plotted at the top, in the middle the signal of the speed of 31 km/h is shown and at the bottom the 41 km/h signal, already introduced in Figure 5.6, is repeated for comparison.

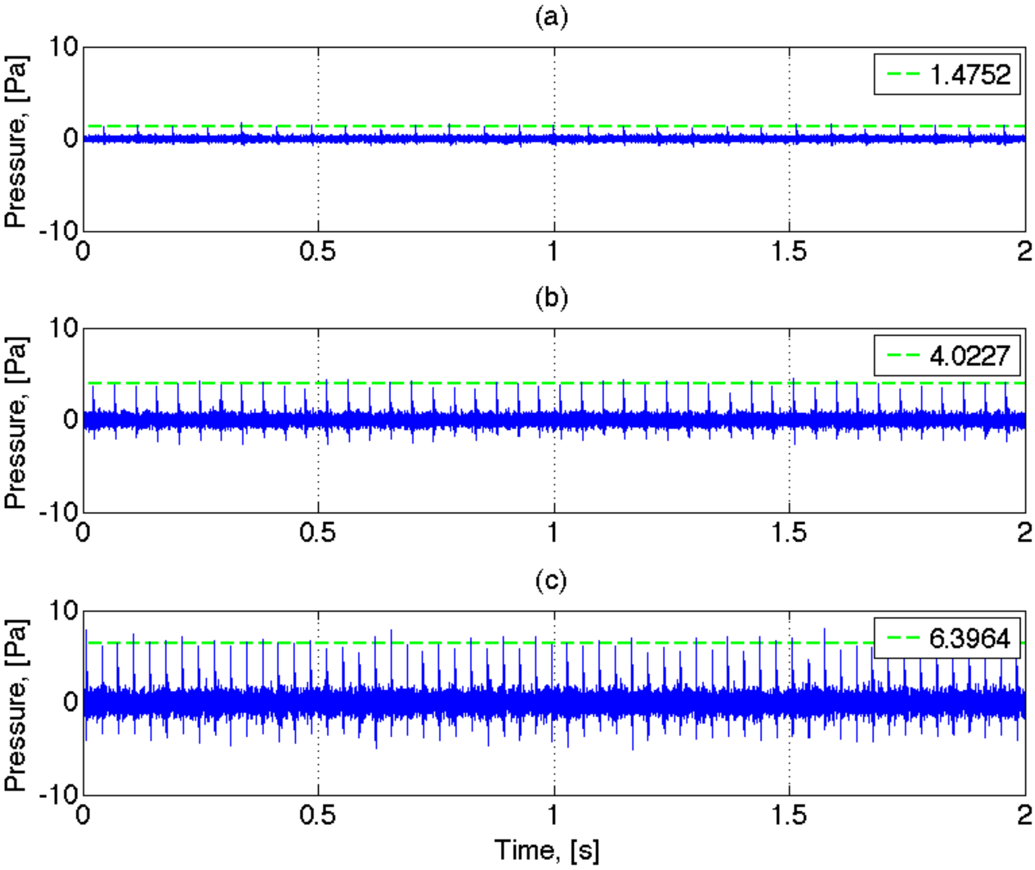

Figure 5.7 Time history of the leading edge signal from the tyre with the 'large cavity' for different speeds including average peak level: (a) 19 km/h; (b) 31 km/h; and (c) 41 km/h

The same bandpass filter is applied to all signals and it is clearly shown that the background noise of the chassis dynamometer driving mechanisms does increase significantly with speed. The repetition frequency of the event at the leading edge does also increase with speed. Thus, the number of peaks in the constant time interval of two seconds reaches from 27 for the lowest speed, until 60 for the highest tyre speed. Furthermore, a dashed green line is added to each plot indicating the average peak amplitude in the two seconds recording for each tyre speed.

	19 km/h	31 km/h	41 km/h
Number of peaks	27	44	60
Average value [Pa]	**1.475**	**4.023**	**6.396**

Table 5.1 Number and average amplitude values of peaks taken from **Figure 5.7** of the leading edge signal of the tyre with the 'large cavity'

Table 5.1 summarises the average peak amplitude values taken from Figure 5.7. It is found that there is a proportional behaviour between average peak amplitude and tyre speed. However, the behaviour is not linear between the amplitudes for two speeds, as when for instance the value of 19 km/h (1.4752 Pa) is compared to 41 km/h (6.3964 Pa). But a quadratic relationship can be identified: the amplitudes in Pascal are dependent on the squared velocity of the tyre. This result is confirmed by the speed exponent v_{exp} introduced by Kuijpers and van Blokland [Kuijpers and van Blokland, 2001] as mentioned in Chapter 2. These authors refer to a speed exponent of four for the sound pressure level difference of the air pumping process at different tyre speeds as it was initially suggested by Hayden [Hayden, 1971].

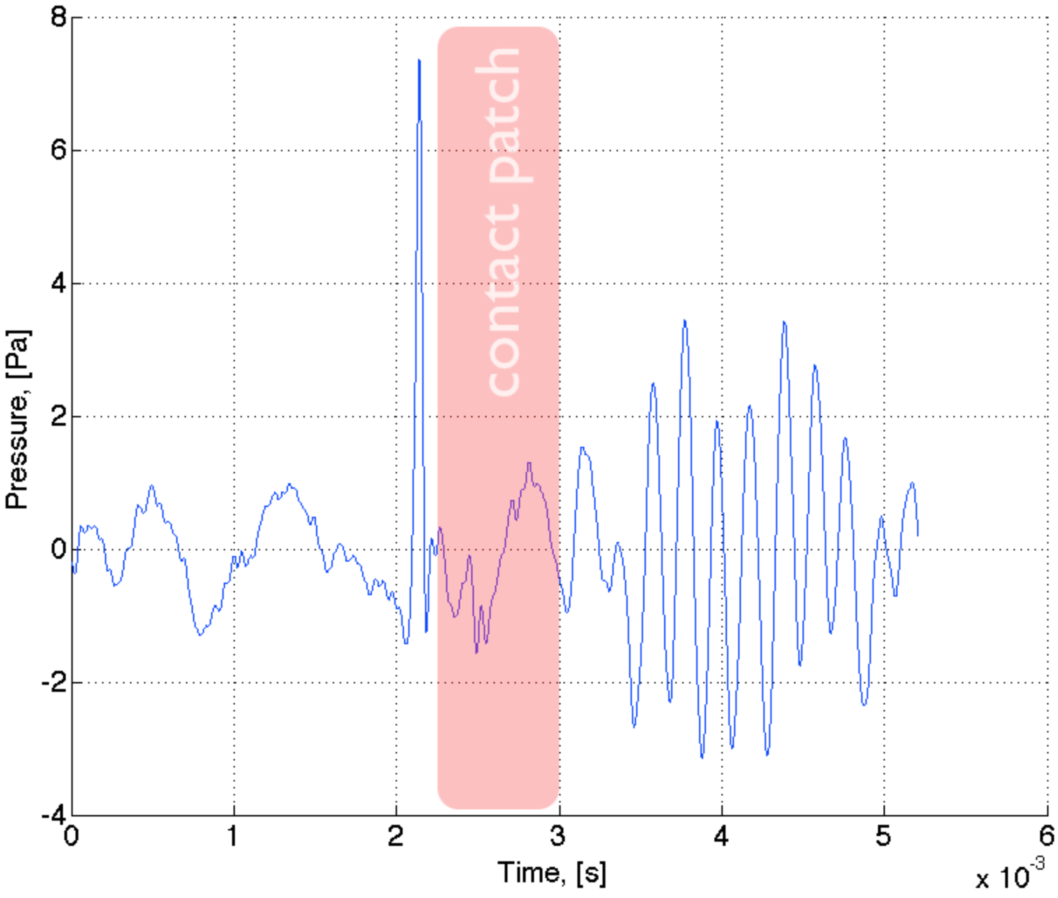

Figure 5.8 Example leading edge signal event of the 'large cavity' contacting the chassis dynamometer drum at 41 km/h, with assumed contact patch area

For a better understanding of the process happening at the leading edge a single event is analysed. Therefore, the highest tyre speed recordings are chosen from Figure 5.7c, this results in the highest amplitude and so the clearest process. In Figure 5.8 an example event of the cavity contacting the chassis dynamometer drum is shown. A sharp peak is shown (at $2.1*10^{-3}$ s) that is identified to be the process happening at the leading edge of the tyre. When the cavity is fully covered little aerodynamic sound is emitted, the red area in the middle of Figure 5.8 marks this assumed phase that lasts about $0.7*10^{-3}$ s. This approximation is in accordance with a contact patch length of 17.5 mm (measurement see Appendix 6). After that, oscillations are initiated produced at the trailing edge of the tyre that is analysed in detail in Chapter 7. As mentioned before, the main noise source is the trailing edge, so it could be possible that the microphone at the leading edge also picks up this signal.

The leading edge signal was also analysed by other authors for instance by Samuels [Samuels, 1979], by Plotkin et al. [Plotkin, 1979] and by Ronneberger [Ronneberger, 1984], they used pockets or grooves in a tyre. Or by Hamet et al. [Hamet, 1990], who used a cylindrical cavity in the road. Except Ronneberger, who tried to develop his own model based on a roughness element on the road, the other Authors always aimed to explain the signal at the leading edge with the monopole theory that was initiated by Hayden [Hayden, 1971]. Here the same approach is used to see if it also applies to results obtained in the experiments.

First of all however the signal is checked to find a reason for such diversity in maximum amplitude of the peak itself. Therefore some of the dominant peaks are compared to the minor ones. This is initially done for the highest speed of 41 km/h. The spline interpolation introduced in Chapter 3 is used to connect the measured points with each other, to generate a smooth signal with higher resolution. As shown in the four sections in Figure 5.9 the peak amplitudes differ significantly: they range from 5.5 Pa up to 7.4 Pa for the highest. However, the peak to trough distance, marked by the red lines is similar for all the examples shown.

Table 5.2 presents the exact values of the example peak amplitudes from Figure 5.9. By comparing the difference between each maximum and minimum value a rather constant range is achieved that leads to an average difference value of 8.078 Pa for the four example readings at the leading edge signal of the tyre running at 41 km/h. When unwanted noise is added from the chassis dynamometer the signal produced by the tyre is prone to be influenced in a significant way. Thus, resulting in high amplitude fluctuations. Even with the applied bandpass filter the fluctuations are still apparent. However, by looking at the whole pulse (oscillation) a satisfactory average value of the amplitude can be found.

	(a)	(b)	(c)	(d)
Peak, [Pa]	7.364	5.511	6.292	6.644
Bottom, [Pa]	-1.248	-1.893	-1.897	-1.463
Difference, [Pa]	8.612	7.404	8.189	8.107
Average, [Pa]		**8.078**		

Table 5.2 Peak value calculation for the leading edge signal of the tyre with the 'large cavity' at 41 km/h

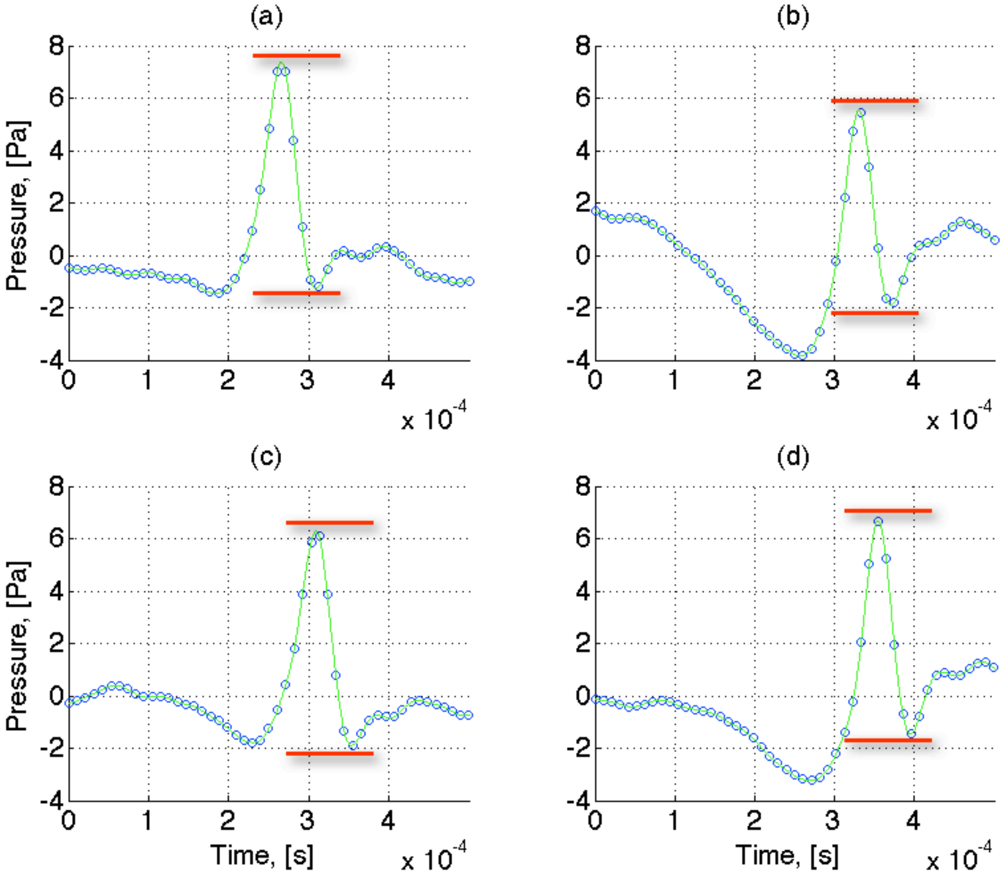

Figure 5.9 Four different example peaks of the leading edge signal at a tyre speed of 41 km/h generated by the 'large cavity'

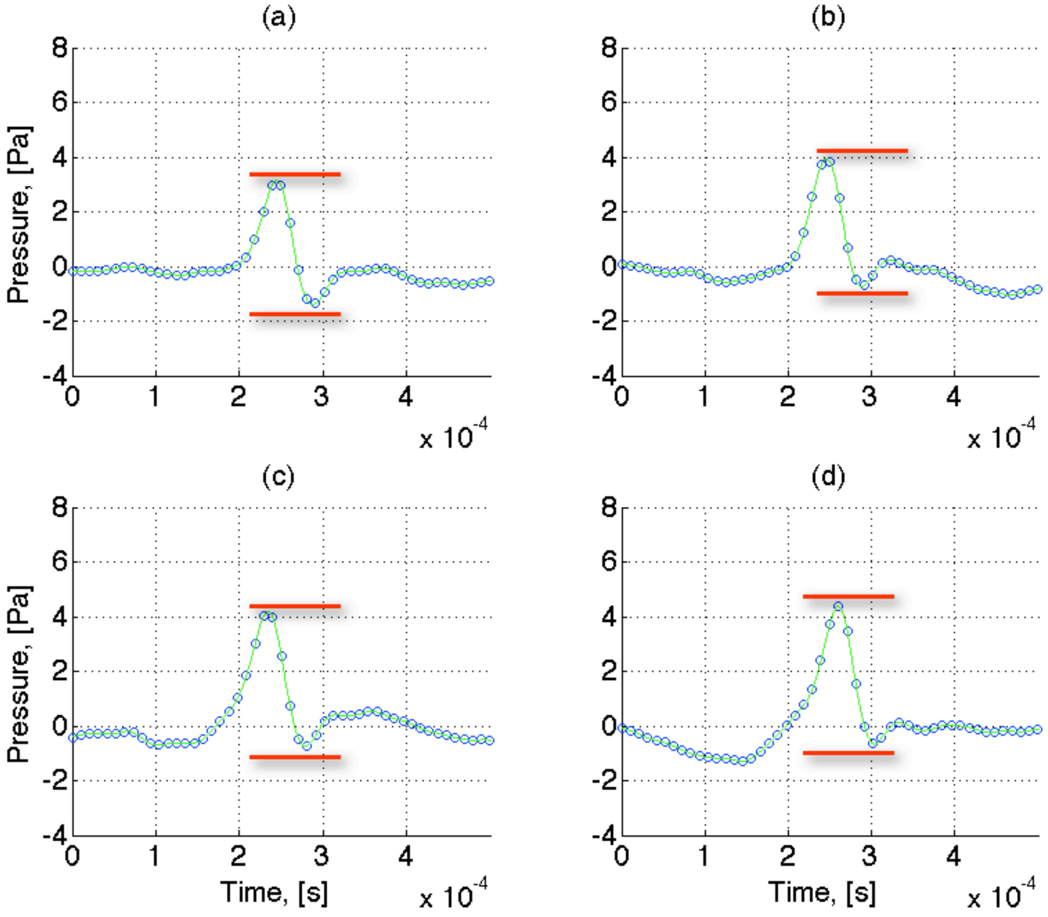

Figure 5.10 Four different example peaks of the leading edge signal at a tyre speed of 31 km/h generated by the ‘large cavity’

	(a)	(b)	(c)	(d)
Peak, [Pa]	3.152	3.930	4.181	4.350
Bottom, [Pa]	-1.391	-0.731	-0.740	-0.660
Difference, [Pa]	4.543	4.661	4.921	5.010
Average, [Pa]	**4.784**			

Table 5.3 Peak value calculation for the leading edge signal of the tyre with the ‘large cavity’ at 31 km/h

The same analysis is conducted for the measured signal of the lower speeds of 31 km/h and 19 km/h. The amplitudes for the peaks generated by the spline interpolation, at 31 km/h, taken from Figure 5.10 are shown in Table 5.3. The maximum peak amplitudes this time reach from 3.152 Pa to up to 4.181 Pa. Again the difference to the bottom value of each peak is measured as indicated by the red lines in Figure 5.10. Finally the average pressure difference is calculated that results in 4.697 Pa, again this is slightly higher than the one calculated for the whole signal in Figure 5.7.

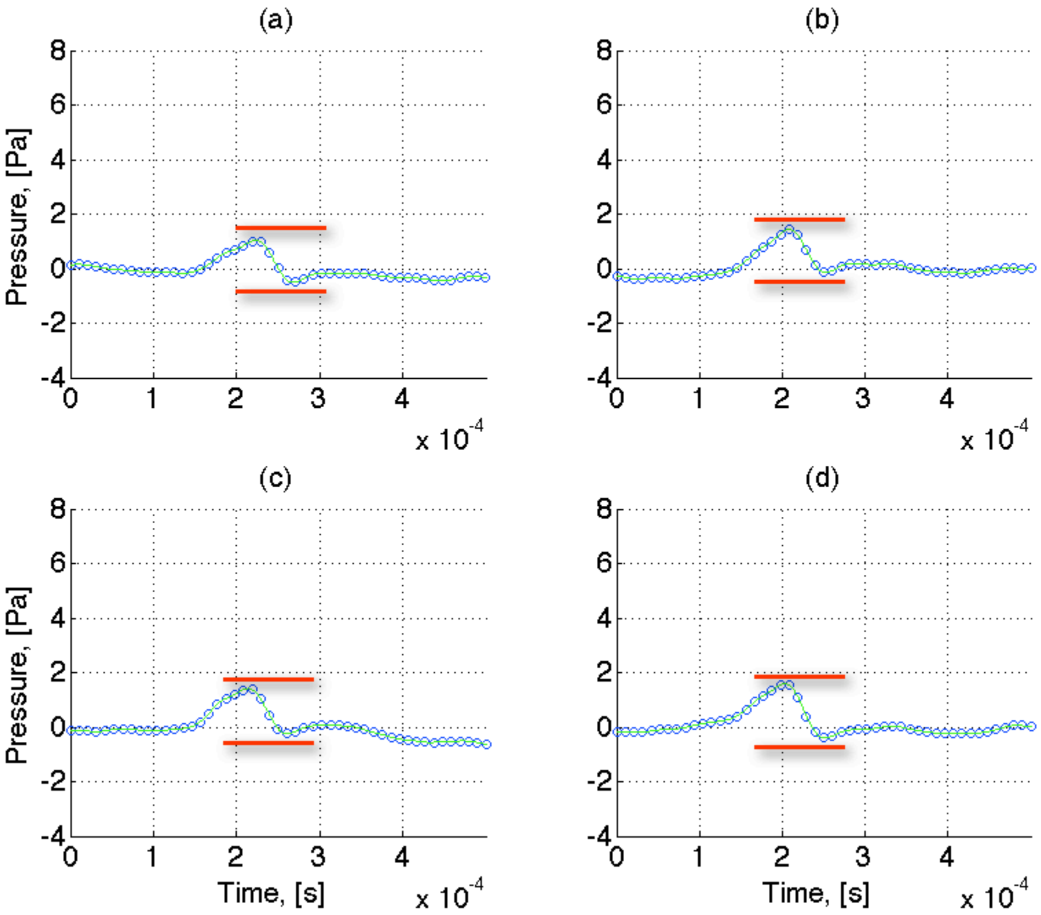

Figure 5.11 Four different example peaks of the leading edge signal at a tyre speed of 19 km/h generated by the 'large cavity'

	(a)	(b)	(c)	(d)
Peak, [Pa]	1.042	1.449	1.421	1.586
Bottom, [Pa]	-0.507	-0.139	-0.239	-0.398
Difference, [Pa]	1.549	1.588	1.66	1.984
Average, [Pa]	**1.695**			

Table 5.4 Peak value calculation for the leading edge signal of the tyre with the 'large cavity' at 19 km/h

Finally the results of the lowest speed of 19 km/h are analysed. The noise level produced by the chassis dynamometer is significantly lower at that speed, however, without the bandpass filter applied not a single event is recognisable in the signal. This time there is nearly no need for the interpolation with the spline function because the peak itself is not very sharp. Figure 5.11 shows four example peaks of the lowest speed time history. The amplitudes range from 1.042 Pa to 1.586 Pa. According to Table 5.4 this results in an average pressure difference of 1.695 Pa at the leading edge when the ‘large cavity’ hits the chassis dynamometer drum. Again this is slightly higher as the before proposed average value of the peak amplitudes only.

Table 5.5 summarises the obtained average values from Table 5.1 to Table 5.4 in dependence of the speed of the tyre. The reference speed v_0 is chosen to be the highest of 41 km/h. As mentioned before, a factor of the square of the velocity is assumed to be the connection between the different obtained pressure values and speeds. First the average amplitudes from Figure 5.7 are compared to the recorded average value of 41 km/h (6.396 Pa). The 31 km/h reading multiplied with the speed factor gives a deviation of 9 % in comparison to the maximum pressure at 41 km/h. A similar result is obtained for 19 km/h. Multiplied with the corresponding speed factor this gives 6.868 Pa, which means a deviation of 7 %.

By taking the manual average from Figures 5.9, 5.10 and 5.11 the fit is more accurate. In this case the highest speed results in an average value of 8.078 Pa, 31 km/h including the speed factor yields to 8.216 Pa and 19 km/h multiplied by the speed factor gives 7.893 Pa. Both deviations are only 3 %, which clearly indicates proportionality between velocity and pressure. The reason for the slightly more different results, when the whole average is taken from the signal, is first of all due to the different number of peaks. For 41 km/h the number of peaks is twice is many as for 19 km/h. Secondly it is due to noise in the signal. For 41 km/h the generated chassis dynamometer noise is more significant and so the peaks are more affected. This influence can be reduced by the other method used where the difference between the peak and the trough is considered.

	41 km/h	31 km/h	19 km/h
Average, [Pa]	*6.396*	4.023	1.475
Speed factor	*1*	$\left(41/31\right)^2$	$\left(41/31\right)^2$
Result, [Pa]	***6.396***	**7.033**	**6.868**
Deviation, [%]		*+9*	*+7*
Manual average, [Pa]	*8.078*	4.784	1.695
Speed factor	*1*	$\left(41/31\right)^2$	$\left(41/31\right)^2$
Result, [Pa]	***8.078***	**8.367**	**7.893**
Deviation, [%]		*+3*	*-3*

Table 5.5 Calculated peak amplitudes for the two lower speeds in comparison to the high speed of 41 km/h for the tyre with the 'large cavity'

For a visual approach of the peak amplitude relationship of the different recordings the Figure 5.12 is introduced. Where Figure 5.12a shows selected peaks of the different tyre speeds with average amplitude values according to Table 5.1. The high-speed case of 41 km/h is shown by the blue line, for 31 km/h red is used, and for 19 km/h the colour green is taken. Remarkable is that the peaks all have the same duration in time, hence the same frequency. The only factor that differs is the amplitude.

By multiplying the lower speeds of 31km/h and 19km/h with the speed difference factor, taken from Table 5.5, Figure 5.12b is generated. For both lower speeds the whole signal is multiplied by this factor and as can be seen not only the maximum amplitude of about 6.4 Pa fits very well, also the slope after it and the minimum value of -2 Pa is similar for at least the two lower speeds. Without the unwanted noise covering the signal the result could be even more accurate. Interesting for the highest speed is the negative pressure part before the peak itself. This is due to the fact that the pressure in the cavity is suddenly occurring, quicker for the high speed and significantly slower for the lower speeds. Some of those initial negative pressure regions are diminished by the filter, thus, later on for the pure signal comparison there will be no filter technique applied. With this example the speed and amplitude of the leading edge for the tyre with the 'large cavity' is shown to be dependent on the squared velocity. In addition to that the signals of the different tyre velocities seem to have all the same duration (0.1*10^{-3} s) that means there is no connection between cavity length and peak duration. A comparison to existing models introduced in Chapter 3 will be approached at the end of this chapter.

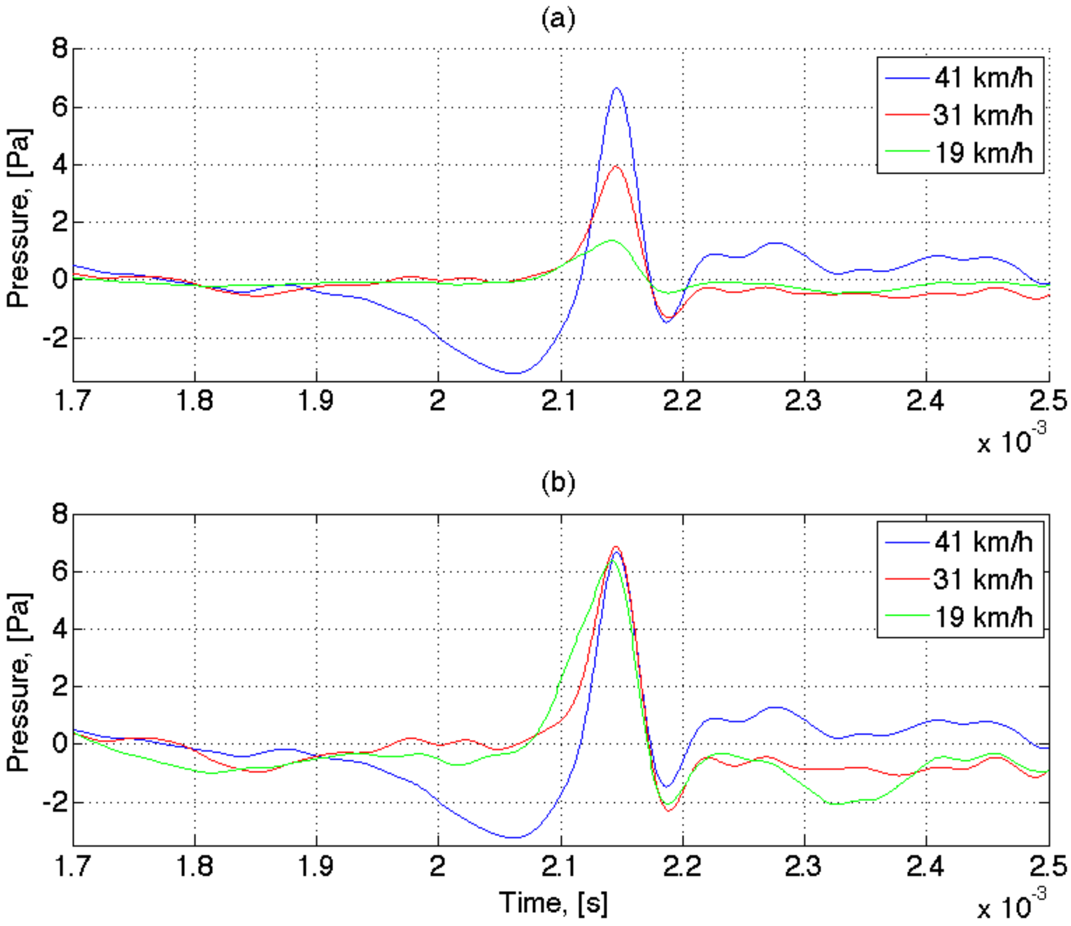

Figure 5.12 Average peak of the leading edge signal from the tyre with the 'large cavity' for the three different speeds: (a) normal recordings; and (b) slower velocity signals multiplied by the speed factor

5.2.2. Small cavity

Figure 5.13 shows the tyre with the other circular cavity cut into the tread: the 'small cavity'. In comparison to the 'large cavity' the volume of this is more than 30 times smaller. So it is interesting to see if there is any noise generated at all at the leading edge of a tyre equipped with such a small cavity.

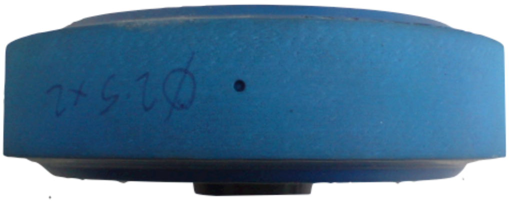

Figure 5.13 Photograph of top view of the tyre equipped with the 'small cavity'

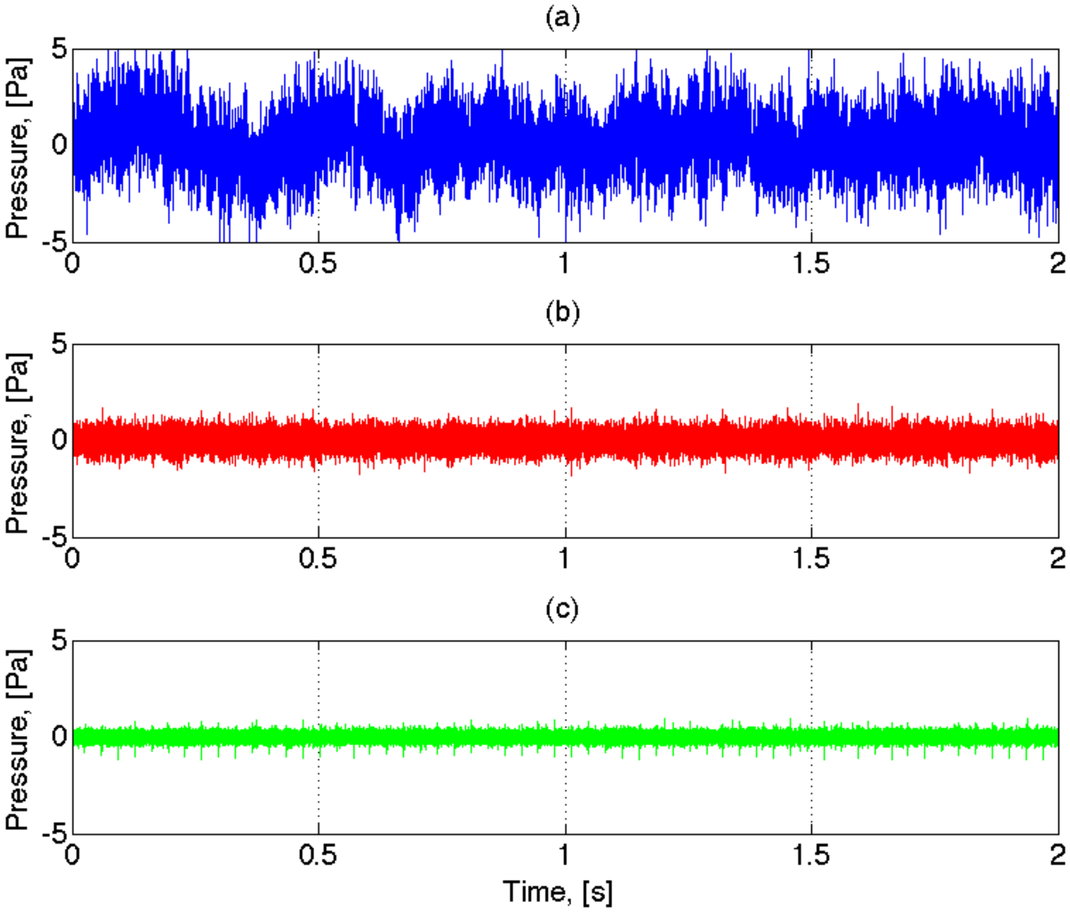

Figure 5.14 Time history of the leading edge signal from the tyre with the 'small cavity' at 41km/h: (a) unfiltered signal; (b) normal bandpass filtered signal; and (c) 3rd order bandpass Butterworth filter used

Figure 5.14 shows the unfiltered and bandpass filtered data of the whole leading edge signal of the tyre with the 'small cavity'. At the top (Figure 5.14a), the unfiltered signal is shown, which is purely dominated by noise. Even in Figure 5.14b with the 2nd order bandpass Butterworth filter according to Chapter 4 applied to the signal, nothing can be identified that indicates the contact of cavity and road at the speed of 41 km/h. Thus, a more powerful filter is introduced. Figure 5.14c shows the signal conditioned with a 3rd order bandpass Butterworth filter with the lower cut-off frequency of 4320 Hertz. However, this is only done to identify the peaks in the signal, not for the actual measurement of peak height because it changes the shape of the peak significantly. The maximum amplitude is now negative as Figure 5.14c shows. With this higher filter order the events can be located and four reference peaks are taken from the signal (Figure 5.14b) to calculate the average peak height.

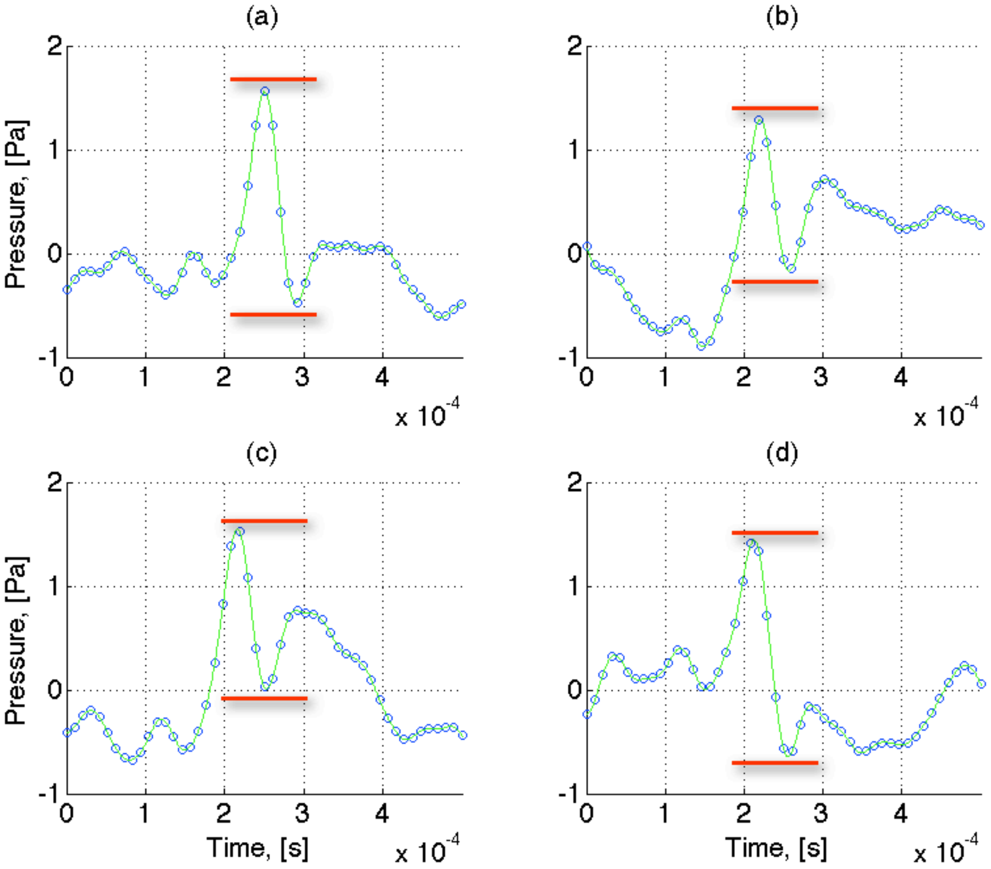

Figure 5.15 Four different example peaks of the leading edge signal at a tyre speed of 41 km/h generated by the ‘small cavity’

Figure 5.15 shows the four reference events chosen. For this plot again the normal 2nd order bandpass Butterworth filter is used, because this filter does not influence the original shape of the signal as significantly. The shape of the peaks is similar to the ones produced by the ‘large cavity’, which is to be expected because the same type of cavity is used. For the ‘small cavity’ however, the maximum of the peak differs significantly. In comparison to the ‘large cavity’ this signal is weaker and thus, prone to be even more influenced by the noise, as can be seen in Table 5.6. The four examples show a quite significant difference between maximum and minimum value. The calculated values reach from 1.458 Pa up to 2.085 Pa and produce an average difference of 1.783 Pa. These significant fluctuations between the peak amplitudes and the low maximum pressure in comparison to the unwanted noise produced by the chassis dynamometer yields to an unsatisfactory accuracy in the results.

	(a)	(b)	(c)	(d)
Peak, [Pa]	1.558	1.289	1.546	1.445
Bottom, [Pa]	-0.475	-0.169	-0.011	-0.640
Difference, [Pa]	2.033	1.458	1.557	2.085
Average, [Pa]	**1.783**			

Table 5.6 Peak value calculation for the leading edge signal of the tyre with the ‘small cavity’ at 41 km/h

The signal generated by the lower speed of 31 km/h is now analysed. Again a stronger filter has to be used to identify the peaks at the leading edge in the first place. Then for the actual peak analysis the normal 2nd order bandpass Butterworth filter is applied to the time history. Figure 5.16 shows the four example peaks despite the cavity size and the low speed it is however possible to identify the events.

	(a)	(b)	(c)	(d)
Peak, [Pa]	0.900	0.7805	0.470	0.757
Bottom, [Pa]	-0.193	-0.373	-0.459	-0.162
Difference, [Pa]	1.093	1.154	0.929	0.920
Average, [Pa]	1.024			

Table 5.7 Peak value calculation for the leading edge signal of the tyre with the ‘small cavity’ at 31 km/h

Table 5.7 summarises all the values taken from the different examples in Figure 5.16. In comparison to each other they are in a similar range, when the difference between maximum and minimum value is considered. This difference ranges from 0.920 Pa to 1.154 Pa, which results in an average difference of 1.024 Pa.

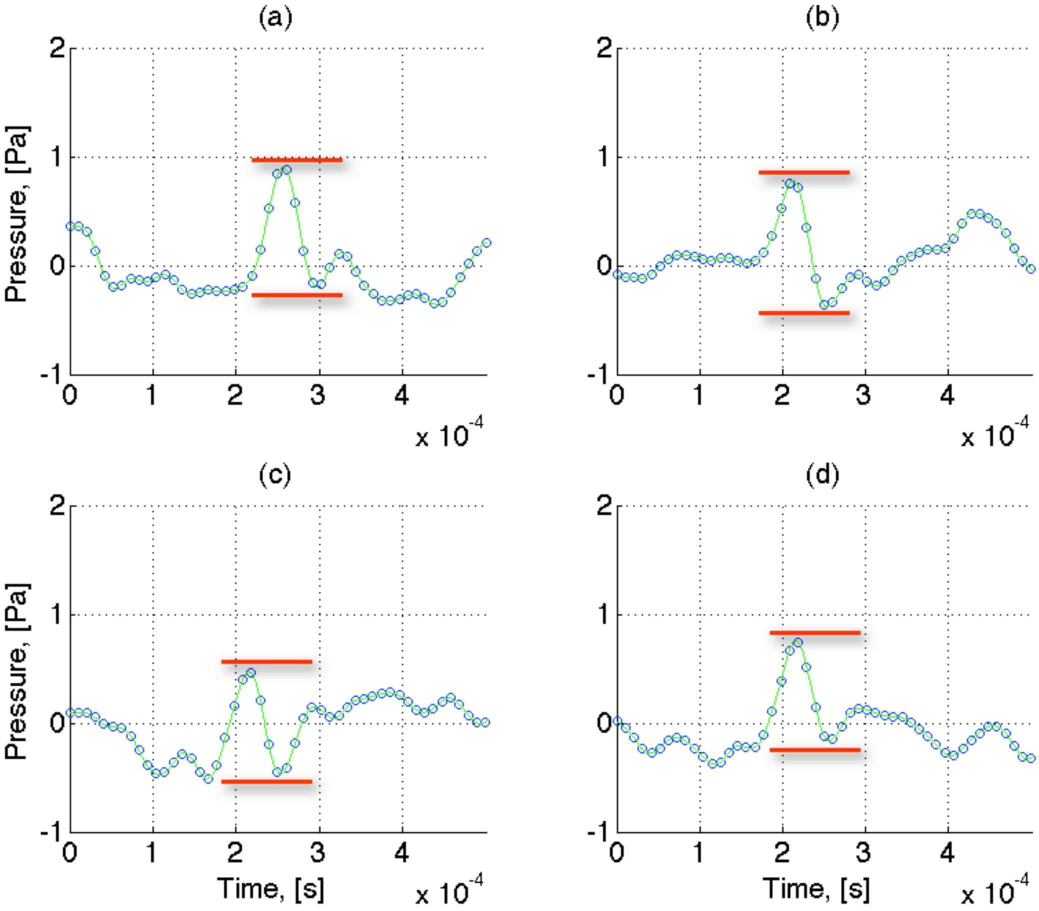

Figure 5.16 Four different example peaks of the leading edge signal at a tyre speed of 31 km/h generated by the ‘small cavity’

At 19 km/h it is not possible to spot the events at the leading edge, because for this ‘small cavity’ a reasonably high tyre speed is needed to produce a significant signal at the leading edge. Therefore the signal was overlaid by the trailing edge signal and so the stronger signal created at the trailing edge helped to identify the right areas for the leading edge peak. Four example peaks are found, but as Figure 5.17 indicates, the amplitude is low and nearly not distinguishable from the noise in the signal. Nevertheless the data is analysed and the results are summarised in Table 5.8. As expected a rather low combined amplitude of 0.209 Pa is the result of the readings from Figure 5.17.

	(a)	(b)	(c)	(d)
Peak, [Pa]	0.191	0.182	0.17	0.201
Bottom, [Pa]	-0.032	0.007	-0.055	-0.01
Difference, [Pa]	0.223	0.175	0.225	0.211
Average, [Pa]	0.209			

Table 5.8 Peak value calculation for the leading edge signal of the tyre with the 'small cavity' at 19 km/h

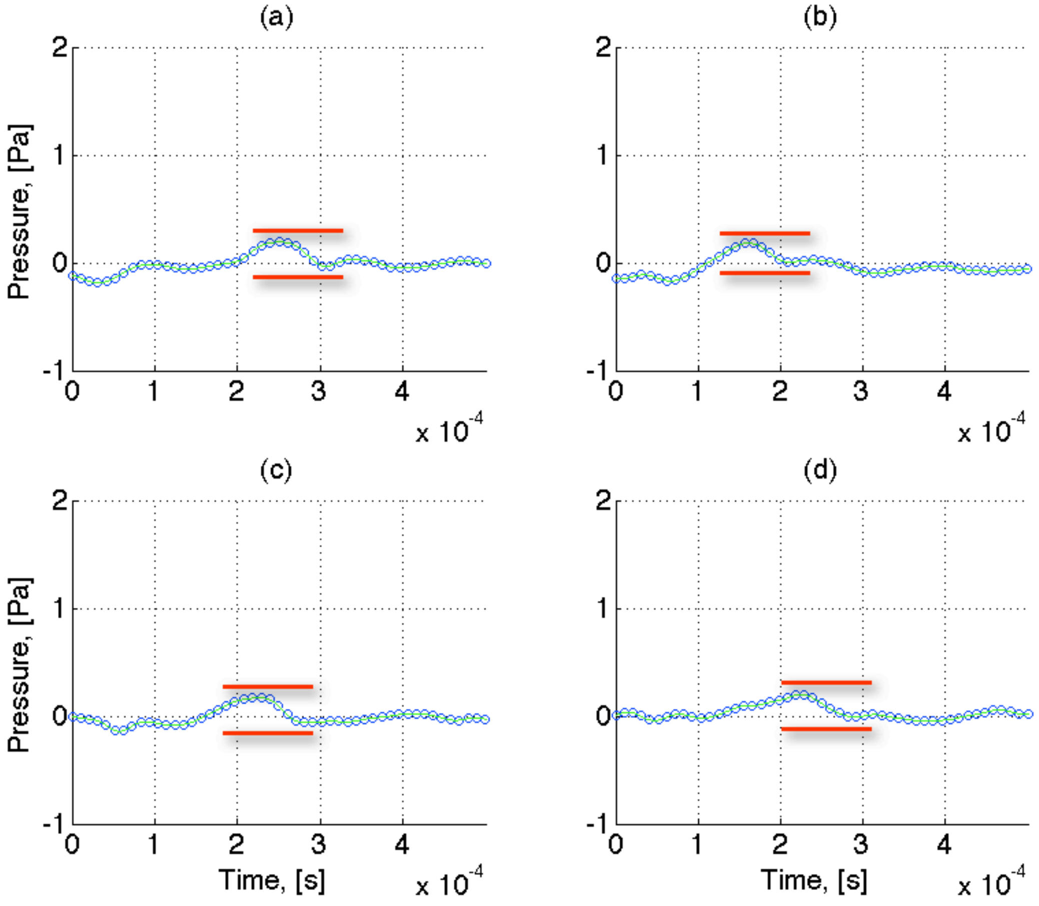

Figure 5.17 Four different example peaks of the leading edge signal at a tyre speed of 19 km/h generated by the 'small cavity'

Table 5.9 summarises the results of the amplitude measurements for the tyre with the 'small cavity' at the different speeds tested. Satisfactory agreement is achieved in between the result of 31 km/h and of 41 km/h (0.3

% deviation) when the speed factor is used. As expected the recording of 19 km/h does not deliver a good result. It is about half the amount as the theory would suggest in this case. The speed of the tyre for this small sized cavity is too low. The chassis dynamometer noise is significantly influencing the sound produced by this cavity/speed combination

	41 km/h	31 km/h	19 km/h
Manual average, [Pa]	*1.783*	1.024	0.209
Speed factor	*1*	$\left(41/31\right)^2$	$\left(41/31\right)^2$
Result, [Pa]	***1.783***	**1.789**	**0.973**
Deviation, [%]		*+0.3*	*-54*

Table 5.9 Calculated peak amplitudes for the two lower speeds in comparison to the reference speed of 41 km/h for the tyre with the 'small cavity'

Due to this low-speed problem higher dynamometer speeds are investigated to see if there is any change, especially in the duration of the peak. The maximum speed the tyre is driven at was 91 km/h. This experiment is only conducted with the 'small cavity' tyre because of safety reasons. The cavity is small in comparison to the tyre thus, is does not affect the structure of the tyre as much. This high speed in combination with the microphones being very close to the tyre was a challenging experiment. It was decided not to be repeated again for the other tyres, due to the vibrations in the rig and the close proximity of the microphones to the tyre. Nevertheless the results are convincing. It is possible to identify pressure peaks generated at the leading edge, even in the signal for the high speeds of 71 km/h and 91 km/h that are overlaid by significant noise generated by the chassis dynamometer. The peaks are not easy to spot in the time history because of the high overall noise levels. However, due to the sharp shape they can still be identified. Figure 5.18 shows a comparison of the following velocities tested: 31 km/h, 51 km/h, 71 km/h and 91 km/h. Again the duration of the pressure peaks in time is the same for all of the results, it is slightly less than a 10th of a millisecond. The initial idea was to reach a speed so the closing time of the cavity would be shorter as the duration of the peak.

However, 91 km/h is just the borderline speed as indicated in Table 5.10. The actual cavity length of the ‘small cavity’ in circumferential direction is 2.5mm. The speed of 91 km/h is equivalent to a velocity of 2528 mm/ms, this value is close to the actual cavity dimension, however, in order to draw meaningful conclusions a higher speed is needed. At 101 km/h the level of noise created by the chassis dynamometer is excessively high, therefore, no contacting signal of cavity and road can be identified at the leading edge for this speed.

Speed (km/h)	Speed (m/s)	Speed (mm/ms)	Speed (mm/s*10^{-4})
91	25.28	25.28	2.53

Table 5.10 Speed unit conversion for the tyre with the ‘small cavity’

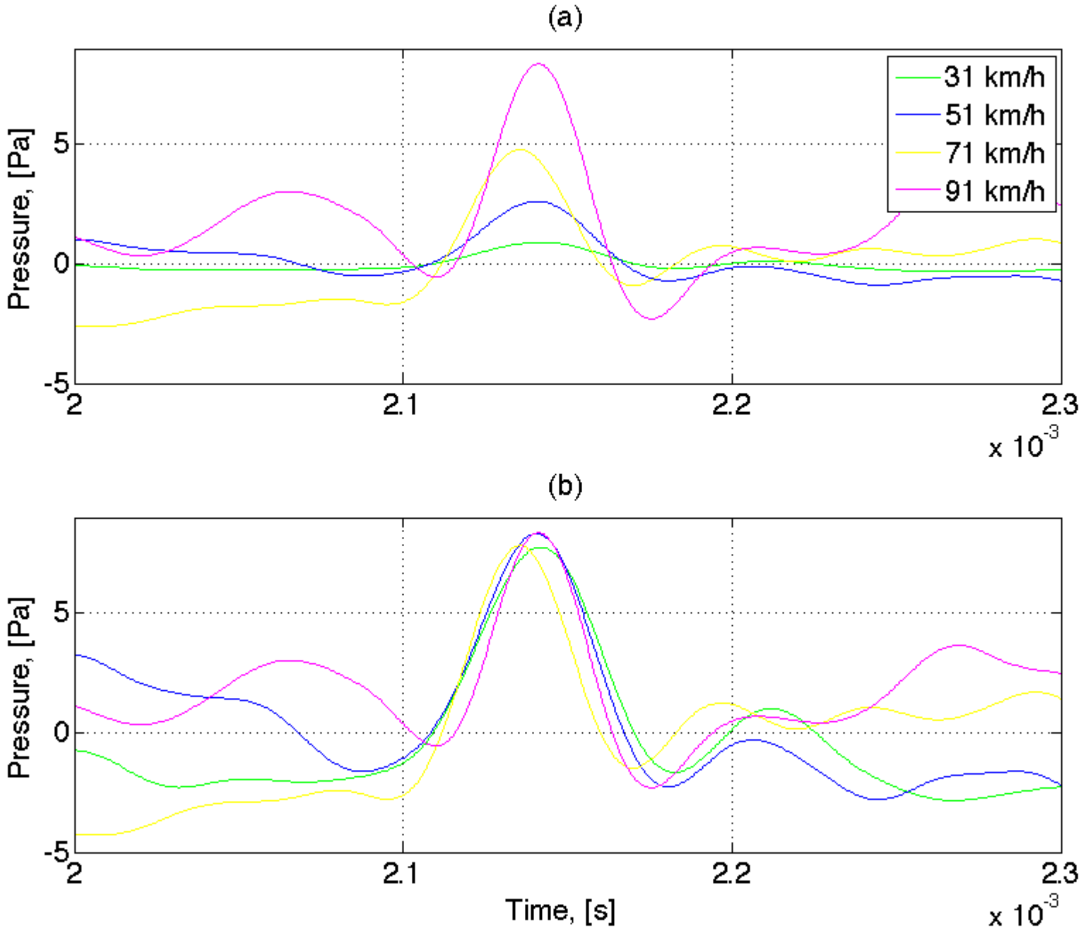

Figure 5.18 Average peak of the leading edge signal from the tyre with the ‘small cavity’ for four different speeds: (a) normal recordings; and (b) slower velocity signals with speed factor multiplied

Figure 5.18 also shows the maximum pressure amplitude comparison between the four different speeds tested. In Figure 5.18b the reference speed v_0 of 91 km/h is plotted in magenta. Good agreement in amplitude and shape is achieved, when lower speeds of 31 km/h, 51 km/h and 71 km/h are multiplied by the squared speed difference to 91 km/h.

It has been found that also for the ‘small cavity’ a signal is produced at the leading edge of the tyre. This signal is similar to the one of the ‘large cavity’ shown earlier on. It shows similar attributes that are: same duration in time for all the speeds; and the amplitudes are proportional to the square of the velocity. This assumption is even valid for much higher velocities up to 91 km/h.

5.3. Rectangular cavities

Previously quick and accurate to manufacture circular cavities have been investigated. Now the same analysis with emphasis on the leading edge is carried out with rectangular cavity types. Here an interesting comparison is conducted where three different cavities have a volume relationship of either half the volume or the same volume, but different orientation of the cavity.

5.3.1. Square cavity

The ‘square cavity’ is similar to the before introduced circular ‘large cavity’. It has the same dimensions in all directions but not the same volume. It is a more realistic design that could be found in a real tyre tread. In comparison to the solid rubber tyre this cavity is rather large, it nearly covers half of the tyre width. Therefore it is expected to produce sufficient noise at the contact patch, for a detailed analysis. Figure 5.19 shows the top view of the tyre with the ‘square cavity’.

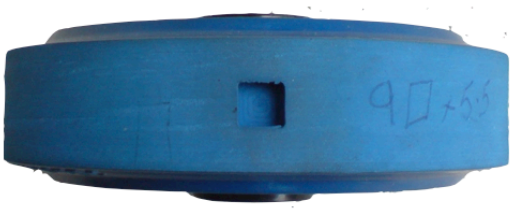

Figure 5.19 Photograph of top view of the tyre equipped with the ‘square cavity’

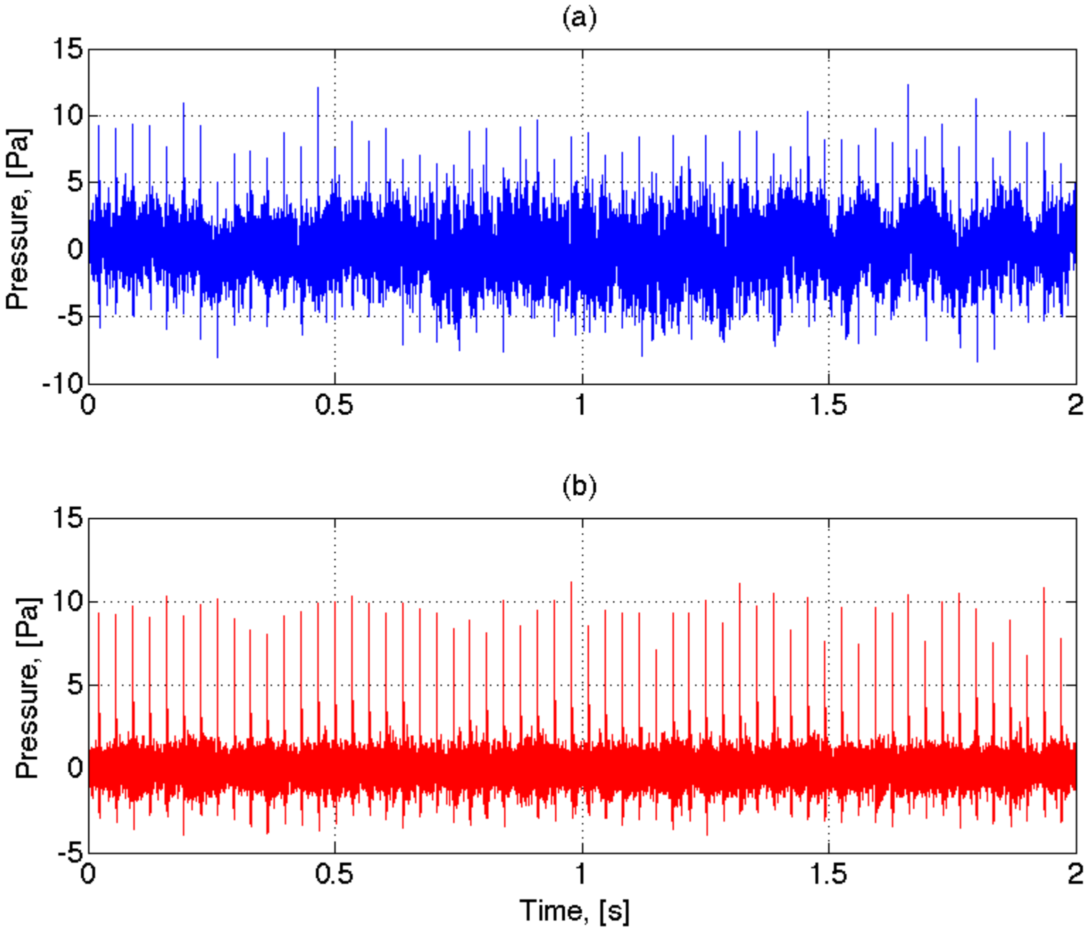

Figure 5.20 Time history of the leading edge signal from tyre with the ‘square cavity’ at 41km/h: (a) unfiltered signal; and (b) bandpass filtered signal

The same approach as previously used is chosen to analyse the leading edge signal. Figure 5.20 shows the leading edge recording of the tyre with the ‘square cavity’. Again at the top of Figure 5.20 the unfiltered signal is shown. In this unfiltered signal peaks of the event can already be identified. However, with the filter applied those peaks become more dominant, as shown in Figure 5.20b. The amplitudes of the peaks show high levels; they are of much greater order than the ones for the tyre with the ‘large cavity’. The square shape of the cavity, resulting in a sudden impact when in contact with the road, could explain this greater order. Also the larger volume, V_0, in comparison to the ‘large cavity’ could contribute to higher-pressure amplitudes in the signal.

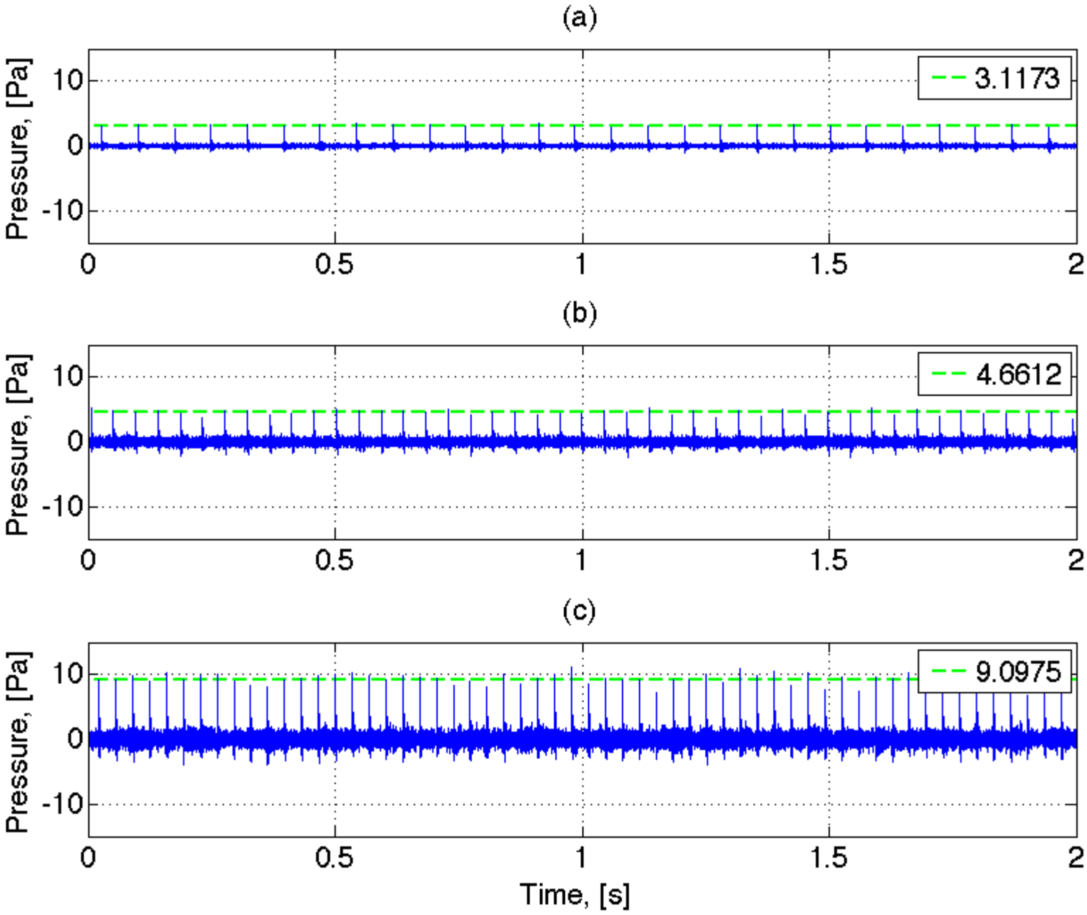

Figure 5.21 Time history of the leading edge signal from the tyre with the ‘square cavity’ for different speeds including average peak level: (a) 19 km/h; (b) 31 km/h; and (c) 41 km/h

	19 km/h	31 km/h	41 km/h
Number of peaks	27	38	60
Average value [Pa]	**3.1173**	**4.6612**	**9.0975**

Table 5.11 Number and average amplitude values of peaks taken from **Figure 5.21** of the leading edge signal of the tyre with the ‘square cavity’

Figure 5.21 shows the filtered measurements for the speeds of 19 km/h, 31 km/h and 41 km/h with the average taken of all peak amplitudes. The values obtained in Figure 5.21 are summarised in Table 5.11. Figure 5.21a shows high peak amplitudes for the slow speed of 19 km/h. This is also confirmed by the high average value of 3.1173 Pa. In comparison to 19km/h, the average value for 31 km/h, which is 4.6612 Pa seems to be rather low. For the top speed of 41 km/h, shown in Figure 5.21c the average amplitude is 9.0975 Pa. The relation of speed of the tyre and peak amplitude at the leading edge is checked later on. But for this ‘square cavity’ the before formulated velocity squared factor in between the peak amplitudes does not seem to be valid, when 19 km/h and 41 km/h are compared.

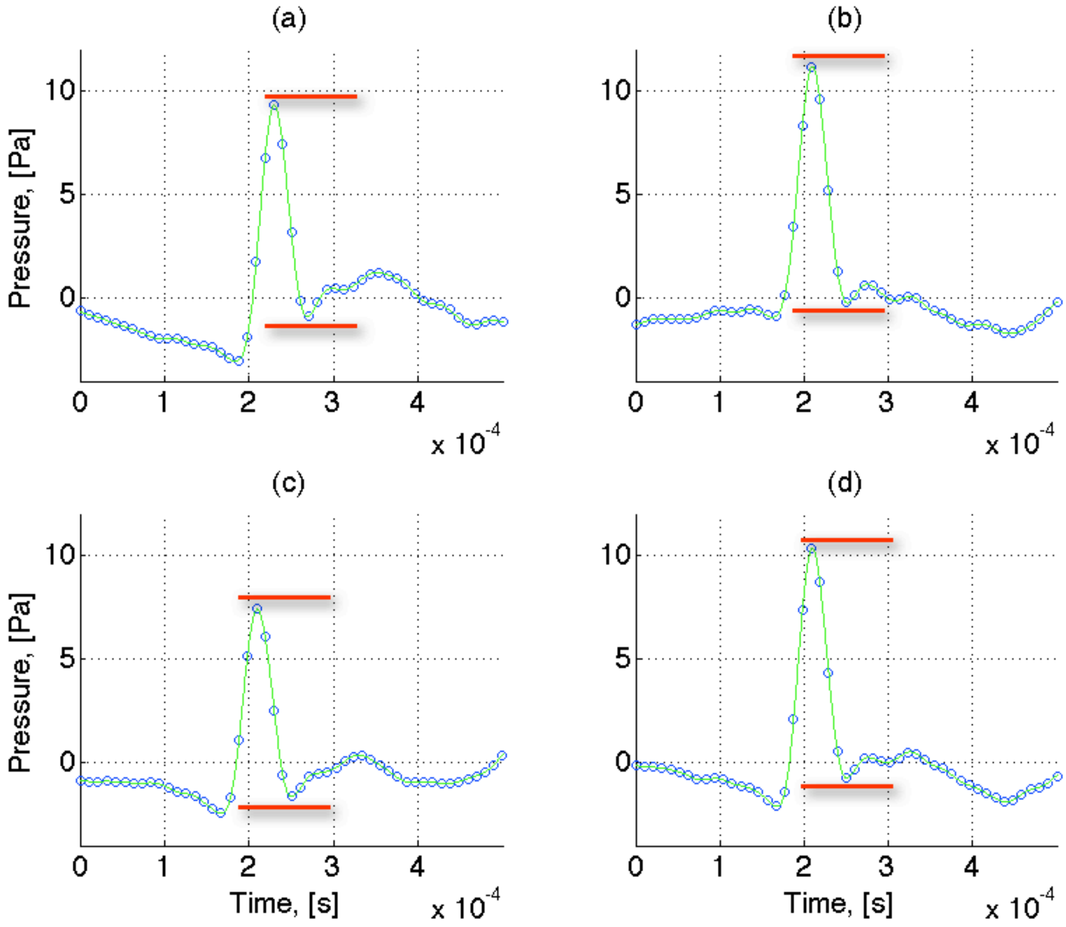

Figure 5.22 Four different example peaks of the leading edge signal at a tyre speed of 41 km/h generated by the ‘square cavity’

	(a)	(b)	(c)	(d)
Peak, [Pa]	9.293	11.190	7.414	10.360
Bottom, [Pa]	-0.880	-0.223	-1.632	-0.747
Difference, [Pa]	10.173	11.413	9.046	11.107
Average, [Pa]	**10.435**			

Table 5.12 Peak value calculation for the leading edge signal of the tyre with the ‘square cavity’ at 41 km/h

Four example events, of the tyre with the ‘square cavity’ recorded at 41 km/h are displayed in Figure 5.22. The structure of the peaks is similar to the ones presented in the previous sections, where the results of the circular cavities are presented. Thus the signature of the pulse is not dependent on the cavity shape. The difference values between peak and trough (after the maximum) indicated by the red lines in Figure 5.22, are calculated and summarised in Table 5.12. There is a significant difference between the highest result of 11.413 Pa and the lowest of 9.046 Pa. The large cavity size could be a reason for that. A big chunk of rubber is missing out of the tyre body that might result in stability issues in the tyre. Thus, leading to a deformation of the cavity, when entering the contact patch, resulting in a more irregular peak behaviour.

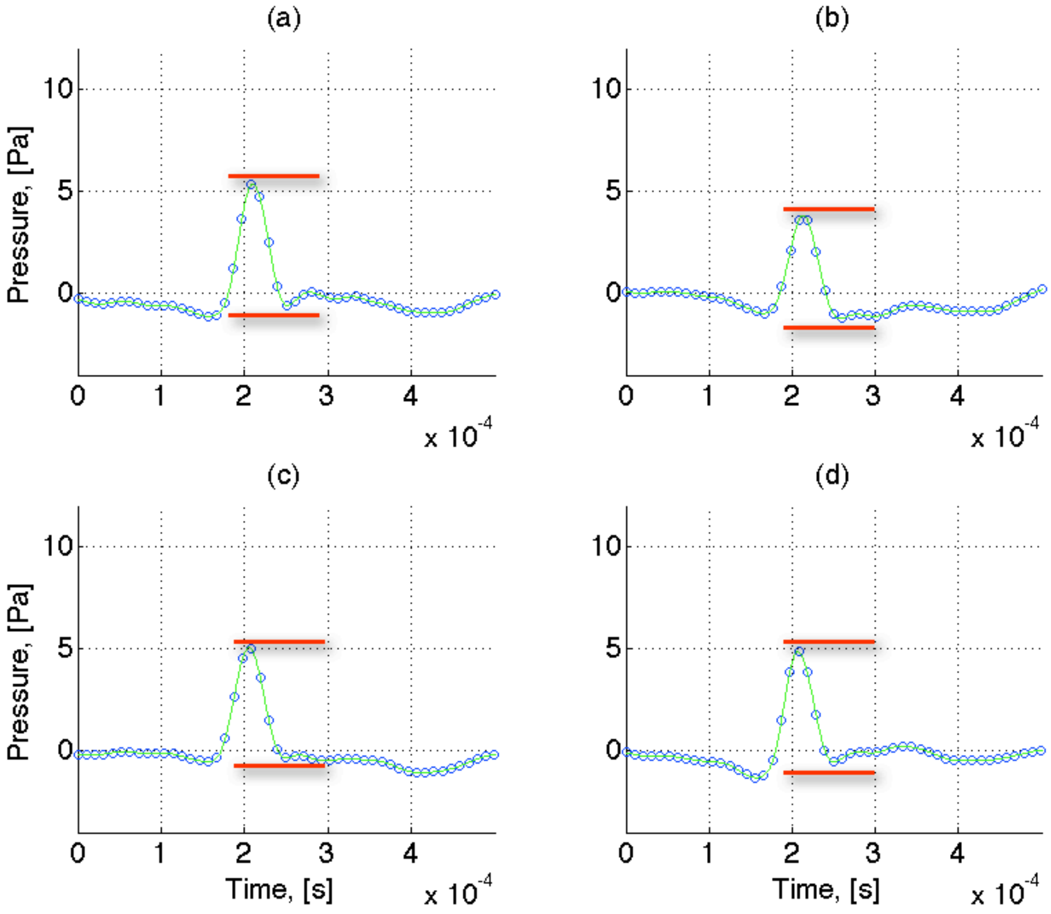

Figure 5.23 Four different example peaks of the leading edge signal at a tyre speed of 31 km/h generated by the ‘square cavity’

Figure 5.23 shows reference peaks of the lower speed of 31 km/h. Again the shape is similar to the ones shown before. A single event consists of a dip at the beginning, followed by a sudden rise and nearly symmetric fall of the amplitude down to a minimum value. In comparison to the measurements conducted at 41 km/h just the amplitude is different.

	(a)	(b)	(c)	(d)
Peak, [Pa]	5.385	3.828	5.070	4.875
Bottom, [Pa]	-0.580	-1.226	-0.342	-0.540
Difference, [Pa]	5.965	5.054	5.412	5.415
Average, [Pa]	**5.462**			

Table 5.13 Peak value calculation for the leading edge signal of the tyre with the ‘square cavity’ at 31 km/h

All four different example maximum and minimum values are summarized in Table 5.13. The highest difference between maximum and minimum value from the two seconds signal is 5.965 Pa and the lowest is 5.054 Pa that is within an acceptable range. The four different peaks result in an average value of 5.462 Pa.

	(a)	(b)	(c)	(d)
Peak, [Pa]	3.569	2.715	2.939	2.699
Bottom, [Pa]	0.132	-0.111	0.110	-0.052
Difference, [Pa]	3.437	2.826	2.829	2.751
Average, [Pa]	**2.960**			

Table 5.14 Peak value calculation for the leading edge signal of the tyre with the ‘square cavity’ at 19 km/h

Figure 5.24 shows the measurement of the tyre with the ‘square cavity’ at 19 km/h. Resulting in lower peak amplitudes in comparison to the ones shown for the higher speeds. The detailed results of the four events are outlined in Table 5.14. The highest difference between the maximum and minimum value is 3.437 Pa and the lowest is 2.826 Pa. These numbers lead to an average value of 3.030 Pa that is slightly lower than the measured average from Figure 5.21a.

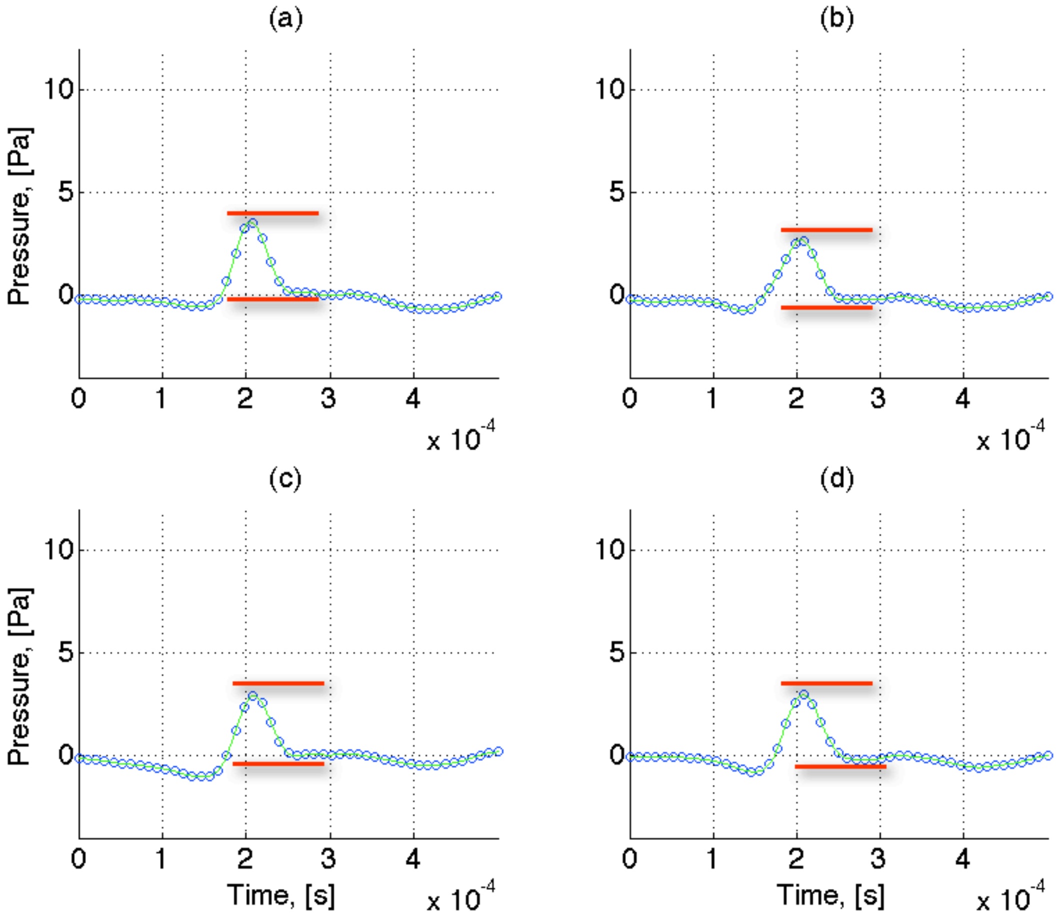

Figure 5.24 Four different example peaks of the leading edge signal at a tyre speed of 19 km/h generated by the ‘square cavity’

The results from Figure 5.21 and from the Tables 6.12 – 6.14 are combined in Table 5.15. As used before the reference speed v_0 is 41 km/h, hence, the other amplitudes are compared to that multiplied by the squared velocity difference. In the first section the data results from the average measurements of Figure 5.21 are presented. As previously indicated at the lowest speed of 19 km/h a rather high average peak amplitude was obtained in combination with the speed factor this results in 14.514 Pa. Compared to the average value for 41 km/h this results in a difference of 5.4 Pa (+59 %), and thus the theory of proportionality of speed and amplitude can not be supported. However, for the velocity of 31 km/h, the theory of proportionality is applicable again. Here in combination with the speed factor a maximum pressure of 8.153 Pa is obtained, resulting in a difference of 10.5 % in comparison to 41 km/h. Similar results are obtained for the manual checked amplitudes. In this case the difference between the average value of 41 km/h and 19 km/h multiplied with the speed difference squared is smaller than before, however, 3.3 Pa still results in a significant difference of 32 %. When the manual taken average of 41 km/h is compared to the average of 31 km/h the difference is in an acceptable (8.5 %) range that can be justified by noise in the recorded signal.

	41 km/h	31 km/h	19 km/h
Average, [Pa]	9.098	4.661	3.117
Speed factor	*1*	$\left(\frac{41}{31}\right)^2$	$\left(\frac{41}{31}\right)^2$
Result, [Pa]	**9.098**	**8.153**	**14.514**
Deviation, [%]		*-10.5*	*+59*
Manual average, [Pa]	10.435	5.462	2.960
Speed factor	*1*	$\left(\frac{41}{31}\right)^2$	$\left(\frac{41}{31}\right)^2$
Result, [Pa]	**10.435**	**9.554**	**13.780**
Deviation, [%]		*-8.5*	*+32*

Table 5.15 Calculated peak amplitudes for the two lower speeds in comparison to the reference speed of 41 km/h for the tyre with the ‘square cavity’

Figure 5.25 finally shows the visual comparison between the events occurring at the leading edge for the tyre with the ‘square cavity’. Figure 5.25a shows the original events and in Figure 5.25b the lower speed recordings are multiplied by the squared velocity difference to be directly comparable to the highest velocity of 41 km/h. As previously assumed there is a satisfactory fit in between the signal of 41 km/h and 31 km/h. However, when the peak from 19 km/h is multiplied by the velocity factor a rather high maximum pressure amplitude is obtained. This high value would not support the theory of a proportional connection between amplitude and velocity.

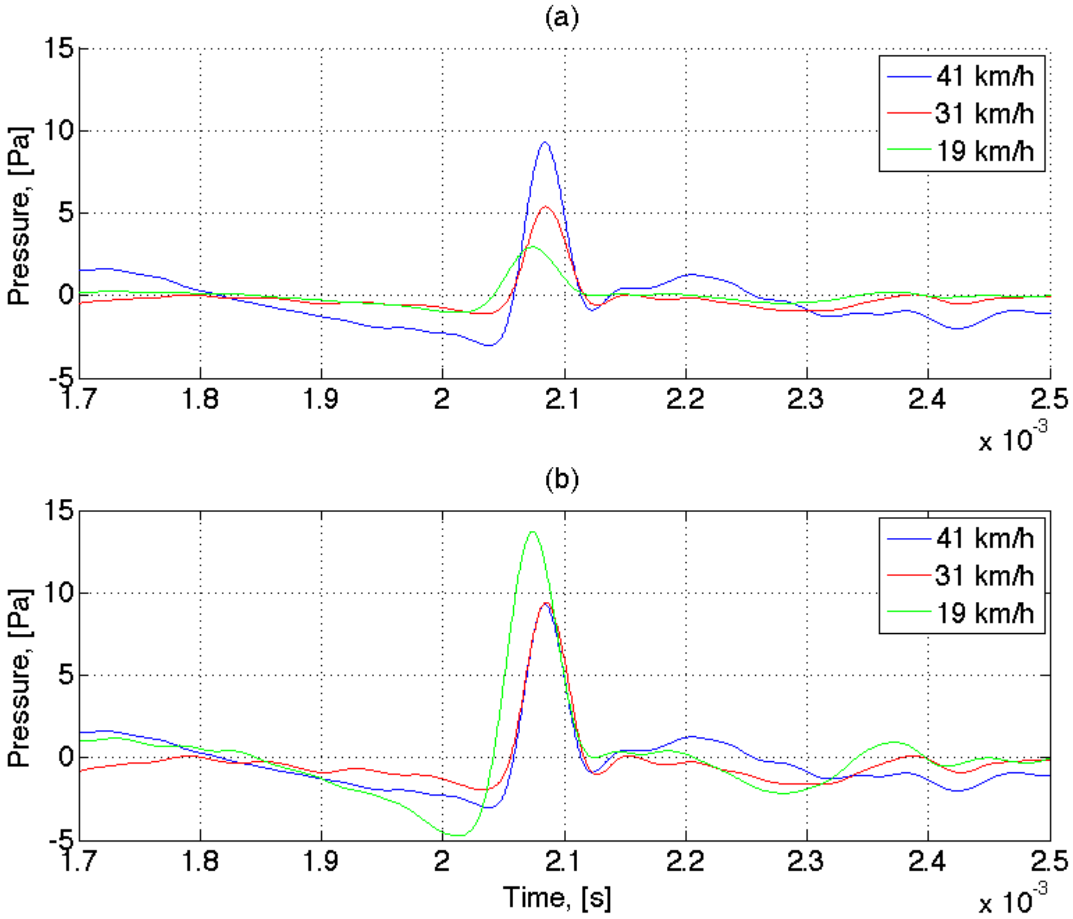

Figure 5.25 Average peak of the leading edge signal from the tyre with the ‘square cavity’ for the three different speeds: (a) normal recordings; and (b) slower velocity signals multiplied by the speed factor

5.3.2. Long cavity

Results of a different rectangular cavity are presented in this section. This ‘long cavity’ has exactly half the volume of the ‘square cavity’. It has the same depth and length as the ‘square cavity’ however the width is half the size. With this volume difference a direct comparison can be carried out considering cavity size and the pressure peak generated at the leading edge.

Figure 5.26 shows a photograph of the tyre with the ‘long cavity’, this cavity is not as accurately manufactured, that is the main problem of the rectangular cavities. Hence deviations in the results could be obtained for this cavity when compared to the other ones.

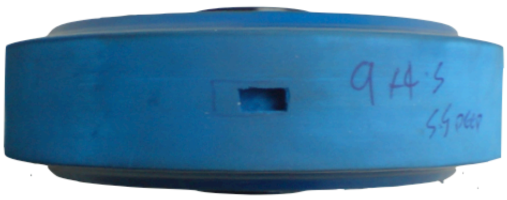

Figure 5.26 Photograph of top view of the tyre equipped with the ‘long cavity’

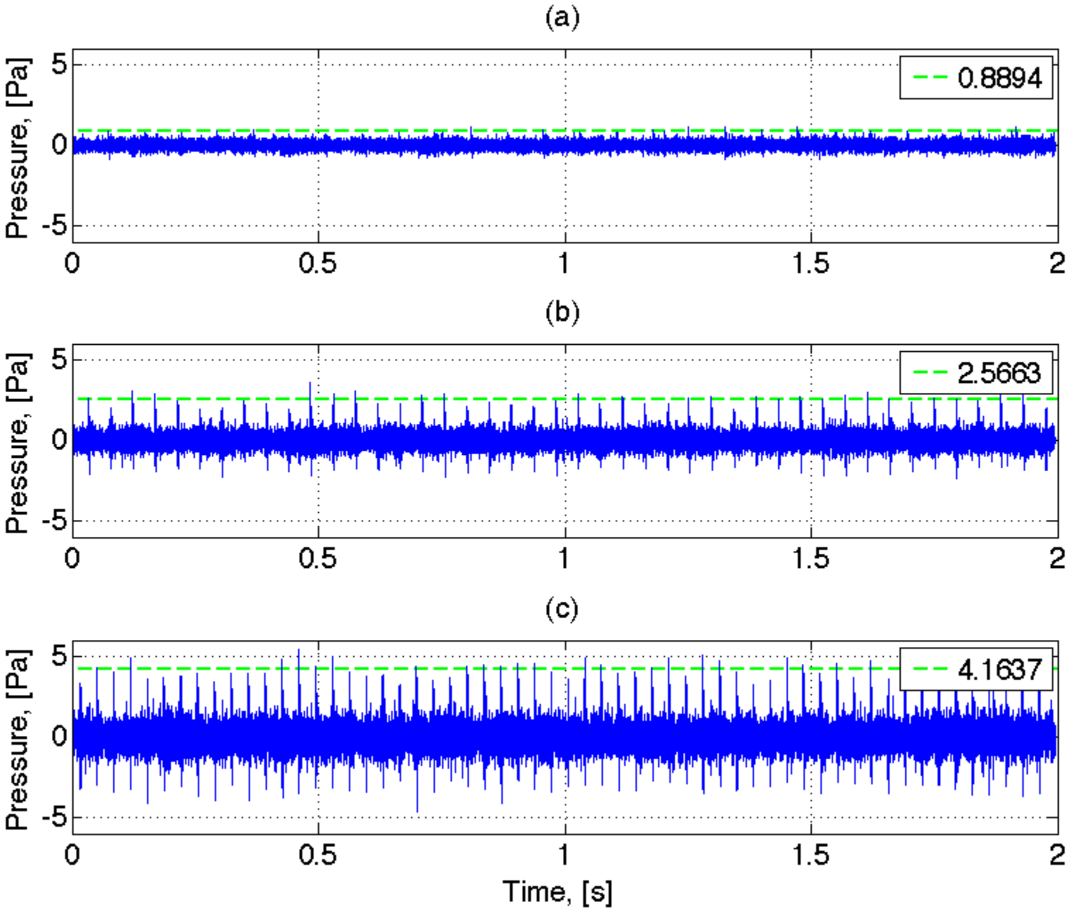

Figure 5.27 Time history of the leading edge signal from the tyre with the ‘long cavity’ for different speeds including average peak level: (a) 19 km/h; (b) 31 km/h; and (c) 41 km/h

Figure 5.27 shows the time histories of the leading edge signal recorded while the tyre equipped with the ‘long cavity’ was running on the chassis dynamometer. The maximum pressure peak for each speed is lower in comparison to the ‘square cavity’ however it is still possible to conduct the computational averaging process. Even for the lowest speed of 19 km/h (Figure 5.27a) there is just about enough maximum amplitude to pick it out of the background noise. Table 5.16 shows the summary of the average peak values from the whole two seconds recording. The amplitudes for all speeds are half the magnitude of the ones recorded for the ‘square cavity’. This presents an interesting fact for the comparison to the existing models at the end of this chapter.

	19 km/h	31 km/h	41 km/h
Number of peaks	27	38	59
Average value [Pa]	**0.8894**	**2.5663**	**4.1637**

Table 5.16 Number and average amplitude values of peaks taken from **Figure 5.27** of the leading edge signal of the tyre with the ‘long cavity’

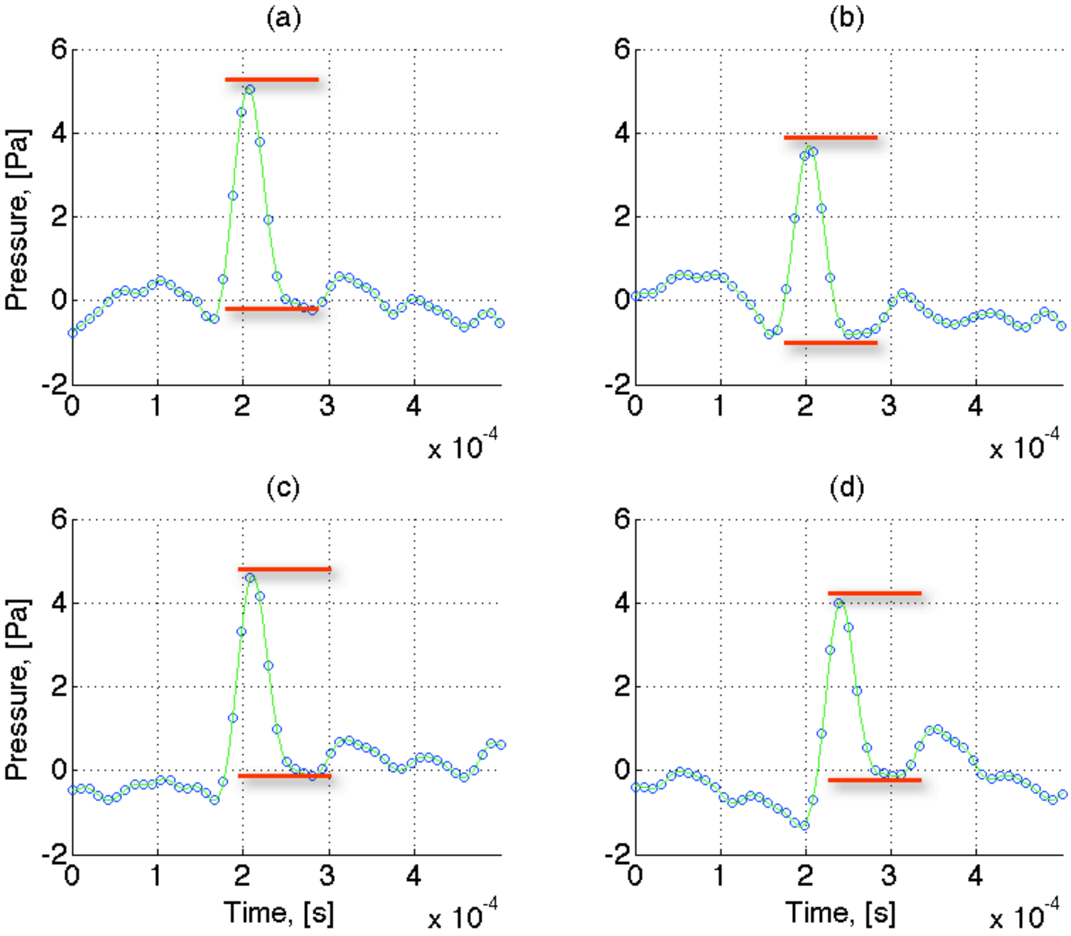

Figure 5.28 Four different example peaks of the leading edge signal at a tyre speed of 41 km/h generated by the ‘long cavity’

	(a)	(b)	(c)	(d)
Peak, [Pa]	5.076	3.698	4.641	4.016
Bottom, [Pa]	0.052	-0.812	-0.003	-0.129
Difference, [Pa]	5.024	4.510	4.644	4.145
Average, [Pa]	**4.581**			

Table 5.17 Peak value calculation for the leading edge signal of the tyre with the ‘long cavity’ at 41 km/h

Figure 5.28 shows a single event at the leading edge of the ‘square cavity’. There is a slight difference in the peak shape in comparison to the other cavities. The end of the actual process seems to be cut off. There is no dip in the signal anymore after the pressure has settled down from the maximum value. Therefore it is difficult to pick the end of the signal, hence the point when the cavity is fully covered by the road. This is essential for the comparison in height for the different speeds. Due to that lack of sharpness in the signal the end-point is chosen to be defined by a significant gradient changes at the end of the signal, as shown in Figure 5.28, marked by the red lines. In Table 5.17 all difference values for the tyre with the ‘long cavity’ taken from Figure 5.28 are enumerated. The highest difference between maximum and minimum in one event is 5.024 Pa and the smallest is 4.145 Pa. The resulting manually calculated average amplitude change is 4.581 Pa that is slightly higher than the average taken from the whole time history in Figure 5.27.

The next tyre velocity to analyse for the ‘long cavity’ is 31 km/h. Four example events picked out of the whole two seconds recording from Figure 5.27b, are shown in Figure 5.29. The maximum peak amplitudes reach from 1.885 Pa up to 3.680 Pa. The difference in between the maximum and minimum points, marked by the red lines, are between 2.208 Pa and 2.920 Pa. All values obtained are summarised in Table 5.18, again the calculated average value of 2.715 Pa is slightly higher than the computed average of the whole time history recording of 2.566 Pa.

	(a)	(b)	(c)	(d)
Peak, [Pa]	3.680	2.995	1.885	2.639
Bottom, [Pa]	0.760	0.060	-0.323	-0.158
Difference, [Pa]	2.920	2.935	2.208	2.797
Average, [Pa]		**2.715**		

Table 5.18 Peak value calculation for the leading edge signal of the tyre with the 'long cavity' at 31 km/h

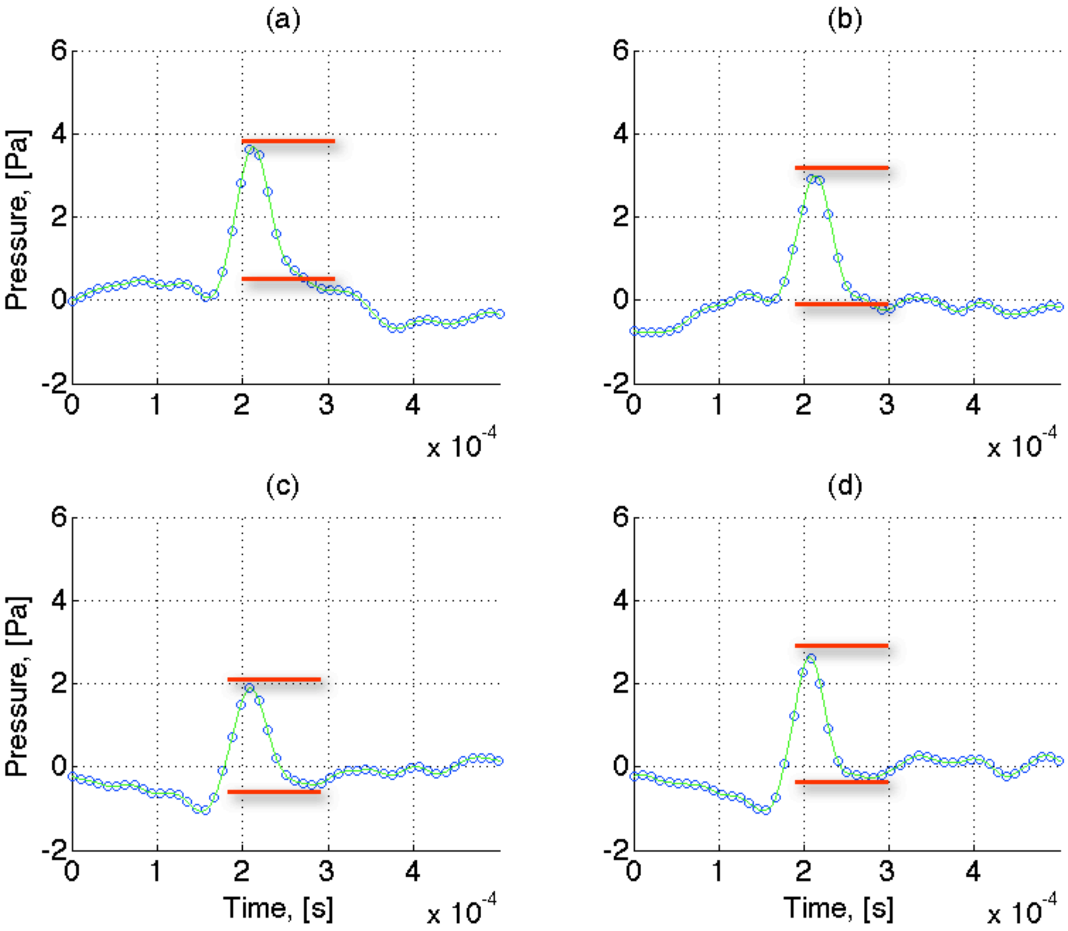

Figure 5.29 Four different example peaks of the leading edge signal at a tyre speed of 31 km/h generated by the 'long cavity'

Four different events, of the 26 in total, taken from the two seconds recording of the tyre with the 'long cavity' running at 19 km/h, are shown in Figure 5.30. The highest value between maximum and minimum amplitude of the event marked by the red lines is 1.100 Pa and the lowest is 0.825 Pa. The average calculated by the four results, shown in Table 5.19, is 0.952 Pa.

	(a)	(b)	(c)	(d)
Peak, [Pa]	1.170	0.913	0.934	0.876
Bottom, [Pa]	0.300	-0.186	-0.080	0.051
Difference, [Pa]	0.870	1.100	1.014	0.825
Average, [Pa]		**0.952**		

Table 5.19 Peak value calculation for the leading edge signal of the tyre with the 'long cavity' at 19 km/h

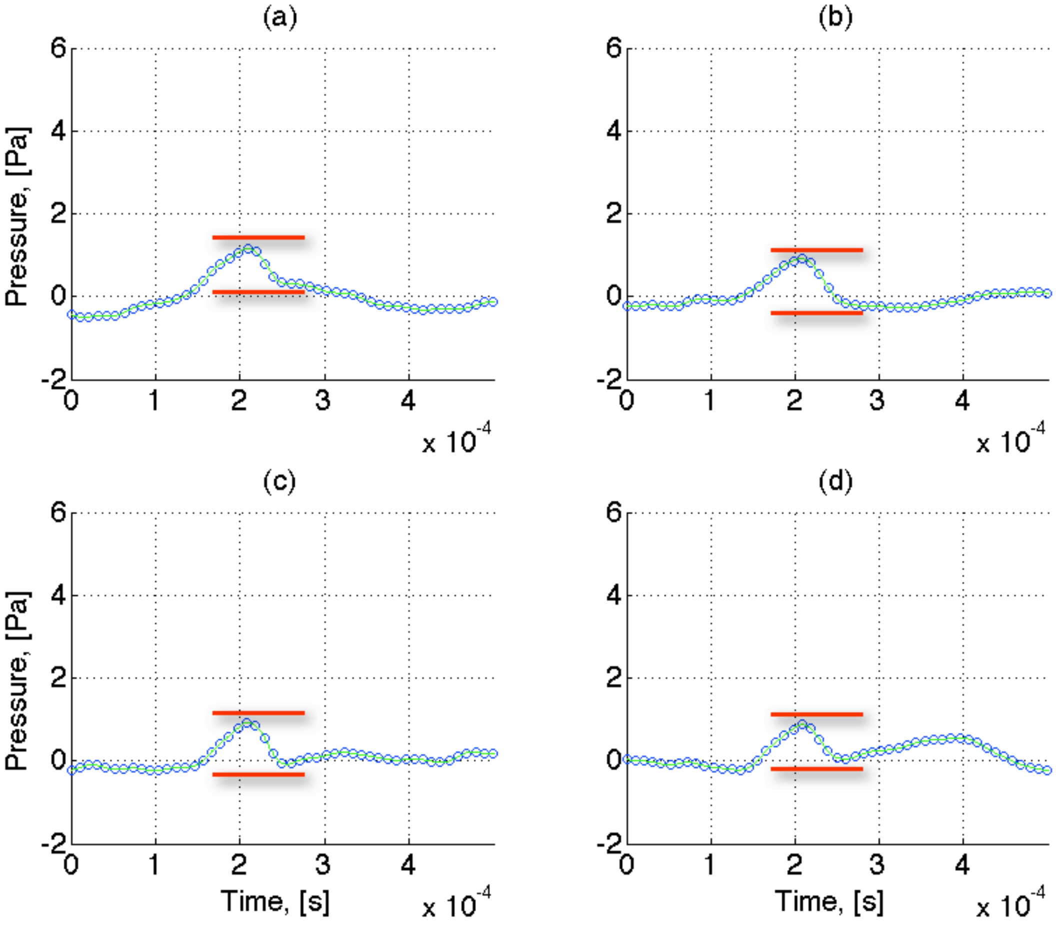

Figure 5.30 Four different example peaks of the leading edge signal at a tyre speed of 19 km/h generated by the 'long cavity'

Finally all different average values obtained for the tyre with the 'long cavity' are combined in Table 5.20. The first section of Table 5.20 shows the average values taken from the whole two seconds recording. 41 km/h is the reference speed with an average peak amplitude of 4.164 Pa. By multiplying the average peak amplitude of 31 km/h with the squared speed difference to 41 km/h an average of 4.489 Pa is obtained that leads to a deviation of 7.8

%. The result of the average peak amplitude taken at a speed of 19 km/h combined with the speed factor gives 4.140 Pa that delivers a good result in comparison to the 41 km/h (0.5 % deviation).

The results in the lower section in Table 5.20 for the manual measured height of a single event confirm the proportionality for both velocity recordings. When 31 km/h is compared to 41 km/h a deviation of 3.6 % is obtained and when 19 km/h is compared to the 41 km/h a deviation of only 3.3 % is the result. Thus also for the ‘long cavity’ a velocity square relationship in between the maximum amplitudes at the leading edge can be confirmed.

	41 km/h	31 km/h	19 km/h
Average, [Pa]	4.164	2.566	0.889
Speed factor	*1*	$\left(41/31\right)^2$	$\left(41/31\right)^2$
Result, [Pa]	**4.164**	**4.489**	**4.140**
Deviation, [%]		*+7.8*	*-0.5*
Manual average, [Pa]	4.581	2.715	0.952
Speed factor	*1*	$\left(41/31\right)^2$	$\left(41/31\right)^2$
Result, [Pa]	**4.581**	**4.749**	**4.433**
Deviation, [%]		*+3.6*	*-3.3*

Table 5.20 Calculated peak amplitudes for the two lower speeds in comparison to the reference speed of 41 km/h for the tyre with the ‘long cavity’

Figure 5.31 shows three example events of the three different recorded speeds. Where in Figure 5.31a the purely recorded signals are shown, with the 19 km/h signal displayed by the green line, the 31 km/h by red and the 41 km/h is shown by the blue graph. In Figure 5.31b the signals of 19 km/h and 31 km/h are multiplied by the factor taken from Table 5.20 in accordance to the reference speed of 41 km/h. A good fit of all the events can be shown, where duration and amplitude of the peak are nearly constant.

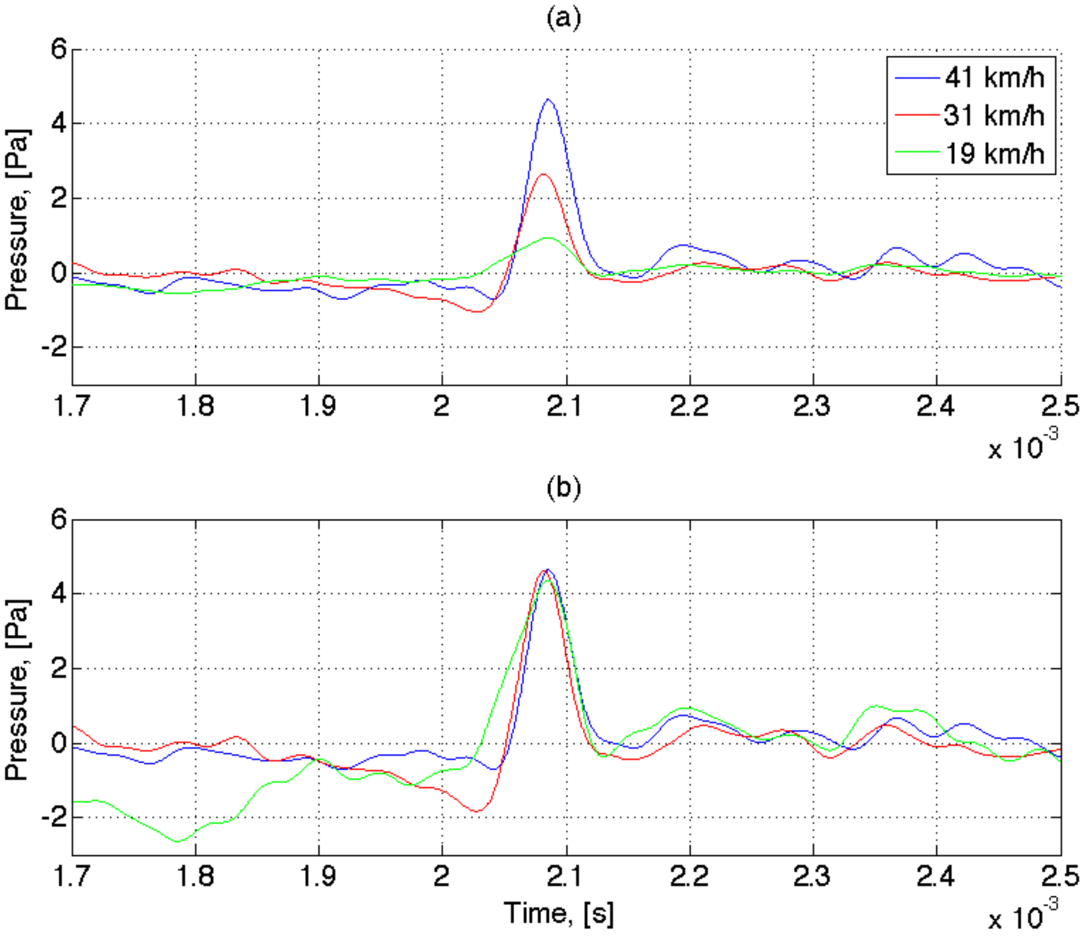

Figure 5.31 Average peak of the leading edge signal from the tyre with the ‘long cavity’ for the three different speeds: (a) normal recordings; and (b) slower velocity signals multiplied by the speed factor

5.3.3. Wide cavity

The last leading edge time history to analyse is generated by the tyre equipped with the ‘wide cavity’. This tyre has a similar cavity design in comparison to the ‘long cavity’. It has the same volume and shape but its orientation is transversal, in respect to the rotation of the tyre, instead of longitudinal as for the ‘long cavity’. By using the same volume it will be investigated if there is a difference in sound radiation depending on orientation of the cavity. This then is compared to the models presented for the leading edge air pumping phenomena. The volume displaced by this cavity is assumed to be the same as for the 'long cavity'. Thus, if sound radiation at the leading edge is proportional to the volume squeezed out the 'wide cavity' and the 'long cavity' should generate the same amount of noise. Figure 5.32 shows a photograph of the top view of the tyre with the 'wide cavity'. The dimensions of the cavity are 4.5 mm in length, 9 mm in width and 5 mm in depth.

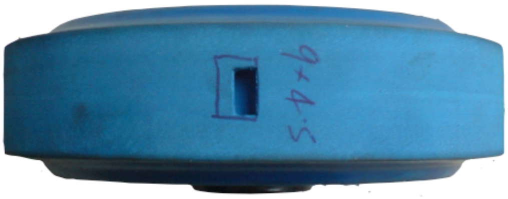

Figure 5.32 Photograph of top view of the tyre equipped with the 'wide cavity'

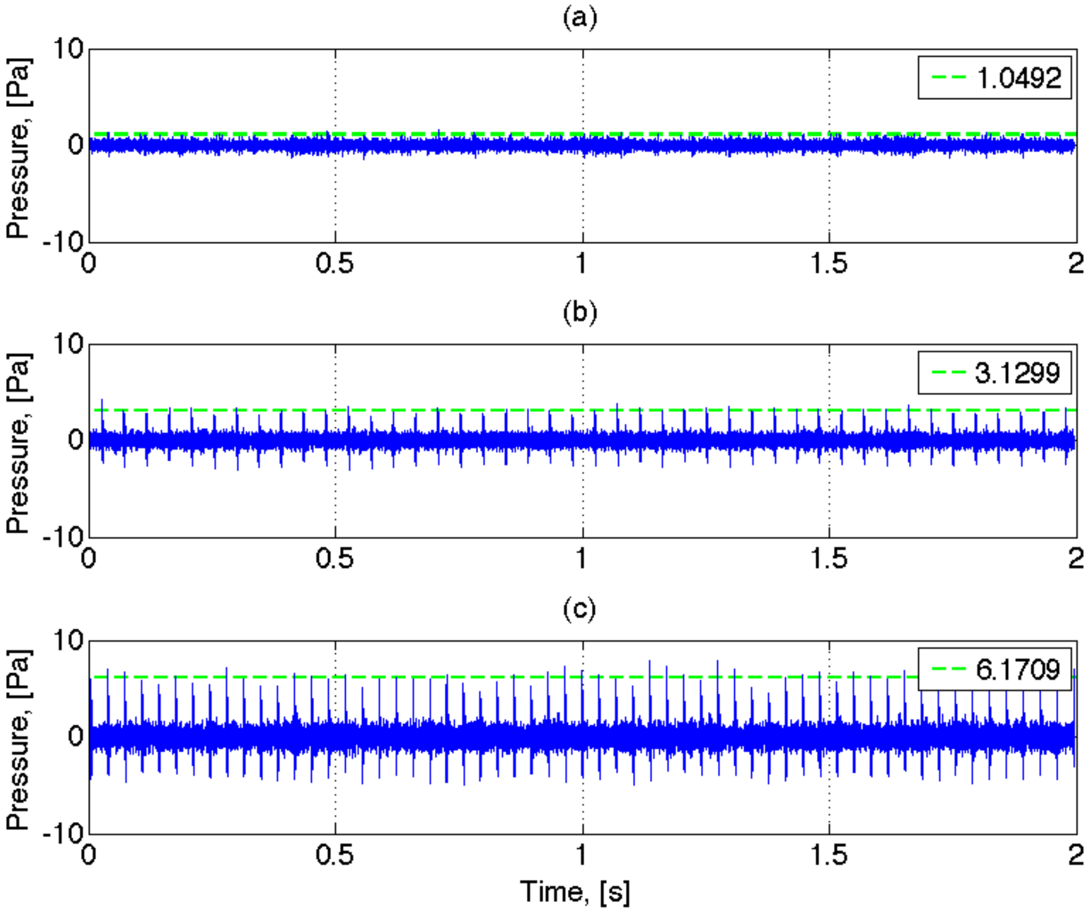

Figure 5.33 Time history of the leading edge signal from the tyre with the 'wide cavity' for different speeds including average peak level: (a) 19 km/h; (b) 31 km/h; and (c) 41 km/h

The average maximum peak amplitudes of the tyre with the 'wide cavity' are presented in Figure 5.33 and summarised in Table 5.21. In comparison to the results obtained by the tyre with the ‘long cavity’ from Table 5.16 these average amplitudes are significantly higher. The higher level could be explained by the orientation of the cavity. The length of the ‘wide cavity’, in respect to the rotation of the tyre, is only half the length of the ‘long cavity’. Thus, the amount of time needed for the air to evacuate the ‘wide cavity’ is also only half of the amount as for the ‘long cavity’. This shorter time could result in higher air speeds, hence more noise generation. The maximum pressure values however result in no obvious relationship of the ‘wide cavity’ to the ‘square cavity’ in respect to sound radiation at the leading edge. Whereas the ‘long cavity’, in comparison to the ‘square cavity’, generated about half the maximum amplitude pressure at the leading edge. The results obtained for the ‘wide cavity’ when compared to each other are promising, only the average of the 19 km/h recording seems to be low in comparison to 31 km/h and 41 km/h.

	19 km/h	31 km/h	41 km/h
Number of peaks	27	38	59
Average value [Pa]	**1.0492**	**3.1299**	**6.1709**

Table 5.21 Number and average amplitude values of peaks taken from **Figure 5.33** of the leading edge signal of the tyre with the ‘wide cavity’

Figure 5.34 shows the example events at the leading edge for the tyre with the ‘wide cavity’. Remarkable for this ‘wide cavity’ is the shape of the peak. This time it is starting much earlier with a significant low-pressure part at the beginning. The end of the event in comparisons to the ‘long cavity’ is not as defined, it more or less settles down to around zero pressure. Defining the end value of the process, when the cavity is completely covered, is not as exact as it is for the other signals. The red lines in Figure 5.34 mark the beginning and end points chosen for the averaging process. The resulting values are summarised in Table 5.22. A maximum difference of 7.299 Pa and a minimum of 6.046 Pa is measured that is a significant variation. For this signal it would be more appropriate to measure the minimum at the beginning of the signal, because this is more strongly defined, however a comparison to the other values in the sections before would not be possible in that case.

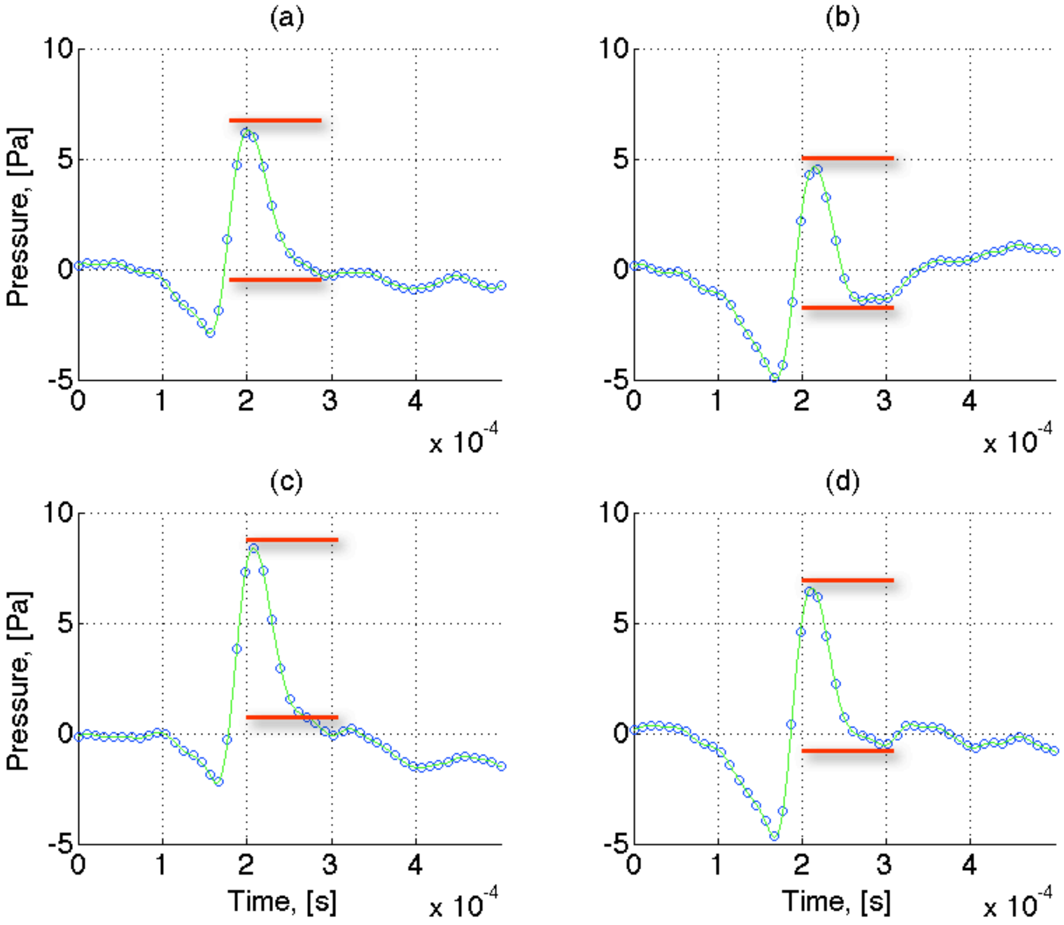

Figure 5.34 Four different example peaks of the leading edge signal at a tyre speed of 41 km/h generated by the ‘wide cavity’

	(a)	(b)	(c)	(d)
Peak, [Pa]	6.292	4.645	8.387	6.567
Bottom, [Pa]	0.090	-1.401	1.088	0.108
Difference, [Pa]	6.202	6.046	7.299	6.459
Average, [Pa]	**6.501**			

Table 5.22 Peak value calculation for the leading edge signal of the tyre with the ‘wide cavity’ at 41 km/h

Examples of the lower speed measurements of 31 km/h are shown in Figure 5.35. The shape of the peak is similar to the one for the higher speed. Table 5.23 displays the collected maximum and minimum values from Figure 5.35. The calculated difference of the peaks is between 2.659 Pa and 3.558

Pa. This leads to an average of 3.206 Pa, which is slightly higher than the average of the whole signal of 3.129 Pa, obtained by the computer.

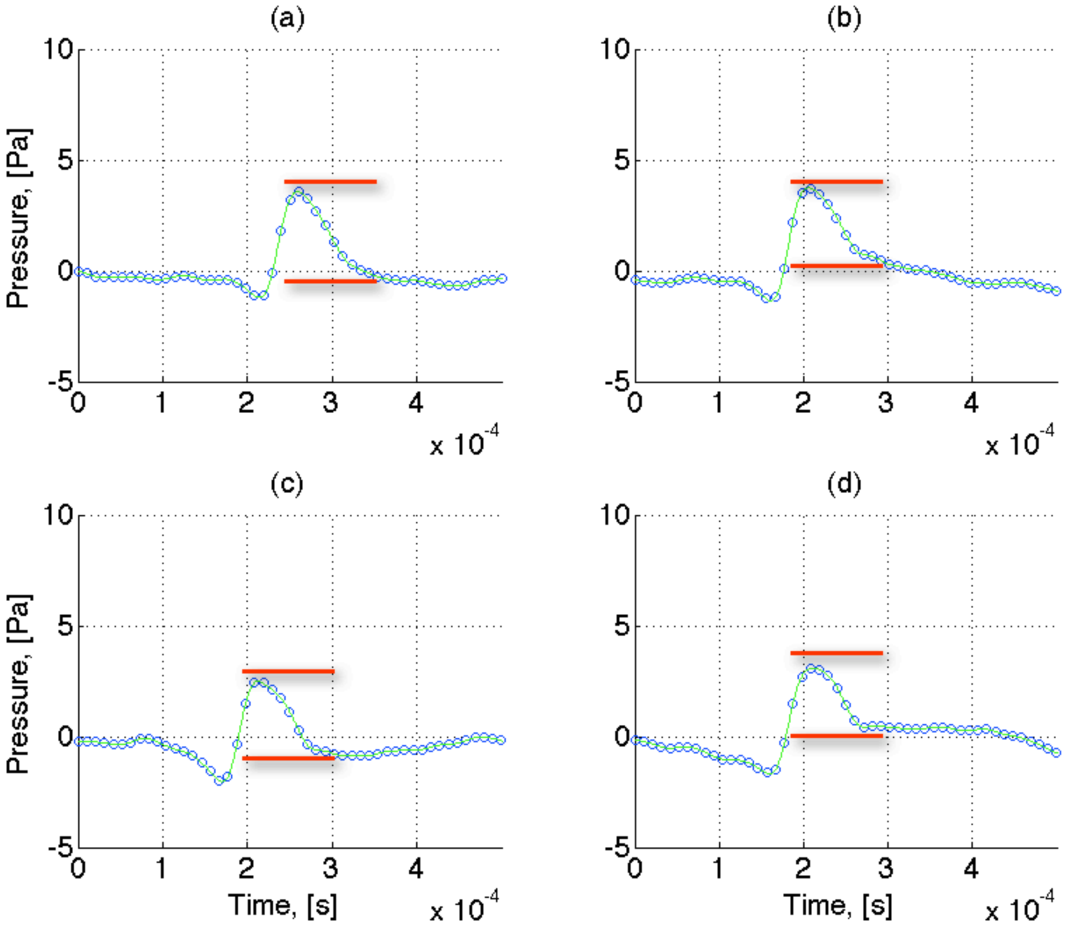

Figure 5.35 Four different example peaks of the leading edge signal at a tyre speed of 31 km/h generated by the 'wide cavity'

	(a)	(b)	(c)	(d)
Peak, [Pa]	3.558	3.741	2.491	3.079
Bottom, [Pa]	0.000	0.326	-0.700	0.420
Difference, [Pa]	3.558	3.415	3.191	2.659
Average, [Pa]	**3.206**			

Table 5.23 Peak value calculation for the leading edge signal of the tyre with the 'wide cavity' at 31 km/h

The last measurement carried out for the tyre with the 'wide cavity' was for the tyre speed of 19 km/h. As previously mentioned the average value of the whole signal does not deliver a satisfactory value. Taking a closer look at the actual signal recorded at the event when this cavity hits the road surface shows that the shape of the event differs a lot from the ones seen before. This low tyre speed results in a double peak at the leading edge of the tyre with the 'wide cavity', as shown for all the four examples drawn in Figure 5.36. Thus, the slow speed might allow the air in the cavity to generate a more complex fluctuation. There could be two waves travelling through the cavity one in the direction of rotation and another one perpendicular to that, resulting in a double pressure peak. Beforehand only one wave travelling in the direction of rotation was assumed.

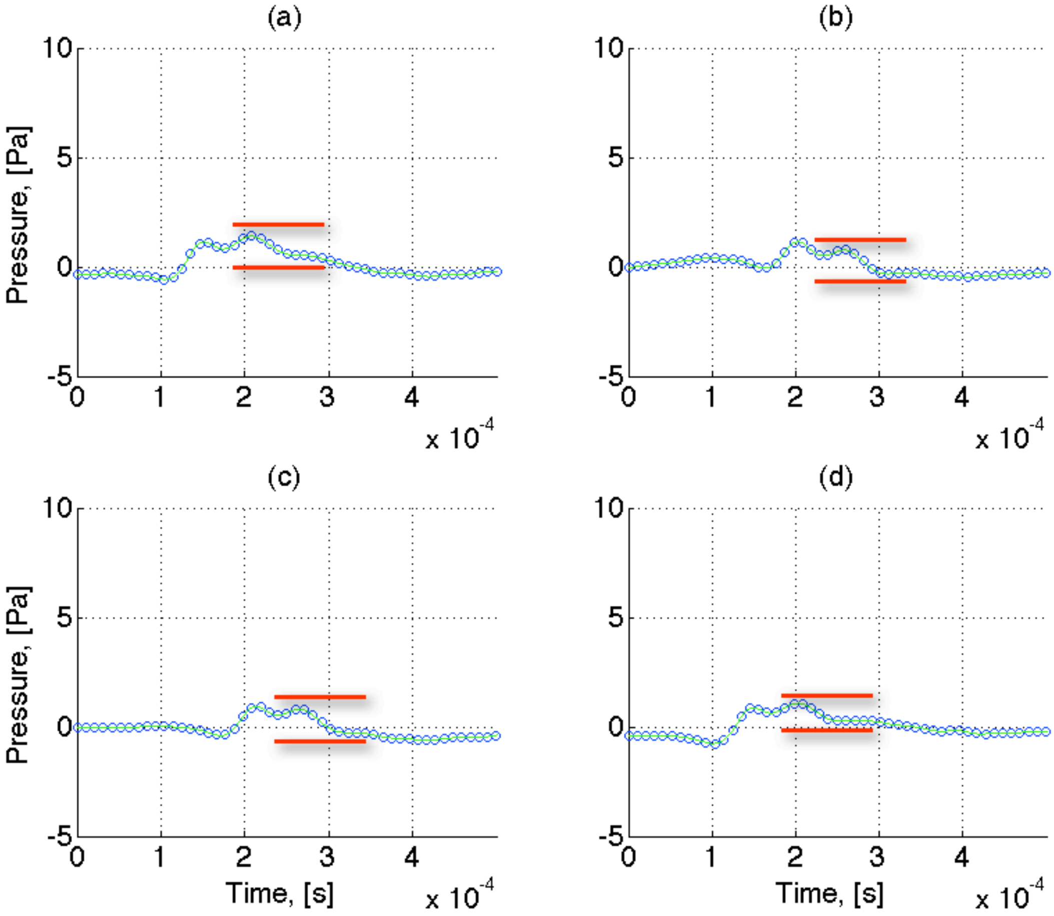

Figure 5.36 Four different example peaks of the leading edge signal at a tyre speed of 19 km/h generated by the 'wide cavity'

The last maximum of each event in Figure 5.36 is taken for the average measurement procedure, because this is closer to the end of the event. The values taken from Figure 5.36 are combined in Table 5.24. The highest difference value is 1.151 Pa and the lowest is 0.827 Pa. By adding the other two examples, an average value of 0.984 Pa is gained. This, however, is lower than the average taken from the whole signal that is 1.049 Pa.

	(a)	(b)	(c)	(d)
Peak, [Pa]	1.399	0.767	0.938	1.077
Bottom, [Pa]	0.521	-0.312	-0.213	0.250
Difference, [Pa]	0.878	1.079	1.151	0.827
Average, [Pa]	**0.984**			

Table 5.24 Peak value calculation for the leading edge signal of the tyre with the 'wide cavity' at 19 km/h

Table 5.25 shows a summary of all values from the tables in this section. The highest tyre velocity of 41 km/h is used as the reference speed for the other recorded velocities. The average values of the whole time history found by the computer are compared to the ones taken manually from the example events. Comparing 31 km/h to 41 km/h leads to a difference of 0.8 Pa (11 %) for the computational method and to 0.9 Pa (13 %) for the manual method. The main challenge is to find the right end point of the event (when the cavity is fully covered by the road). For the low speed of 19 km/h a slightly higher difference of 1.3 Pa (20 % deviation) and 2 Pa (30 % deviation) is obtained when compared to 41 km/h.

	41 km/h	31 km/h	19 km/h
Average, [Pa]	6.171	3.130	1.049
Speed factor	*1*	$\left(41/31\right)^2$	$\left(41/31\right)^2$
Result, [Pa]	**6.171**	**5.475**	**4.885**
Deviation, [%]		*-11.3*	*-20.8*
Manual average, [Pa]	6.501	3.206	0.984
Speed factor	*1*	$\left(41/31\right)^2$	$\left(41/31\right)^2$
Result, [Pa]	**6.501**	**5.608**	**4.582**
Deviation, [%]		*-13.3*	*-30*

Table 5.25 Calculated peak amplitudes for the two lower speeds in comparison to the reference speed of 41 km/h for the tyre with the 'wide cavity'

Figure 5.37 summarises the comparison of the three different speeds. The example event for 41 km/h is shown in blue, 31 km/h is red and 19 km/h is drawn in green. In Figure 5.37a the different original examples are overlaid and shifted so they end at the same time. Figure 5.37b shows the same graphs but in this case the lower speed signals are multiplied by the squared speed difference to 41 km/h as taken from Table 5.25. By comparing the signal of 41 km/h to 31 km/h a perfect overlay is shown. The signal generated at 19 km/h has a different shape as previously shown, a double peak is measured which makes the comparison difficult. However, the main amplitude of the signal approaches the maximum of the other two. In the next section these results are compared against the models available for the leading edge signal of a tyre.

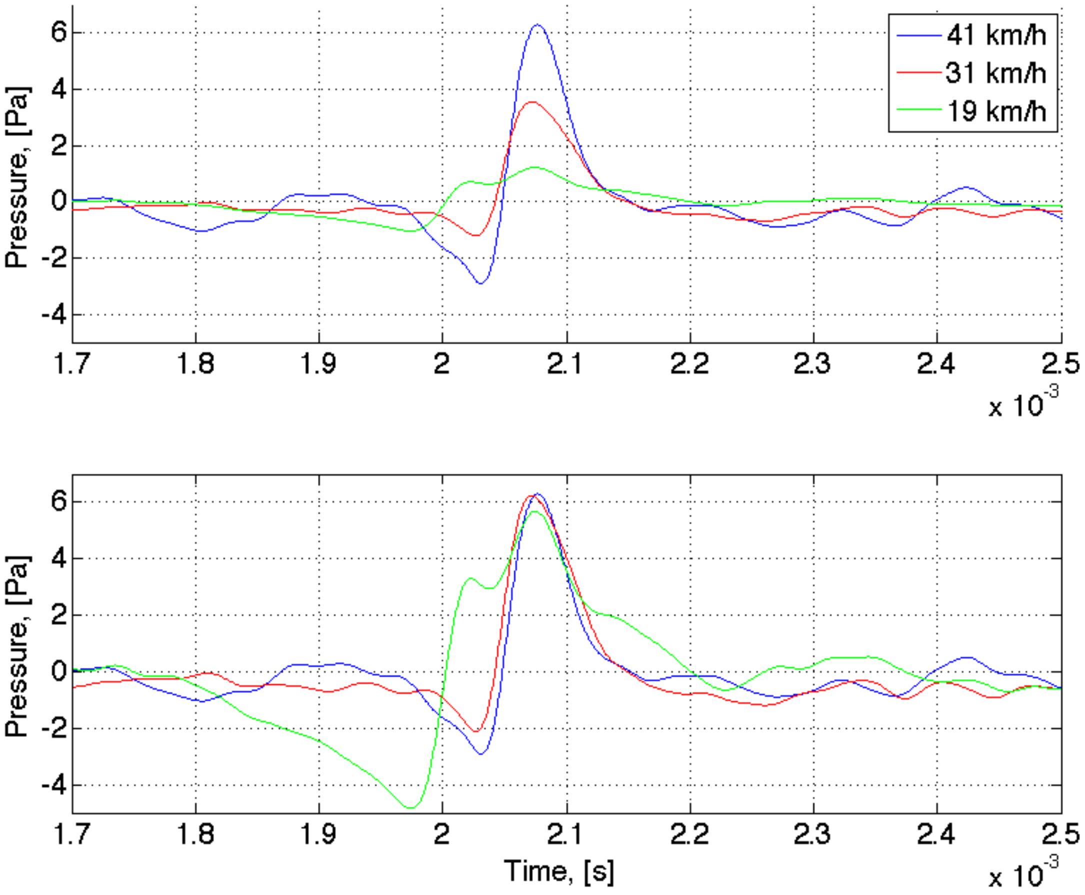

Figure 5.37 Average peak of the leading edge signal from the tyre with the ‘wide cavity’ for the three different speeds: (a) normal recordings; and (b) slower velocity signals multiplied by the speed factor

5.4. Comparison of the effect of cavity geometry

After this analysis of pulse height and duration of the leading edge signal for different types of cavities the results are compared to the models introduced in Chapter 3. First of all the signals of the different cavities are compared to each other, to investigate into the cavity dimensions and resulting noise generation. Figure 5.38 shows the events combined for the circular cavities at the top and the rectangular cavities at the bottom for a tyre speed of 41 km/h. For the circular cavities in Figure 5.38a it is noticed that the ‘large cavity’ produces a sound at the leading edge that is about four times higher than the one produced by the ‘small cavity’. However the duration (or frequency) of the peak is exactly the same (0.05 ms) and does not depend on the cavity dimension. A connection between cavity dimensions and sound radiation cannot be found for those cavities, mainly because all three dimensions of the cavities (length, width and depth) are different.

For a comparison of cavity geometry and noise generation the rectangular cavities are introduced in Figure 5.38b. All peaks have the same duration in time, also a duration of about 0.05 ms. This is remarkable because the length in the direction of rotation of the ‘wide cavity’ is only half the amount in comparison to the ‘long cavity’ and the ‘square cavity’ respectively. The tyre with the ‘square cavity’ generates the highest sound pressure amplitude (9.4 Pa) at the leading edge. The tyre with the ‘long cavity’ generates half of that sound pressure (4.7 Pa). The only difference in the geometry in between both cavities is the width. The ‘square cavity’ has double the width of the ‘long cavity’ hence double the volume. Thus a linear relationship between the width of a cavity and the maximum pressure amplitude of the leading edge signal can be found. For the ‘wide cavity’ it is different, despite having the same volume as the ‘long cavity’ the sound radiation is significantly higher. By comparing the dimensions and sound radiation of the ‘long cavity’ to the ‘wide cavity’, the relation between the peak amplitudes of the signal and cavity length is found to be $2 \cdot \sqrt{L}$.

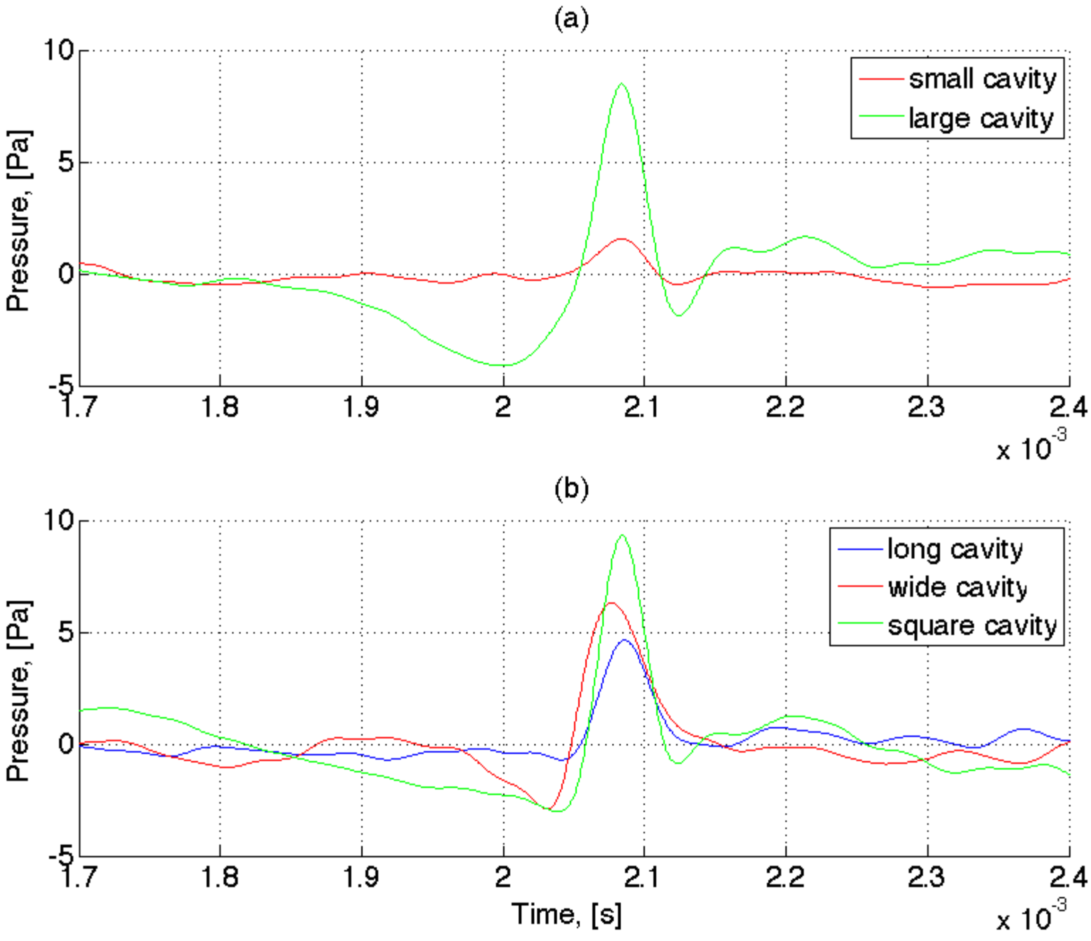

Figure 5.38 Leading edge signal example events of the different cavities at the same tyre velocity of 41 km/h: (a) circular cavities; (b) rectangular cavities

Similar results to those discussed previously are obtained for the lower speed of 31 km/h shown in Figure 5.39. Here the relation between the signals generated is equivalent to the higher speed measurements, this is due to the square velocity connection in between the peak amplitudes for all the introduced cavities. Only the shape of the event is not as sharp as with the higher speed previously shown. The shape of the peaks shown in this Dissertation is similar to measurements conducted by Ronneberger [Ronneberger, 1984] and to results of simulations presented by Conte [Conte and Jean, 2006] for a cavity in the road surface. So the peak itself can be seen as a real effect and is not a creation of the filter technique applied. Comparing filtered and unfiltered signal also confirmed this. However, Ronneberger and Conte do not mention a relation between the signal amplitudes and volume of a cavity or the speed of a tyre.

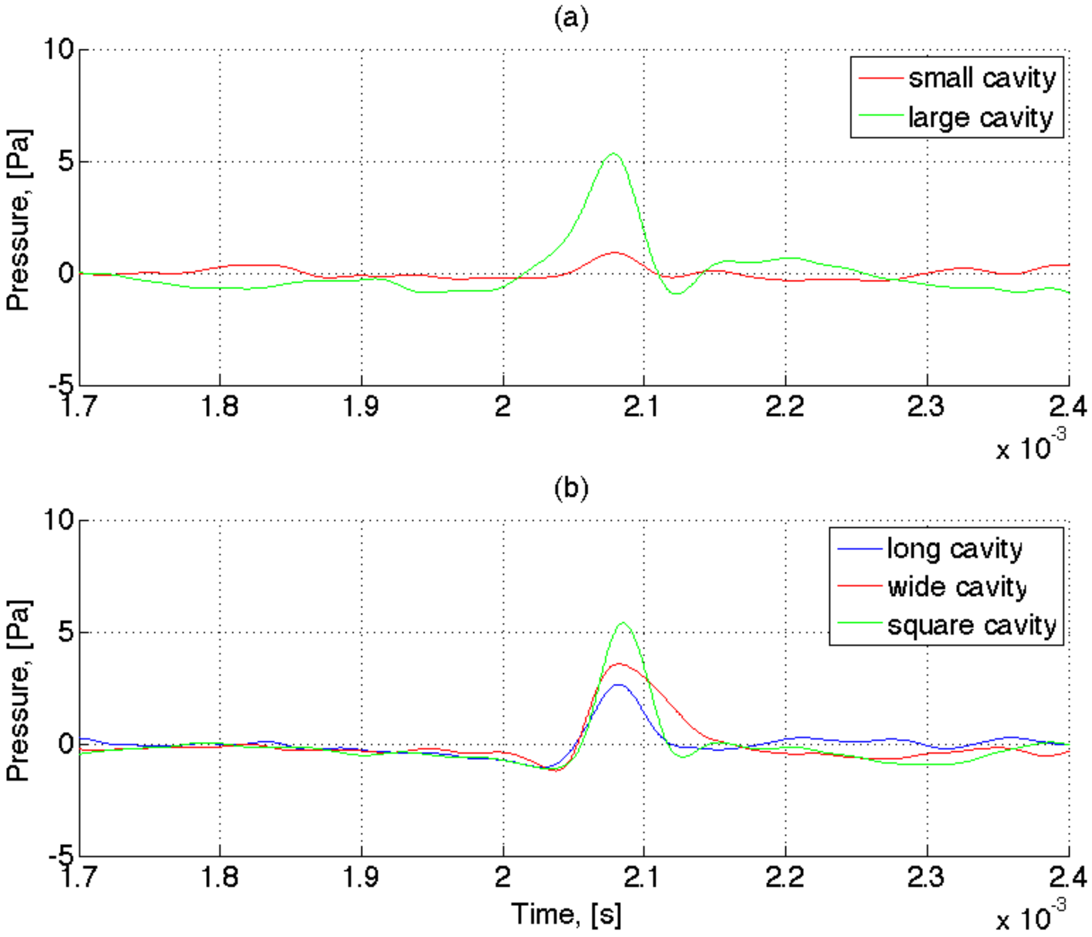

Figure 5.39 Leading edge signal of the different cavities at the same tyre velocity of 31 km/h: (a) circular cavities; (b) rectangular cavities

5.5. Frequency analysis

Hayden [Hayden, 1971] introduced the first theory regarding air pumping and therefore his idea is always referred to when this effect is analysed. As described in detail in Chapter 3 Hayden proposed a model based on the monopole radiation theory, to predict the sound pressure generated by a tyre with cavities. This sound pressure is predicted at the frequency of excitation for the monopole, calculated with Equation (A1.5). Where v is the forward velocity that the dynamometer or tyre is driven at and x_{circ} is the circumferencial distance of the cavities. In our case there is one cavity only in the whole tyre. Thus the circumference of the tyre of 0.38 m is taken as the cavity distance. Table 5.26 shows the frequencies of reoccurrence for the tyre cavity as well as for the dynamometer drum (1.570 m circumference) at the different speeds analysed.

	41 km/h	31 km/h	19 km/h
Frequency tyre, [Hertz]	29.9	22.7	13.9
Frequency dynamometer, [Hertz]	7.3	5.5	3.4

Table 5.26 Repetition frequencies of the cavity and the chassis dynamometer in dependence of tyre speed

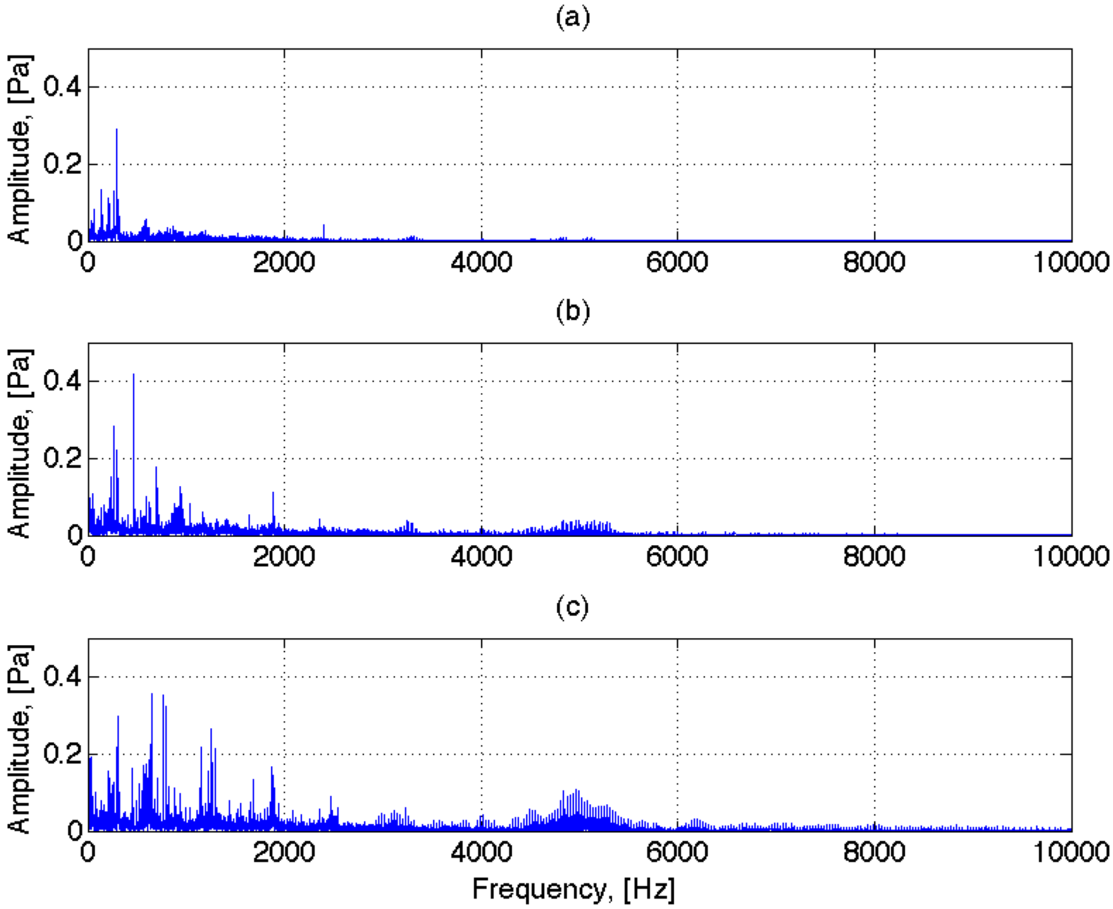

Figure 5.40 Fast Fourier Transform of leading edge signal of the tyre with the 'large cavity': (a) 19 km/h; (b) 31 km/h; and (c) 41 km/h

As previously discussed the low frequency region of the recorded signals is dominated by the unwanted noise of the chassis dynamometer driving mechanism. Due to the long distance in between the cavities (only one per tyre) the frequency of reoccurrence of each cavity falls into this low frequency region. Thus, at the fundamental reoccurrence frequencies named in Table 5.26 no peak can be identified in the frequency analysis of the time signal at the leading edge. Figure 5.40 shows the Fast Fourier Transform of the leading edge signal recorded from the tyre with the 'large cavity'. As shown for all the three different tyre speeds the main area of interest lies between 4000 and 6500 Hertz. The single peak at the leading edge cannot generate this broadband frequency area. It is in fact due to the oscillations at the trailing edge that were recorded by the leading edge microphone as well, as shown in Figure 5.8.

The structure of the frequency plots in between 4000 and 6500 Hertz consists of a high number of single peaks that build the envelope broadband frequency area. A magnified view of the spectrum in between 4800 and 5200 Hertz is shown in Figure 5.41. At the top the frequency analysis of the 19 km/h signal is plotted. The distance between the low amplitude peaks correspond perfectly to the repetition frequency of the cavity hitting the chassis dynamometer drum shown in Table 5.26. Figure 5.41b shows the magnified 31 km/h recording. The high level peaks correspond to the repetition frequency for the cavity hitting the drum at 22 Hertz. Also the quarter harmonics in between those peaks are present that could be generated by the chassis dynamometer as explained by Chang et al. [Chang et al., 1997]. The tyre/chassis dynamometer drum ratio is about four: this would support Chang's theory. Similar observations can be made for the frequency content of the high speed of 41 km/h Figure 5.41c, showing very high amplitudes.

Conclusively, the repetition frequency can be picked up in the frequency spectrum of the leading edge signal, but only harmonics of it and not the fundamental. For this reason the initial model presented by Hayden from Equation (3.4) cannot be applied, because it defines the amplitude pressure at the fundamental of the repetition frequency. In addition to that the approach from Samuels [Samuels, 1979] cannot be used either, because the first harmonic cannot be found in the frequency spectrum of the leading edge signal.

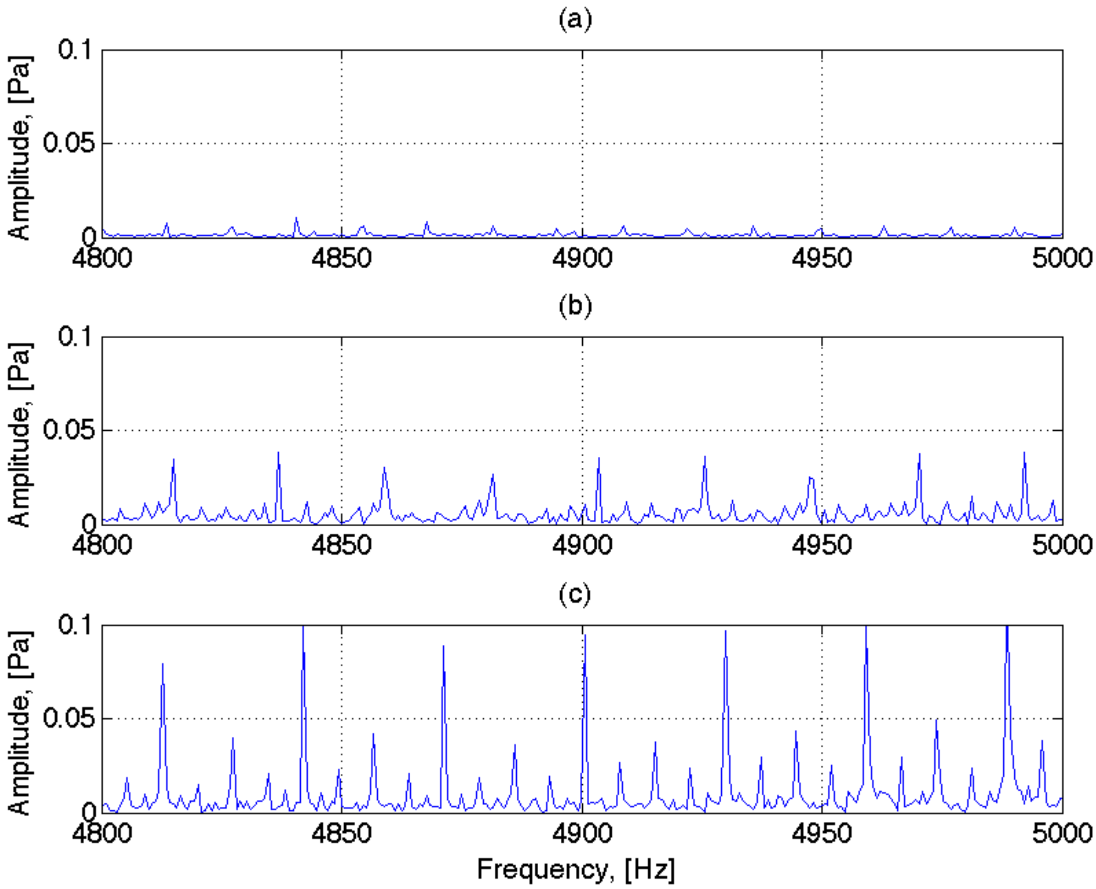

Figure 5.41 Magnified Fast Fourier Transform of leading edge signal of the tyre with the ‘large cavity’: a) 19 km/h; b) 31 km/h; and c) 41 km/h

5.6. Comparison of theoretical models

5.6.1. Monopole theory

This leaves the last approach from Plotkin et al. [Plotkin et al., 1979], where the initial monopole idea from Hayden is transformed to calculate the displaced volume of a cavity or groove when entering the contact patch. According to Hayden this process is initiated as soon as the edge of the cavity touches the road, introducing a squeezing process, where the air is squeezed out continuously until the whole cavity is covered. Table 5.27 shows the closing times in dependence of cavity length *L* (in circumferential direction) and rotational speed.

		Cavity length (*L*)		
		9 mm	4.5 mm	2.5 mm
Speed	41 km/h	$7.90*10^{-4}$ s	$3.95*10^{-4}$ s	$2.19*10^{-4}$ s
	31 km/h	$10.45*10^{-4}$ s	$5.23*10^{-4}$ s	$2.90*10^{-4}$ s
	19 km/h	$17.05*10^{-4}$ s	$8.53*10^{-4}$ s	$4.74*10^{-4}$ s

Table 5.27 Duration for the cavity to be completely closed in dependence of cavity length and rotational speed of the tyre

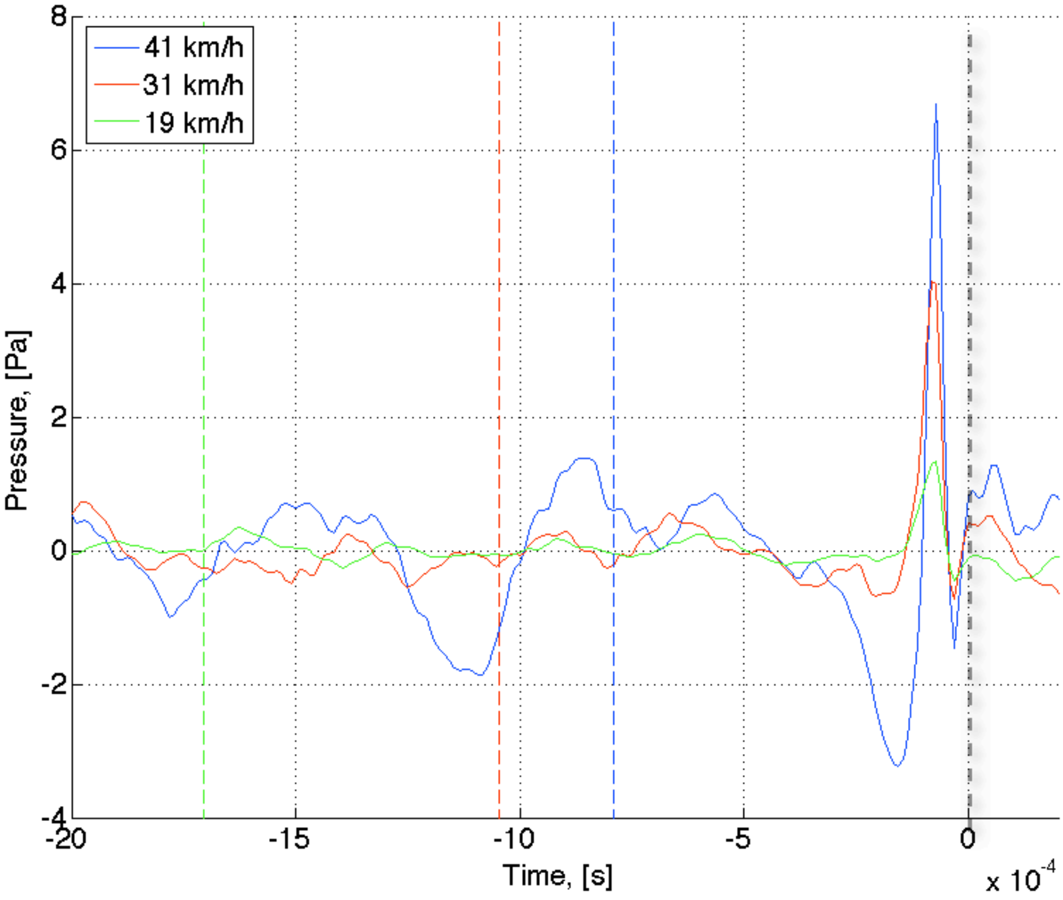

Figure 5.42 Zoomed example event at the leading edge of the tyre equipped with the 'large cavity' for the three different speeds, the time when the cavity edge touches the road is marked

In Figure 5.42 one example event of the leading edge of the tyre with the 'large cavity' is shown for each of the three different speeds recorded. A possible initiation of the closing time in dependence of the tyre speed is marked with the coloured dashed line in accordance to the speed it is for. The cavity is assumed to be fully closed when the event is finished; this position is marked by the black dashed line at time zero on the x-axis. The blue line indicates the start for the tyre speed of 41 km/h. Due to noise in the signal identification of a start of the process that indicates an air movement out of the cavity at that time is impossible. However, as described previously there is a pressure drop in the signal from the dashed line on so the theory of Hayden could be supported. But a negative pressure is recorded that indicates air moving away from the microphone. For the other speeds the closing time of the cavity is of such a big order, so that due to noise in the signal no pressure drop is noticeable at the assumed beginning.

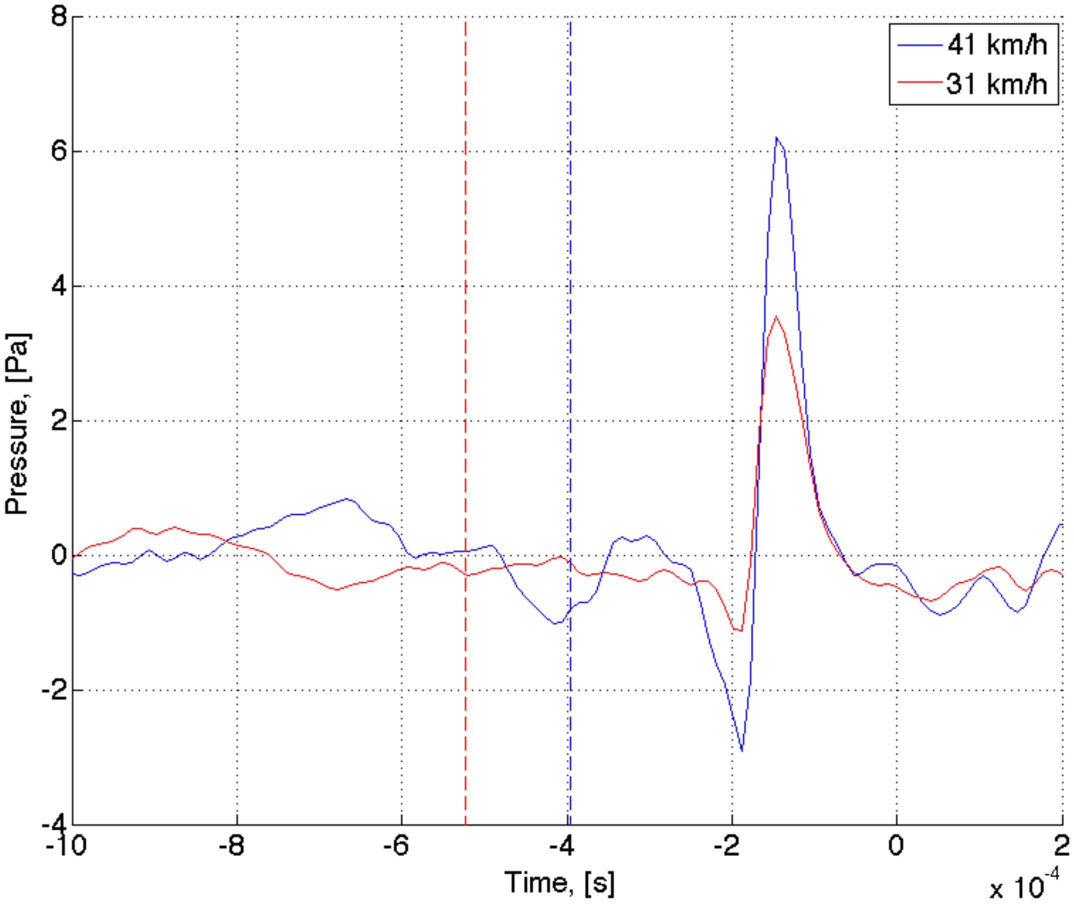

Figure 5.43 Zoomed example event at the leading edge of the tyre equipped with the ‘wide cavity’ for two different speeds, the time when the cavity edge touches the road is marked

Hence for the setup used the speed needs to be significantly high to see the initiation of the event at the leading edge. Nevertheless Plotkins's theory is checked with a signal to identify if it applies to the measurements conducted for this Thesis. Instead of going for higher speeds, because this would introduce more noise, the 'wide cavity' with a shorter length *L*, hence quicker closing time, is chosen.

Figure 5.43 shows the event at the leading edge for the tyre with the 'wide cavity'. This cavity is just half the length of the 'large cavity', thus resulting in half the closing time, see Table 5.27 for the exact times. Only 31 km/h and 41 km/h are shown because the 19 km/h reading does not give a satisfying pressure drop. Again the vertical dashed red line marks the assumed time when the cavity starts to cover up for the tyre speed of 31 km/h. Slightly later this happens for the speed of 41 km/h as indicated by the blue dashed line. Similar behaviour for both of the signals can be identified. In comparison to the signal produced by the 'large cavity' the negative pressure part is much more developed, even for the lower speed of 31 km/h.

As stated in Chapter 3 Plotkin and his co-authors measured the volume change in a groove during a slow motion experiment, with the amount of fluid squeezed out of a bladder that was located in the groove with one open end. The results were then linked to air pressure fluctuations measured on the side of the leading edge of the tyre at higher speed. For our experiments no such volume change measurements were possible. Nevertheless, the recorded pressure data is transformed into the resulting volume change based on Equation (3.8) [Plotkin et al., 1979], to verify if this results in a realistic volume change. Equation (3.8) is transformed so it can be solved for the second derivative of the volume. Also a factor of 2 is implemented because of a different microphone location in front of the tyre instead of at the side (only one mirror source underneath the road surface). Thus the second derivative of the volume change becomes

$$V'' = \frac{p \cdot 2\pi \cdot r_{mic}}{\rho \cdot v^2}. \tag{5.1}$$

In this equation also the speed has an exponent of two that is equivalent to the proportionality of pressure amplitude and speed found during the experiments. As noted, the second derivative of the volume is needed to calculate the resulting pressure. This means an integration of the pressure signal to obtain the volume change. A spatial way of integration is programmed into the software MATLAB and applied to the time signal. The results are shown in the next figure.

In Figure 5.44a the signals from Figure 5.43 are repeated just cut to the exact length of the closing time for the cavity, depending on the tyre speed. The green line shows the 41 km/h recording and the blue dashed line the 31 km/h recording for the tyre with the wide cavity. Figure 5.44b shows the same signal just over distance, not time, in this case the signals have the same length according to the length of the cavity of 4.5 mm. The bottom part of the figure shows the results of the spatial integration and so the volume change over time and distance, respectively. The graph of the displaced volume shows a similar shape for both speeds. Actually the minimum value should be at the same level, but due to noise in the signal there is a slight deviation. The minimum value reached by the integrated signal is about -$3.5*10^{-9}$ m^3. This corresponds to a volume change of 1.5 % when compared to the actual cavity volume of $222*10^{-9}$ m^3. In terms of an expected volume change of 4.2 % calculated in the Appendices (A6) this is significantly lower (10 % volume change is normally assumed in the literature [Hayden, 1971]). In addition to that the volume is of negative order that was not obtained by Samuels. However, both signals result in a similar minimum value that could be seen as the initiation of the dominant positive pulse at the leading edge.

The final value reached by the volume calculation in Figure 5.44 is different for both signals. This is explained by the peak duration. When the cavity impacts onto the road surface there is an airwave generated in the cavity. On the outside this is recorded as a negative pressure that yields to a positive pressure peak at the end. This peak occurs for all the cavities, as shown before. The amplitude of the event is dependent on the speed squared but has the same duration for all speeds. Thus, the peak at the end of the signal is not connected to Hayden’s theory, because its length does not change with speed. The monopole theory is only valid until this sharp peak starts. Until then the volume calculation would result in a similar volume change, because it is assumed that the process for the lower speeds starts earlier. However, this would result in a negative volume change and this is not the way Hayden suggested it. If the positive peak only would be considered for the volume calculation the volume change would be of greater magnitude for higher speeds because the amplitude changes, but not the duration. Gagen [Gagen, 1999, 2000] introduced a theory with a wave travelling through the groove after the initial impact and being squeezed out at a later stage. This theory is compared to our measured results for the cavity as well.

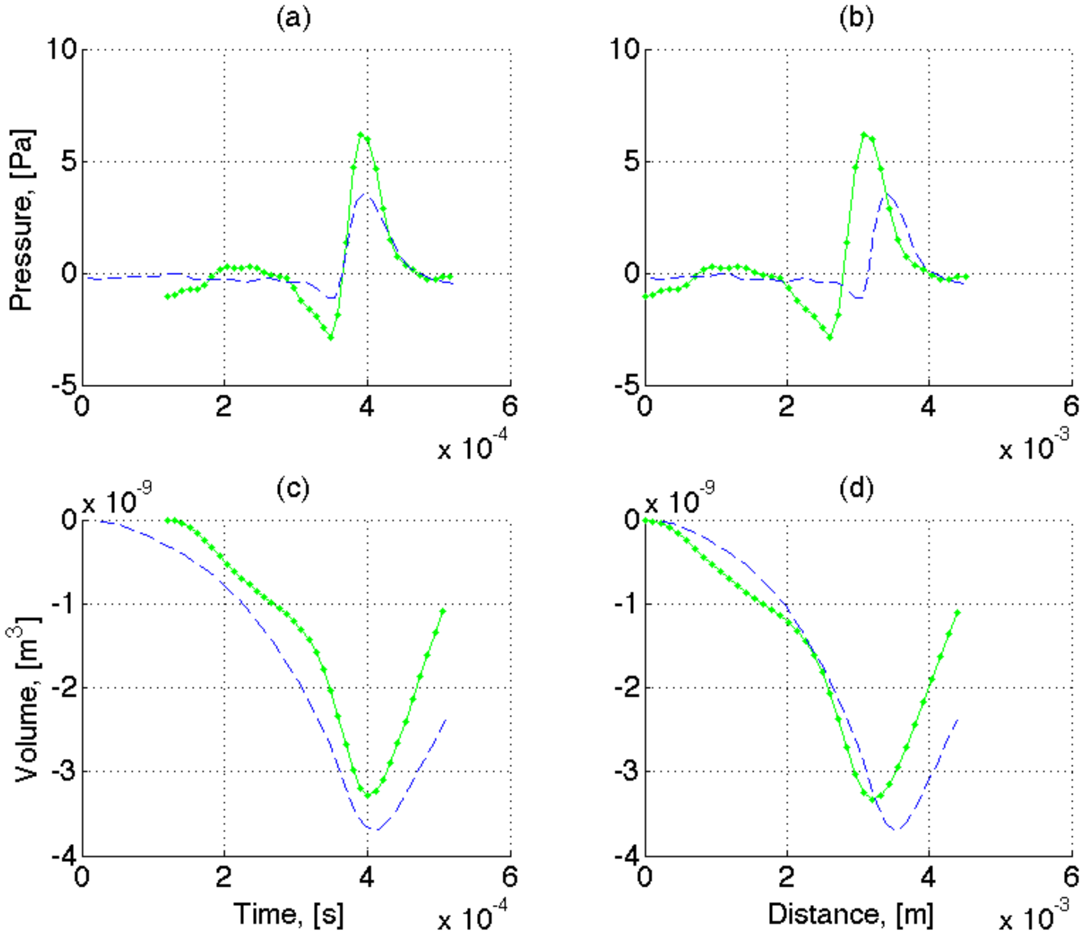

Figure 5.44 Sound pressure pulses recorded at the leading edge for the tyre with the ‘wide cavity at 41 (dotted green) and 31 km/h (dashed blue) over: (a) time; and (b) distance; and prediction of the displaced cavity volume over: (c) time; and (d) distance

5.6.2. Gagen model

The model derived by Gagen is based on computer simulation and has not yet been verified by experiments. In addition to that it was initially developed for grooves with one open end. For our case this does not apply because the results presented are from cavities in a tyre tread only. Gagen assumes a wave travelling in direction of the width *W*, towards the exit of the groove (perpendicular to the tyre rotation) hence, a change of volume in the length of the groove. In this Thesis a change of volume in the depth *D* due to the impact onto the road and a wave travelling in the direction of the tyre rotation is assumed. Therefore Equation (3.12) is changed to

$$E = \frac{\rho \cdot W \cdot A^3 \cdot L^3 \cdot v^2}{2\left(1 - \frac{A}{D}\right) \cdot D^4}. \tag{5.2}$$

The tyre geometries are used in Equation (5.2) with the assumption of a 5 % volume change of the cavity when compressed by the load. This is chosen mainly because of investigations presented in the Appendices (A6). However, as previously mentioned the assumed volume change to be found in the literature is up to 10 %.

Table 5.28 lists the energy results of the Gagen model together with the maximum amplitude values from the investigations for the different types of cavities. All measured results show a velocity square relation for the cavity, this can also be seen for the energy, as the velocity is also squared in Equation (6.2). The other factor where energy and amplitude deliver a similar result is for the width of the cavity. When the results of the ‘square cavity’ are compared to the results of the ‘long cavity’ exactly half the amount of energy and also half the amplitude is generated by the long cavity. So the Gagen model and the measurements deliver similar results in this case. Only the results of the ‘wide cavity’ do not fit to Gagen’s model. This cavity actually generates more noise than the ‘long cavity’ but Equation (6.2) delivers a significantly lower energy radiation. The difference in energy generated by the ‘small cavity’ and the ‘large cavity’ is also too high in comparison to the measurement results. Although Gagen's model looked promising when comparing the results of the 'long cavity' and the 'square cavity' it cannot be successfully applied to all of the results presented from cavities in the tyre. The velocity relationship can be supported; the width relationship does deliver a satisfactory result as well. However Gagen's model does not deliver the right energy when the influence of the cavity length towards peak amplitude is tested. Therefore a different approach is presented to explain the phenomena happening at the leading edge of a tyre equipped with a cavity.

		41 km/h	31 km/h	19 km/h
Pressure and energy comparison	Large cavity, [Pa]	8.078	4.784	1.695
	Gagen model, [W]	$7.55*10^{-9}$	$4.32*10^{-9}$	$1.62*10^{-9}$
	Small cavity, [Pa]	*1.783*	1.024	0.209
	Gagen model, [W]	$0.13*10^{-9}$	$0.07*10^{-9}$	$0.03*10^{-9}$
	Square cavity, [Pa]	10.435	5.462	2.960
	Gagen model, [W]	$12.72*10^{-9}$	$7.27*10^{-9}$	$2.73*10^{-9}$
	Long cavity, [Pa]	4.581	2.715	0.952
	Gagen model, [W]	$6.36*10^{-9}$	$3.64*10^{-9}$	$1.37*10^{-9}$
	Wide cavity, [Pa]	6.501	3.206	0.984
	Gagen model, [W]	$1.59*10^{-9}$	$0.91*10^{-9}$	$0.34*10^{-9}$

Table 5.28 Comparison of maximum pressure amplitudes to the energy model presented by Gagen for the different types of cavities

5.6.3. Inverse air-resonant model

By comparing the measurement results in this project another route can be taken that explains the signal occurring at the leading edge. This is a visual approach and can be identified when the leading and trailing edge signals are compared to each other. As previously mentioned the chassis dynamometer generates high levels of unwanted noise, otherwise higher speeds could have been tested and so more data could be used for verification. However, the main process happening at the leading edge can be identified already with these low speeds. The signal at the leading edge consists of one peak, whose width is independent of the speed when the main shape of the peak is considered. The amplitude of the peak is the only speed dependent variable. Similar behaviour shows the trailing edge of the signal. Thus the next figure is composed where leading and trailing edge signal are overlaid. To produce this figure the leading edge signal is reversed and shifted towards the start of the trailing edge signal.

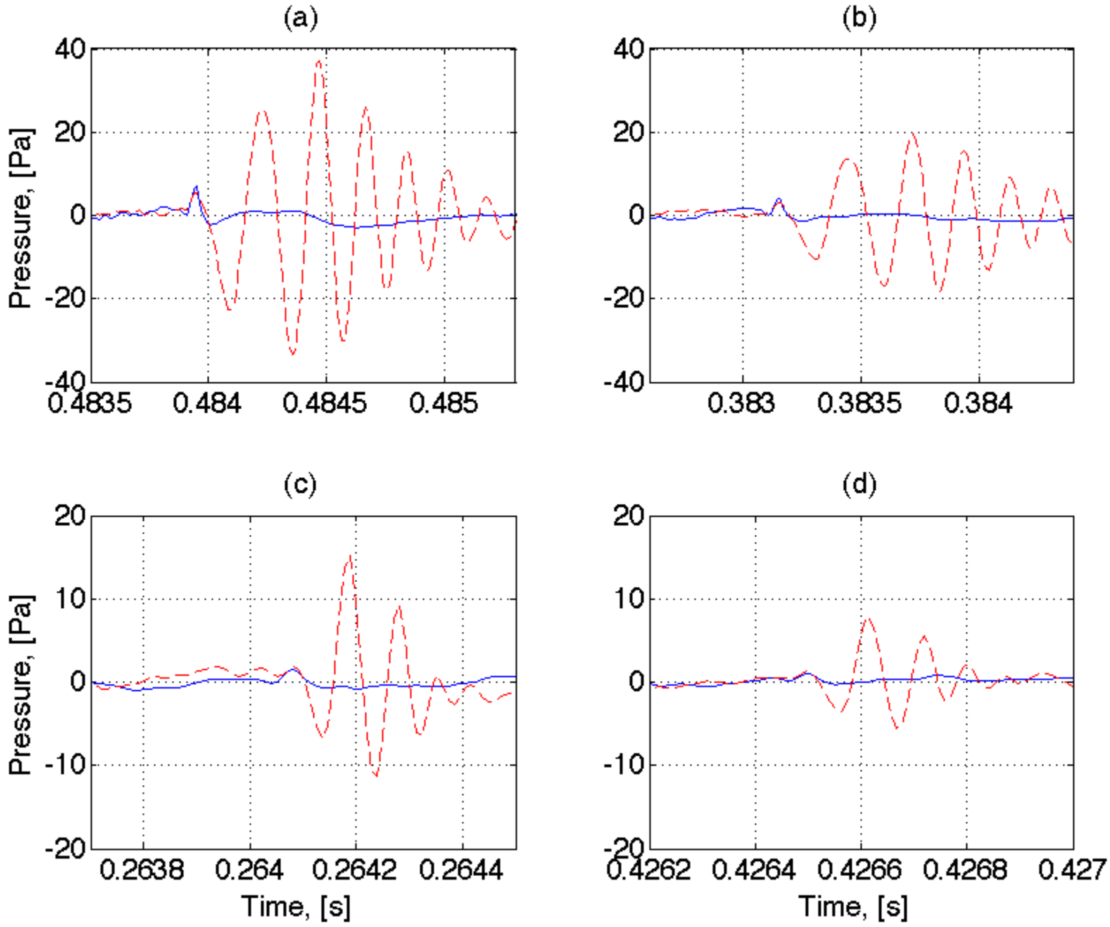

Figure 5.45 Overlaid leading and trailing edge signal for the tyres equipped with the circular cavities: (a) ‘large cavity’ at 41 km/h; (b) ‘large cavity’ at 31 km/h; (c) ‘small cavity’ at 41 km/h and (d) ‘small cavity’ at 31 km/h

Figure 5.45 shows this procedure done for the circular cavities. The shifted leading edge signal is drawn by the solid blue line and the trailing edge signal is displayed by the dashed red line. On the left hand side example events of 41 km/h are shown and on the right hand side the lower speed of 31 km/h. The top of Figure 5.45 shows an example event of the tyre with the ‘large cavity’. When overlaid the leading edge pulse shows a similar shape as the initial part of the signal at the trailing edge. The same visual approach can be applied to the tyre equipped with the ‘small cavity’ that is shown at the bottom of Figure 5.45.

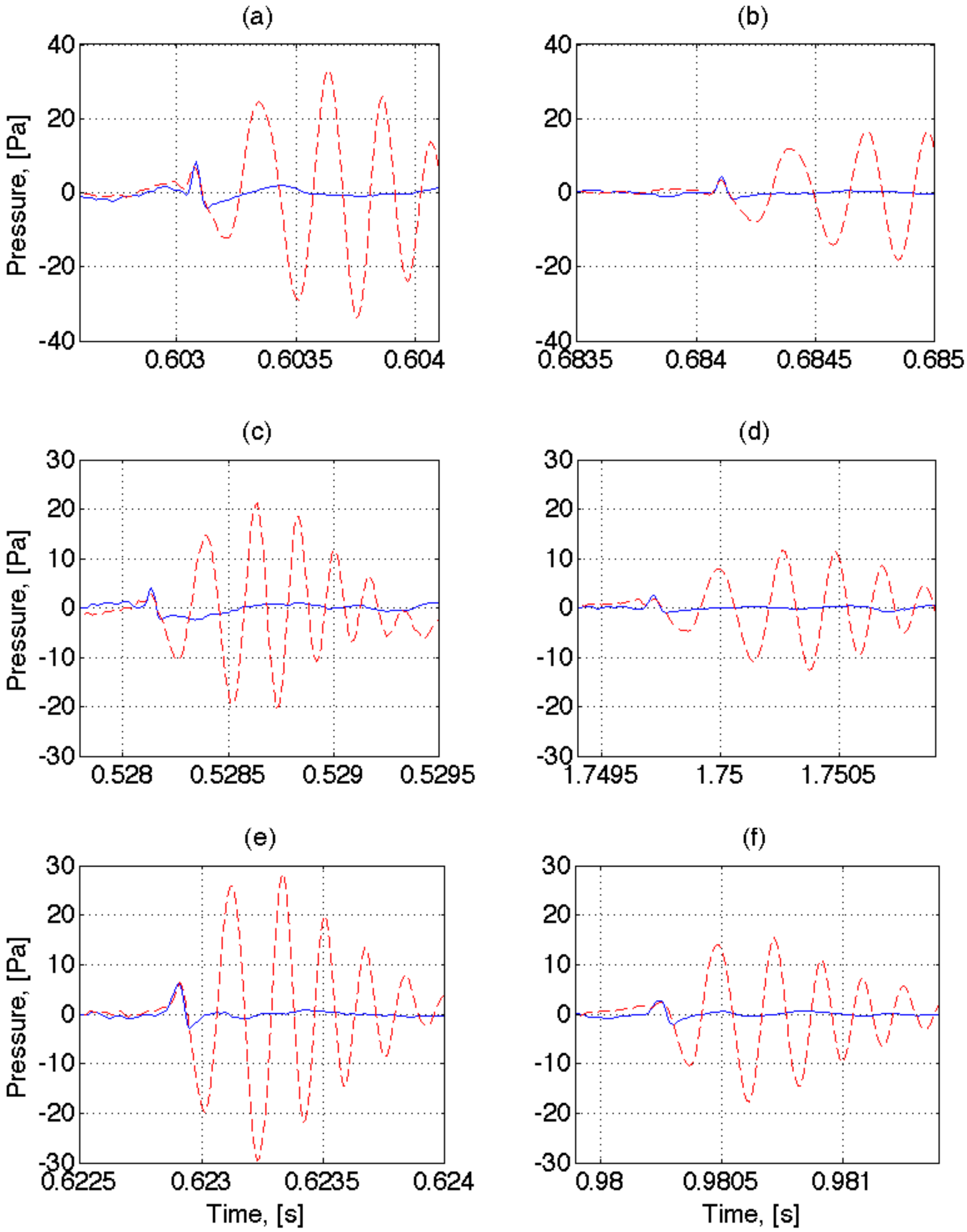

Figure 5.46 Overlaid leading and trailing edge signal for the tyres equipped with the rectangular cavities: (a) ‘square cavity’ at 41 km/h; (b) ‘square cavity’ at 31 km/h; (c) ‘long cavity’ at 41 km/h; (d) ‘long cavity’ at 31 km/h; (e) ‘wide cavity’ at 41 km/h and (f) ‘wide cavity’ at 31 km/h

Figure 5.46 shows example events of the tyres equipped with the rectangular cavities. At the top of this figure the results for the ‘square cavity’ are shown, in the middle an example signal produced by the ‘long cavity’ is plotted and the bottom results for the ‘wide cavity’ are drawn. Again leading edge pulse and initiation of the trailing edge signal overlay nicely, for all cavities and speeds shown. The only difference to the circular cavities is a sharper end of the leading edge signal, because of the shape of cavity.

The amplitudes of the leading and the trailing edge signal show not always a similar level the main reason for that is the influence of noise. Nevertheless, the shape at the end of the signal at the leading edge is similar to the beginning of the signal at the trailing edge. Thus the initial part of the air resonant radiation that dominates the trailing edge signal, as it is confirmed in Chapter 8 is also to be found at the leading edge. However, only when the cavity at the leading edge is nearly covered by the road, thus pressure in the cavity is built up sufficiently to initiate the resonator. This initiation time of the resonator is dependent on the speed and cavity dimensions and can be linked to the monopole theory, the shape of the pulse however is purely due to the air resonant radiation and a volume displacement of a cavity cannot be predicted in this case.

5.7. Conclusion

All the different measured types of cavities show a similar behaviour at the leading edge. It is found that the pressure peak amplitudes of the leading edge generated by the cavity on the road are proportional to the square of the speed of the rotating tyre. This can be confirmed by the literature where mainly sound pressure level is analysed as stated by Heckl [Heckl, 1986], Kim et al. [Kim et al. 1997] and Kuijpers and van Blokland [Kuijpers and van Blokland, 2001].

In these experiments the generated maximum pressure also seems to be linearly dependent on the width *W* of the cavity. The dependence of cavity length and generated sound is found to be $2 \cdot \sqrt{L}$. The duration in reference to time of the peak at the leading edge is the same for all cavities and speeds. It is not dependent on cavity size for the measurements presented, as proposed by Hayden initially. The peak amplitude relation is shown for the speed comparison from 31 km/h and 41 km/h and is expected for higher speeds as indicated by the results of the 'small cavity'. Only at low speeds some irregularities occur for wider cavities as the results of the tyre with the 'square cavity' and the tyre with the 'wide cavity' show.

The model presented by Hayden could not be applied to the signal at the leading edge. The volume displacement and resulting sound radiation theory from Plotkin et al. [Plotkin et al., 1979] are only valid for the low pressure part before the sharp peak starts. When this low pressure part is converted into volume change it results in similar volume fluctuation for different speeds, however, it is of negative order. Also the model presented by Gagen [Gagen, 1999 and 2000] for grooves with one open end in the tyre cannot be applied to the measurement results presented in this Thesis. However, the idea presented by Gagen seems plausible, because Gagen stated that the air behaves sluggishly when the first impact to the groove takes place. This can be confirmed by the measurement because only at the very end, when the cavity is nearly closed a pressure change can be measured. Guidelines are given for the created pressure amplitude at the leading edge in dependence of cavity dimensions. Also a connection between the leading and the trailing edge is presented that could explain the shape of the pulse at the leading edge and might reveal this as an inverse air resonant radiation phenomenon.

This air resonance is already generated at low speeds for a cavity in a tyre. At high speed the phenomenon is more visible, however the main difficulty during the measurements conducted in the facilities at Loughborough University proves to be the noisy chassis dynamometer. The generated background noise results in heavy fluctuations of the peak amplitude measured at the leading edge. To avoid this, as presented in here, the peak needs to be analysed in detail. Further irregularities in the measurements occurred because of the temperature of the tyre, as rubber stiffness changes when the temperature changes. Therefore it was tried to heat the tyre up beforehand, to have a similar temperature throughout the short measurement period for each speed.

It would be interesting to see what happens when the closing time of the cavity is so short that it reaches the duration of the pressure peak of the signal. As shown for the tyre with the small hole very high speeds are needed for this to happen that are out of the region of interest for normal driving conditions. After these presented results for the leading edge the contact patch and the trailing edge are investigated to see if similar relations between noise generation and cavity dimensions can be found.

Chapter 6

Results and discussion: contact patch

After the measurement analysis of the leading edge signal the tyres with a groove cut into the tread are considered. In this chapter the emphasis is mainly on the groove resonance that occurs in the contact area between tyre and road. However, also the event that occurs at the trailing edge after this resonance is looked into. Three different types of tread are used. These are: a large ‘square groove’, a ‘small groove’ and a ‘chevron’ type of groove. In the literature different groove sizes and their contribution to noise generation in the far field of the tyre have been covered widely already [Ejsmont et al., 1984]. In this Thesis the results of the grooved tyres are compared to those obtained by the tyres with cavity. This comparison is done to investigate into the air mechanisms generated by more realistic tyre treads.

6.1. Grooves

The first groove to be investigated is a square transversal groove. In comparison to the size of the tyre this groove is of large size and will also introduce a significant amount of vibration to the rig.

6.1.1. Square groove

As with the other large cavities before, this one is more realistic to a real tyre from its size, but in comparison to the model tyre it is rather large. Figure 6.1 shows the 'square groove' from the top view with the dimensions of 5 mm in depth and 5 mm in length in regard to the rotational direction.

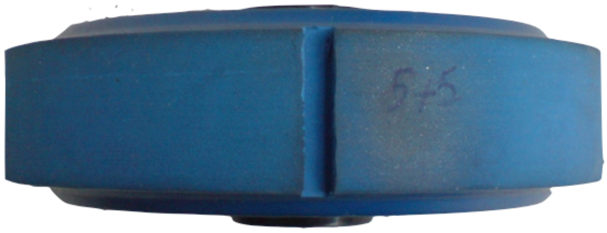

Figure 6.1 Photograph of top view of the tyre equipped with the 'square groove'

Separate microphones as used before record the leading and trailing edge signals. For this kind of tyre, it is challenging to distinguish between the signal purely generated at leading edge and the one at the trailing edge. This is due to the pipe resonance happening when the groove is closed by the road surface. Thus, a continuous signal is generated that is changing dependent on the position of the cavity to the road. In addition to that, non-dominant peak amplitudes are expected in comparison to the tyre with cavities because air has always time and space (on the sides) to escape out of the groove when the tread is covered by the road.

The whole two seconds signal recorded at the trailing edge is shown in Figure 6.2, where the top (Figure 6.2a) shows the unfiltered signal that is overlaid by a substantial amount of noise. Thus, a narrower 2nd order bandpass Butterworth filter with a lower cut-off frequency of 3840 Hertz is chosen and the upper cut-off frequency is the same as used before (24000 Hertz). The result of the bandpass filtering process is shown in Figure 6.2b. Now the events when the groove is in contact with the road surface can be identified. This gives an idea about the rather complex process happening at the contact patch of the tyre with the 'square groove'. The same filtering is applied to the leading edge signal that results in a similar signal.

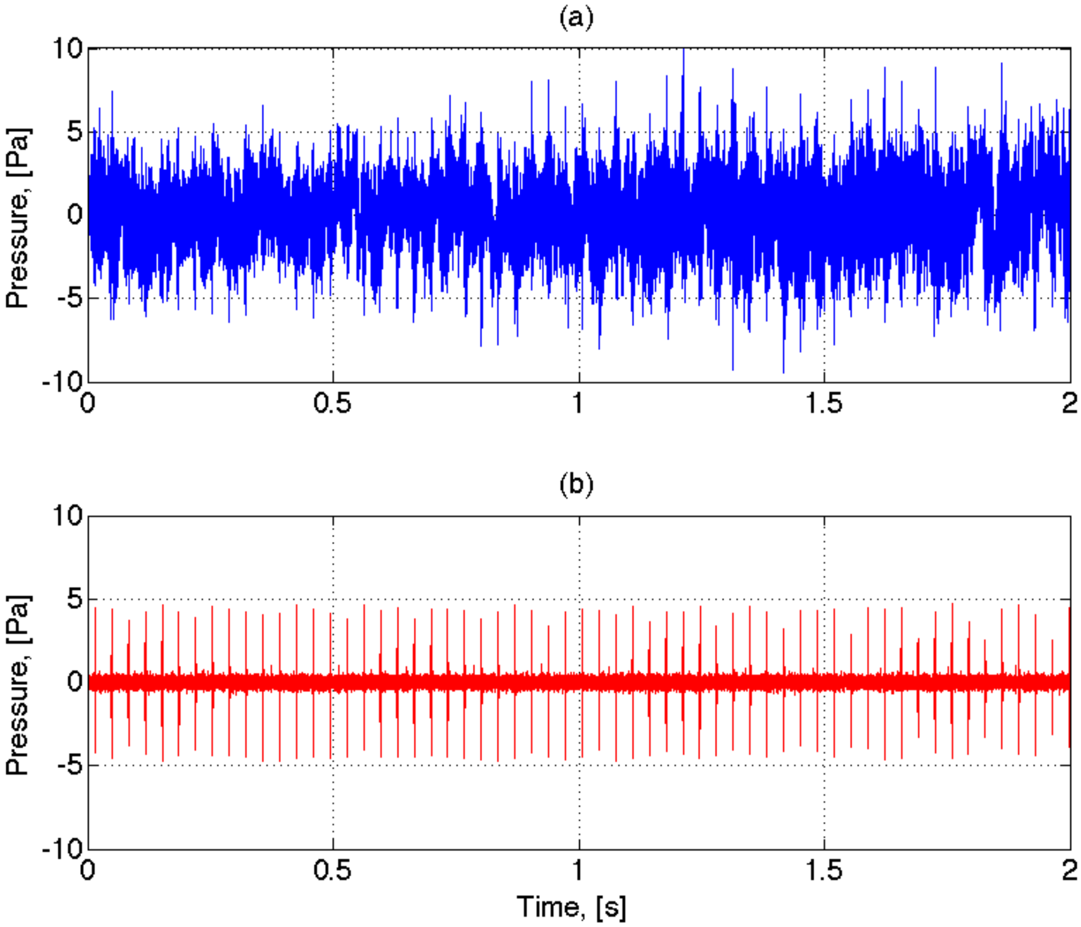

Figure 6.2 Recorded signals of the trailing edge of the tyre equipped with the ‘square groove’ at 41km/h: (a) unfiltered signal; and (b) bandpass filtered signal

Both signals, leading and trailing edge are combined in one graph to draw conclusions about the process happening at the contact patch of a grooved tyre. Figure 6.3 shows an example of both signals recorded simultaneously. The blue line displays the data recorded by the leading edge microphone and the red line the recording at the trailing edge. By comparing both lines, a difference at the beginning and at the end of the event can be identified. When the groove is in contact with the road (assumed green area lasting for about 0.0007 s) both signals show similar behaviour. Although the groove is ventilated (open at both sides in this case) and does have possibilities for the air to escape, the leading edge pulse is still quite significant (0.6983 s). It looks similar to the high amplitude trailing edge recording at the end of the signal (0.6992 s), from the frequency and amplitude point of view. In the middle of the signal leading and trailing edge recordings show an overlay. At the end of the process, when the groove lifts off the road, high amplitude oscillations occur that could be related to the air resonant radiation introduced for the tyres with cavities in the next chapter. This resonance is recorded by the trailing edge microphone only. The leading edge signal shows oscillations that appear to be influenced by the groove resonance. Measuring the frequency content of the signal will present additional information about the processes happening in the contact patch of the tyre with the 'square groove'.

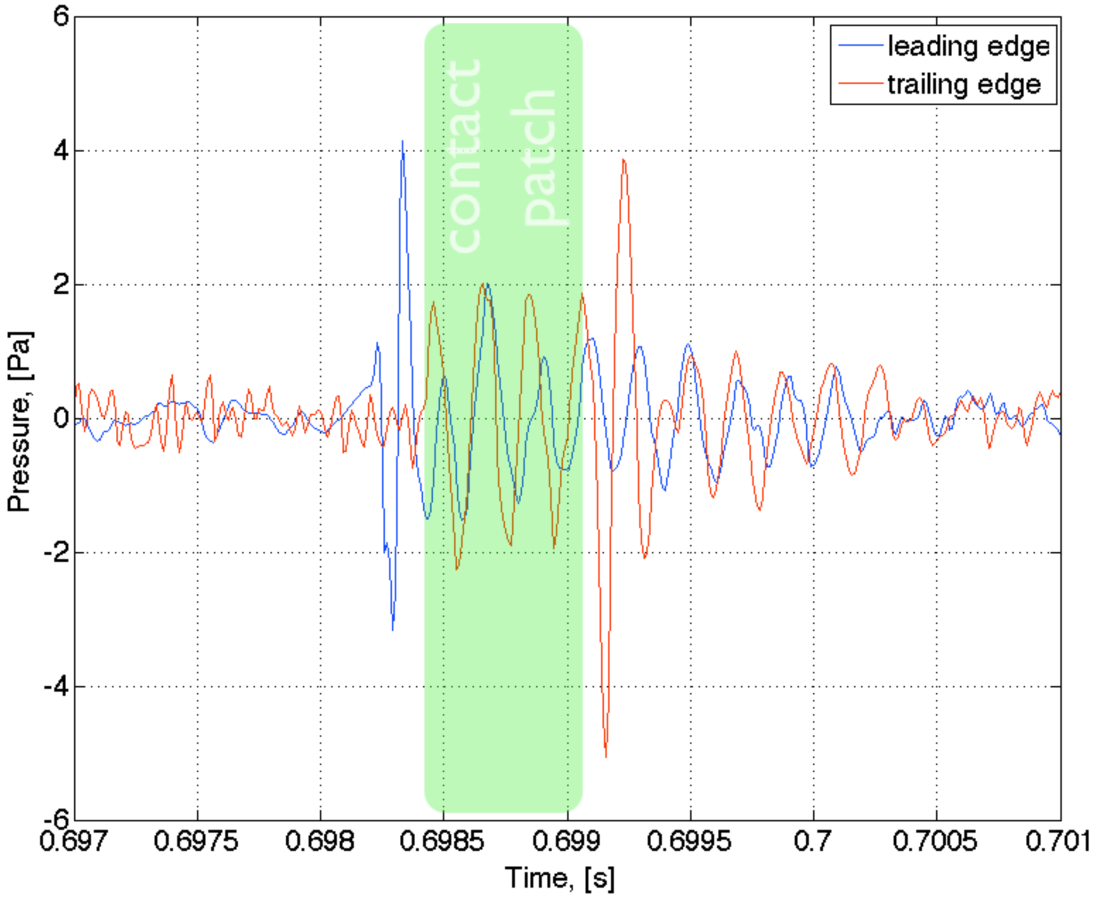

Figure 6.3 Leading and trailing edge signal of the tyre with the 'square groove' at 41 km/h and assumed contact patch area

Figure 6.4 shows a sample event for the lower tyre speed of 31 km/h. The amplitude of the signal is lower, as it would be expected. The shape of the event is similar to the higher speed recordings previously shown in Figure 6.3. The only difference is at the leading edge at 0.9115 s where there is a negative double peak that could be due to a frequency change when the groove resonance is initiated. It also occurs for the high-speed example at

0.6983 s but just not as significantly. After this first visual inspection the frequencies of the signal are analysed, so they can be compared to the models presented in Chapter 3. Especially the effect of groove resonance and the air resonant radiation shall be considered here.

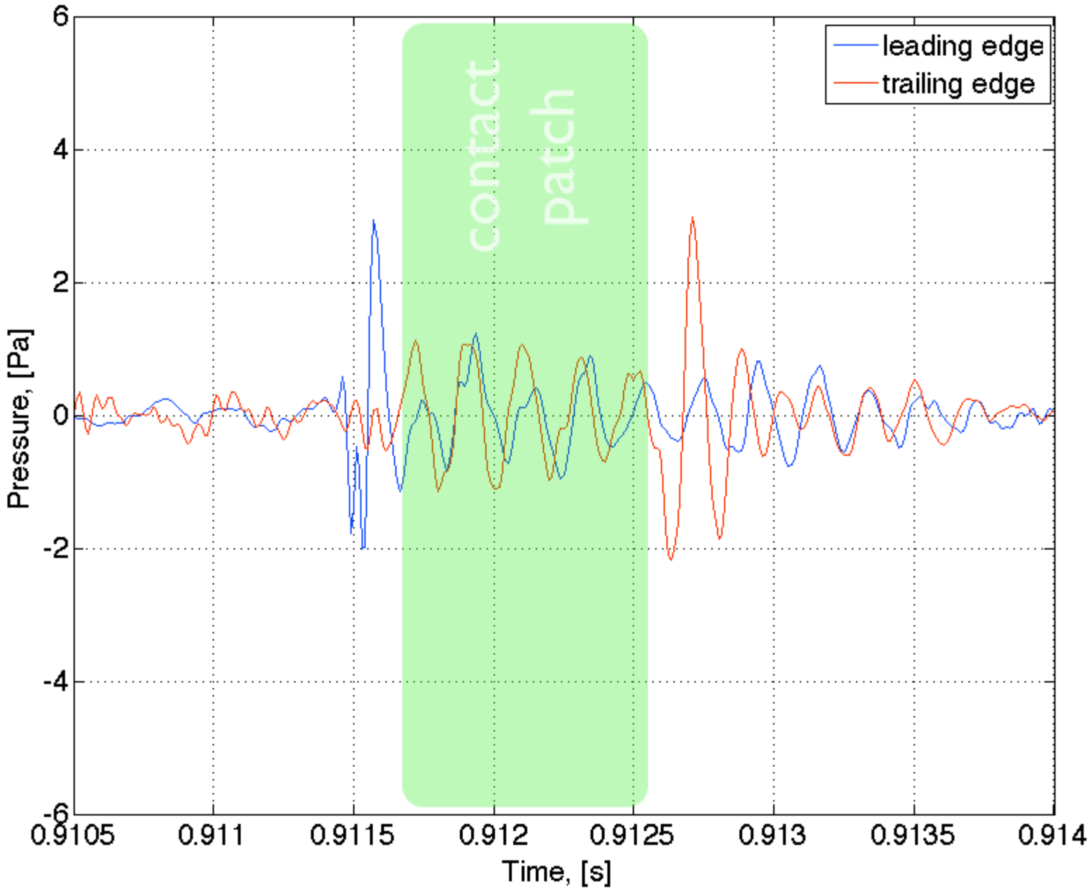

Figure 6.4 Leading and trailing edge signal of the tyre with the 'square groove' at 31 km/h and assumed contact patch area

The resonance frequency of a pipe with two open ends is dependent on the dimensions of the groove used, it can be calculated in conjunction with Equation (3.14). In this equation the diameter of a pipe is needed to calculate the resonance frequency of a pipe. The pipe/groove found in the tread of the tyre used is equipped with a square section, therefore, the diameter is approximated by the area of the square section. The dimensions of the groove *L* and *D* are used to calculate the area of the square section (0.000025 m^2). To get the same area with a circular shape a diameter of 0.0056 m is needed as shown in Table 6.1. The resulting pipe resonance for should be in a region between 5576 Hertz and 5790 Hertz.

	Length, [m]	Diameter, [m]	Resonance frequency, [Hz]
Square groove	0.026	0.0056	5576-5790

Table 6.1 Groove resonance frequency calculation for the tyre with the 'square groove'

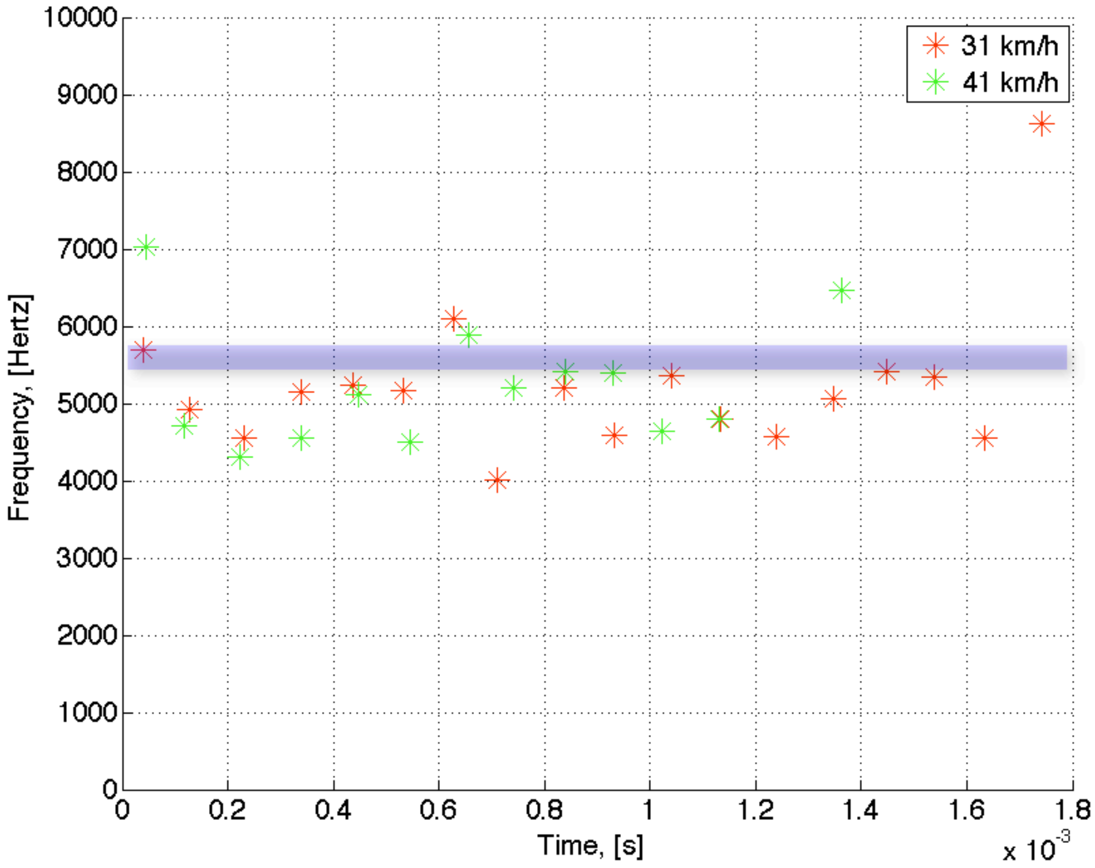

Figure 6.5 Instantaneous frequency at the leading edge for the tyre with the 'square groove' at 41 km/h and 31 km/h

Figure 6.5 shows the instantaneous frequencies that are taken off the signal via the maximum and minimum values of the oscillations by the software MATLAB. Both speeds are shown in this graph by the crosses, where the red colour marks the frequencies for 31 km/h and the green colour shows the results for 41 km/h. Both speeds present a more or less linear behaviour of the frequency over time. However, the mean value of the crosses is a bit lower than the actual calculated resonance frequency. The factors influencing this deviation can be the unwanted noise in the recorded signal, and a not accurately cut groove. In addition to that it has to be considered that the cross section of the groove is a square shape, instead of a circular, as needed for the pipe resonance calculations. Also the shape of the cross section is different when the groove is compressed due to the load of the tyre. At the beginning of the signal a slight decrease in frequency is shown for the first three crosses, this can be an indication for an inverse air resonant radiation at the leading edge.

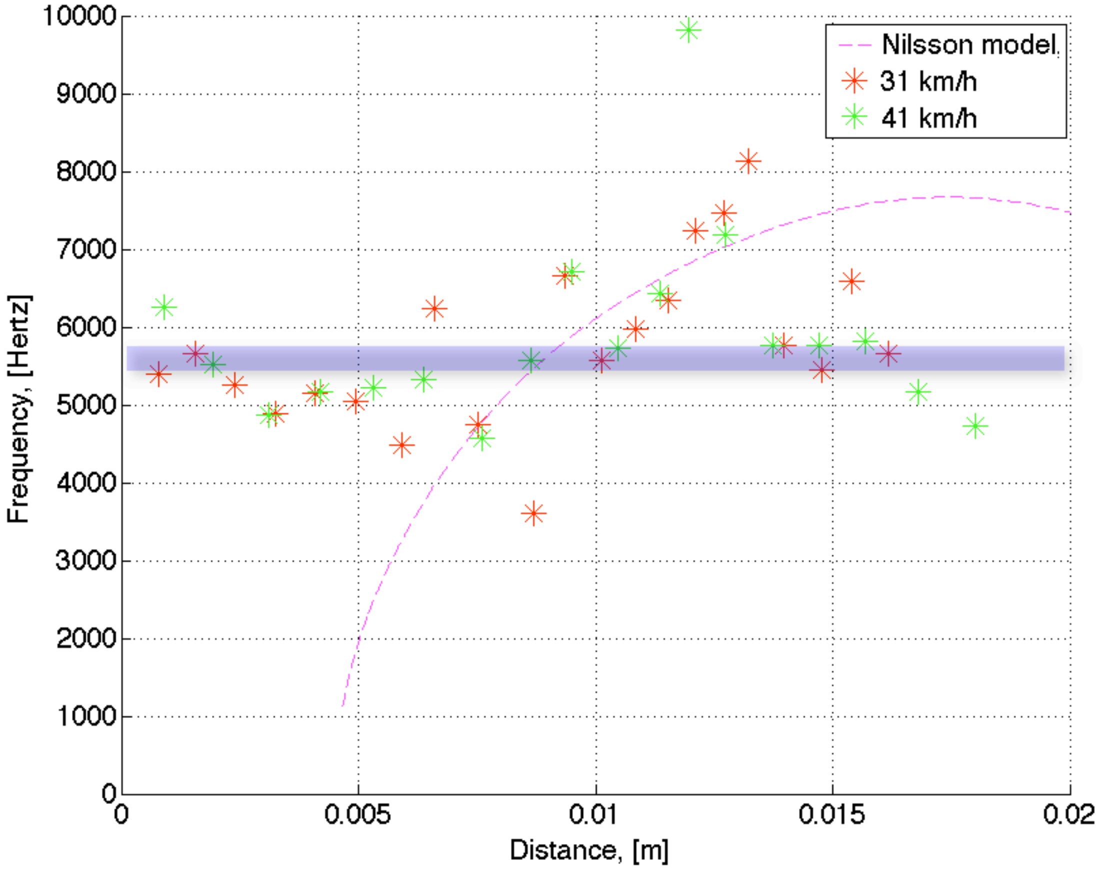

Figure 6.6 Instantaneous frequency at the trailing edge for the tyre with the 'square groove' at 41 km/h and 31 km/h

The frequency analysis of the recording of the trailing edge microphone shown in Figure 6.6 is very interesting. Again, both speeds are shown by the crosses and the pipe resonance frequency is marked with the blue horizontal line. In addition, the air resonant radiation model proposed by Nilsson [Nilsson, 1979] is drawn in the figure. This model introduced in Chapter 3 describes the frequency behaviour at the trailing edge of a tyre with a groove. The model is dependent on the location of the groove in relation to the trailing edge, therefore in Figure 6.6 the frequency is plotted over distance not over time. The distance zero corresponds to the start of the signal at 0.6984 s in Figure 6.3 where it is assumed that the groove is fully covered. As already shown in the time history plot, the initial part of the recording shows a constant frequency that could be explained by the pipe resonance happening at the contact patch. In the middle of the signal however, the frequency rises (at about 0.011 m). This change of frequency could be explained by the air resonant radiation that takes place when the groove lifts off the road. However the fit between the frequencies predicted by Nilsson and the measured instantaneous frequency is not accurate, furthermore it can only be achieved because of the applied bandpass filter to the initial signal. At the very end of the time recording shown in Figure 6.6 the pipe resonance dominates again due to the fact that the crosses settle down around the area of the blue bar.

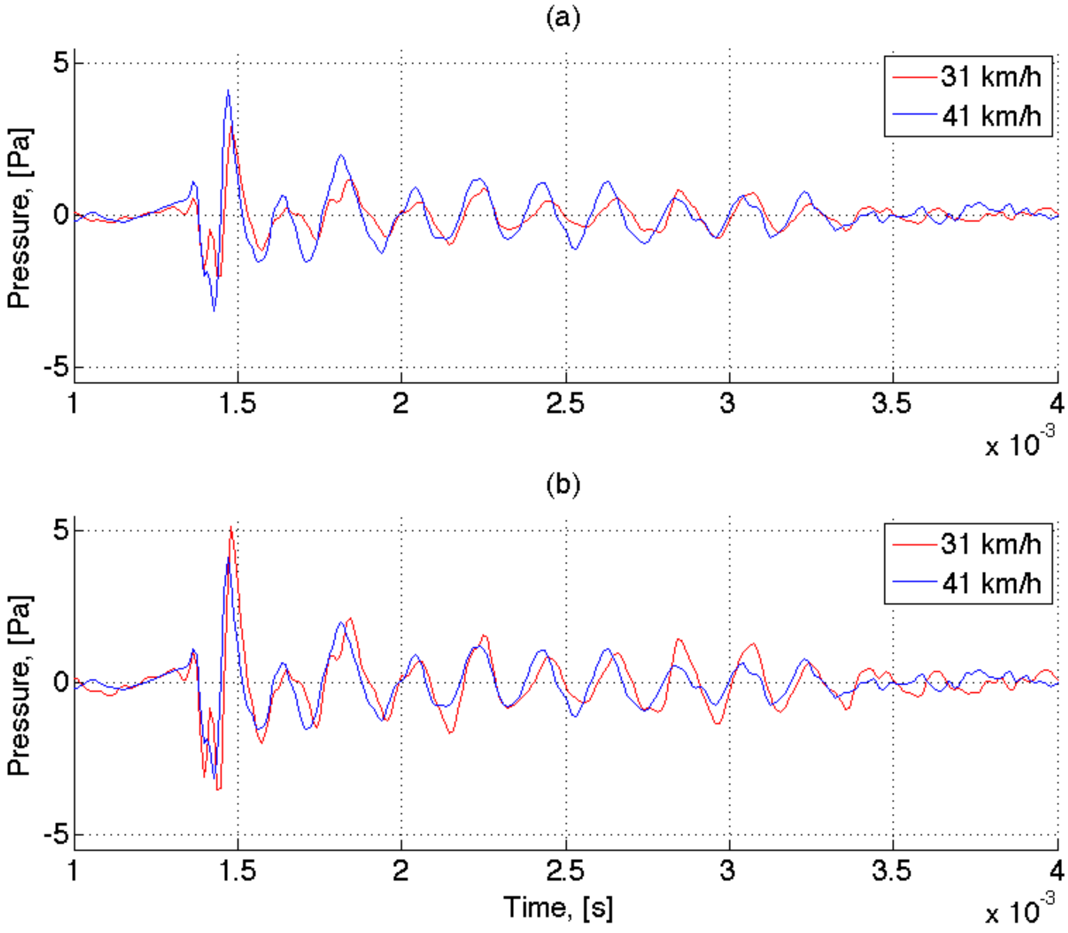

Figure 6.7 Example of the leading edge signal from the tyre with the ‘square groove’ for two different speeds: (a) normal recordings; and (b) slower velocity signal multiplied by speed factor

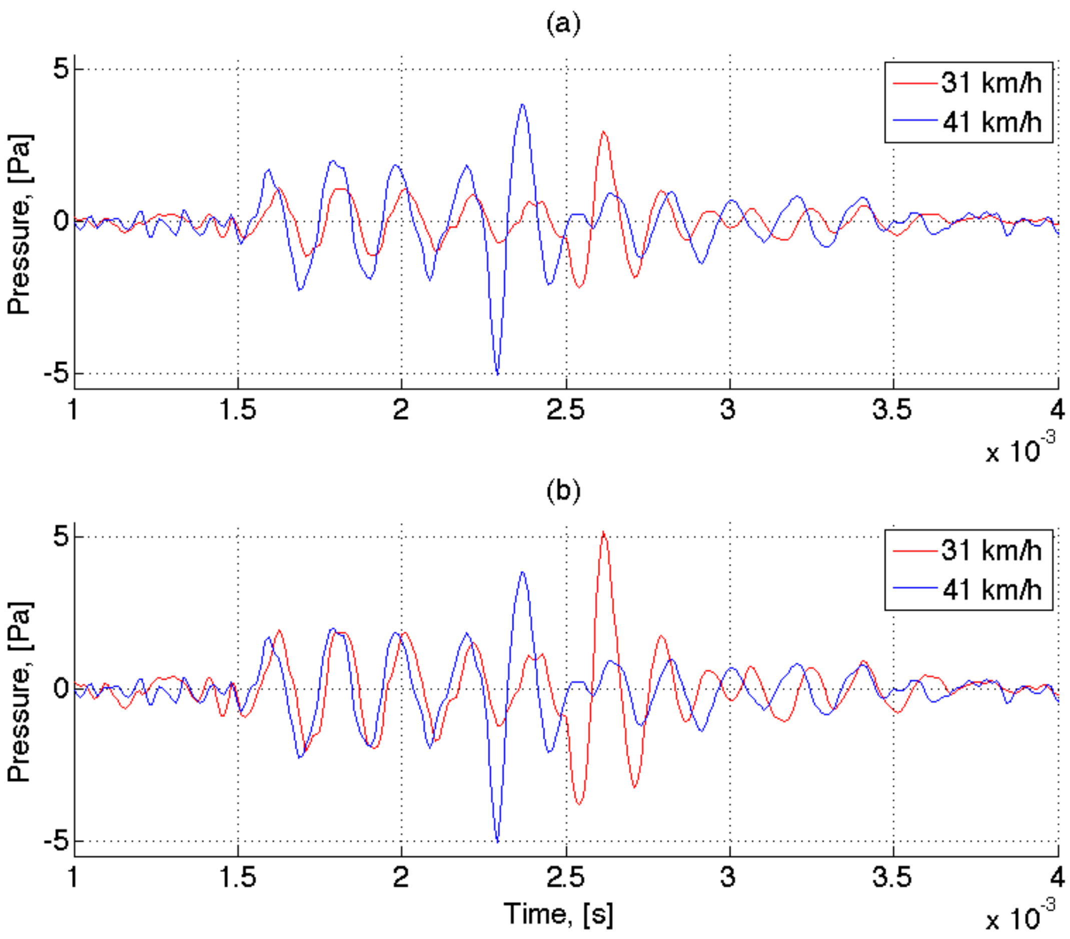

Figure 6.8 Example peak of the trailing edge signal from the tyre with the 'square groove' for two different speeds: (a) normal recordings; and (b) slower velocity signal multiplied by speed factor

As previously shown at the contact patch of a tyre with a groove a rather complex air process occurs. It is difficult to judge from the signal when a process starts at the leading or trailing edge because the transition is influenced by the pipe resonance. However, the models from the literature for the pipe resonance and the air resonant radiation could indicate both processes. Neither of those measured frequencies for the models are dependent on the speed of the tyre. However, the amplitudes are speed dependent. This is clearly recognisable when the 31 km/h signal is directly compared to the signal at 41 km/h as shown in Figure 6.7 and Figure 6.8, separately for the leading and trailing edges. At the top of both figures the plain example signals are plotted, where 41 km/h is in blue and 31 km/h is in red. At the bottom of both figures the 31 km/h recording is multiplied by the speed factor to the reference speed 41 km/h, as introduced in the previous chapter. These plots reveal a similar relationship between the amplitudes as presented in Chapter 5. Again the amplitude is dependent on the square of the velocity difference. This dependence applies to the constant frequency groove resonance section in the middle of the signal and also to the air resonance radiation occurring at the end of the signal.

The signal for the tyre with the ‘square groove’ is as best explained in the following way: At the entrance to the contact patch an air movement is initiated that is converted to the groove resonance. When the groove lifts off the road the air resonant radiation is dominating, however, at the end this is converted into the groove resonance again. In the next section a significantly smaller groove in the tyre is investigated, to compare the results to the ones obtained for the ‘square groove’.

6.1.2. Small groove

This time the groove is smaller in the dimensions so it fits better to the size of the tyre and does not lead to that much vibrational impact into the rig when contacting the chassis dynamometer drum. With a cross section still nearly square and the length obviously the same as before, it is hoped that the results will look similar to the ones previously obtained by the groove with the larger square section. The volume is significantly smaller in comparison to the tyre with the ‘square groove’, thus, the overall sound generation by this tyre is expected to be lower.

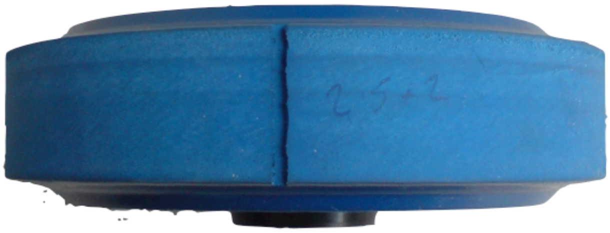

Figure 6.9 Photograph of top view of the tyre equipped with the ‘small groove’

As shown in Table 6.2 the smaller calculated diameter results in a slightly higher resonance frequency range. This time the pipe resonances are supposed to be in between 6073 and 6184 Hertz.

Figure 6.10 shows the recordings at the leading and trailing edge at 41 km/h for the ‘small groove’. Again with the bandpass filter used the events are clearly visible in the time history. The leading edge signal (blue) has an initial peak followed by a good fit to the trailing edge signal. In the middle however there is a section with a drop in the amplitude (1.5853 s). A similar thing happens to the trailing edge signal (red). This drop could either be due to noise in the signal or the change of air effect from groove resonance to air resonant radiation, because the frequencies do not match up. Another explanation might be that the energy of the initiation for the groove resonance is simply dissipated. This time the trailing edge signal is dominating, whereas for the ‘square groove’ before the leading and trailing edge had similar maximum amplitudes

	Length, [m]	Diameter, [m]	Resonance frequency, [Hz]
Small groove	0.026	0.0025	6073-6184

Table 6.2 Groove resonance frequency calculation for the tyre with the ‘small groove’

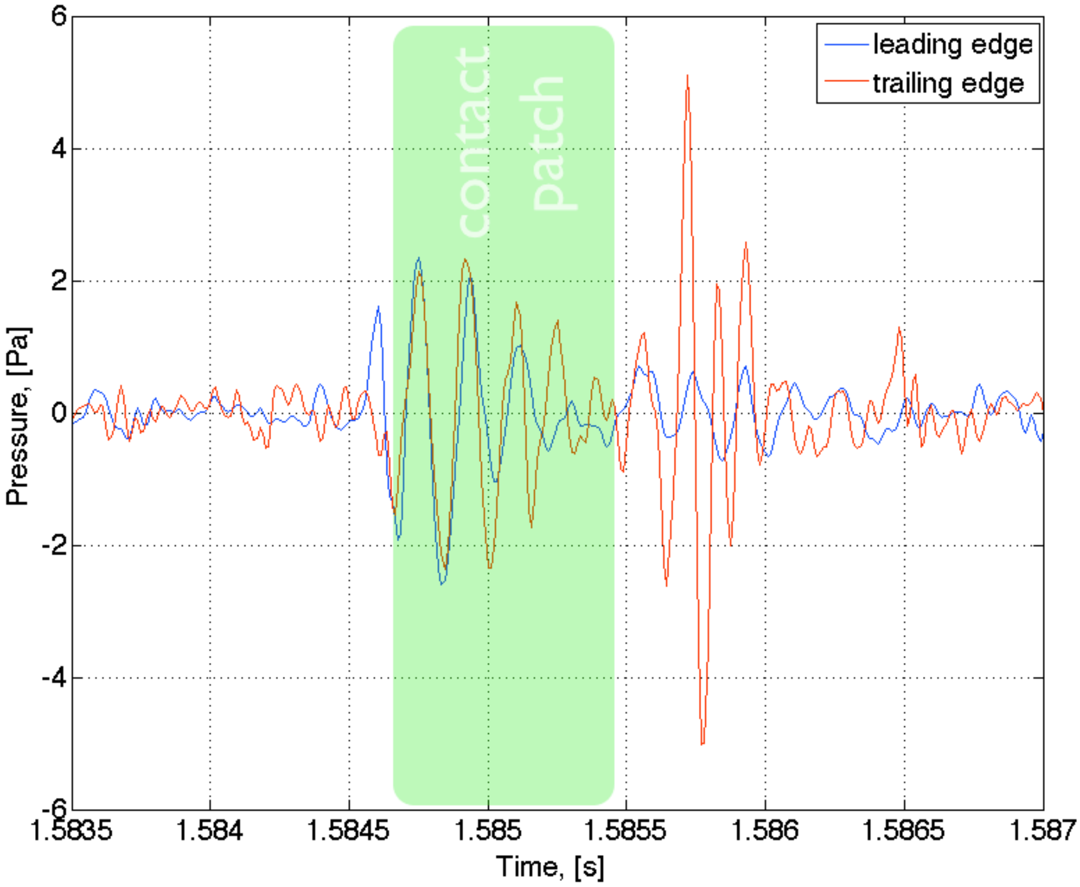

Figure 6.10 Leading and trailing edge signal of the tyre with the ‘small groove’ at 41 km/h and assumed contact patch area

The next plot shows the recording for the lower speed of 31 km/h. In the leading edge recording in between 0.2136 s and 0.2141 s no significant signal is recorded that is also shown to some extend in the trailing edge recordings. When Figure 6.11 is compared to Figure 6.10 it becomes apparent that the shape of the signals is similar only the amplitude differs. Thus, both signals are expected to contain similar frequencies.

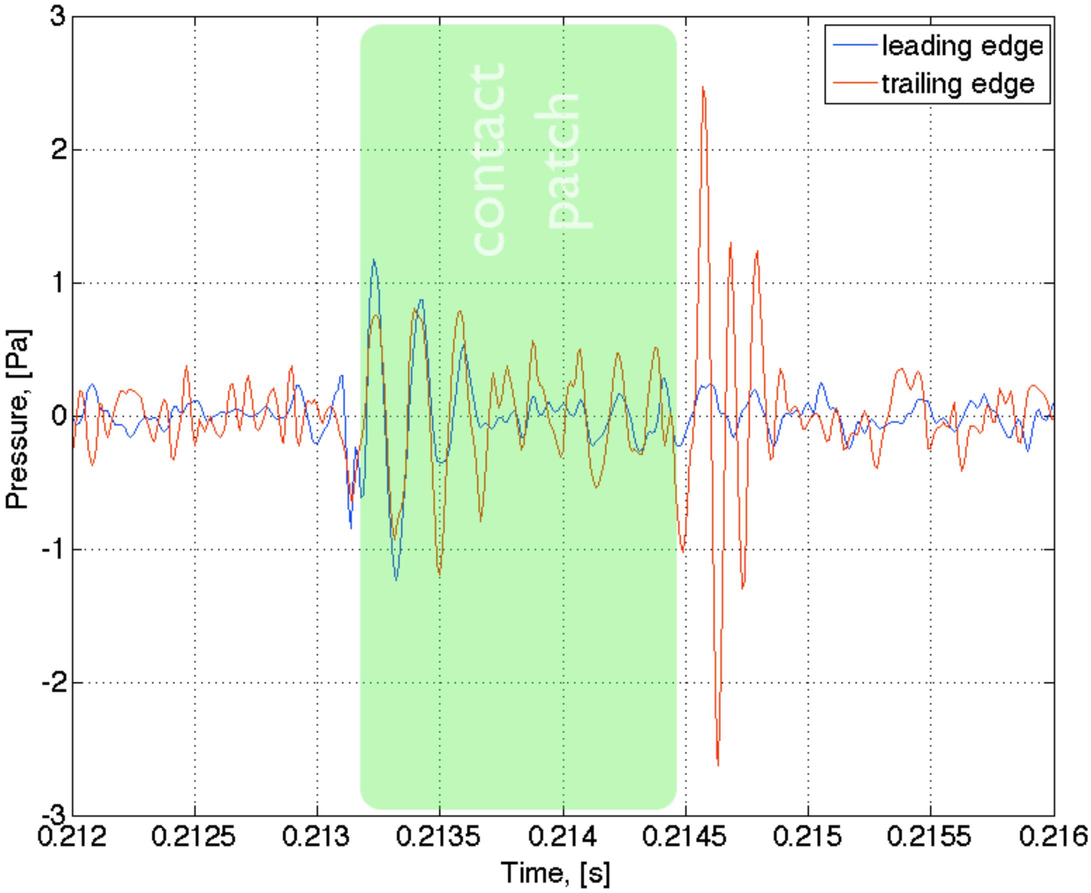

Figure 6.11 Leading and trailing edge signal of the tyre with the ‘small groove’ at 31 km/h and assumed contact patch area

Figure 6.12 shows the instantaneous frequency content of the leading edge signal for both speeds of the tyre with the ‘small groove’. The red crosses display the measurements for 31 km/h the green ones for 41 km/h, respectively. The pipe resonance frequency range taken from Table 6.2 is shown with the blue broad line. By comparing the crosses generated by the measured data to the bold line a similar trend is shown. However, in the middle (between 0.8 s and 1.1 s) measured and calculated results differ. This difference could be due to the corrupted data from the measurements.

Nevertheless the pipe resonance seems to occur. Again as shown for the ‘square groove’ the measured resonance frequency is slightly lower than the predicted one from Table 6.2.

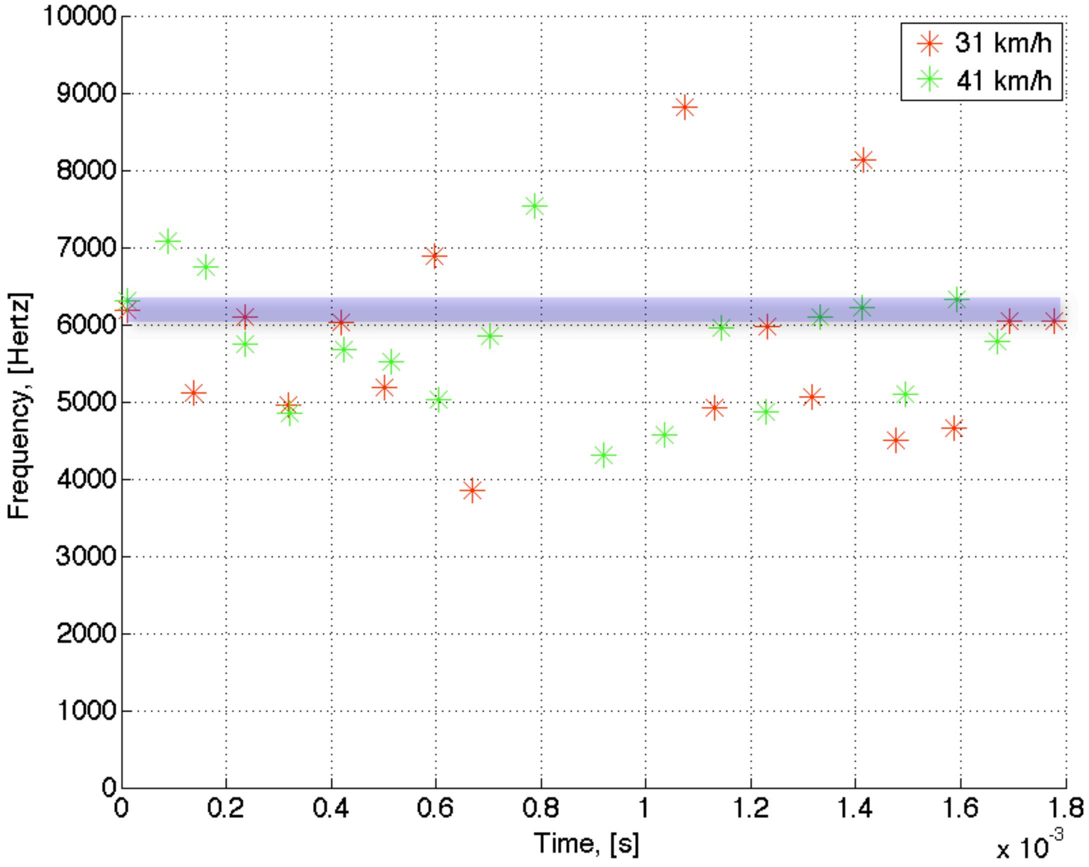

Figure 6.12 Instantaneous frequency at the leading edge for the tyre with the ‘small groove’ at 41 km/h and 31 km/h

The results for the frequency calculations of the trailing edge signal are shown in Figure 6.13. Both speed recordings show similar frequency behaviour. There is a good fit to the pipe resonance area (blue) at the beginning and just before the model introduced by Nilsson is applied. In the middle section, however, the frequencies taken from the time signal are much higher than expected. Again at the very end of Figure 6.13 after 0.013 m the Nilsson model is also shown in the graph. The distance zero corresponds to the start of the oscillations when the groove is supposed to be completely covered by the road at the leading edge. This time the Nilsson model is shifted to a further distance in comparison to the tyre with the ‘square groove’. This shifting is due to the fact that a constant contact patch length is assumed for the tyre, hence a groove with smaller width lifts off the road at a later stage than a wider groove. The measured frequencies show good agreement to the predicted frequency modulation from Nilsson. The trailing edge and so the air resonant radiation delivers the highest levels of noise generated by this kind of groove.

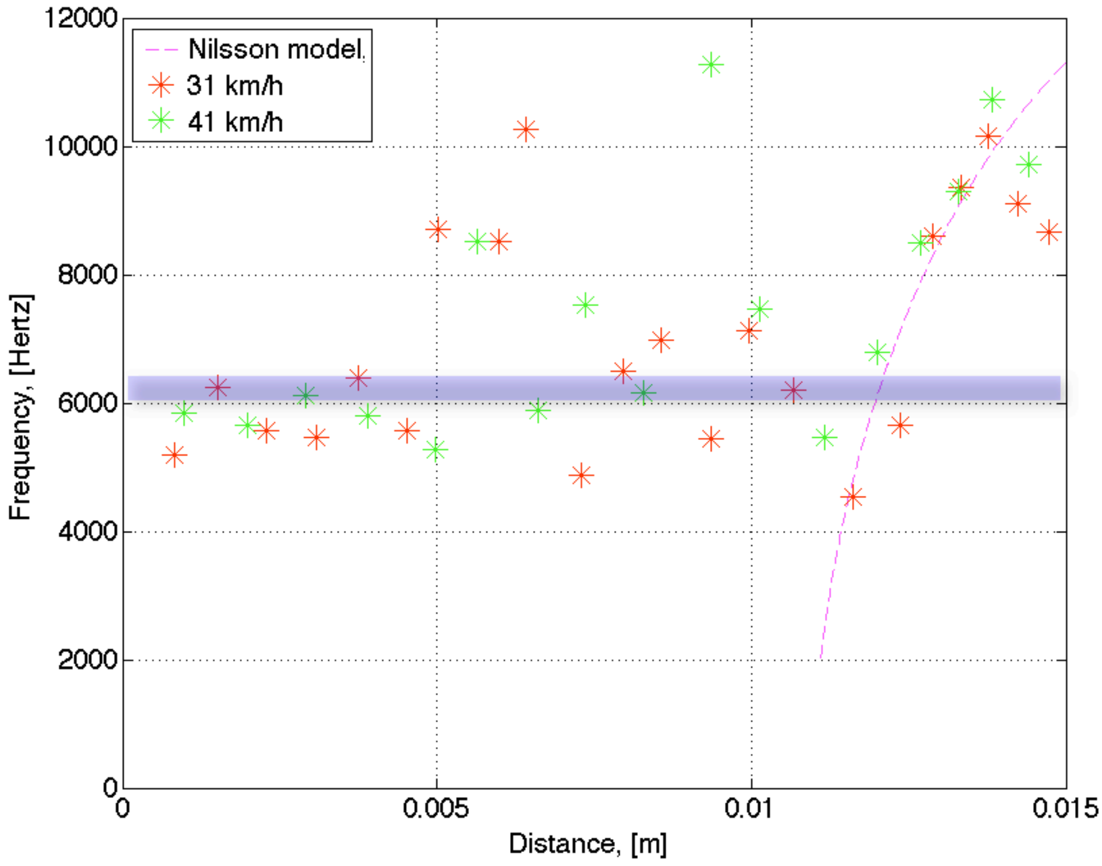

Figure 6.13 Instantaneous frequency at the trailing edge for the tyre with the ‘small groove’ at 41 km/h and 31 km/h

In comparison to the ‘square groove’ the ‘small groove’ generates less noise and does not present the expected groove resonance frequencies as well. The ‘small groove’ does show a similar behaviour, however, the unwanted chassis dynamometer noise seems just too significant for this type of tyre. For the tyre with the ‘square groove’ the maximum amplitudes generated at the leading and trailing edge are similar, whereas for the tyre with the ‘small groove’ the trailing edge signal clearly dominates. The ventilation of the groove could explain the aplitude difference at the trailing edge. The ‘square groove’ has a larger square section, hence more room for the air to escape at the contact patch, whilst having the same length. Thus the air resonant radiation is not as significant for the ‘square groove’.

Figure 6.14 shows the recordings of the leading edge signal for 41 km/h in blue and 31 km/h in red. Both recordings are combined in one plot to investigate into the speed and amplitude relationship of the tyre with the ‘small groove’. At the top of the figure both originally recorded signals are plotted. When the slower signal is multiplied by the speed factor that is the squared difference to the reference speed (41 km/h) both signals show a similar amplitude as shown Figure 6.14b.

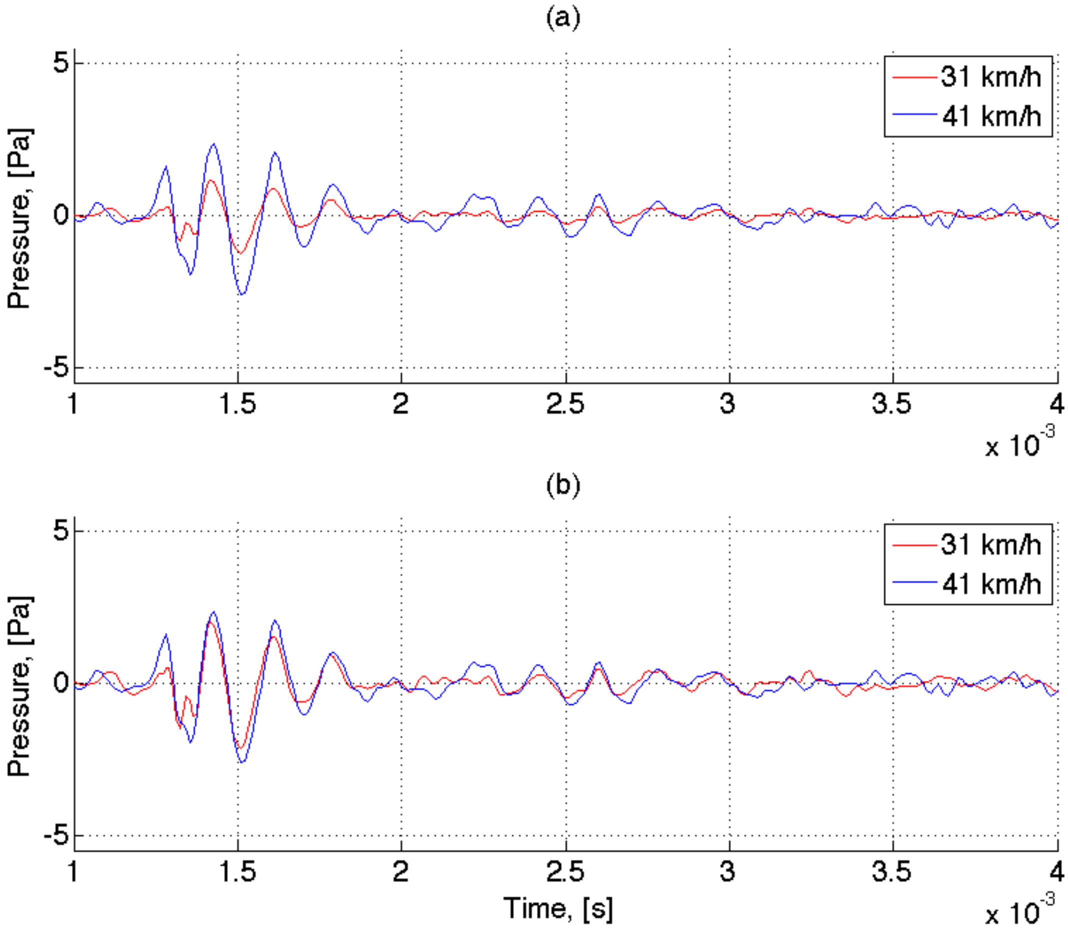

Figure 6.14 Example of the leading edge signal from the tyre with the ‘small groove’ for two different speeds: (a) normal recordings; and (b) slower velocity signal multiplied by speed factor

The same is generated for the trailing edge recordings as shown in Figure 6.15. Here again the blue line presents 41 km/h and 31 km/h is displayed by the red line. The time of the process at 41 km/h is much shorter in comparison to 31 km/h. Hence, the signals are not overlaying perfectly.

However, the amplitude comparison in Figure 6.15b again shows good agreement for the groove resonance area (1.3 s until 2.2 s). Also for the air resonance radiation, when comparing the signal of 41 km/h in between 2.2 s and 2.7 s to the signal of 31 km/h in between 2.5 s and 3.1 s. Thus, the speed dependence of the pressure amplitude of the signal is also to be found for the tyre with the ‘small groove’.

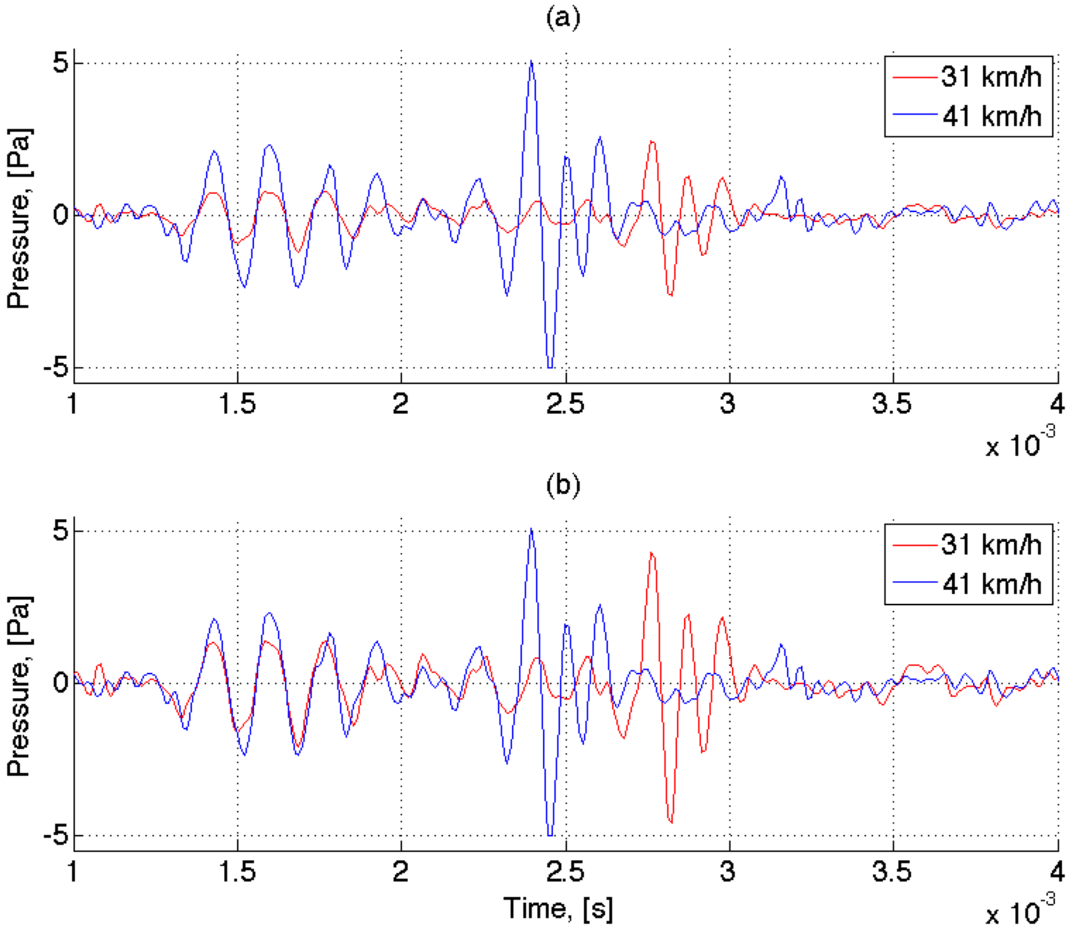

Figure 6.15 Example peak of the trailing edge signal from the tyre with the ‘small groove’ for two different speeds: (a) normal recordings; and (b) slower velocity signal multiplied by speed factor

6.1.3. Chevron

This groove type is of a very special signature. It is a realistic shape for tyres used for agriculture vehicles or for vehicles in the construction business. The chevron is chosen to simulate a directivity of a tyre tread. This special arrangement of the groove means the chevron can either be pointing in the direction of rotation of the tyre or against it. Thus, measurements are conducted with the chevron running either way, to investigate into the difference in noise radiation.

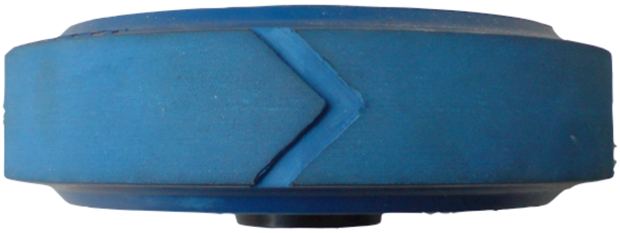

Figure 6.16 Photograph of top view of the tyre equipped with the 'chevron' shape of groove

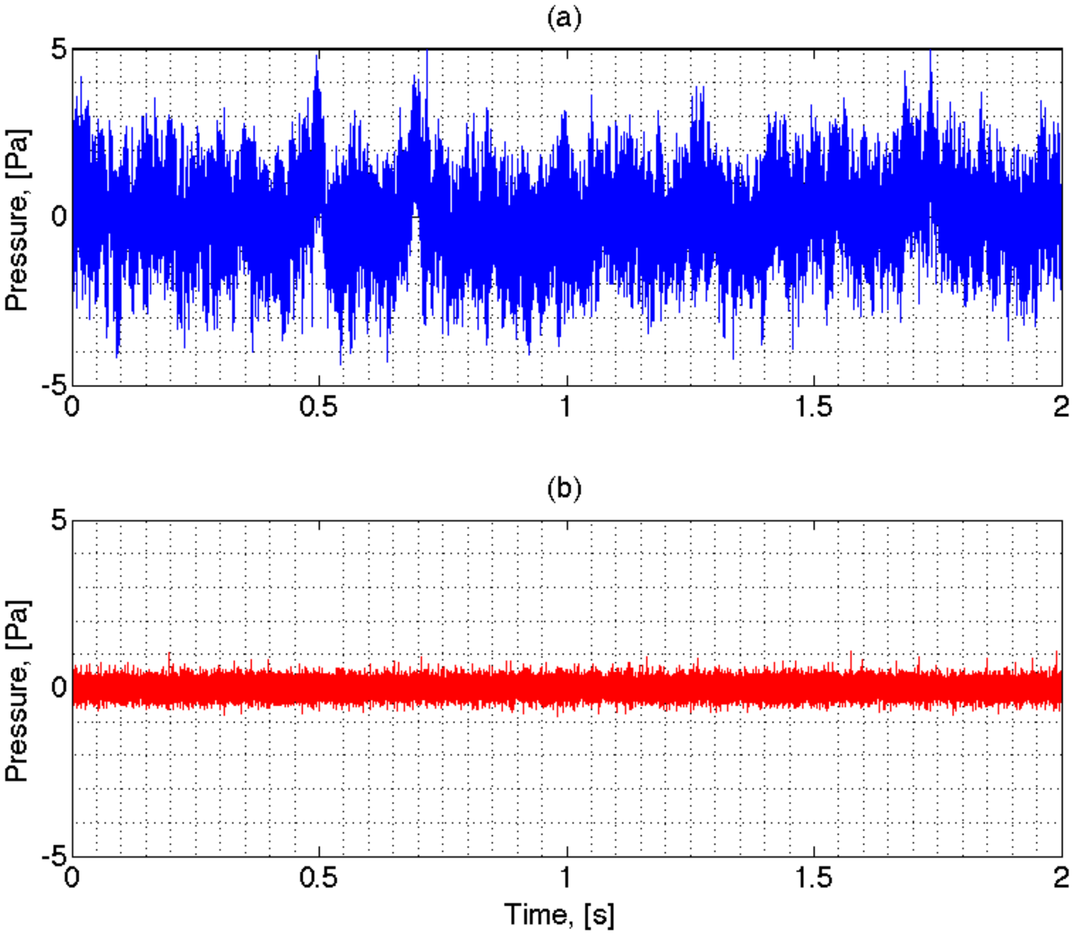

Figure 6.17 Recorded signals of the trailing edge of the tyre equipped with the 'chevron' shape of groove at 41km/h: (a) unfiltered signal; and (b) bandpass filtered signal. The chevron points in the direction of rotation

Figure 6.17 shows the results at the trailing edge of this tyre moving at a speed of 41 km/h with the chevron pointing into the direction of rotation. In this case where the chevron points to the actual road surface while rotating no event can be identified in the signal. The unfiltered recording in Figure 6.17a is purely dominated by noise even in the bandpass filtered recording in Figure 6.17b. Thus, it can be concluded that for the setup used and the chevron pointing in the direction of rotation of the tyre no significant air related noise generation is identified. This phenomenon could be explained by the fact that the air is easily squeezed out of the tread, towards the open end of the chevron, when it enters the contact patch. Thus no air is captured in the tread and, hence, no significant resonance behaviour.

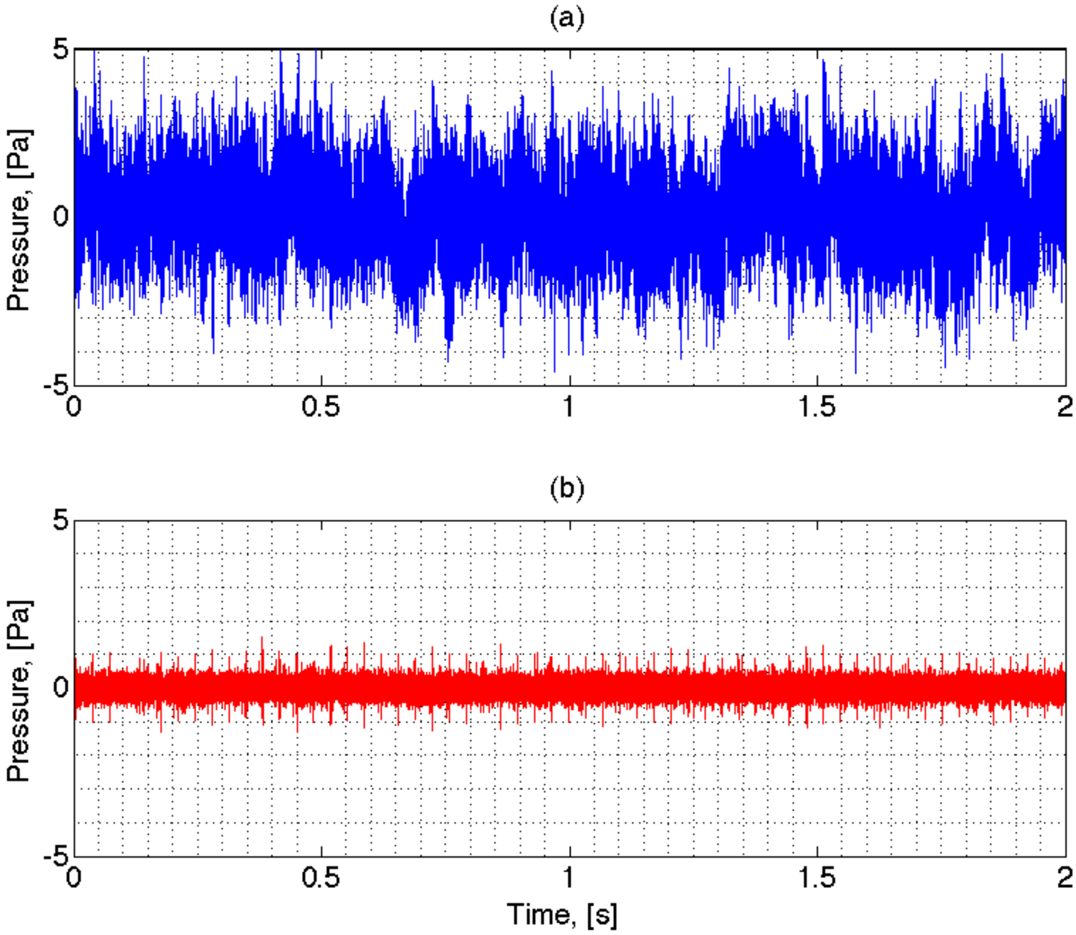

Figure 6.18 Recorded signals of the trailing edge of the tyre equipped with the ‘chevron’ shape of groove at 41km/h: (a) unfiltered signal; and (b) bandpass filtered signal. The chevron points against the direction of rotation

Figure 6.18 shows the signal at the trailing edge produced by the chevron in the tread pointing in the other direction in respect to the rotation of the tyre at a tyre speed of 41 km/h. In the unfiltered part, Figure 6.18a, there is nothing obvious to identify, however, in the bandpass filtered signal recording (Figure 6.18b) peaks with a constant distance related to the frequency of reoccurrence, of the chevron contacting the chassis dynamometer drum, can be identified.

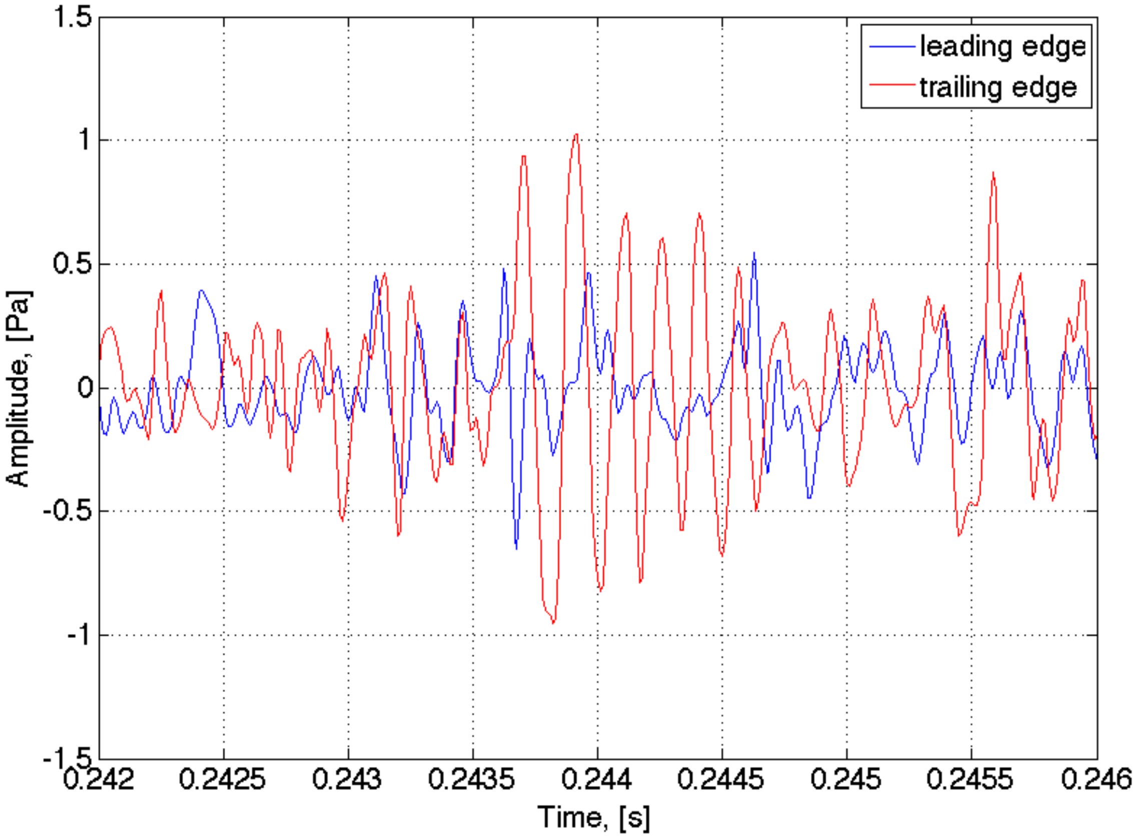

Figure 6.19 Leading and trailing edge signal of the tyre with the ‘chevron’ shaped groove at 41 km/h, the chevron points against the direction of rotation

A reference peak of this trailing edge signal is shown in Figure 6.19 alongside with the leading edge signal in blue. There are no significant air movements at the leading edge of the tyre when the chevron hits the road surface. However, at the trailing edge some considerable oscillations can be identified with changing amplitude. For this special kind of groove it is difficult to judge what kind of signal that is. Due to the fact that there is no indication at the leading edge the initiation of the signal, in reference to the chevron location at the contact patch, cannot be identified. The open ends of the chevron point towards the trailing edge microphone therefore no signal is picked up at the leading edge. To identify the responsible mechanism for this noise further research needs to be conducted.

	Length, [m]	Diameter, [m]	Resonance frequency, [Hz]
Chevron	0.0368	0.0032	4327-4398
Half chevron	0.0184	0.0032	8126-8382

Table 6.3 Groove resonance frequency calculation for the tyre with the 'chevron' shaped groove

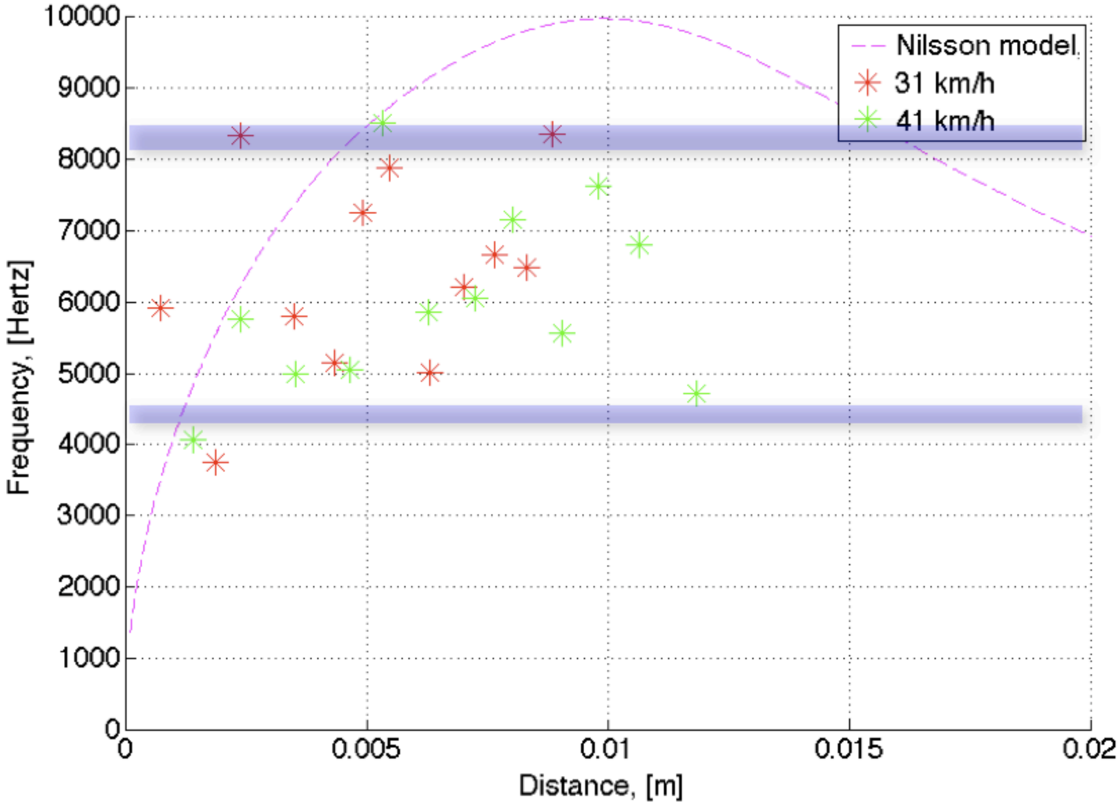

Figure 6.20 Instantaneous frequency at the trailing edge for the tyre with the 'chevron' shaped groove, pointing against the direction of rotation, at 41 km/h and 31 km/h

Therefore, the frequency content of the recorded signal is analysed. In Figure 6.20 the frequencies of the pulse for both speeds (31 km/h and 41 km/h) in comparison to the model derived by Nilsson are shown. Due to the fact that the oscillations are at the trailing edge only, Nilsson's model this time starts at the cavity distance of zero meters. However, the fit is not satisfactory. The frequency values for both speeds seem to be rising at the beginning, however, are eventually rather oscillating. Thus, groove resonance could be the mechanism that generates those oscillations. With this kind of groove the resonance frequency is rather complex to define, so there are two simple attempts presented.

In Table 6.3 two different resonance regions are shown that are also plotted in Figure 6.20 by the blue line. Those are derived from the geometry of the chevron. The lower region is the frequency calculation over the whole length of the chevron that results in a very low resonance frequency, much lower than the measured values. The higher resonance frequency region only considers half the length of the chevron to give an idea what pipe resonance frequency this would produce. Unfortunately, this one is much higher than the measured values; therefore it could be something in between of both calculations due to the fact that the chevron is a special kind of groove.

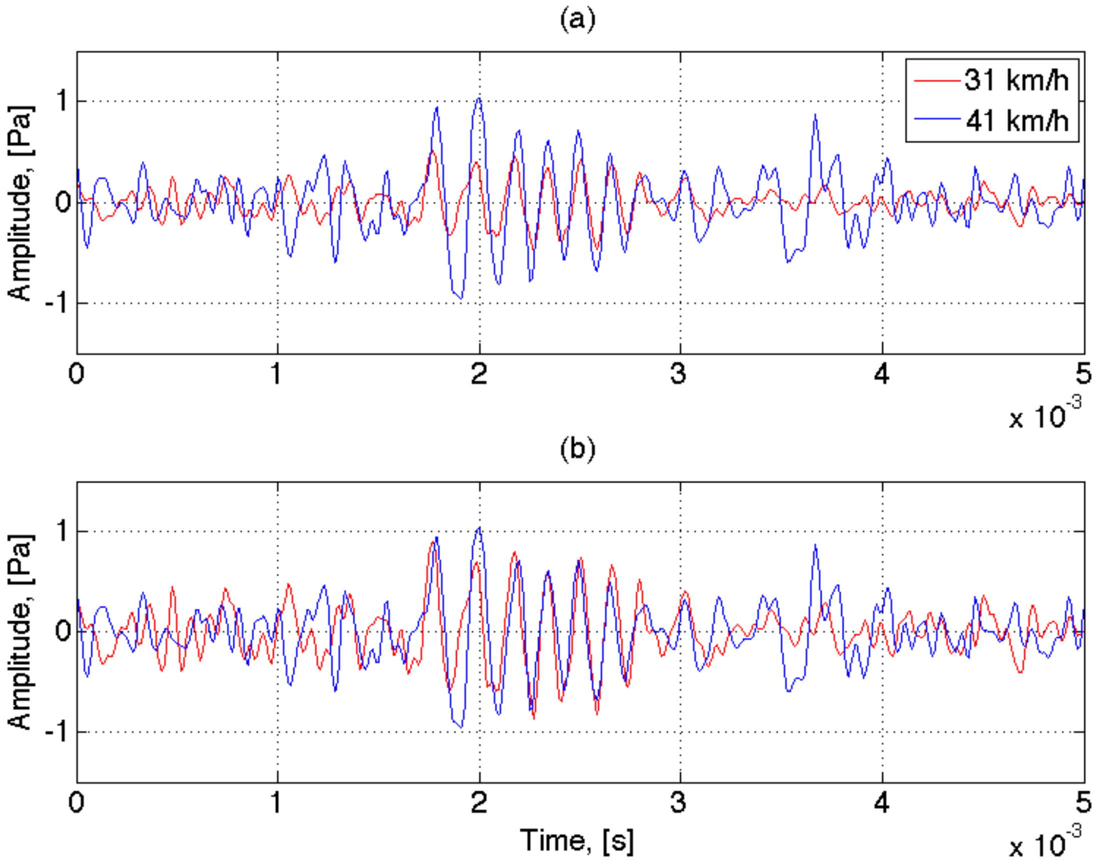

Figure 6.21 Example peak of the trailing edge signal from the tyre with the ‘chevron groove’ for two different speeds: (a) normal recordings; and (b) slower velocity signal multiplied by speed factor

Figure 6.21 shows the comparison of the trailing edge signals of 31 km/h and 41 km/h for the tyre equipped with the chevron type of groove. The signals show a similar shape. In Figure 6.21b the slower speed recording (red) is multiplied by the speed factor that again leads to similar amplitudes of the oscillations when compared to the recording of 41 km/h (blue). Hence, an air effect is supposed to be the source of that oscillation at the trailing edge.

6.2. Conclusion

Interesting results have been presented for more realistic treaded tyres. However, it is shown that with those kind of grooves the complexity of the whole signal generated by air movements at the contact patch is increased significantly. For the grooved tyres first of all a signal is generated when the groove enters the contact patch. This then is converted into the groove resonance and afterwards into the “air resonant radiation”. At the very end of the process it can go back to the groove resonance depending on groove size. The first three stages could be observed for both types of grooves used during the experiment. When the maximum peaks are compared the tyre with the ‘square groove’ shows very similar maximum pressure amplitudes for both leading and trailing edge. However, for the tyre with the small groove the maximum amplitude of the oscillation at the trailing edge is more significant. The “ventilation” of the groove could explain this. The ‘small groove’ is not as effectively ventilated because of the smaller square section in comparison to the ‘square groove’ (both have the same groove length). Thus, the air resonant radiation dominates for the tyre with the ‘small groove’ as it does for the tyres equipped with cavities. The signal at the trailing edge also is not converted into the groove resonance anymore after the air resonant radiation occurred. For the ‘small groove’ the leading edge recording only shows the groove resonance, until the very end of the signal.

Again the amplitudes of the signals are dependent on the speed of the tyre. The pressure amplitudes are, as in the previous chapter, proportional to the squared velocity of the tyre. This is found for the groove resonance recorded at the leading and trailing edge and also for the air resonant radiation only recorded at the trailing edge

The tyre with the chevron cut into the tread, only produces noise in one direction of rotation. When the chevron points to the direction of rotation no recognisable noise is generated. The shape of the chevron could explain this. While the chevron points in the direction of rotation the air can escape at the leading edge towards the open ends of the chevron. However, when the chevron points against the direction of rotation an air movement can be recorded at the trailing edge. Due to the fact that the open ends of the chevron are squeezed first at the leading edge an air movement into the chevron is initiated. Thus, an airwave is moving towards the inside of the chevron. At the trailing edge this airwave that is reflected at the inside, is released out of the chevron. This movement generates a sound that is explained by the groove resonance rather than by the air resonant radiation. Again the amplitude of the signal produced by the tyre with the chevron is shown to be proportional to the squared tyre velocity. This experiment could be an explanation for the high amount of tyres, equipped with a directional tread, that are used recently. The directivity leads to a reduction in aerodynamic noise generation on both sides: the leading and the trailing edge of a tyre.

Chapter 7

Results and discussion: trailing edge

In this chapter the event at the trailing edge of tyres with cavities is analysed. Results in Chapter 5 indicated a higher pressure amplitude at the trailing edge in comparison to the leading edge. In addition to that, the leading edge microphone recorded oscillations generated at the trailing edge as well, as presented in Chapter 5. Therefore, a clear signal is expected at the trailing edge. The trailing edge pulse is also more consistent than the leading edge one [Ronneberger, 1989], thus there is no averaging process applied as used for the leading edge signal.

7.1. Circular cavities

The first tread shapes investigated are the circular cavities. In analogy to Chapter 5, the 'large cavity' is considered first. For the trailing edge signal only one model is available that is presented by Nilsson [Nilsson et al., 1979]. This mathematical approach to predict the frequencies of oscillations at the trailing edge of a tyre with a groove is explained in detail in Chapter 3. The recordings produced by all cavities are compared to the model and it is expected to find a similar relationship between the signals for the different speeds as it was found for the single leading edge pulse.

7.1.1. Large cavity

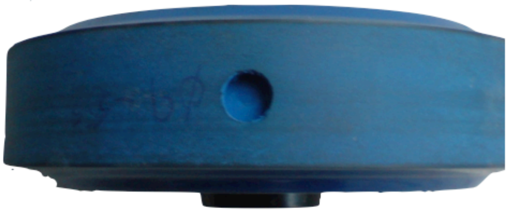

Figure 7.1 Photograph of top view of the tyre equipped with the 'large cavity'

The signal produced at a speed of 41 km/h by the tyre with the 'large cavity' at the trailing edge is shown in Figure 7.2. For comparison the unfiltered (Figure 7.2a) and bandpass filtered signal (Figure 7.2b) are shown. Even with no filter applied, the signal produced is strong and the event happening at the trailing edge can be identified clearly. The amplitudes are sharp and the variations in the maximum pressure reached by each peak are not significant.

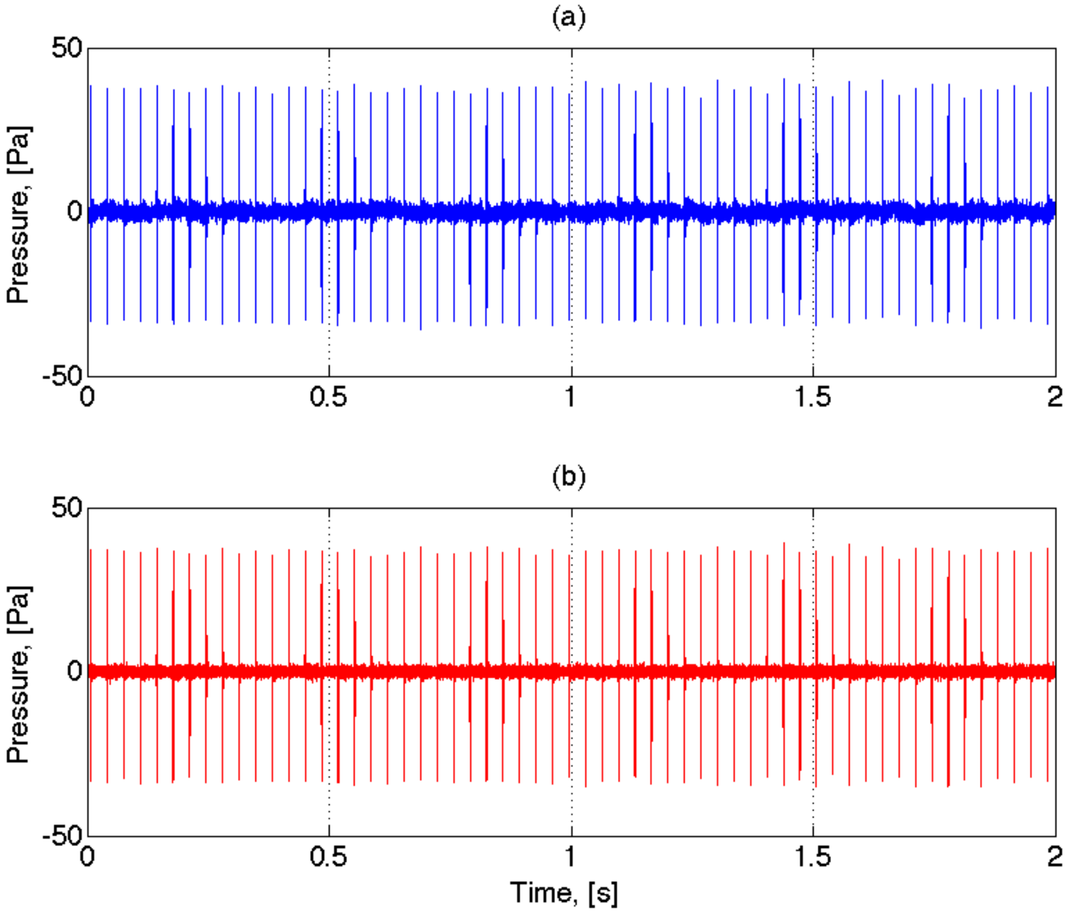

Figure 7.2 Time history of the trailing edge signal generated by the tyre with the 'large cavity' at 41 km/h: (a) unfiltered; and (b) bandpass filtered signal

For the filtered signal in Figure 7.2b, as for the leading edge signal, a 2nd order bandpass Butterworth filter is implemented via the software Matlab. The only difference between the unfiltered and the filtered signal is the noise around the centreline of the signal that is significantly reduced by the filter used. A detailed example event of the filtered signal from Figure 7.2b is presented in Figure 7.3.

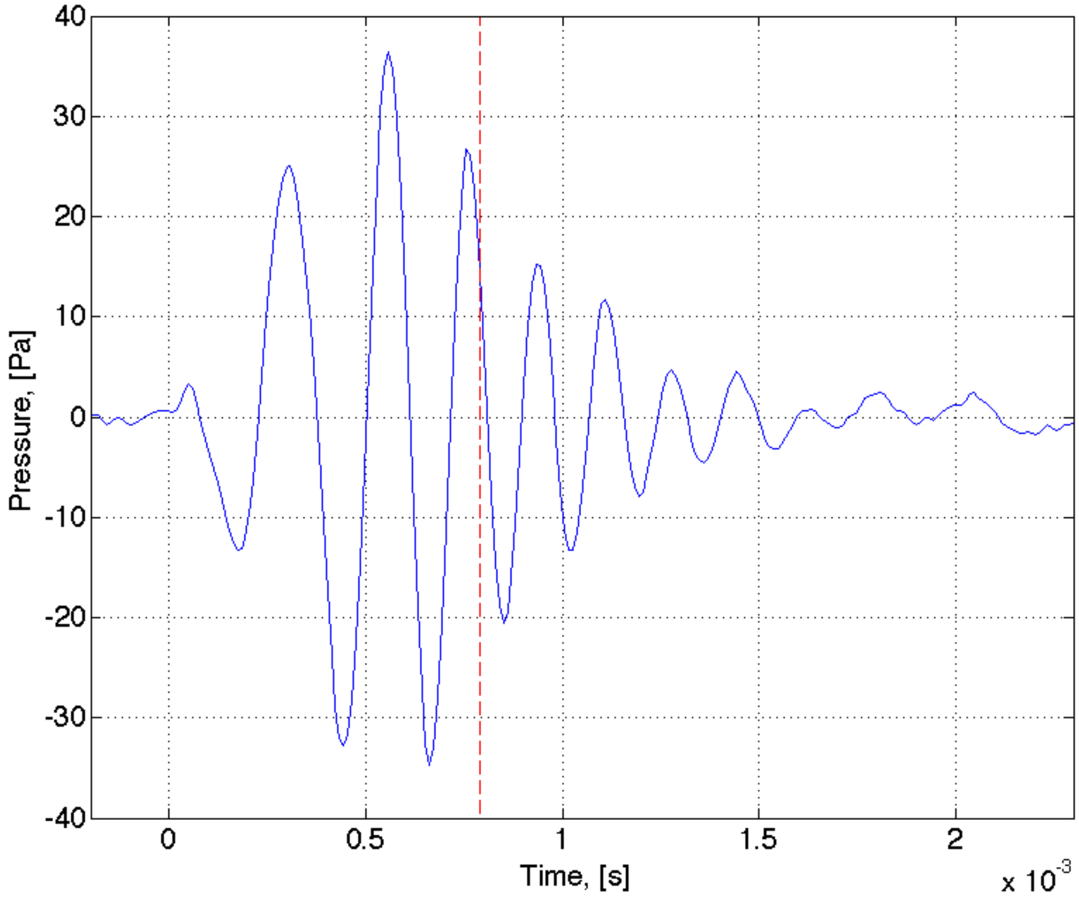

Figure 7.3 Magnified example event of the trailing signal generated by the tyre with the 'large cavity' at 41 km/h, including marked position "cavity fully open" (red dotted line)

For a better analysis this event is shifted towards zero on the time axis that now marks the beginning of the signal. The trailing edge recording consists of an oscillation, whose amplitude increases first until a certain point (0.6 s), then decreases again until it is overlaid by the noise of the chassis dynamometer (1.6 s). This oscillation is also picked up by the microphone at the leading edge, as Figure 5.8 reveals. To clarify the relationship between cavity position and the oscillation, the red dashed line is introduced into

Figure 7.3. It marks the time when the ‘large cavity’ is fully open and not partly covered by the road surface anymore. The time for this to happen at a speed of 41 km/h is taken from Table 5.27. The maximum amplitude of the oscillation is reached before the cavity is fully open. This means that the resonator is most efficient when the road still covers about 1/3 of the cavity. Furthermore a frequency change takes place in the signal, showing a low frequency at the beginning that is rising towards the end of the oscillation. So the next logical step is to analyse the frequency content of this oscillation. The Fast Fourier Transform of the leading edge signal in Figure 5.40 shows a broadband frequency content in between 2000 and 6500 Hertz for the whole recorded time signal. To analyse a single oscillation adequately the instantaneous frequency is needed that will give information about the frequency at a certain time instead of just for the complete signal analysed.

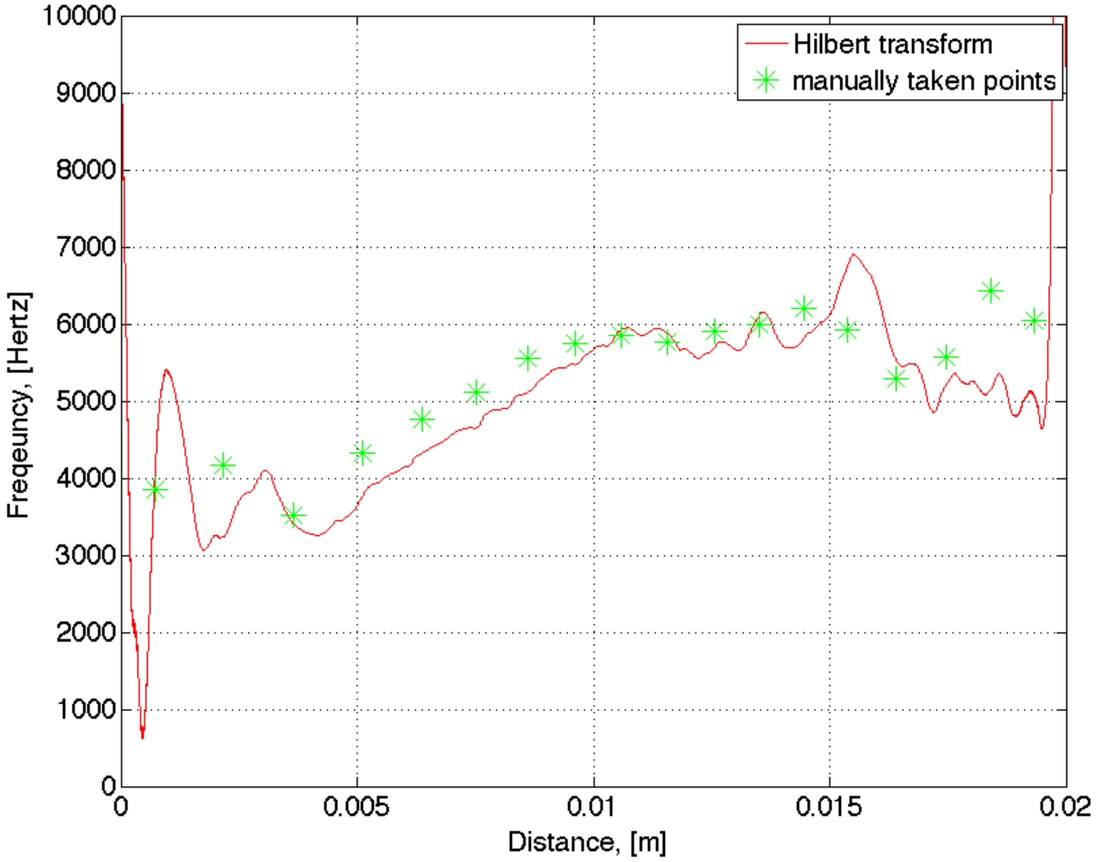

Figure 7.4 Instantaneous frequency in comparison to the frequency calculation via the maxima and minima of the oscillation found at an example event at the trailing edge of the tyre with the ‘large cavity’ at 41 km/h

Initially two different approaches are used to obtain the instantaneous frequency. These are a manual approach and the Hilbert Transform, explained in Chapter 4. For the manual approach the inverse difference of a neighbouring minimum and maximum value is calculated, multiplied by the factor 0.5. This results in the frequency in between the two points. The Hilbert Transform analyses the whole time signal and gives out the frequency at each point of the oscillation. Figure 7.4 shows a comparison of both ways for the instantaneous frequency, of the example oscillation from Figure 7.3. This time however the frequency is plotted over distance and not time, that enables a comparison of the different tyre speeds to each other. The green double crosses in Figure 7.4 mark the manually taken frequencies of all maxima and minima in Figure 7.3, the red line is the converted signal by the Hilbert transform. Both show good agreement indicating both ways deliver a decent analysis for the instantaneous frequency of the reviewed signal. For further investigation the manual approach is preferred to the Hilbert Transform. This is taken for two reasons, first of all due to the fact that it delivers quick results when implemented by a routine in Matlab and secondly because it is less influenced by noise in the signal. The Hilbert Transform is very sensitive when noise is present in a signal, as the beginning and the end of the red line in Figure 7.4 indicates.

The frequency content of the example oscillation lies between 3500 and 6200 Hertz that is similar to the results obtained by the Fast Fourier Transform of the whole time history as shown in the Frequency analysis section of Chapter 5. Starting at 3500 Hertz the frequency rises while the distance from the cavity to the road is increasing. The maximum frequency is reached at a cavity position of about 0.015 m away from the road surface, after that the frequency decreases again. Now the instantaneous frequency of events at lower tyre speeds is determined to draw conclusions for different velocities.

One example oscillation of the trailing edge signal for each speed measured is presented in Figure 7.5. In the top plot of Figure 7.5 the 41 km/h recording is shown in the middle it is 31 km/h and at the bottom 19 km/h. The first remarkable thing is the magnitude of the oscillations that increases with speed. The maximum amplitude of the oscillation is not at the same time for every speed recorded, this could be dependent on the cavity position. Again the red dashed line marks the point of the fully open cavity. Similar to the leading edge signal the duration of the oscillation is nearly the same for all tyre speeds. At the beginning of the process the frequencies decrease with speed this fact makes it difficult to overlay the signals and compare the amplitudes. The comparison of the instantaneous frequency of those three oscillations to the predictions calculated by Nilsson [Nilsson et al., 1979] is shown in the next figure.

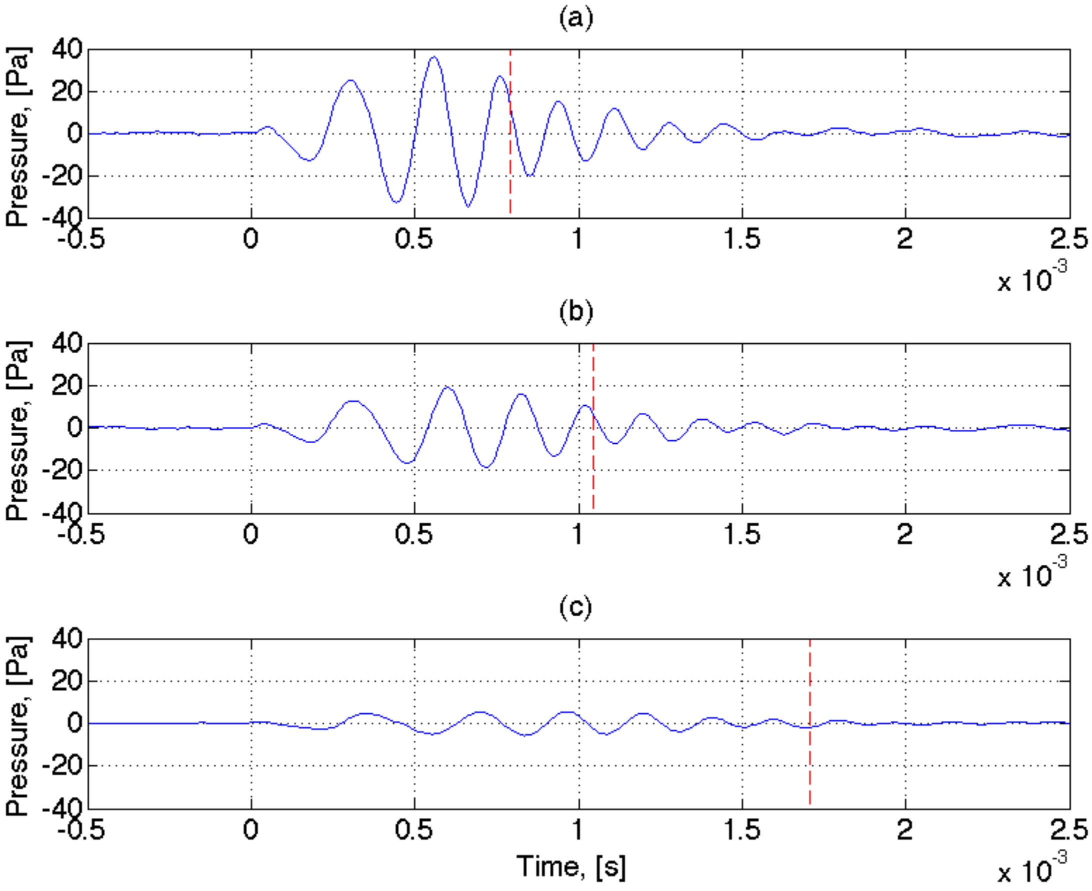

Figure 7.5 Example events of trailing edge signal from the tyre with the 'large cavity' at: (a) 41 km/h; (b) 31 km/h; and (c) 19 km/h

As mentioned in Chapter 3, where the Nilsson model is explained in detail, Nilsson supposes a frequency modulation of the resonance frequency measured at the trailing edge of a tyre with a transversal groove in the tread. This frequency change occurs due to the fact that the air volume in between the groove and road changes when the groove progresses away from the road. In this chapter Nilsson's model is compared to cavities in the tyre. Equation (3.24) shows the mathematical method developed by Nilsson. With this equation the air resonance radiation frequency at the trailing edge can be predicted in dependence of the position of the cavity in respect to the road. The only parameters needed are tyre geometry and cavity dimension. In addition to that Nilsson introduces two variables whose quantity (between zero and one) can be freely chosen for best fit to the measured data. Those two variables are β and γ. The chosen values for them in accordance to the measurements are listed in Table 7.1. These two determined values are used for all the different cavity types analysed in this thesis. Thus, they are tyre dependent not cavity dependent.

Nilsson model variables

β	γ
0.16	0.3

Table 7.1 Chosen variables for best fit of predicted frequency (by Nilsson) to results

Figure 7.6 presents the results obtained by comparing the instantaneous frequency of the three tyre speeds of the tyre with the 'large cavity'. The red crosses mark the frequencies for 19 km/h, the blue ones for 31 km/h and the green double crosses show the results of the tyre velocity of 41 km/h. The purple line indicates the instantaneous frequencies predicted by the Nilsson model for this kind of cavity. A good fit of the measured frequencies to the predictions by Nilsson is achieved nearly over the whole range of the measurements. At the beginning (the first two crosses for each speed) there is a slight mismatch between the model and the measurements. This could be due to the fact that the cavity is still mainly covered by the road, hence compressed by the load. Thus, the cavity volume is changing that in the Nilsson model is assumed to be constant. Also the reference point for the position of the cavity used by Nilsson to compute the area underneath the cavity is actually the middle of the cavity. This means the Nilsson model is only valid when the middle of the cavity lifts off the road, for the 'large cavity' this at a position of 0.0045 m. From this point on, model and measured data overlay nicely. However, this does not mean that there is no noise generation at an earlier point, when the cavity just lifts off the road. A noise is generated with slightly higher frequencies that are increasing with speed (this is similar to the leading edge pulse behaviour), but this is not incorporated in Nilsson's model. At the end of the oscillation the signal is not of a strong nature anymore, the noise from the chassis dynamometer becomes dominant again. Therefore, the match between the Nilsson model and the measured frequencies is not satisfactory for higher distances than 0.015 m. Nevertheless over the whole range a good agreement is presented for the signal at the trailing edge of the tyre with the 'large cavity' in comparison to the model derived by Nilsson.

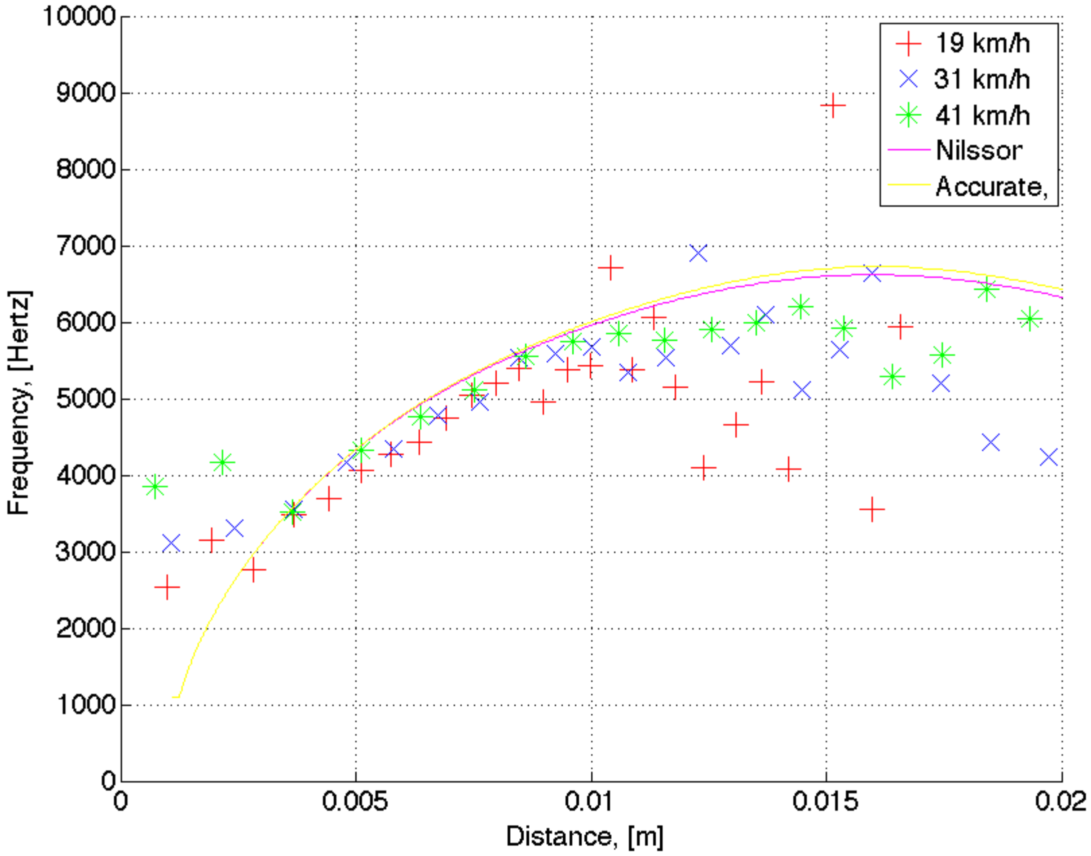

Figure 7.6 Instantaneous frequency of the oscillations at the trailing edge produced by the tyre with the 'large cavity' in comparison to the frequency change predicted by Nilsson [Nilsson et al., 1979]

In Chapter 3 it is mentioned that Nilsson used a mathematical simplification to calculate the area *S* underneath the cavity in his model. But as previously stated until a distance of 0.015 m the differences between the accurate calculation and the assumptions made by Nilsson are negligible.

This is also confirmed by the yellow line in Figure 7.6 that shows the frequency predictions for the accurate area, *S*, calculated by Equation (3.19).

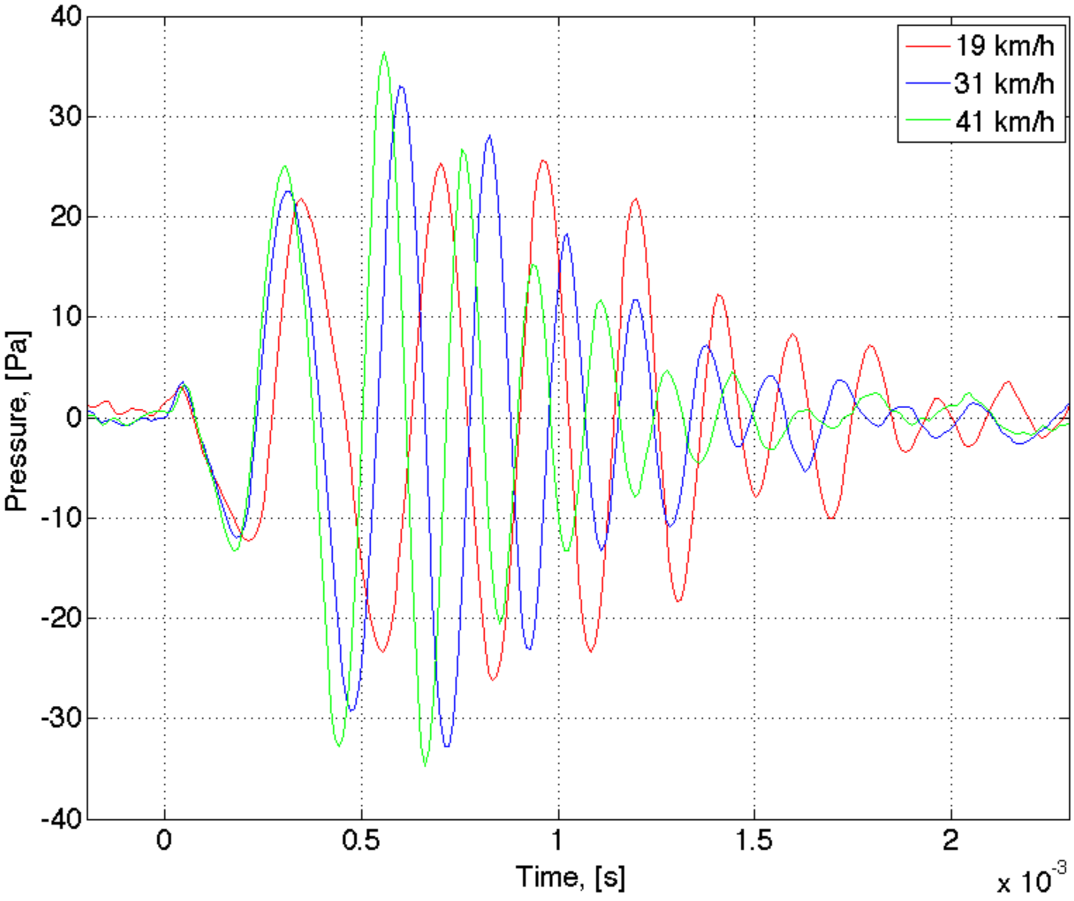

Figure 7.7 Trailing edge signal comparison of an example event of the tyre with the 'large cavity' in reference to the speed of 41 km/h, the other signals are multiplied by the speed factor

Now the three different example events are compared visually over time. The pressure at the leading edge appears to be proportional to the squared power of velocity as shown in Chapter 5. This is also tested for the trailing edge signal. Figure 7.7 shows the oscillations of the three speeds now combined in one plot. The lower speed oscillations are multiplied by the difference of velocity squared in relation to the reference speed of 41 km/h. Again red is used for 19 km/h, blue for 31 km/h and green for 41 km/h. At the beginning of the oscillation a good fit is obtained between the amplitude and phase of the different signals. Afterwards, however, the oscillations differ in signature. One important point is the maximum value reached by each oscillation. This value differs with speed, the higher the speed the earlier the oscillation reaches its maximum value. Another difference is the frequency; with higher speed the frequency of the oscillation also changes quicker. Thus, a comparison of the oscillations generated at different tyre speeds is difficult. Generally speaking the pressure oscillation at the trailing edge seems to be proportional to the squared power of velocity, however, due to the different speed and damping included, this can only be confirmed for the initial oscillations at the trailing edge, that are similar to the leading edge signal as shown in Chapter 5.

7.1.2. Small cavity

The next results presented are the trailing edge recordings of the tyre with the 'small cavity' (Figure 7.8). As shown for the leading edge signal even this small whole in the tyre tread produces an air movement that was picked up by the microphone. Thus, for the trailing edge the signal should be even more significant.

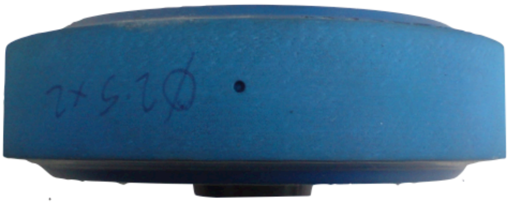

Figure 7.8 Photograph of top view of the tyre equipped with the 'small cavity'

Figure 7.9 presents example events of the trailing edge oscillation of the 'small cavity' for the three tyre speeds measured. At the top the event for 41 km/h is plotted, in the middle 31 km/h and at the bottom 19 km/h. In comparison to the oscillations produced by the 'large cavity' those ones are smaller, in duration and amplitude. Again the maximum amplitude of the signal is reached before the point when the cavity is fully open (marked by the dashed red line). The frequency content of this rather weak signal is analysed in the next figure.

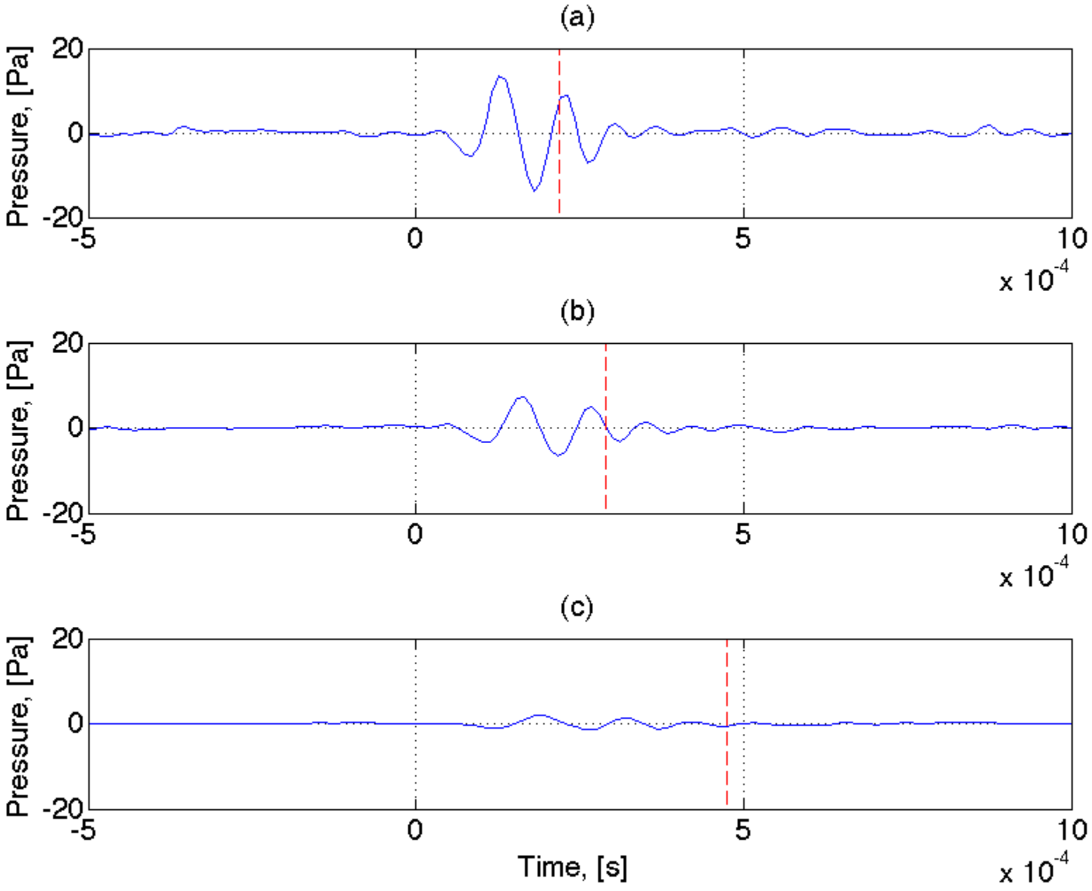

Figure 7.9 Example events of trailing edge signal from the tyre with the 'small cavity' at: (a) 41 km/h; (b) 31 km/h; and (c) 19 km/h

To compare the model from Nilsson to the frequencies of the oscillations produced by the 'small cavity', the cavity dimensions implemented in the model need to be adjusted. However, the factors β and γ introduced before, remain constant because the tyre geometry is still the same. Figure 7.10 shows the frequency change predicted by Nilsson's model with a purple line. Red crosses are used for 19 km/h, blue ones for 31 km/h and green double-crosses for a tyre velocity of 41 km/h. Although the amplitude of the oscillations is not high, it still produces satisfactory results regarding the instantaneous frequency, when compared to the predicted frequency modulation. However, the results are not as good as for the 'large cavity'. This is due to the fact that the air pressure movements generated by the 'small cavity' are of small amplitude; hence, the produced signal in comparison to the noise of the chassis dynamometer is low. However, nevertheless air resonant radiation seems to be active even for the tyre with the ‘small cavity’.

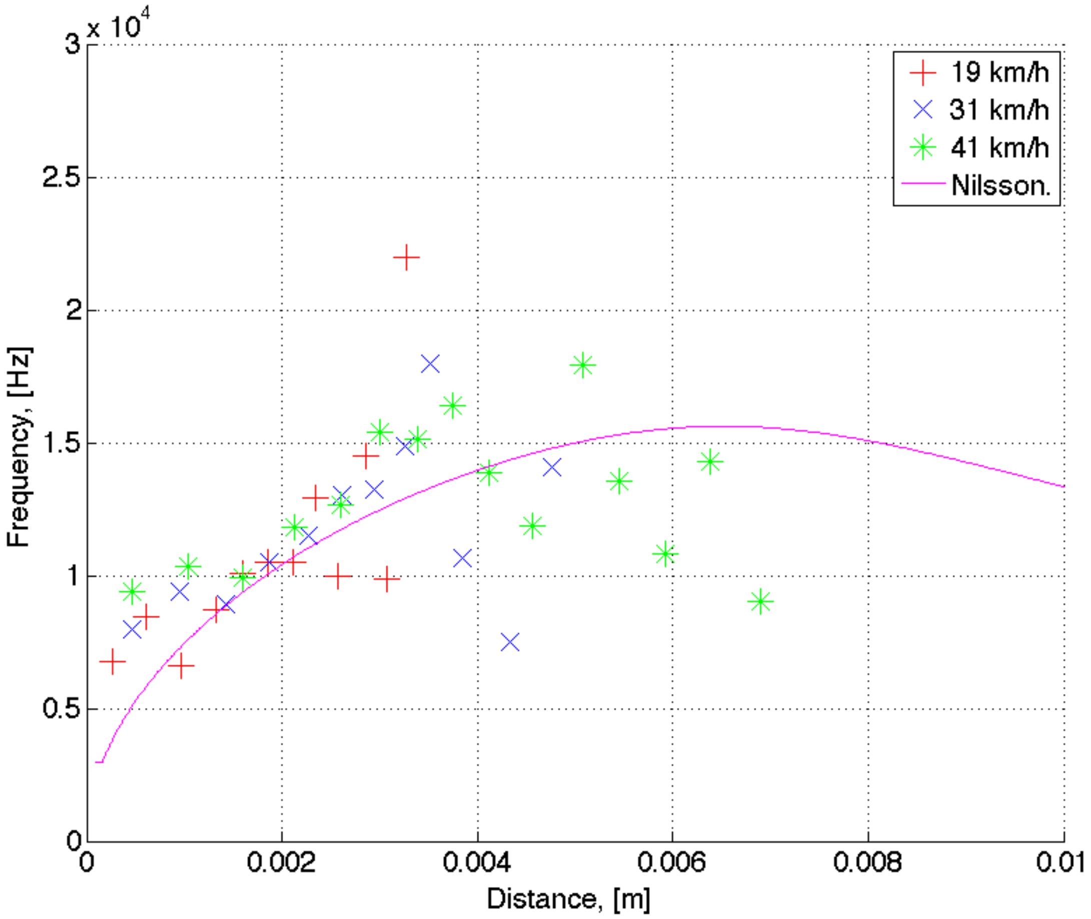

Figure 7.10 Instantaneous frequency of the oscillations at the trailing edge produced by the tyre with the ‘small cavity’ in comparison to the frequency change predicted by Nilsson [Nilsson et al., 1979]

The example oscillations from the different velocity recordings of Figure 7.9 are combined in Figure 7.11. 41 km/h is the reference speed drawn in green. The other two signals from 31 km/h (blue) and 19 km/h (red) are multiplied by the according speed factor used for the leading edge signal introduced in Chapter 5. In comparison to the results of the ‘large cavity’ the fit for the different speeds is better. An explanation for this could be the cavity length (in rotational direction). When the resonance is initiated by the ‘small cavity’ the time needed to fully open the cavity is shorter, so it is not that influenced by damping of the surrounding air. It is shown that the amplitudes of the oscillations generated by the ‘small cavity’ at the trailing edge are proportional to the squared tyre velocity.

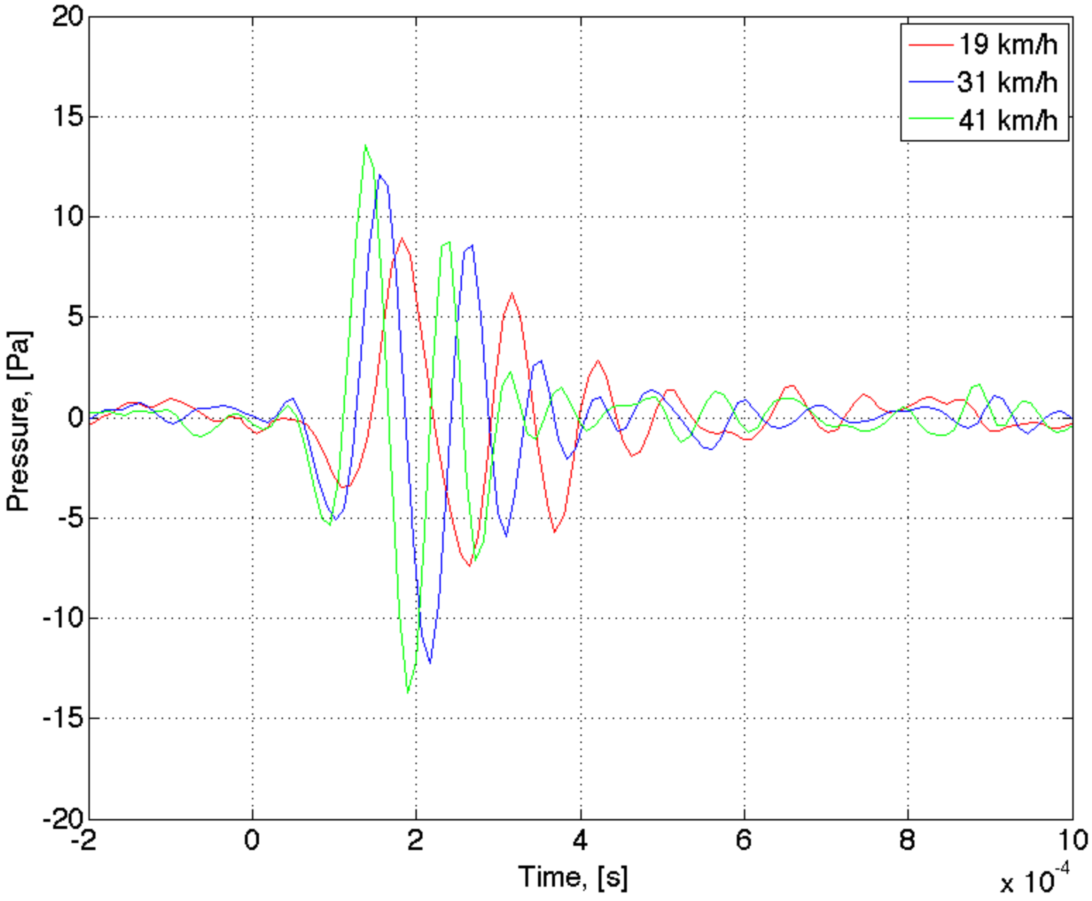

Figure 7.11 Trailing edge signal comparison of an example event of the tyre with the ‘small cavity’ in reference to the speed of 41 km/h, the other oscillations are multiplied by the speed factor

7.2. Rectangular cavities

As the air resonant radiation is found to be the mechanism at the trailing edge for the tyres with circular cavities tested in this Thesis, it is interesting to see if there is any connection between the amplitude of the resonance and the cavity geometry. Therefore the results of the rectangular cavities are presented.

7.2.1. Square cavity

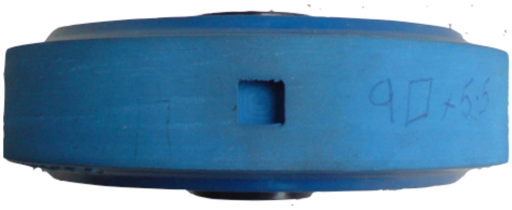

Figure 7.12 Photograph of top view of the tyre equipped with the ‘square cavity’

The ‘square cavity’ shown in Figure 7.12 has the largest volume of all the cavities tested in this Thesis. This tyre is therefore expected to produce the highest level of noise. In comparison to the circular cavities it should yield to even better results at the trailing edge, due to the fact that the square shape is more realistic to a real tyre and this is what the Nilsson model was developed for.

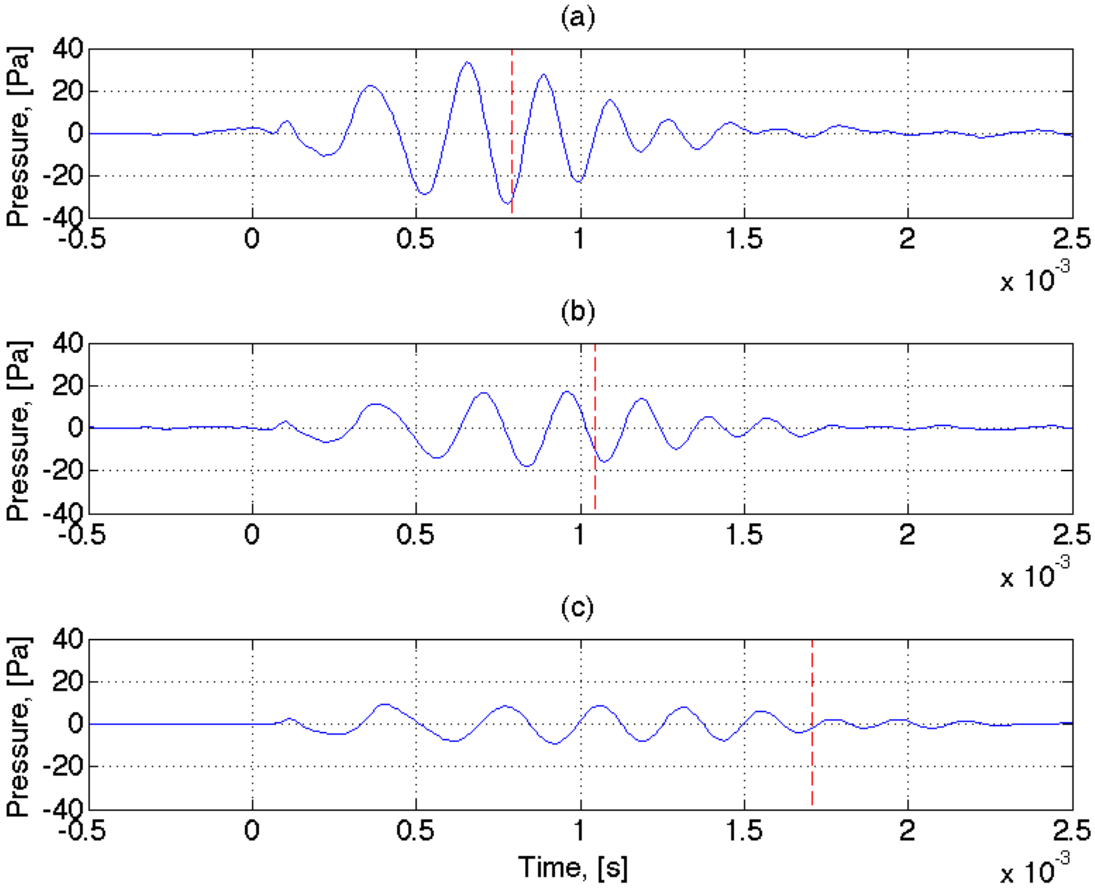

Figure 7.13 Example events of trailing edge signal from the tyre with the ‘square cavity’ at: (a) 41 km/h; (b) 31 km/h; and (c) 19 km/h

The time history of a single event at the trailing edge for the three different tyre velocities are shown separated by their speed in Figure 7.13. Figure 7.13a shows the oscillations of the highest tyre velocity of 41 km/h. This produces the highest amplitude in comparison to the lower speeds of 31 km/h (Figure 7.13b) and 19 km/h (Figure 7.13c). This time the maximum amplitude reached is closer to the time when the cavity is fully open. All the signals have again a similar duration in time, however, the initial frequencies of the oscillations are lower with lower tyre velocities.

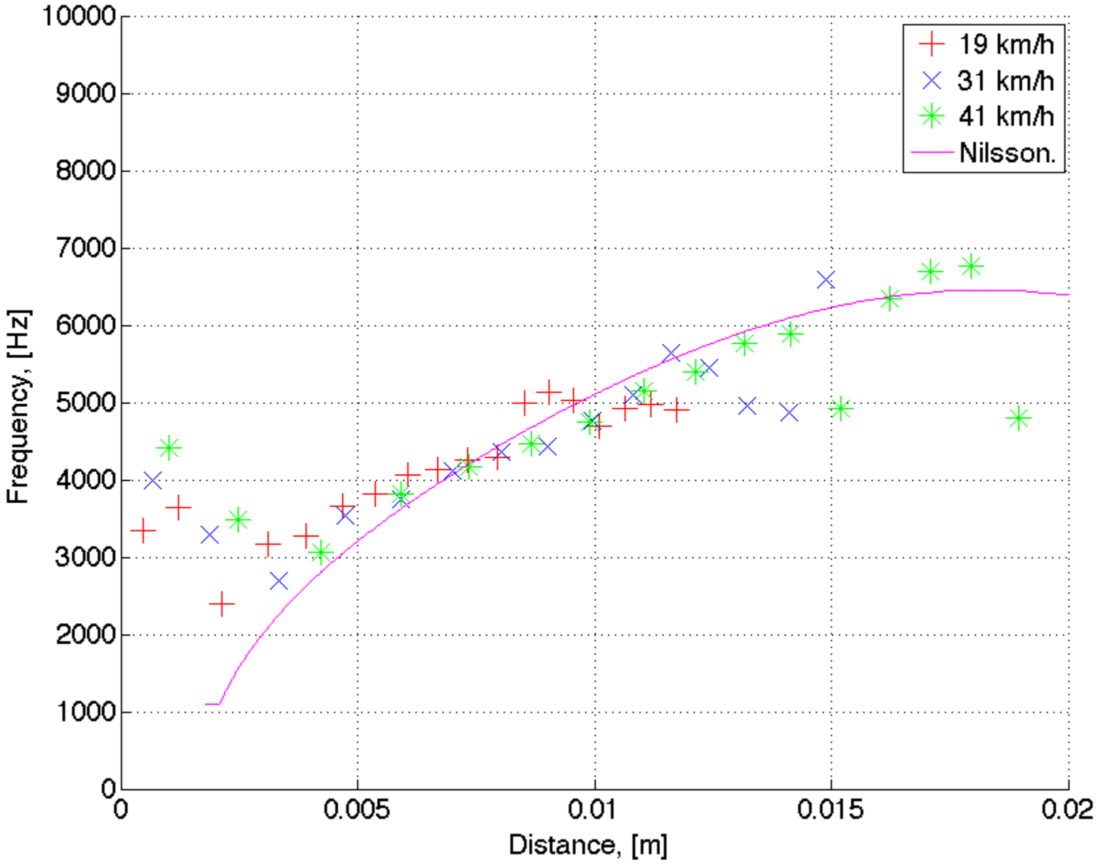

Figure 7.14 Instantaneous frequency of the oscillations at the trailing edge produced by the tyre with the ‘square cavity’ in comparison to the frequency change predicted by Nilsson [Nilsson et al., 1979]

This behaviour is also presented in the analysis of the frequency content of the three signals. Figure 7.14 shows the frequencies measured in comparison to calculated ones from the Nilsson model adjusted to the geometry of this cavity. The green double-crosses mark the instantaneous frequencies of the tyre velocity of 41 km/h the blue crosses mark 31 km/h and the red ones 19 km/h. The initial frequencies for all speeds are higher than predicted by the Nilsson model (purple line), they rise with speed as mentioned before for the other cavities. When the cavity has reached the reference point for the Nilsson model (the middle of the cavity just lifts off the road surface) at 0.0045 m, model and measured frequencies show a good agreement. For this cavity even at the end of the resonance process the agreement between predicted frequency and measured results is good. In addition to that, it is clearly shown that with higher speeds the maximum frequency reached is higher as well. This increase is due to the fact that the oscillation lasts longer (in respect to distance) for a higher tyre velocity.

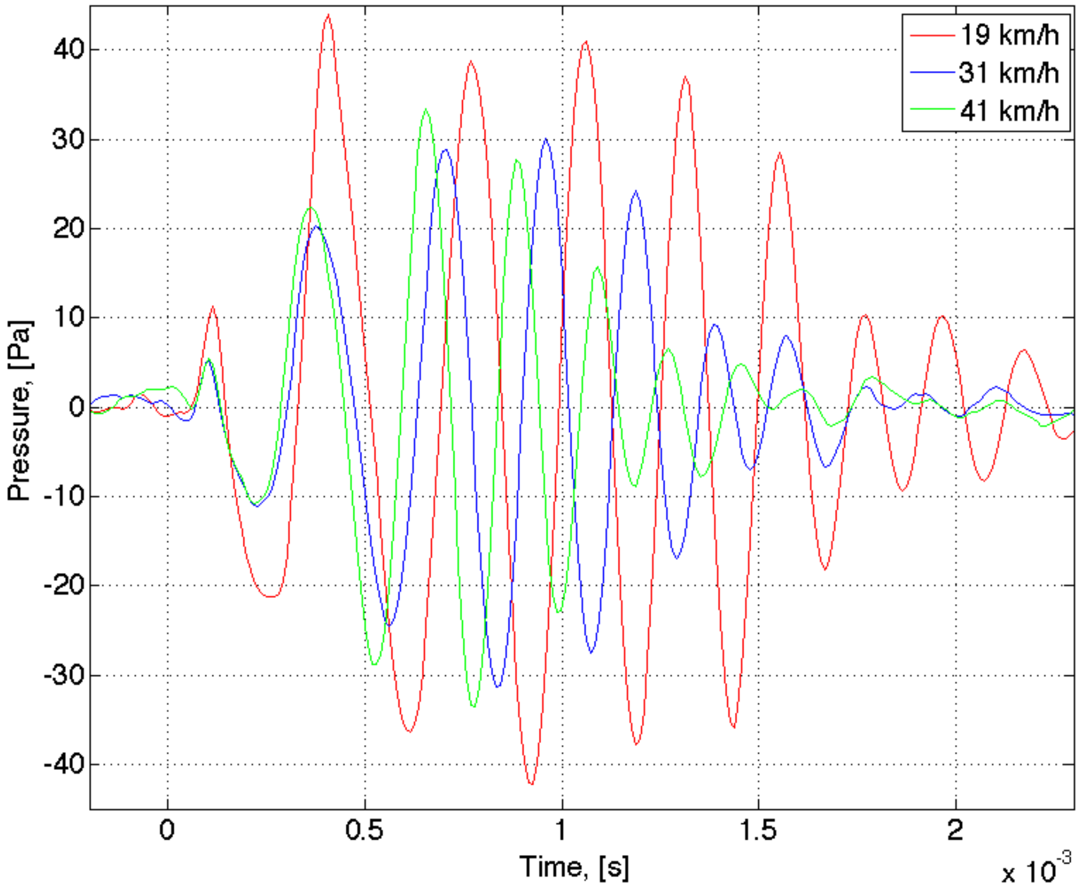

Figure 7.15 Trailing edge signal comparison of an example event of the tyre with the ‘square cavity’ in reference to the speed of 41 km/h, the other oscillations are multiplied by the speed factor

The oscillations for the different velocities are combined for direct comparison in Figure 7.15. Here 41 km/h (green) is the reference signal again which the other examples are compared to. The signals of 31 km/h (blue) and 19 km/h (red) are multiplied by the speed factor according to the velocity difference to 41 km/h. When the blue signal (31 km/h) is compared to the green one (41 km/h) regarding the amplitude and shape a good agreement is achieved. However, this does not work well for the 19 km/h example oscillation. As for the leading edge for this kind of cavity the amplitude at 19 km/h is high in comparison to the other two tyre velocities. This phenomenon would support the idea that the initial excitation of the resonance at the trailing edge is a similar mechanism to that occurring at the leading edge. However, none of the existing models give an explanation why the amplitude of the low speed of 19 km/h is that high in comparison to the other speeds measured.

7.2.2. Long cavity

The trailing edge signal of the tyre with the long cavity is the next to be looked at in detail (Figure 7.16). At the leading edge, presented in Chapter 5, the pressure amplitude seems to be half the magnitude of the one generated by the square cavity that is equivalent to the volume relationship of both cavities. A similar behaviour is expected to be found for the trailing edge signal.

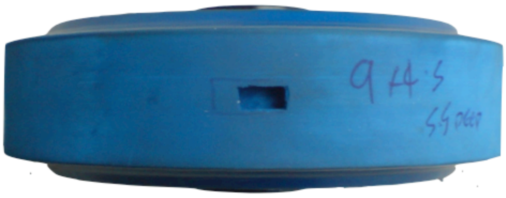

Figure 7.16 Photograph of top view of the tyre equipped with the 'long cavity'

Figure 7.17 shows the events at the trailing edge produced by the 'long cavity' at the three different speeds. The oscillation with the highest amplitude is generated by the tyre velocity of 41 km/h shown at the top of

Figure 7.17. In analogy to a decrease in speed the amplitude decreases as can be seen for 31 km/h (Figure 7.17b) and 19 km/h (Figure 7.17c). The maximum pressure of the oscillation is reached before the cavity is fully open (marked by the red dashed line). Again this approximately takes place when a third of the cavity is still covered by the road.

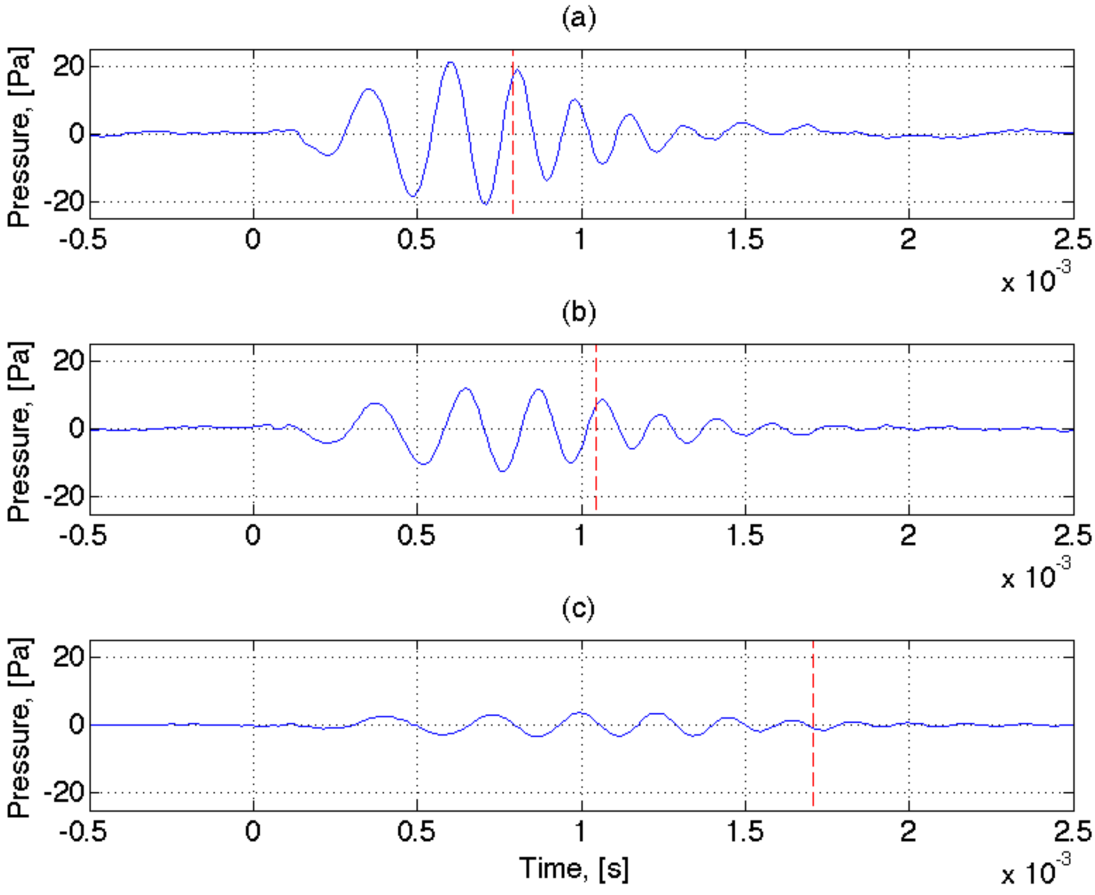

Figure 7.17 Example events of trailing edge signal from the tyre with the 'long cavity' at: (a) 41 km/h; (b) 31 km/h; and (c) 19 km/h

The frequency content of the three signals is shown in Figure 7.18. The purple line in Figure 7.18 marks the predicted frequencies by Nilsson, adjusted to the geometry of the 'long cavity'. The instantaneous frequencies of the three measured oscillations from Figure 7.17 are plotted with the crosses in the colour according to the tyre speed as explained in the legend. Again the first two crosses of every result do not fit to the predictions from the mathematical model. This means that the measured frequencies are actually higher than predicted by Nilsson. Again this takes place before half of the cavity has cleared the road, thus out of the range for the Nilsson model. However, it is still assumed to be the initiation of the air resonant radiation process only this time dependent on the velocity of the tyre. A higher speed results in a higher frequency. The other measured values deliver an especially satisfactory fit to the model, even at the end of the oscillations

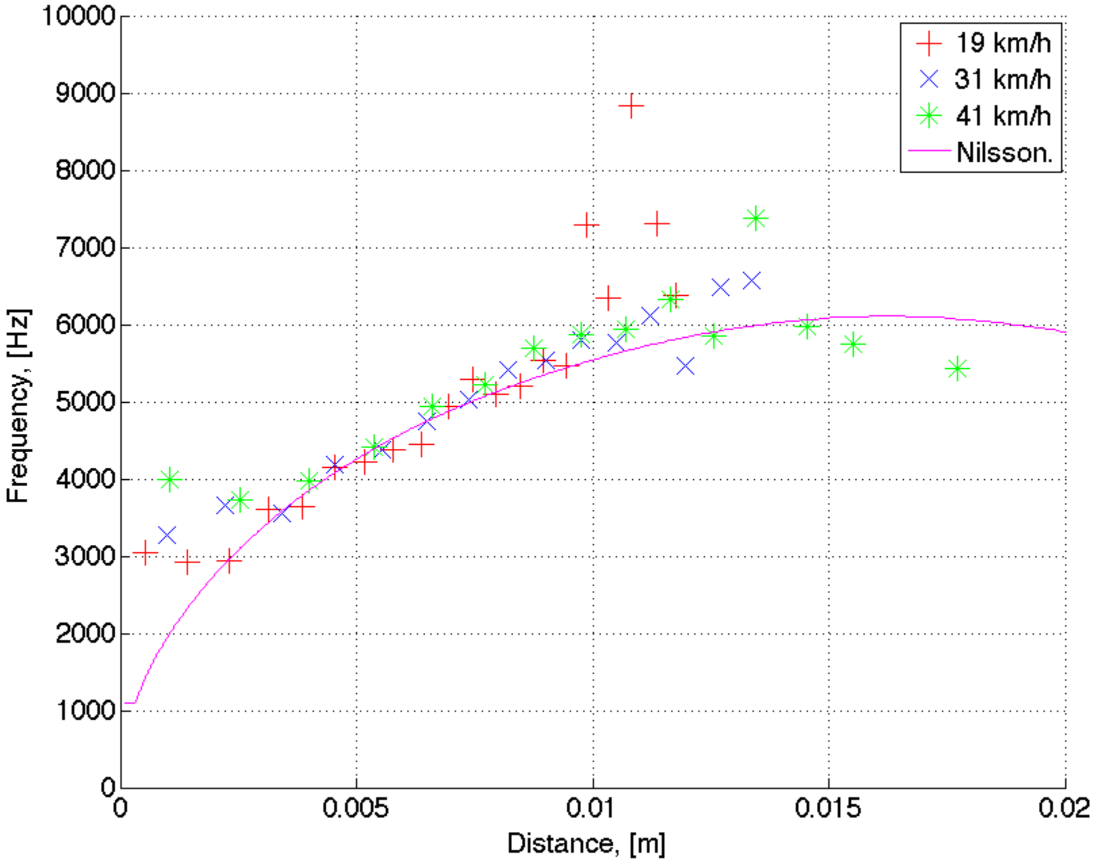

Figure 7.18 Instantaneous frequency of the oscillations at the trailing edge produced by the tyre with the 'long cavity' in comparison to the frequency change predicted by Nilsson [Nilsson et al., 1979]

The last figure for the 'long cavity' shows the amplitude comparison for the different tyre velocities. In Figure 7.19 the oscillation in green generated by the 'large cavity' at the trailing edge at 41 km/h, is the reference signal where the other ones are compared to. Again when the blue signal generated at 31 km/h is multiplied by the squared speed difference it shows similarities when compared to the green signal. For the lower speed of 19 km/h shown in red the fit is not that satisfactory. At the start of the oscillation it is good, however, due to the fact that the cavity moves slower the highest amplitude is lower and reached later.

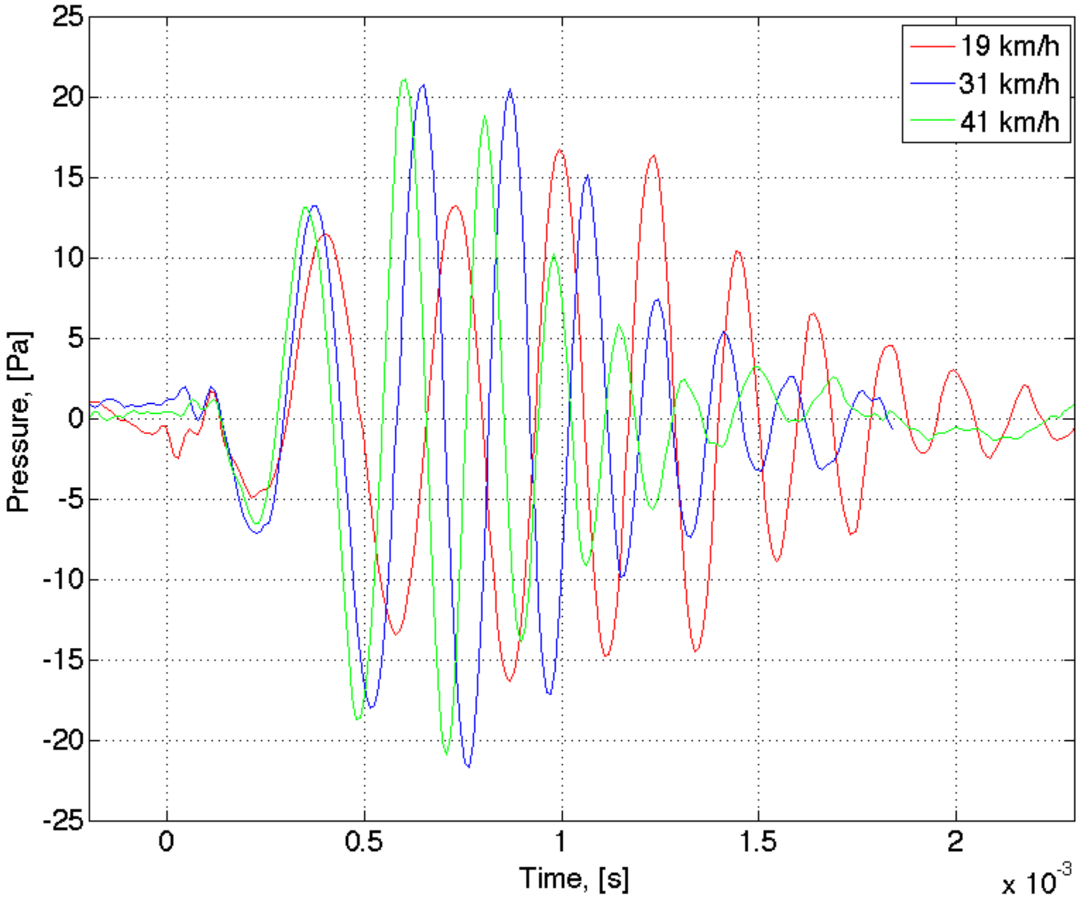

Figure 7.19 Trailing edge signal comparison of an example event of the tyre with the 'long cavity' in reference to the speed of 41 km/h, the other oscillations are multiplied by the speed factor

7.2.3. Wide cavity

The tyre with the 'wide cavity' shown in Figure 7.20 is analysed in this last results section. This tyre has the same cavity volume cut into the tread as the tyre with the 'long cavity' just at a different orientation. Due to this different layout the duration needed for the cavity to be completely open is just half the length in comparison to the other rectangular cavities. At the leading edge this resulted in a higher pressure amplitude as the 'long cavity'.

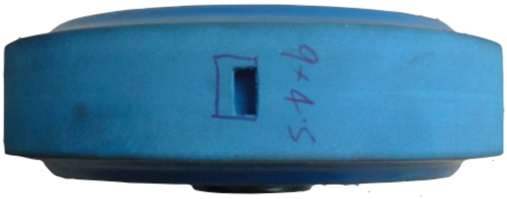

Figure 7.20 Photograph of top view of the tyre equipped with the 'wide cavity'

Figure 7.21 shows three different example events of the trailing edge recordings for the three different speeds analysed. This time, due to the short cavity length in the rotational direction, the maximum amplitude of the oscillations is reached close to the actual time where the cavity is fully opened marked by the red dashed line. Again the length of the signals is similar but the amplitude varies with speed. To get an idea about the frequencies occurring throughout the oscillations the instantaneous frequency is plotted in the figure overleaf.

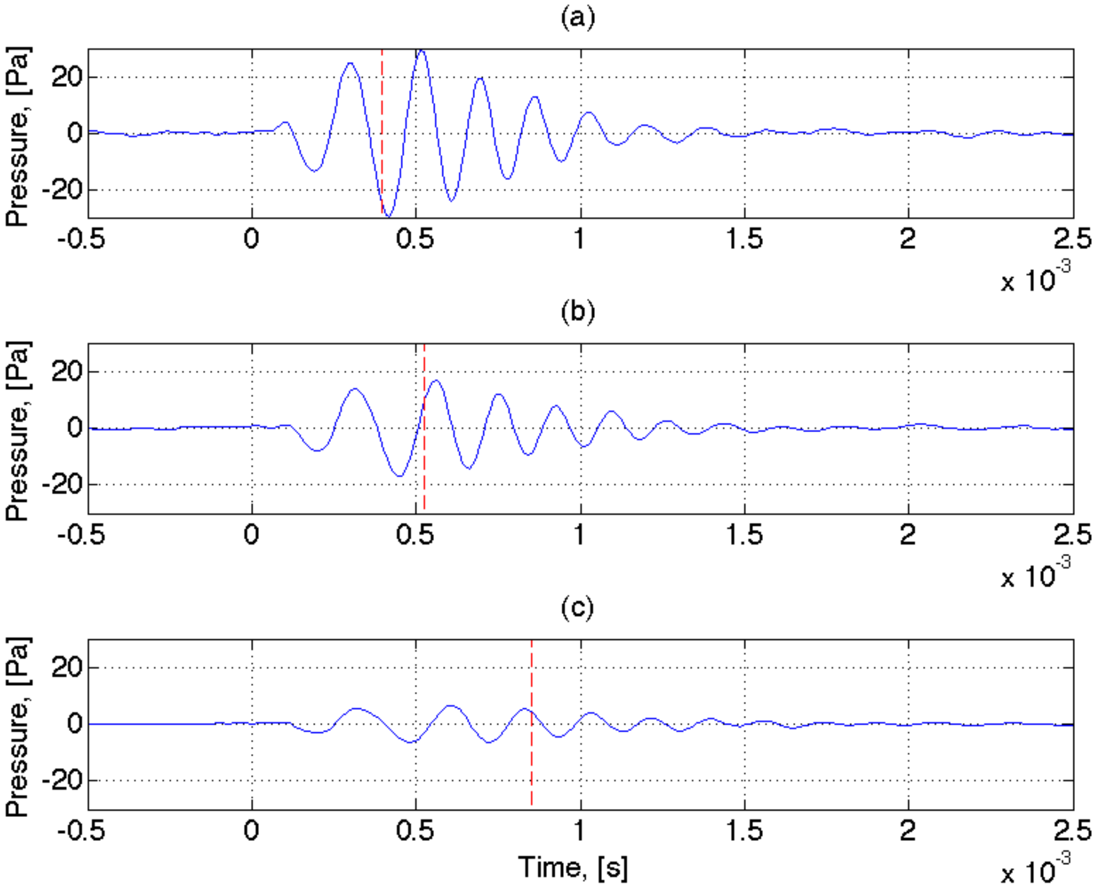

Figure 7.21 Example events of trailing edge signal from the tyre with the 'wide cavity' at: (a) 41 km/h; (b) 31 km/h; and (c) 19 km/h

In Figure 7.22 the comparison of measured frequencies and the Nilsson predictions are shown. Similar behaviour as previously shown is achieved. The first two frequencies points measured do not fit to the Nilsson model and again they are influenced by the rotational speed of the tyre. High frequency values are obtained for the speed 41 km/h (green double cross) and lower ones for the lower speeds of 31 km/h (blue cross) and 19 km/h (red cross). After those two points at the beginning, the measured values of the different velocities plotted over distance result in a similar frequency rise that is predicted by the model from Nilsson. At the end of the process however, lower frequencies are measured as compared to those predicted by Nilsson.

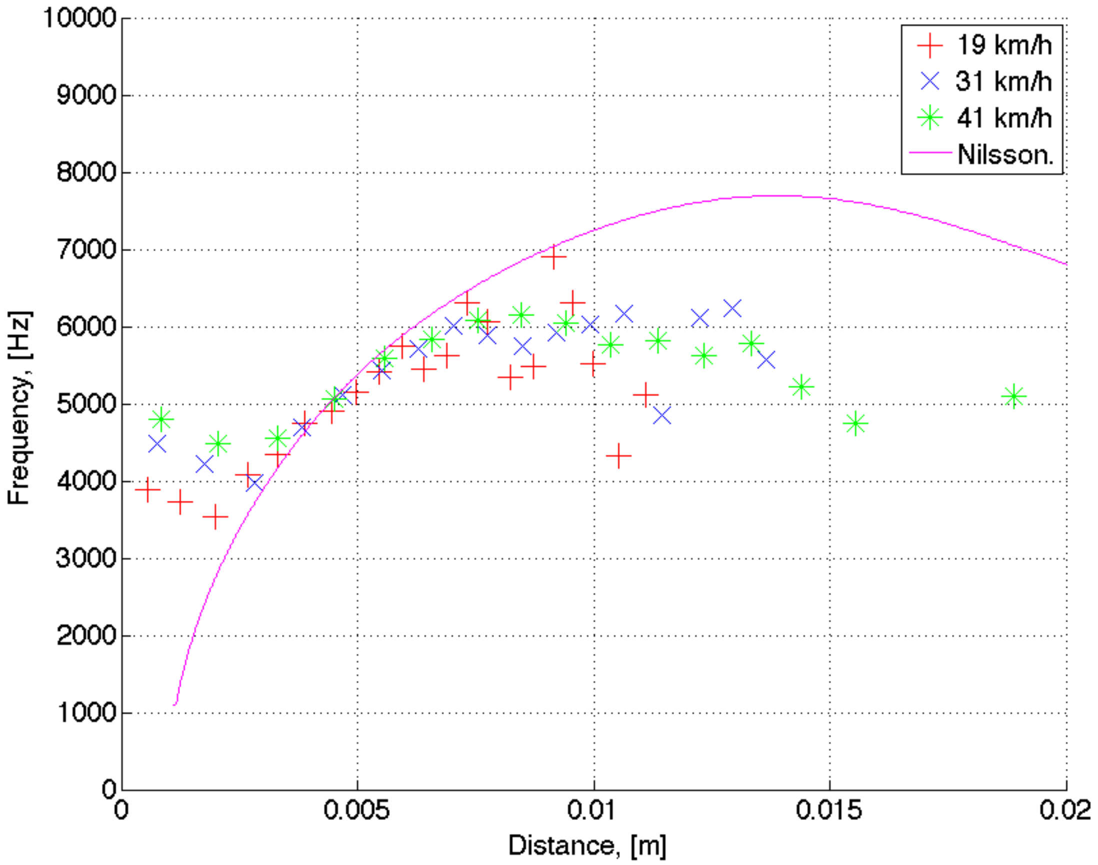

Figure 7.22 Instantaneous frequency of the oscillations at the trailing edge produced by the tyre with the ‘wide cavity’ in comparison to the frequency change predicted by [Nilsson et al., 1979]

The direct comparison of the oscillations, multiplied by the squared velocity difference to 41 km/h, is shown in Figure 7.23. This time the results show a similar shape, even for the low speed of 19 km/h (red). The maximum pressure amplitude reached is the same for all velocities. This is due to a shorter cavity length in the direction of tyre rotation. Therefore, the damping of the surrounding air has not such a big impact on the resonance produced at the trailing edge. It is also remarkable that for the 'wide cavity' a rather high maximum amplitude is reached that is similar to the one produced by the 'square cavity' at the trailing edge.

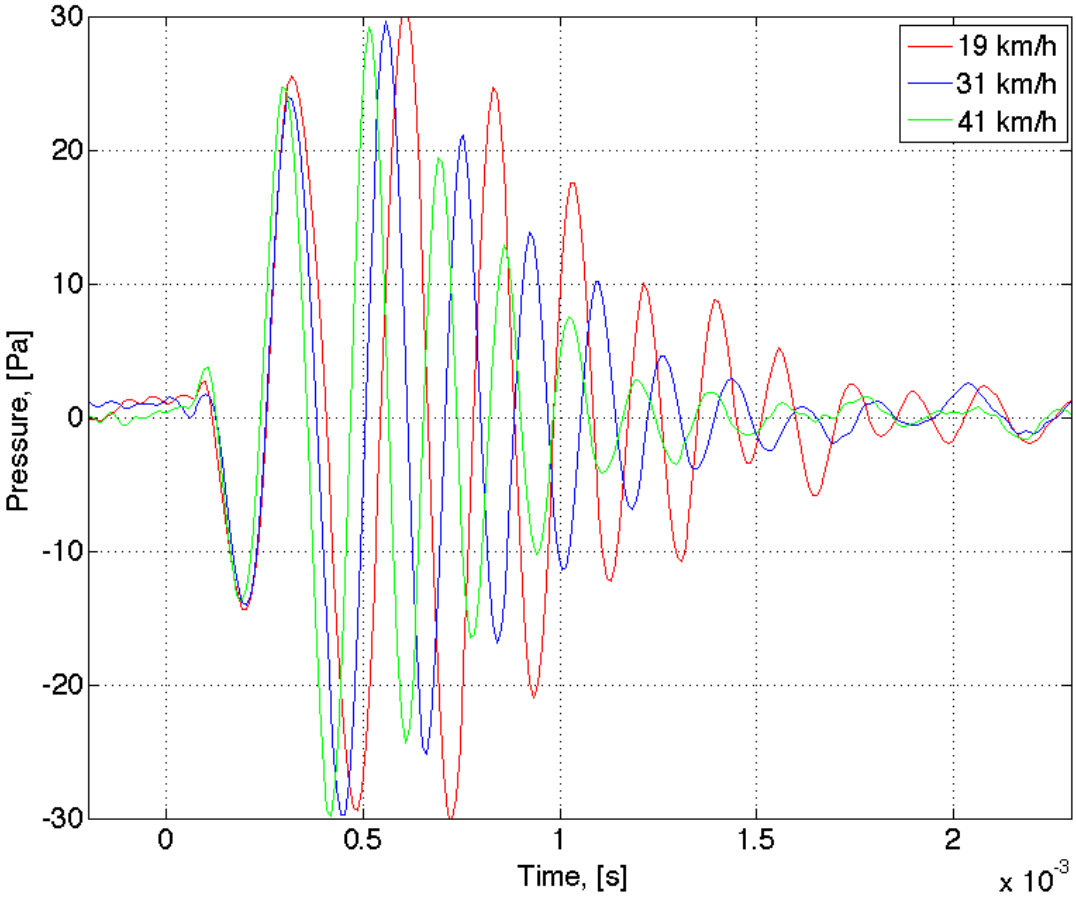

Figure 7.23 Trailing edge signal comparison of an example event of the tyre with the 'wide cavity' in reference to the speed of 41 km/h, the other oscillations are multiplied by the speed factor

7.3. Comparison of the effect of cavity geometry

As presented for the leading edge signal, example oscillations of the different cavities tested are compared to each other at the same speed measured.

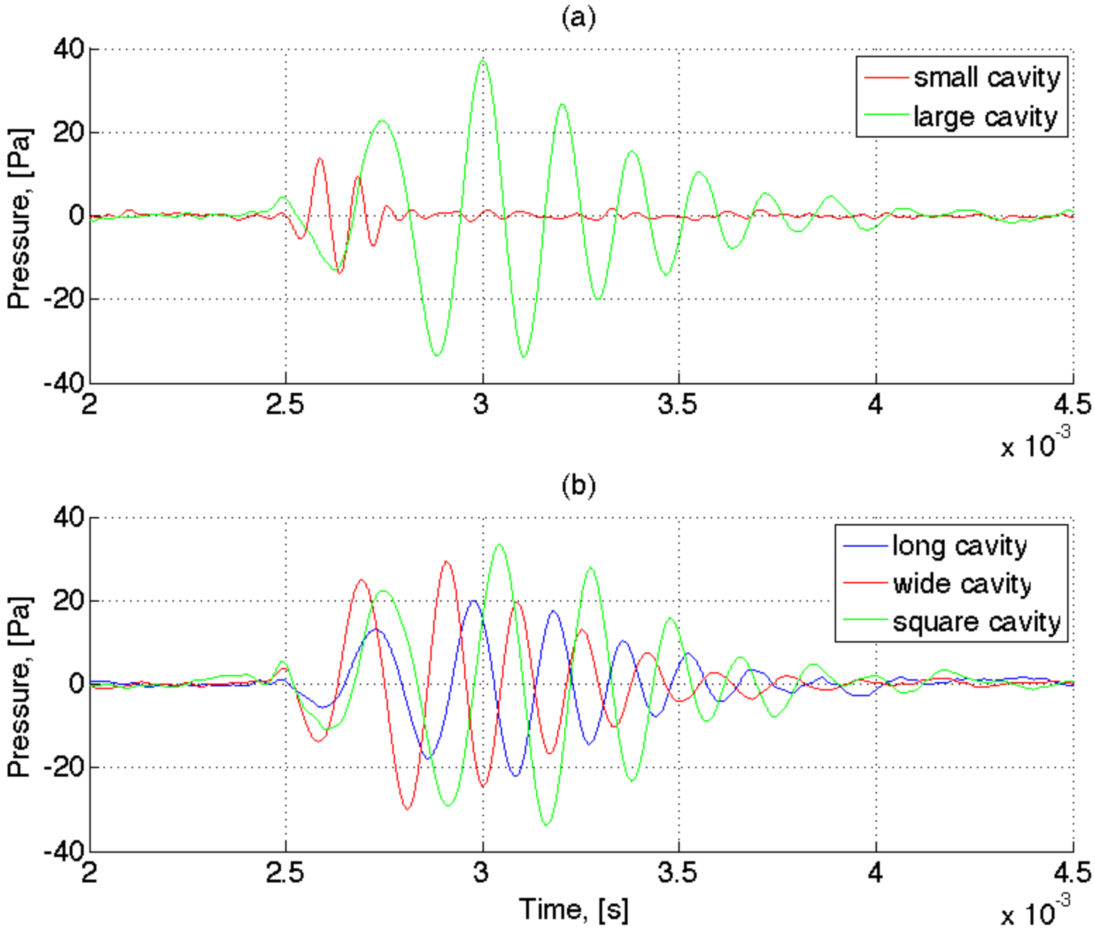

Figure 7.24 Trailing edge signal example events of the different cavities at the same tyre velocity of 41 km/h: (a) circular cavities; (b) rectangular cavities

Figure 7.24 shows example signals for a tyre velocity of 41 km/h. The two circular cavities are plotted at the top and the rectangular ones are plotted at the bottom graph of the figure. For the circular ones there is a big difference at the trailing edge. The shape of the signal is similar but duration amplitude and frequency differ significantly. There is a factor of 35 between the volume of both cavities but this is not obviously linked to the sound generation at the trailing edge. The result shown for the rectangular cavities in Figure 7.24b give more possibilities for interpretation. The relationship between cavity dimension and noise generation, as formulated for the leading edge pulse, cannot be confirmed at the trailing edge. Although also here the ‘long cavity’ (blue) generates the lowest level of noise that was similar at the leading edge. However it is not half of the amplitude of the one produced by the ‘square cavity’ (green). This connection can only be found at the beginning of the signal that is found to be the same as the leading edge event. The time of the oscillation is nearly constant for the different rectangular cavities. The time when the maximum peak amplitude is reached (3.1 ms) is similar in between the ‘long cavity’ and the ‘square cavity’, the tyre with the ‘wide cavity’ peaks earlier this could be due to a shorter cavity length, *L*. The maximum amplitude of the ‘wide cavity’ and the ‘square cavity’ approach nearly the same value.

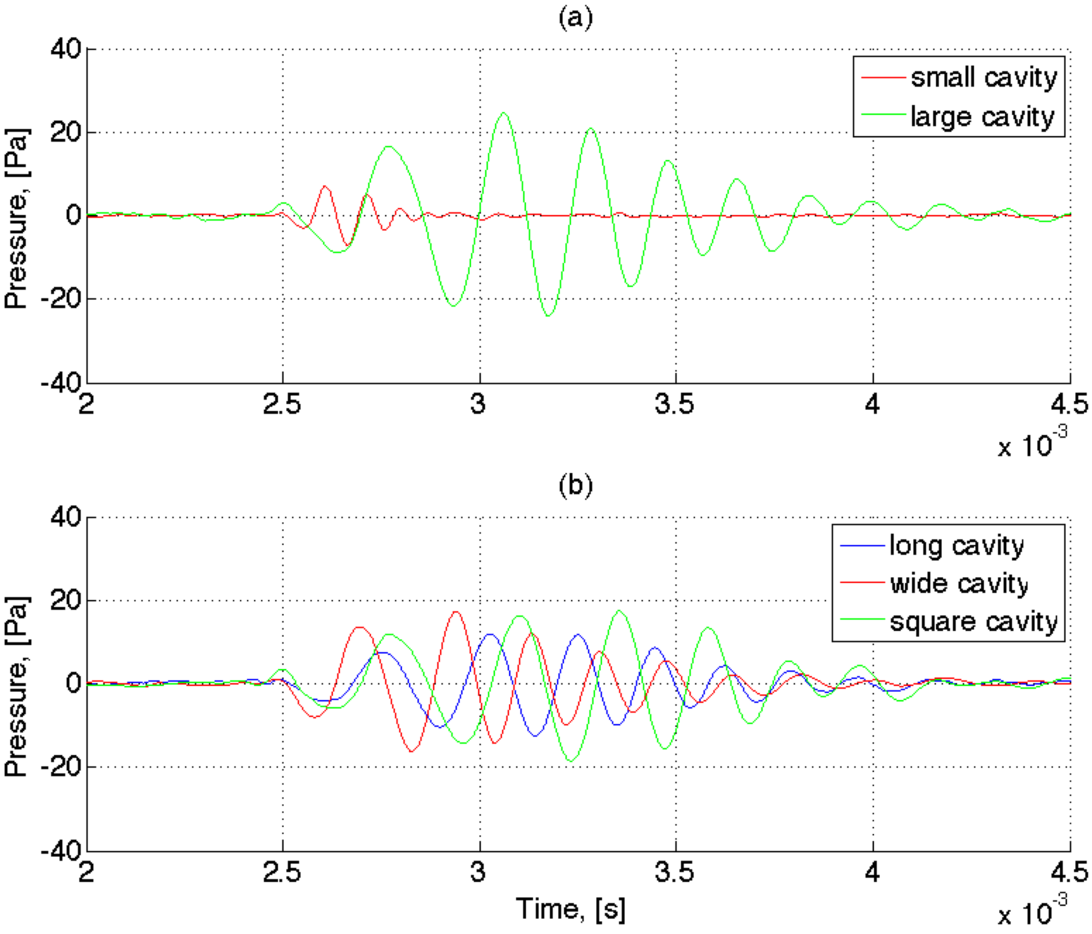

Figure 7.25 Trailing edge signal of the different cavities at the same tyre velocity of 31 km/h: (a) circular cavities; (b) rectangular cavities

Similar conclusions can be drawn for the measurements of the tyre speed of 31 km/h. Figure 7.25 shows the results of the oscillations produced separated for the circular and rectangular cavities.

7.4. Frequency analysis

In accordance to the leading edge signal also a frequency analysis is conducted for the trailing edge. The instantaneous frequency of a single event for all the tyres tested has already been analysed. Now the whole time history generated by the tyre with the 'large cavity' is converted into the frequency domain for the three different speeds the tyre was driven at.

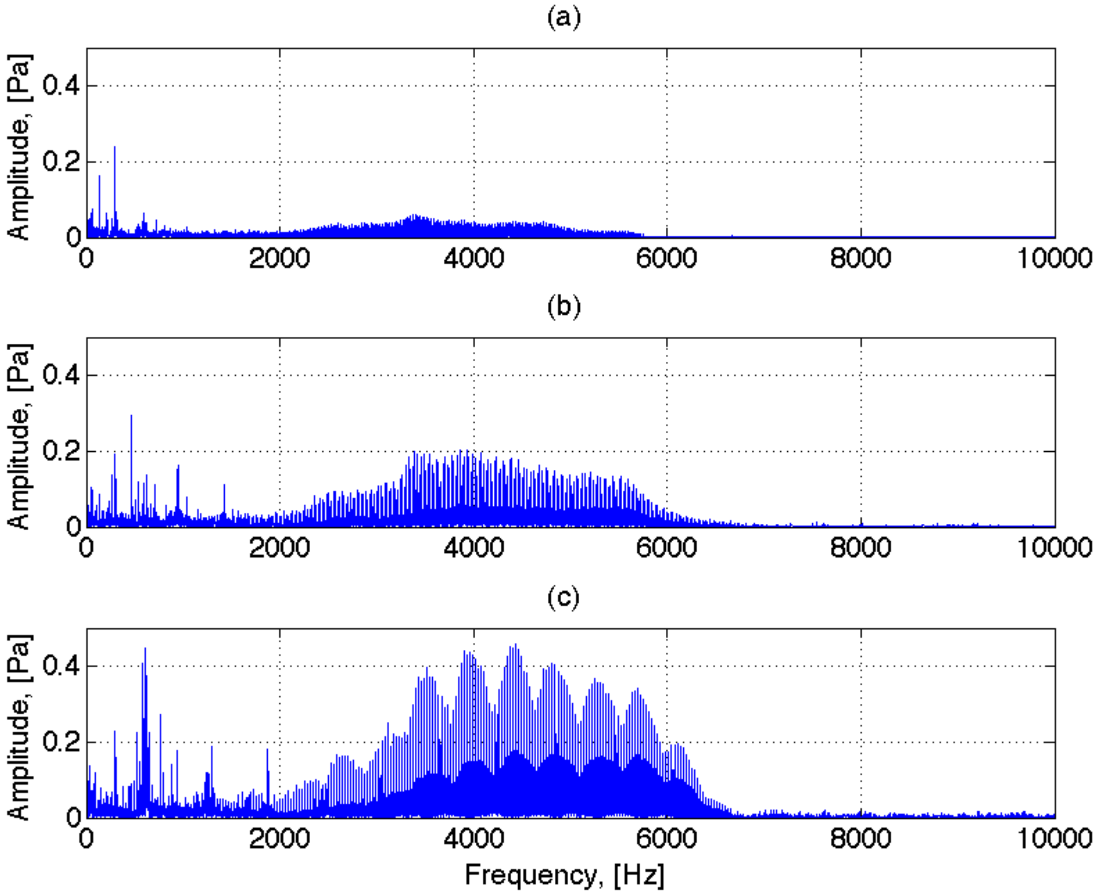

Figure 7.26 Fast Fourier Transform of trailing edge signal generated by the tyre with the 'large cavity': (a) 19 km/h; (b) 31 km/h; and (c) 41 km/h

Figure 7.26 shows the Fast Fourier Transform of the whole two seconds recording for the unfiltered trailing edge signal of the tyre with the ‘large cavity’. The result for a tyre velocity of 19 km/h is shown at the top of the figure, in the middle 31 km/h and at the bottom the result of 41 km/h is plotted. As for the oscillations at the trailing edge, the amplitude of the frequency transformation is also dependent on the speed that is shown clearly in the area in between 2000 and 6500 Hertz. The low frequency region is dominated by the noise of the chassis dynamometer driving mechanism. As for the leading edge signal, the repetition frequency of the cavity contacting the chassis dynamometer drum is low and also here nothing can be picked up at the fundamental frequencies from Table 5.26.

The instantaneous frequency calculations earlier in this chapter showed the frequency modulation of an example trailing edge signal. The same resulting frequencies can be seen in Figure 7.26 where the whole time history of two seconds is analysed. For all the three different tyre speeds the area of interest is constant in between 2000 and 6500 Hertz that are the same values predicted by Nilsson and measured by the instantaneous frequency. The structure of that frequency area consists of a high number of single peaks that build the envelope for the broadband frequency peak.

A more detailed view of the actual high amplitude area is presented in Figure 7.27 that shows only a section of the frequency area in between 3200 and 3400 Hertz for all the three speeds. At the top the frequency spectrum of the 19 km/h signal is plotted. All the fine peaks are shown and the distance of those corresponds perfectly to the repetition frequency (13.9 Hertz) of the cavity hitting the chassis dynamometer drum. Figure 7.27b clarifies the structure of the broadband frequency at the 31 km/h. The high peaks correspond to the repetition frequency for the cavity hitting the drum at 22.7 Hertz. In addition to that peaks of lower amplitude are present as well, these are the quarter harmonics that could be generated by the chassis dynamometer due to the tyre/chassis dynamometer drum ratio of about four. The same applies to the frequency content for the high speed of 41 km/h shown in Figure 7.27c. Here peaks are shown for the repetition frequency of 29.9 Hertz and the quarter harmonics occur as well. Hence, the repetition frequency can be picked up at the trailing edge, however, only harmonics of it and not the fundamental. These are similar observations as for the leading edge signal.

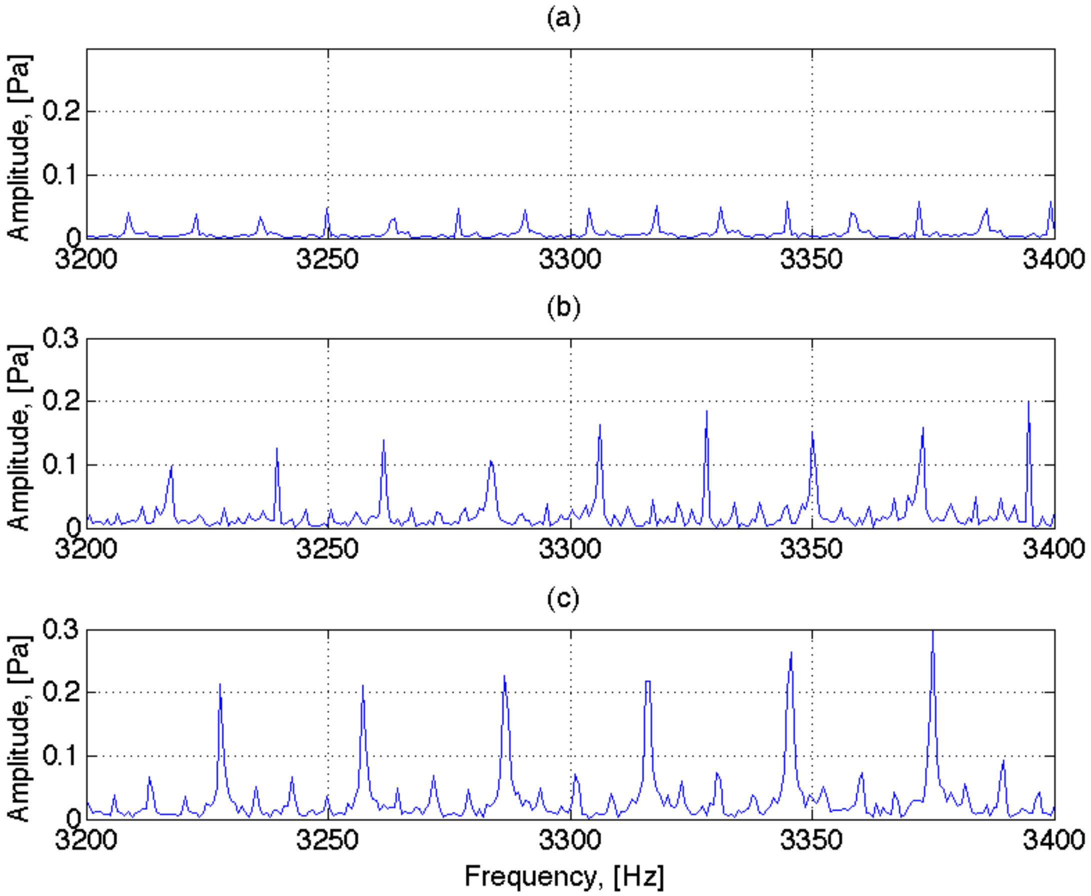

Figure 7.27 Zoomed Fast Fourier Transform of the trailing edge signal generated by the tyre with the 'large cavity': (a) 19 km/h; (b) 31 km/h; and (c) 41 km/h

7.5. Conclusion

This last chapter shows a detailed analysis of the trailing edge signal of tyres with different types of cavities in the tread. The recorded time signal was analysed regarding the instantaneous frequency and the amplitude produced. The instantaneous frequencies measured at the trailing edge were compared to a mathematical model introduced by Nilsson. Satisfactory agreement is presented between the model and the measured data, for different shaped cavities.

Therefore, it could be concluded that air resonant radiation is found to produce the main noise at the trailing edge for the tyres used in this research project. And Nilsson delivers an appropriate model to explain this phenomenon. Frequencies in between 2000 and 7000 Hertz can be found in the signal that is also proven by a Fast Fourier Transform applied to the recordings. It is noted that the first measured frequencies for each cavity and each speed do not fit to the predictions from the Nilsson model. Nilsson uses the middle of the cavity as the starting point. However, noise is already generated when the cavity just clears the road surface that could be seen as the initiator of the air resonant radiation. In this early stage, the middle of the cavity is still covered by the road. As soon as the middle of the cavity has cleared the road the Nilsson model is valid. In comparison to the Nilsson model, the highest speed always produces slightly higher frequencies than the lower speeds measurements. The Doppler effect could explain this because the source is moving towards the microphone. This is however only a minor difference because of the rather low speed of the tyre.

A model for the amplitude of the air resonant radiation is not available in the literature. Some findings from this project regarding the amplitude behaviour at the trailing edge are:

- The amplitude of the oscillation changes with cavity position
- The amplitude is dependent on the squared velocity of the tyre. Although much better agreement has been shown for the leading edge regarding this.
- The relationship of volume of the cavity and sound radiation found for the single leading edge pulse is different in comparison to the trailing edge oscillations.
- The number of oscillations is similar for different tyre speeds but dependent on the cavity.
- The frequency change is quicker with higher tyre speeds but constant with distance.

Chapter 8

Conclusions and future work

As shown during the experimental work in this Thesis, the air related mechanisms at the tyre/road interface are of a difficult nature to investigate and to explain. This Thesis gives an inside view and understanding about the air effects occurring, especially when a tyre with a cavity enters and leaves the contact patch. A detailed analysis about different cavity sizes could not be found in the literature, neither experiments with a solid rubber tyre, where other known active noise mechanisms at the tyre/road noise interface can be neglected. Therefore, the experimental work presented in this Thesis helps clarify theories of air pumping which have come into question recently.

8.1. Conclusion and summary of results

Due to the initial literature survey an experimental project regarding the air related mechanisms at the contact patch of a tyre rolling over a road surface was defined. The models described in the literature consider different stages of the air related processes. However, the understanding about these models has been questioned especially by Gagen [Gagen, 2000]. By choosing a simple tyre design mounted onto a constructed rig acoustic measurements of high resolution could be carried out within the facilities available at

Loughborough University. This led to a detailed analysis of the leading and trailing edge signals of rubber tyres with cavities that are presented in this Thesis.

Generally the sound radiation measurements conducted and the comparison of the separate leading and trailing edge recordings show that for tyres with cavities the main aerodynamic noise source is at the trailing edge. Even for the low maximum tyre velocity of 41 km/h significant levels of noise were generated. This supports the theory from Sandberg [Sandberg, 2001], that tyre road noise is dominant already at low speeds. The air effects for tyres with pockets or even grooves are a dominant source for the generation of that noise. The frequencies found in the signal at the trailing edge can be partly modelled by the air resonant radiation theory developed by Nilsson [Nilsson et al., 1979]. Attempts have been made to model the trailing edge signal amplitude. However, a mathematical explanation could not be found (A8), especially because the duration of the oscillation does not appear to be speed dependent. Neither is there a relation between cavity volume or change in cavity volume and duration of the pulse. The only factor that has not been investigated is the depth of the cavity. This could give more clarification about the duration of the oscillation when the cavity lifts off the road surface.

The mathematical frequency description presented by Nilsson overlays well with the obtained results of the trailing edge recordings. However, the first oscillation of a single event does not fit to the frequencies predicted by Nilsson for either of the tyres tested. The generated signal starts as soon as the cavity opens up at the trailing edge. The Nilsson model is valid when the middle of the cavity starts to lift off the road and this is when the model can be compared to the results of the measurements. The first part of the oscillations could be seen as the initiator of the air resonance radiation. The frequencies for this initial part of the oscillation are speed dependent, they increase with speed. Therefore, in the time domain those initial parts of the resonance overlay when the different speed recordings are compared. This beginning section is also similar in comparison to the signal found at the leading edge. Here the frequency of the signal changes proportionally with speed as well. By overlaying, the leading edge and the trailing edge signal from a tyre with a cavity, a connection between both signals can be presented. The initial part of the trailing edge signal can be found at the leading edge as well, however, the oscillation of the Helmholtz resonator are not occurring at the leading edge.

The process described by Hayden [Hayden, 1971], to explain the effect happening at the leading edge of a tyre with cavities could not be applied. First of all the frequency of repetition could not be identified in the frequency analysis of the time signal. Also the monopole theory could not be applied successfully to explain the results obtained. The volume change of a cavity due to the load of a tyre, when entering the contact patch could be constant. However, a connection in between the volume change and the sound pressure generated at the leading edge cannot be confirmed by the calculations in Chapter 5. Gagen [Gagen, 2000] presents a more plausible description of the process happening at the leading edge. However, the model derived by Gagen for the energy of an expelled jet at the leading edge of a tyre with a groove with one open end cannot be completely applied to the tyres with cavities either, even after alteration. However, Gagen's theory about the behaviour of air in the compressed grooves seems realistic, especially when the peaks at the leading edge are analysed in detail. The duration of the peak at the leading edge and cavity length cannot be linked. Thus, the explanation of the air in a cavity behaving sluggishly as presented by Gagen could be supported. It is assumed that the peak at the leading edge occurs only at the end when the cavity is nearly closed. This would indicate that the initial air movement in a cavity is not recorded at the outside, hence, no noise is emitted into the environment at that stage. Only at a late stage of the cavity closing process can a noise be recorded.

Similar peaks at the leading edge were also found by other authors: Ronneberger [Ronneberger, 1984] for cavities in tyres and Conte [Conte and Jean, 2006] for cavities in the road surface. This fact and also a comparison of unfiltered and filtered leading edge signals reveal this sharp peak as a real effect that is not influenced by the filter applied. It is found that the peak amplitudes generated at the leading edge are dependent on the speed of the tyre. The higher the speed, the higher the pressure peak. However, the duration in time of the peak stays constant, even for different types of cavities. The maximum amplitude values of that peak in the time history of one recording do vary, as also mentioned by Ronneberger [Ronneberger, 1989]. However, this is found to be due to noise in the signal. Actually the difference between the peak and trough of the short oscillation is rather constant when every peak is analysed in detail. The results reveal proportionality to the square of the velocity for the leading edge peak pressure amplitude. This dependency can also be found for the acceleration level when impact measurements are conducted at the contact patch [Perisse, 2002]. The speed exponent for the sound pressure level presented by Kuijpers and van Blokland [Kuijpers and van Blokland, 2001], explained in Chapter 2, is of an order of four to five for air pumping in accordance to the initial model from Hayden. This order can be confirmed for the leading edge signal because the amplitude of the sound pressure level, when compared for different speeds, is proportional to the squared velocity. Furthermore this relationship could also be found for the groove resonance and the trailing edge signal (air resonant radiation) for all different tyre treads tested in the experiments. However this proportionality is not mentioned in the publications of Kuijpers and van Blokland. Instead they suggest a speed exponent of zero for the groove resonance and also the air resonant radiation phenomena. This exponent would indicate no amplitude change for the air resonant radiation or groove resonance, when the tyre speed is changing. This does not seem to be the case for the results presented in this Thesis. When the tyre load is decreased, the volume change of a cavity passing the contact zone should decrease. This would lead to a lower level of sound generation at the leading and the trailing edge. However, the frequencies are not influenced by a load change at all, as shown in the appendices (A7).

When measurements are conducted there is always a possibility to introduce inaccuracy to the recordings. During the experiments carried out for this Thesis mainly the following points could have influenced the results obtained:

- Changing tyre rubber stiffness due to temperature
- Noise of chassis dynamometer

- Reflections from the walls, floor and ceiling of the chassis dynamometer chamber
- Inaccuracy in cutting the tread

The main point in the list is the noise from the chassis dynamometer and the resulting reflections in the chamber. Thus, for more accurate measurements an anechoic environment should be built around the chassis dynamometer also the noise of the driving mechanisms should be reduced significantly.

8.2. Future work suggestions

To get an even better understanding of the air processes at the tyre/road interface measurements with a higher number of different cavity shapes could be carried out. This would give an advanced understanding about what is happening at the leading and trailing edge. Investigation into the depth of a cavity to see if this changes the results in a different radiated maximum sound pressure, would also be interesting. Specifically, the energy prediction presented by Gagen could be tested with this additional parameter.

Another suggestion would be to try and compare a cavity to a groove with one open end, where both should have the same dimensions. This would give an interesting insight into the change of amplitude for both the leading and the trailing edge. Further information would be collected to derive a mathematical prediction of the pressure signal generated by a groove with two open ends that is a more realistic shape.

The measurements presented could be repeated with a different, larger solid rubber tyre. This would give clarification about the influence of the tyre dimensions to the radiated sound especially for the constants γ and β used in Nilsson’s model. The cavity dimension should stay the same to compare it to the results obtained here. Also a real tyre filled with air could be tested with similar cavities/grooves for validation of the statements made in this Thesis.

References

Anthony, D. A. (2007). The horse, the wheel, and language: how Bronze-Age riders from the Eurasian steppes shaped the modern world**.** *Princeton, N.J: Princeton University Press,* **6**, 2007.

Blackcircles.com Ltd (2008). *The History of the Tyre* [online]. Available: http://www.blackcircles.com/general/history [accessed 16 July 2008].

Beckenbauer, T. (2003). Reifen-Fahrbahn-Geraeusche – Minderungs-potentiale der Strassenoberflaeche. *Documenta Acustica,* 2003, 70-79

Chanaud, R. C. (1969). Experimental Study of Aerodynamic Sound from a Rotating Disc. *The Journal of the Acoustical Society of America*, **45**(2), 1969.

Cheng, S.-P., Griffiths, D., Gu, P. P. (1997). Chassis Dynamometer Simulation of Road Noise. *Society of Automotive Engineers,* 1997, 971893.

Conte, F., Jean, P. (2006). CFD Modelling of Air Compression and Release in Road Cavities During Tyre/Road Interaction. *Proceedings of Euronoise*, 2006.

de Graff, D. F. (2000). Noise of Passenger Cars 1974-1999 – The Paradox of a 2 dB(A) Increase in Traffic Noise and a 8 dB(A) Decrease in Type Approval Limits. *VROM Project 2000130079*. ‘s-Hertogen-bosch, 2000.

Deffayet, C. (1989). Bruit de Contact Pneumatique/Chaussee – Emission Acoustique d’une Cavite de Chaussee – Resultats Experimentaux Satolas. INRETS Research Report NNB 8907. Bron, 1989.

Duhamel, D., Hamet, J. F., Klein, P., Anfosso, F., Yin, H., Gautier, J.-L., Meunier, Y. (2006). Effect of Absorbing Grounds on Acoustic Radiation of Tyres. *Proceedings of Euronoise*, 2003.

Dunlop Tires, (2008). About us [online]. Available: http://www. dunloptires.com/about/ [accessed 30 July 2008].

Ejsmont,J.A., Sandberg,U., Taryma,S. (1984). Influence of Tread Pattern on Tire/Road Noise. *Society of Automotive Engineers,* 1984, 847138.

EU commission (1996). *The Green Paper on Future Noise Policy* [online]. Available: http://ec.europa.eu/environment/noise/ greenpap.htm#situ [accessed 16 July 2008].

Favre, B. (1979). Some Results Concerning Current Research on Tire Noise in France. *Proceedings of the International Tire Noise Conference*, 1979, 273-281.

Gagen, M. J. (1999). Novel Acoustic Sources from Squeezed Cavities in Car Tires. *Journal of the Acoustical Society of America*, 1999, **106** (2), 794-801.

Gagen, M. J. (2000). Nonlinear Acoustic Sources in Squeezed Car Tyre Cavities. *Noise and Vibration Worldwide*, 2000, **31**(4), 9-19.

Ghesquiere, H., Clairet, J. M., Hamet, J. F. (1988). Elaboration d'un Modele Simple pour l'Emission Acoustique d'un Pneumatique d'Automobile. INRETS Research Report 68. Bron, 1988.

Graf, R. A. G., Kuo, C.-Y., Dowling, A. P., Graham, W. R. (2002). On the horn effect of a tyre/road interface, Part I: Experiment and computation. *Journal of Sound and Vibration*, 2002, **256**(3), 417-431.

Graf, R.A.G. (2002). Tyre-road interaction noise. *PhD thesis*, December 2002, University of Cambridge, Department of Engineering, Corpus Christi College, UK.

Hamet, J. F., Deffayet, C., Pallas, M. A. (1990). Air-Pumping Phenomena in Road Cavities. *Proceedings of the International Tire/Road noise Conference*, 1990, **1**, 19-29.

Hamet, J. F., Deffayet, C., Pallas, M. A. (1990). De Quelques Phenomenes d'Air-Pumping dans le Bruit de Contact Pneumatique/Chaussee. INRETS Research Report 128. Bron, 1990.

Hamet, J. F., Deffayet, C., Pallas, M. A. (1991). Phenomenes d'Air-Pumping dans le Bruit de Contact Pneumatique/Chaussee Cas d'une Cavite Amenagee dans la Chaussee. INRETS Research Report 132. Bron, 1991.

Hayden, R. E. (1971). Roadside Noise from the Interaction of a Rolling Tire with the Road Surface. *Proceedings of the Purdue Noise Control Conference*, 1971, 59-64.

Heckl, M. (1986). Tyre Noise Generation. *Wear*, **113**, 1986, 157-170.

Institute of Environment and Health (1997). The Non-Auditory Effect of Noise, *IEH Research Report R10*. Page Bros, Norwich, 1997.

Iwao, K., Yamazaki, I. (1996). A study on the mechanism of tire/road noise. *Society of Automotive Engineers of Japan*, 1996, **17**, 139-144.

Jennewein, M., Bergmann, M. (1984). Investigations Concerning Tyre/Road Noise Sources and Possibilities of Noise Reduction. *Journal of Mechanical Engineering Science*, **C150**(84), 1984, 235-245.

Kim, G. J., Holland, K. R., Lalor, N. (1997). Identification of the Airborne Component of Tyre-Induced Vehicle Interior Noise. *Applied Acoustics*, **51**(2), 1997, 141-156.

Kim, S., Jeong, W., Park, Y., Lee, S. (2006). Prediction Method for Tire Air-pumping Noise Using a Hybrid Technique. *The Journal of the Acoustical Society of America*, **119**(6), 2006, 3799-3812.

Kroeger, M., Lindner, M., Popp, K. (2004). Influences of Friction noise and Vibrations of Tyres. *Proceedings of International Congress and Exhibition on Noise Control Engineering*, 2004.

Kropp, W. (1989). Structure-Borne Sound on a Smooth Tyre. *Applied Acoustics*, **26**(3), 1989, 181-192.

Kropp, W. (2006). Trends in modeling – have we reached the end of the road. *Silentroads 2006 workshop*, [online] http://www.silentroads.nl /index.php?section=research&subject=workshop2006 [accessed 17 July 2008].

Kropp, W., Bécot, F. X., Barrelet, S. (2000). On the sound radiation from tyres. *Acta Acustica united with Acustica*, 2000, **86**(5), 769-779.

Kropp, W., Larsson, K., Wullens, F., Andersson, P. (2004). Tyre/Road Noise Generation – Modelling and Understanding. *Proceedings of the Institute of Acoustics*, 2004, **26**(2).

Kuijpers, A., van Blokland, G. (2001). Tyre/road noise models in the last two decades: a critical evaluation. *Proceedings of International Congress and Exhibition on Noise Control Engineering*, 2001.

Kuo, C.-Y., Graf, R. A. G., Dowling, A. P., Graham, W. R. (2002). On the horn effect of a tyre/road interface, Part II: Asymptotic theories. *Journal of Sound and Vibration*, 2002, **256**(3), 433-445.

Kuo, F. F. (1966). *Network Analysis and Synthesis.* Toppan Company Ltd., Tokyo, 1966.

Larsson, K., Barrelet, S., Kropp, W. (2002). The modelling of the Dynamic Behaviour of Tyre Tread Blocks. *Applied Acoustics*, **63**(6), 2002, 659-677.

Lay, M. G. (1992). *Ways of the World.* Rutgers University Press, New Brunswick, 1992.

Nilsson, N.-A. (1979). Possible Methods of Reducing External Tyre Noise. *Proceedings of the International Tire Noise Conference*, 1979, 247-259.

Nilsson, N.-A. (1979). Air Resonant and Vibrational Radiation - Possible Mechanisms for Noise from Cross-Bar Tires. *Proceedings of the International Tire Noise Conference*, 1979, 93-109.

Nilsson, N.-A., Söderqvist, S., Bennerhult, O. (1979). Air Resonant Radiation - a Possible Mechanism for High Frequency Noise from Cross-Bar Tires. *IFM Akustikbyran Research Report 6.084.02.* Stockholm, 1979.

Öhrström, E. (2004). Longitudinal Surveys on Effects of Changes in Road Traffic Noise: Effects on Sleep Assessed by General Questionnaires and 3-Day Sleep Logs. *Journal of Sound and Vibration,* **276**(3-5), 2004, 713-727.

Perisse, J. (2002). A study of radial vibrations of a rolling tyre for tyre-road noise characterization. *Mechanical Systems and Signal Processing,* **16**(6), 2002, 1043-1058.

Periyathamby, H. (2004). Helmholtz Resonator for Reducing Tire Cavity Resonance and In-vehicle Noise. *Canadian Acoustics*, 2004, **32**(4), 27-31.

Plotkin, K., Fuller, W., Montroll, M. (1979). Identification of Tire Road Noise Generation Mechanisms Using a Roadwheel Facility. *Proceedings of the International Tire Noise Conference*, 1979, 127-141

Plotkin, K., Montroll, M., Fuller, W. (1980). The Generation of Tire Noise by Air Pumping and Carcass Vibration. *Proceedings of International Congress and Exhibition on Noise Control Engineering*, 1980, 273-276.

Richards, M. G. (1974). Automotive Tire Noise-A Comprehensive Study. *Sound and Vibration,* **8**(5), 1974, 42-47.

Ronneberger, D. (1989). Towards Quantitative Predictions of Tire/Road Noise*. A Workshop on Rolling Noise Generation*. Berlin, 1989.

Ronneberger, D. (1984). Experimentelle und theoretische Untersuchungen spezieller Mechanismen der Rollgeraeuschentstehung und Abstrahlung. *Proceedings of Internationales Seminar Reifengeraeusche und Fahrbahn, 1984,* **57**, 79-116.

Ruhala, R. J., Burroughs, C. B. (1998). Identification of Sources of Tire/Pavement Interaction Noise. *The Journal of the Acoustical Society of America*, **103**(5), 1998, 2919.

Saburchill.com (2008). *The Development of roads* [online]. Available: http://www.saburchill.com/history/chapters/IR/024.html [accessed 20 July 2008].

Saemann, E.-U. (2006). Developments in Reducing Tyre/Road Noise. *Proceedings of Euronoise*, 2006.

Samuels, S. (1979). Recent Australian Tyre/Road Noise Research. *Proceedings of the International Tire Noise Conference*, 1979, 111-125.

Sandberg, U. (1982). Will Tyre-Noise Limit Future Vehicle Noise Reductions? *Proceedings of the International Congress and Exhibition on Noise Control Engineering*, 1982.

Sandberg, U. (2001). Tyre/Road Noise - Myths and Realities. *Proceedings* *of the International Congress and Exhibition on Noise Control Engineering*, 2001.

Sandberg, U. (2003). The Multi-Coincidence Peak around 1000 Hz in Tyre/Road Noise Spectra. *Proceedings of Euronoise*, 2003.

Sandberg, U. (2004). *A Closer Look at the Tread Groove Resonance in Tyre/Road Noise.* Proceedings of the International Congress on Acoustics, 2004, **3**, 2195-2198.

Sandberg, U., Ejsmont, J. A. (2002). *Tyre/Road Noise Reference Book*. INFORMEX, Kisa, 2002.

Schaaf, K., Ronneberger, D. (1982). Noise radiation from rolling tires – Sound amplification by the "Horn Effect". *Proceedings of International Congress and Exhibition on Noise Control Engineering*, 1982, 131-134.

Schaaf, K., Ronneberger, D., Neuwald, P. (1990). Noise of a Rolling Tire-Flow and Pressure Variations in the Region of the Contact Patch. *Proceedings of the International Tire/Road Noise Conference*, 1990, **1**, 9-17.

Sun, M., Sclabassi, R. J. (1993). Discrete-Time Instantaneous Frequency and its Computation. *Institute of Electrical and Electronics Engineers Transactions on Signal Processing*, **41**(5), 1993, 1867-1880.

Taylor, N.C.; Bridgewater, A.P. (1998). Airborne Road Noise Source Definition. *IMechE Conference Transactions,* 1998, C521/011, 251-260.

The Goodyear Tire and Rubber Company (2008). The Charles Goodyear Story [online]. Available: http://www.goodyear.com/corporate/history/history_story.html [accessed 28 August 2008].

Torra i Fernandez, E., Nilsson, N. (2004). Acoustic Modes in the Air Cavity of Tyres - Prediction and Reduction on Noise in Automobile Interiors. *Proceedings of the International Congress and Exposition on Noise Control Engineering*, 2004.

Virmalwar, A.D., Athavale, S.M., Sajanpawar, P.R. (1999). Application of FEM and Experimental Techniques for Simulation of Tyre/Road Air

Pumping Noise, Horn Effect and Vibration of Tyre Sidewalls. *Proceedings of International Congress and Exhibition on Noise Control Engineering*, 1999, 1817-1825.

Yokohama Tire Corporation (2008). Understanding Your Tires, *Construction* [online]. Available: http://www.yokohamatire.com/ customer_service/construction.aspx [accessed 16 July 2008].

Appendices

A1. Hayden model

Hayden [Hayden, 1971] proposed a model of a noise generation mechanism at the leading edge of a tyre due to air movements when the tread is compressed. This section of the Appendix gives a further inside view of the model developed by Hayden.

The monopole theory is the base for Hayden's model. Equation (3.3) shows the basic understanding of that theory. By differentiation with respect to time Hayden assumes the volumetric flow rate per time is equal to the volumetric flow rate Q times the circular frequency ω

$$\frac{\partial Q}{\partial t} = \omega \cdot Q = \frac{\partial^2 V}{\partial t^2}, \tag{A1.1}$$

Combining Equations (3.3) and (3.4) for a narrow band of frequencies an expression for the mean squared acoustic pressure at a distance r_{mic} from the source is given by

$$\overline{p^2}(r_{mic}, \omega) = \frac{\rho^2 \omega^2 \overline{Q^2}}{16 \cdot \pi^2 \cdot r_{mic}^2}. \tag{A1.2}$$

The groove or cavity initial volume V_0 is calculated by

$$V_0 = L \cdot D \cdot W. \tag{A1.3}$$

Where *L* is the circumferential dimension of a cavity, *D* is the depth of the cavity (tread depth), and finally *W* is the width of a single cavity in the direction of the tyre width (Figure 3.1). The only unknown variables in Equation (A1.2) are the mean volumetric flow rate *Q(v)* and the circular frequency of reoccurrence of the cavity *ω*. An assumption for the mean volumetric flow rate according to Hayden is

$$\overline{Q(v)} = \frac{volume\ change}{time} = \frac{(fc)\cdot D\cdot W\cdot L}{L/v} = (fc)\cdot D\cdot v\cdot W\,. \tag{A1.4}$$

Where *fc* shall be the fractional change in cavity volume V_0, and *v* is the forward velocity. Note the circumferential dimension of the tread grooves/cavities *L* is eliminated, so there is no influence of this factor in the model. Hayden wanted to take this further so the frequency of this volume change can be predicted as well. Thus Hayden approximated the circular frequency of reoccurrence of the cavities by

$$\omega(v) = \frac{2\pi\cdot v}{x_{circ}}, \tag{A1.5}$$

where x_{circ} is the circumferential distance between the cavities in the tread. This fundamental circular frequency *ω* shall be referred to as the 'repetition frequency' for the cavity hitting the road surface. By combining Equations (A1.2), (A1.4) and (A1.5), the sound pressure at a certain distance r_{mic} generated by a groove with *n* as the number of cavities per tyre width can be calculated.

$$p(r_{mic},v) = \frac{\rho\cdot v^2\cdot (fc)\cdot D\cdot W}{2\cdot x_{circ}\cdot r_{mic}}\cdot n\,. \tag{A1.6}$$

With the use of this equation Hayden aimed to predict the sound pressure at the repetition frequency from Equation (A1.5).

A2. Gagen model (wave equations)

The model for squeezed cavities in the contact patch of a tyre derived by Gagen [Gagen, 1999, 2000] is based on computational fluid dynamics. Gagen combines the small amplitude acoustic wave equation with terms from fluid dynamics in squeezed cavities and calls this squeezed acoustic wave equations. This part of the Appendix explains the details Gagen's model is based on.

Gagen developed his equation by simulating a volume deformation in a groove with one open end. The volume deformation is assumed to be in one direction of the groove only. This direction is equivalent to the parameter *L* defined as length of groove in this Dissertation (Figure 3.1). The function of changing groove length, $f_L(t)$, with respect to time according to Gagen is given by

$$L_f(t) = L \cdot f_L(t) \,. \tag{A2.1}$$

When the groove is fully closed, Equation (A2.1) can be written as.

$$A = L \cdot fc \,. \tag{A2.2}$$

Here *A* is the part of the length that *L* is shortened by, due to the squeezing of the groove. According to the notations used the variable *A* is given by the product of length, *L*, and fractional change of volume, *fc*.

Gagen states that for a pure cavity with no open ends the density change with respect to time is defined as the inverse of cavity size change. Thus,

$$\rho(t) = \frac{1}{f(t)} \,. \tag{A2.3}$$

The speed of cavity size change, $v(y,t)$, for an open ended groove is assumed to be

$$v(y,t) = \frac{\dot{f}(t) \cdot y}{f(t)} \qquad \text{(A2.4)}$$

where the speed of the air inside the groove travels in transversal direction *y* of the tyre rotation, i.e. the direction along the parameter *W*. So the air moves to the direction where the open end of the groove is. The initial mass change of the fluid in the groove at a certain time, *t*, is defined as

$$\delta m = \rho \cdot D \cdot W \cdot L_0 \cdot \dot{f}(t) \cdot \delta t \, . \qquad \text{(A2.5)}$$

When integrating Equation (A2.5) to the total mass, *m(t)* , which is expelled at time *t,* Hayden gets

$$m(t) = m_0 \left(1 - f(t)\right) . \qquad \text{(A2.6)}$$

Hayden assumes linear squeezing of the groove with a volume loss, *fc*, as introduced in Equation (A2.2), then Equation (A2.8) turns into

$$m = \frac{A}{L} m_0 . \qquad \text{(A2.7)}$$

For the kinetic energy, *E*, which Gagen defines as the expelled mass, *m,* at a velocity $v(L_f,t)$. Thus,

$$\delta E = \frac{1}{2} \delta m \cdot v\left(L,t\right)^2 . \qquad \text{(A2.8)}$$

After integration the total kinetic energy *E* at closure time, *T*, becomes

$$E(t) = -E_p T^2 \int_0^t dt \left(\frac{\dot{f}^3(t)}{f^2(t)} \right) . \qquad \text{(A2.9)}$$

For a constant volume velocity, hence linear squeezing with loss of volume Gagen gets

$$\frac{\delta V}{V}=\frac{t}{T}=\frac{A}{L}. \tag{A2.10}$$

Substituting into for Equation (A2.9) Hayden defines the kinetic energy of the expelled yet

$$E=\frac{A}{L_f-A}E_p. \tag{A2.11}$$

A3. Nilsson model (wave equations)

The model of the trailing edge signal generated by tyres with grooves developed by Nilsson, is based on propagating wave motion. This section of the Appendix gives further inside into the mathematical background of Nilsson's air resonant radiation phenomenon.

As the space between the tyre and the road is regularly referred to as being the shape of a horn (Figure 2.8) Nilsson uses the wave equation of a conical horn as the base of the air resonant radiation model.

$$\frac{\partial^2\phi}{\partial t^2}-\frac{2c^2}{x}\frac{\partial\phi}{\partial x}-c\frac{\partial^2\phi}{\partial x^2}=0, \tag{A3.1}$$

where ϕ is the velocity potential, x the distance and c the speed of sound. For a stationary signal at an angular frequency ω and with the variable B as a constant, Equation (A3.1) can be expressed as

$$\phi(\omega,x)=\frac{B}{x}\cdot e^{j(\omega t\pm kx)}. \tag{A3.2}$$

According to Nilsson the pressure *p(ω,x)* and volume velocity *u(ω,x)* can be deduced from the velocity potential (A3.1) as

$$p(\omega,x) = -\rho \frac{\partial \phi}{\partial t}, \tag{A3.3}$$

and

$$u(\omega,x) = S(x) \frac{\partial \phi}{\partial x}. \tag{A3.4}$$

When the observer is located in the vicinity of the contact patch the only wave that is seen is the wave travelling away from the source through the horn. Very close to the source there would be one wave only in the direction perpendicular to the trailing edge. There the pressure according to Nilsson would be defined as

$$p(\omega,x) = -\frac{j\omega\rho \cdot B}{x} \cdot e^{j(\omega t - kx)}. \tag{A3.5}$$

The volume velocity *u(ω,x)* can be written as

$$u(\omega,x) = -\frac{S(x) \cdot B}{x^2} \cdot (1 + jkx) \cdot e^{j(\omega t - kx)}. \tag{A3.6}$$

The impedance *Z(ω,x)* for a monopole (for $x=x_1$) is defined as pressure divided by the volume velocity

$$Z(\omega,x) = \frac{p(\omega,x)}{u(\omega,x)} \tag{A3.7}$$

With both Equations (A3.5) and (A3.6) inserted into Equation (A3.7) the following standard expression for a monopole can be obtained

$$Z(\omega,x) = \frac{\rho \cdot c \cdot (kx_1)}{S(x)\left[1 + (kx_1)^2\right]} \cdot \left[(kx_1) + j\right]. \tag{A3.8}$$

In our case the impedance can be divided into a resistance and mass reactance according to a simple spring mass damper relationship. This can be written as follows

$$Z(\omega,x) = R(\omega,x) + j\omega \cdot M(\omega,x) \quad \text{(A3.9)}$$

Splitting Equation (A3.8) in accordance to Equation (A3.9) reveals the actual Resistance (3.20) and Mass (3.21) part of the damper/mass system.

The spring constant is derived in a different way. The volume of the groove/cavity in the tyre is assumed to be the spring in accordance to Nilsson. Thus, this time the observer is located outside the tyre facing the trailing edge. There are two parallel standing waves to be seen, with the same components from Equation (A3.5) and (A3.6) as the travelling wave before. One standing wave towards the contact patch (for *x=0*) with the impedance $Z_2(\omega,x)$ of

$$Z_2(\omega,x) = \frac{1}{j\omega} \cdot \frac{\omega \cdot \rho \cdot x}{S(x)} \cdot \frac{1}{1 - \frac{kx_1}{\tan(kx_1)}} . \quad \text{(A3.10)}$$

There is a second standing wave with a spring like impedance $Z_3(\omega,x)$, in the cavity itself defined as

$$Z_3(\omega,x) = \frac{1}{j\omega} \cdot \frac{\omega \cdot \rho \cdot x}{S(x)} \cdot \frac{1}{1 - \frac{kx_1}{\tan(kx_1)}} . \quad \text{(A3.11)}$$

The impedances from Equation (A3.6) and (A3.7) connected in parallel result in the spring stiffness *K*

$$\left(\frac{1}{Z_2(\omega,x)} + \frac{1}{Z_3(\omega,x)} \right) \cdot \frac{1}{j\omega} = \frac{1}{K(\omega,x)} , \quad \text{(A3.12)}$$

yielding to Equation (3.22).

The mass, damper and spring coefficients can be combined to a resonance circuit. For a free movement vibration of the oscillating volume of air *V(ω,t),* initiated by the impulse, generated when the cavity lifts off the road, the circuit can be written as

$$M(\omega,x)\cdot\ddot{V}+R(\omega,x)\cdot\dot{V}+K(\omega,x)\cdot V=0\,. \tag{A3.13}$$

Where the oscillating volume of air, *V(ω,t),* is defined as

$$V(\omega,t)=V_1\cdot e^{j\omega t}\,. \tag{A3.14}$$

By combining this function of volume *V(ω,t)* with Equation (A3.13) the circular frequency *ω(x)* can be calculated. It is a damped oscillation with a real and imaginary part

$$\omega(x)=\frac{R(\omega,x)}{2M(\omega,x)}j\pm\sqrt{\frac{K(\omega,x)}{M(\omega,x)}-\left(\frac{R(\omega,x)}{2M(\omega,x)}\right)^2}\,. \tag{A3.15}$$

A4. Sound radiation plots: anechoic chamber

As shown in Chapter 5 the sound radiation measurements in the chassis dynamometer laboratory were influenced a lot by unwanted noise and reflections. To check if the used equipment delivers suitable results measurements were done in a room with anechoic termination in place. This could guarantee that there is less unwanted reflections in the recordings. The chassis dynamometer was not located in the anechoic chamber; thus, it was decided to use a speaker generating a sine wave with a constant frequency. The rig used to accommodate the microphones around the speaker was explained in Chapter 3. Seven microphones were used at a time to cover 60 degrees of the circular measurements one meter away from the speaker. The microphone stand needed to be repositioned five times and then the full circle around the source was covered. The recorded time signal then was transformed within the software Matlab into the frequency domain and the peaks at that frequency where the sine wave was generated at was compared for the 42 measurement positions. Actually just 36 microphone position would be needed, however, with the microphones overlapping the results could be checked to see if the same level was recorded at the end position during the next set of measurements.

The next figures show the sound radiation of 8 different frequencies checked from 7000 Hertz down to 500 Hertz. Those frequencies were chosen in accordance to the frequency modulation measured at the trailing edge signal of the tyre with the ‘large cavity’. For all the measurements the speaker was pointing to the right hand side, according to the direction of the trailing edge of the tyre, which produced the highest-pressure amplitude. This measurements show very smooth sound radiation plots around the source, which clearly indicates the importance of an anechoic environment. For the middle frequencies (1000 and 3000 Hertz) nearly no directivity can be seen. These plots are compared to recordings taken in the chassis dynamometer lab to see the influence of reflections in the next section.

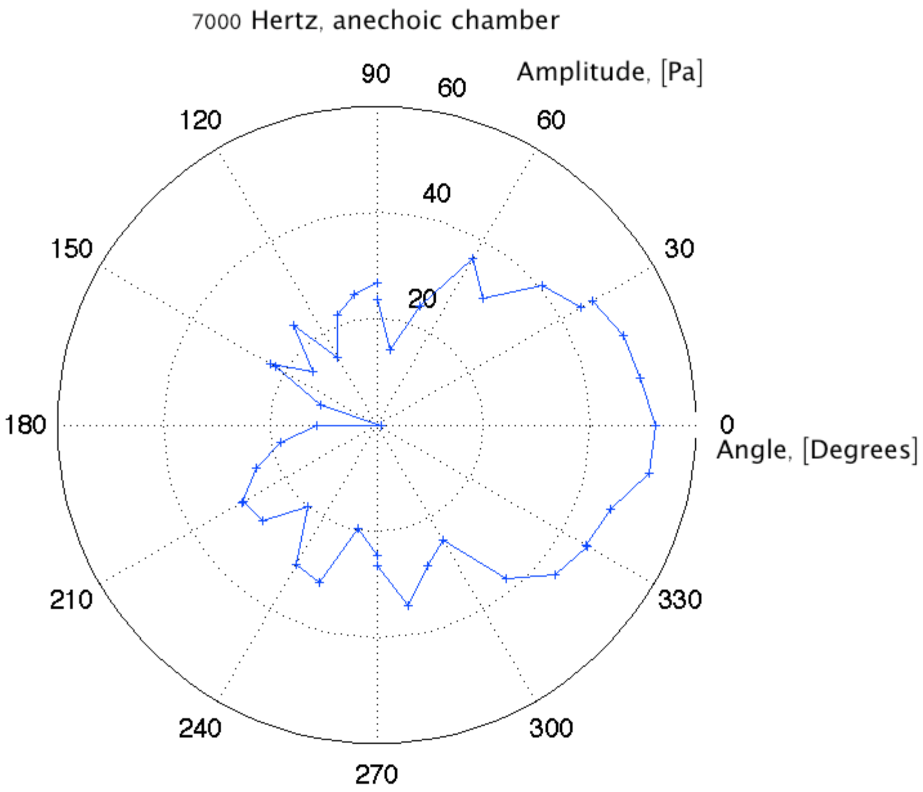

Figure A4.1 Sound radiation, at a frequency of 7000 Hertz, generated by a speaker facing to the right hand side of the plot, recorded in the anechoic chamber

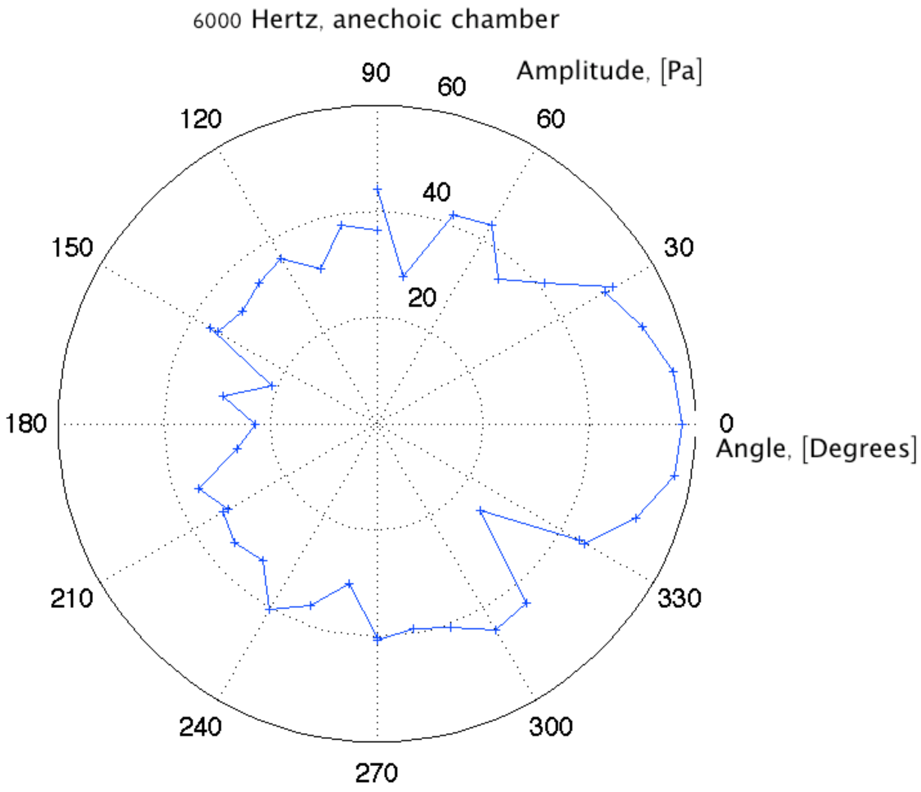

Figure A4.2 Sound radiation, at a frequency of 6000 Hertz, generated by a speaker facing to the right hand side of the plot, recorded in the anechoic chamber

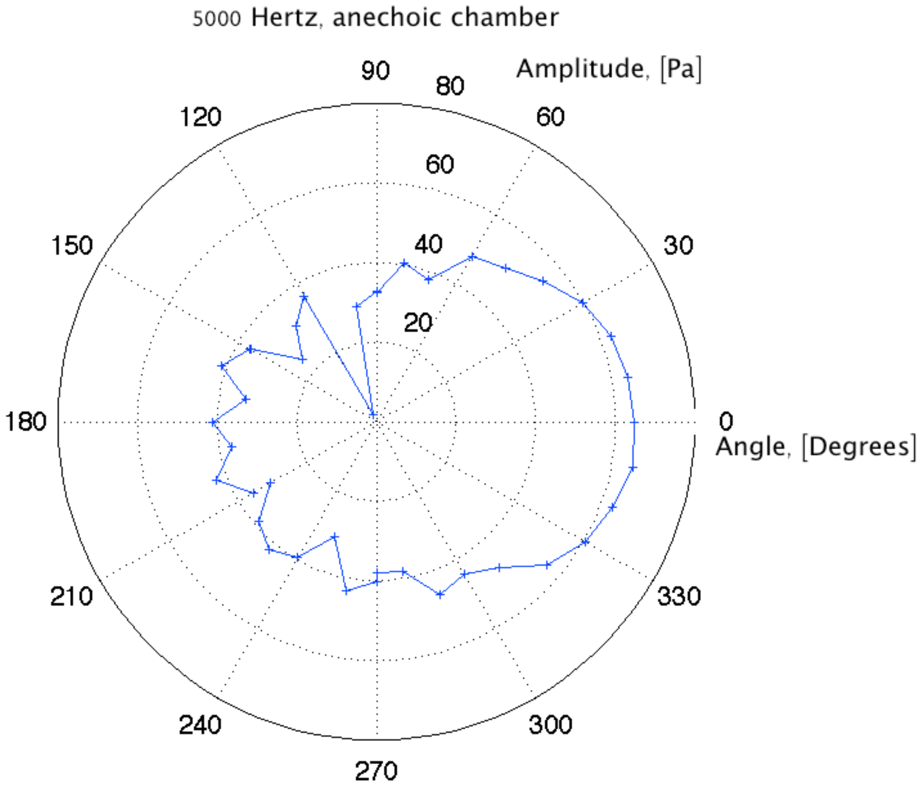

Figure A4.3 Sound radiation, at a frequency of 5000 Hertz, generated by a speaker facing to the right hand side of the plot, recorded in the anechoic chamber

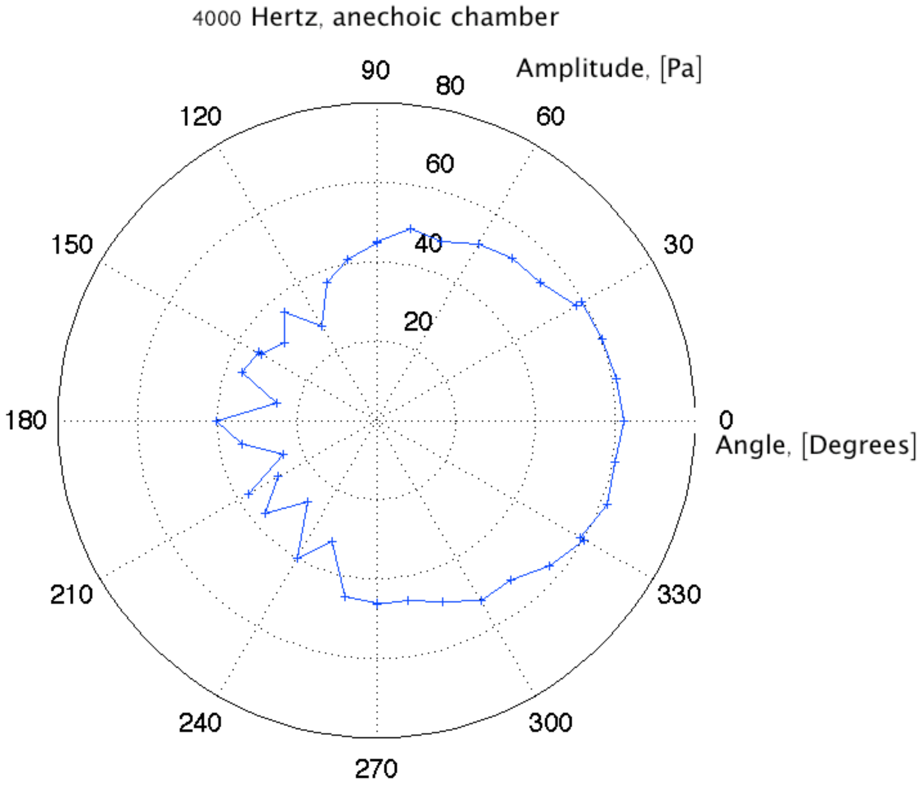

Figure A4.4 Sound radiation, at a frequency of 4000 Hertz, generated by a speaker facing to the right hand side of the plot, recorded in the anechoic chamber

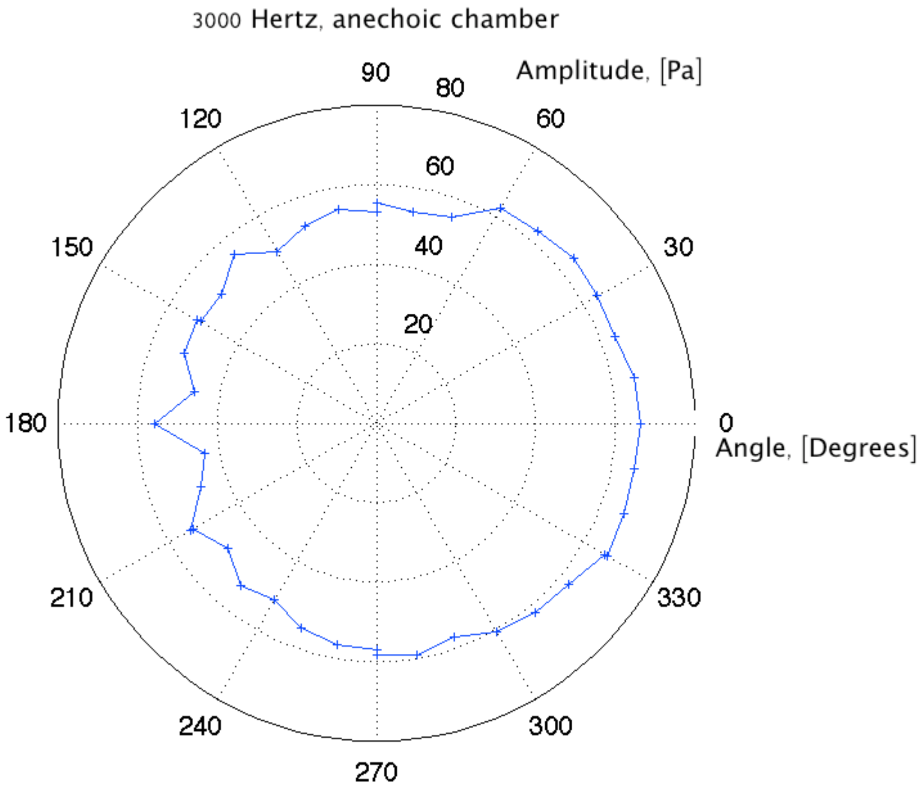

Figure A4.5 Sound radiation, at a frequency of 3000 Hertz, generated by a speaker facing to the right hand side of the plot, recorded in the anechoic chamber

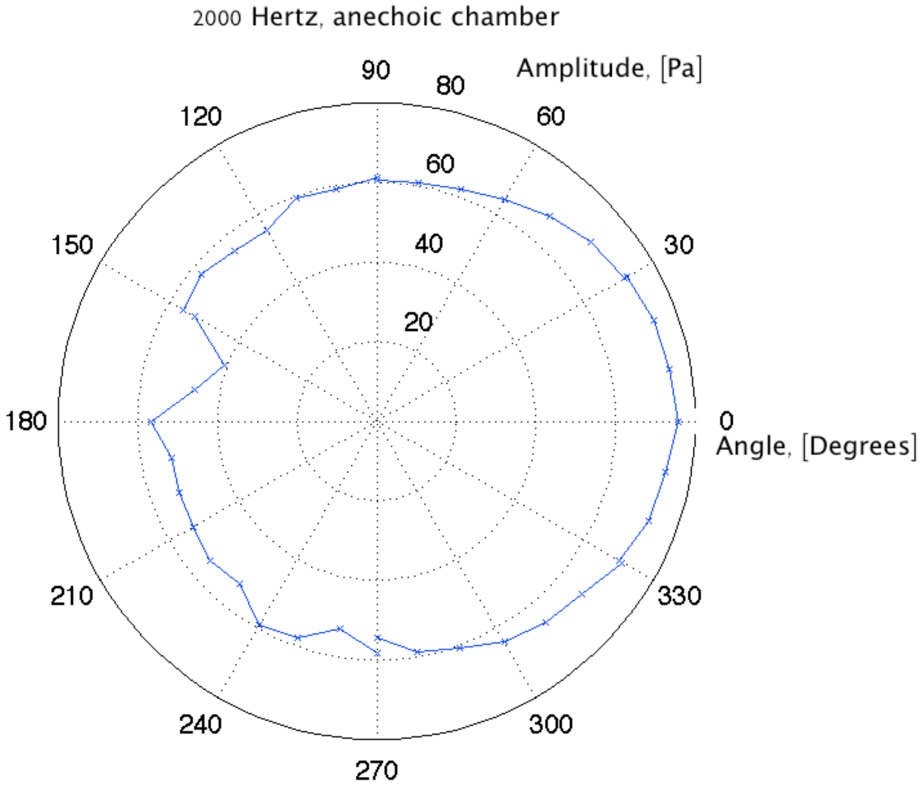

Figure A4.6 Sound radiation, at a frequency of 2000 Hertz, generated by a speaker facing to the right hand side of the plot, recorded in the anechoic chamber

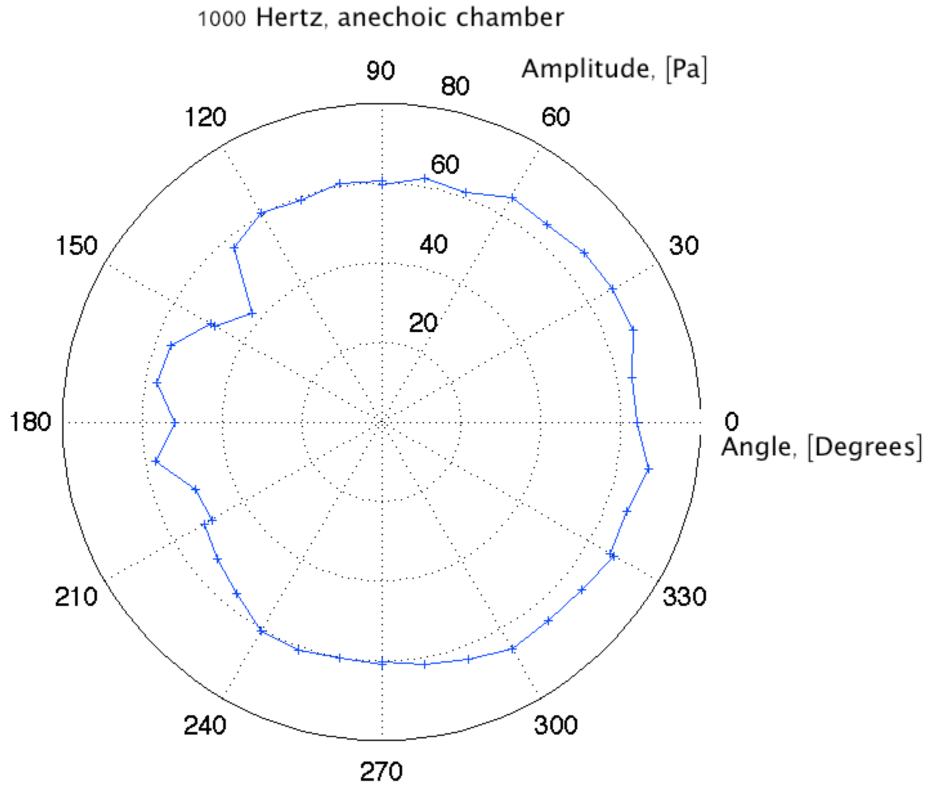

Figure A4.7 Sound radiation, at a frequency of 1000 Hertz, generated by a speaker facing to the right hand side of the plot, recorded in the anechoic chamber

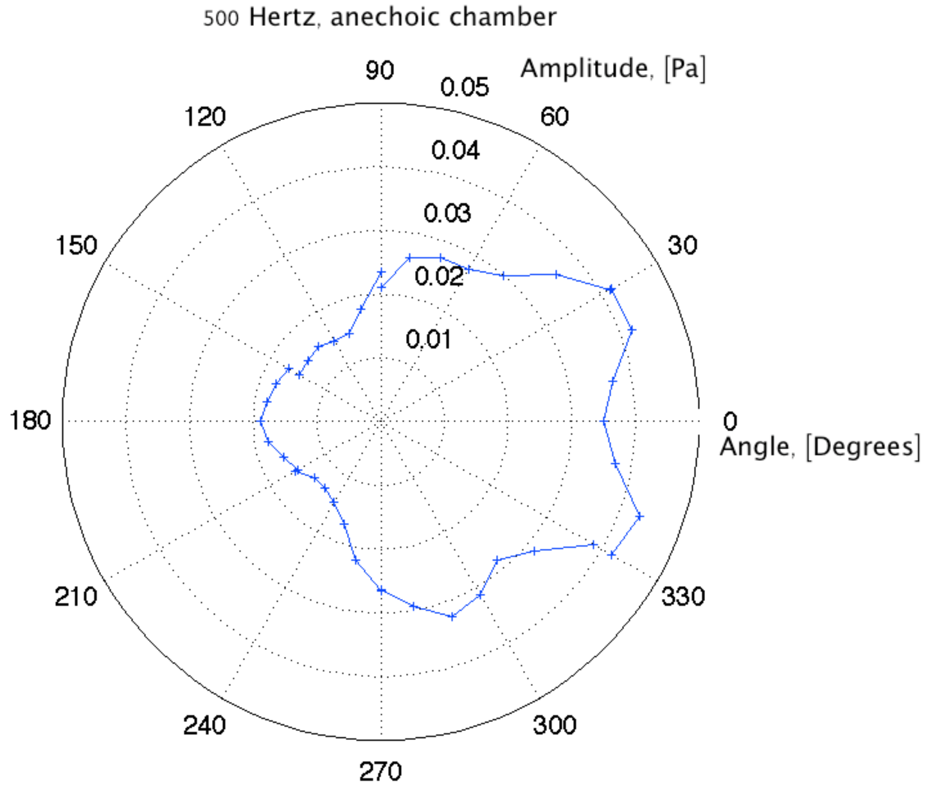

Figure A4.8 Sound radiation, at a frequency of 500 Hertz, generated by a speaker facing to the right hand side of the plot, recorded in the anechoic chamber

A5. Sound radiation plots: chassis dynamometer lab

The results from the anechoic chamber before are compared to results obtained with the same measurement setup, done in the chassis dynamometer laboratories. Again a speaker is used to generate sinusoidal signals at the same fixed frequencies in between 500 and 7000 Hertz. The only difference is this time there is no anechoic termination.

As to be seen in Figure A5.1 and the following ones for the lower frequencies this time the sound radiation recordings are distorted. Again the speaker is pointing to the right hand side, which could clearly be identified for the higher frequencies measured in the anechoic chamber. This time however nearly no directivity is to be seen. There is a lot of influence of reflection in this recordings especially with a constant sinusoidal signal in a reflective room standing waves could be generated that would not be that bad for a transient signal as it is produced by the tyre at the trailing edge. Nevertheless the influence of the reflections is clearly shown in those plots which explains the inaccuracy of the sound radiation plots generated for the tyre running on the chassis dynamometer.

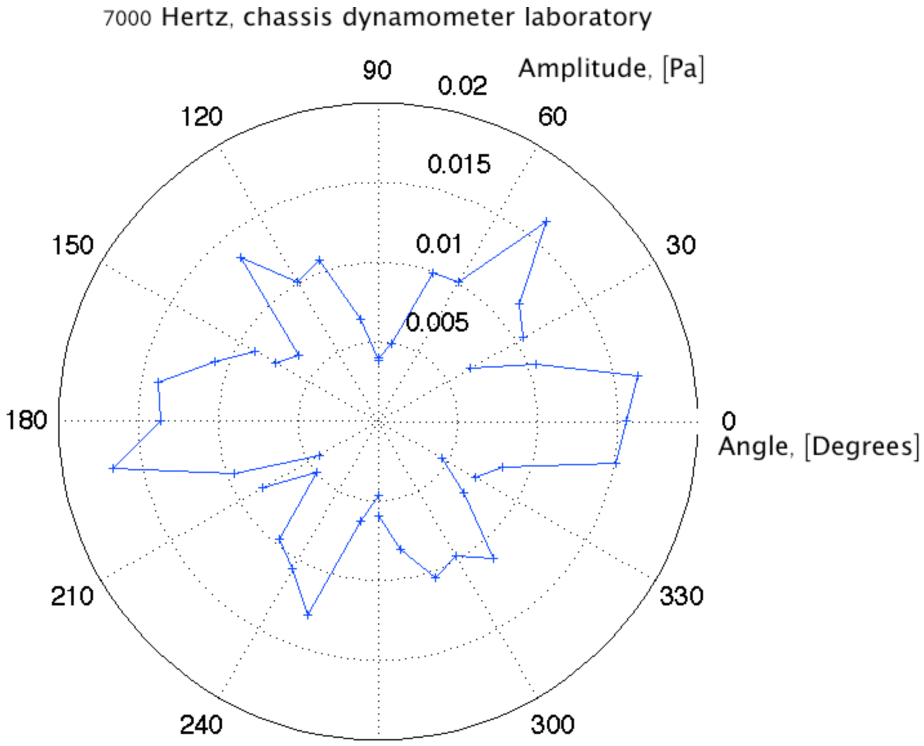

Figure A5.1 Sound radiation, at a frequency of 7000 Hertz, generated by a speaker facing to the right hand side of the plot, recorded in the chassis dynamometer laboratory

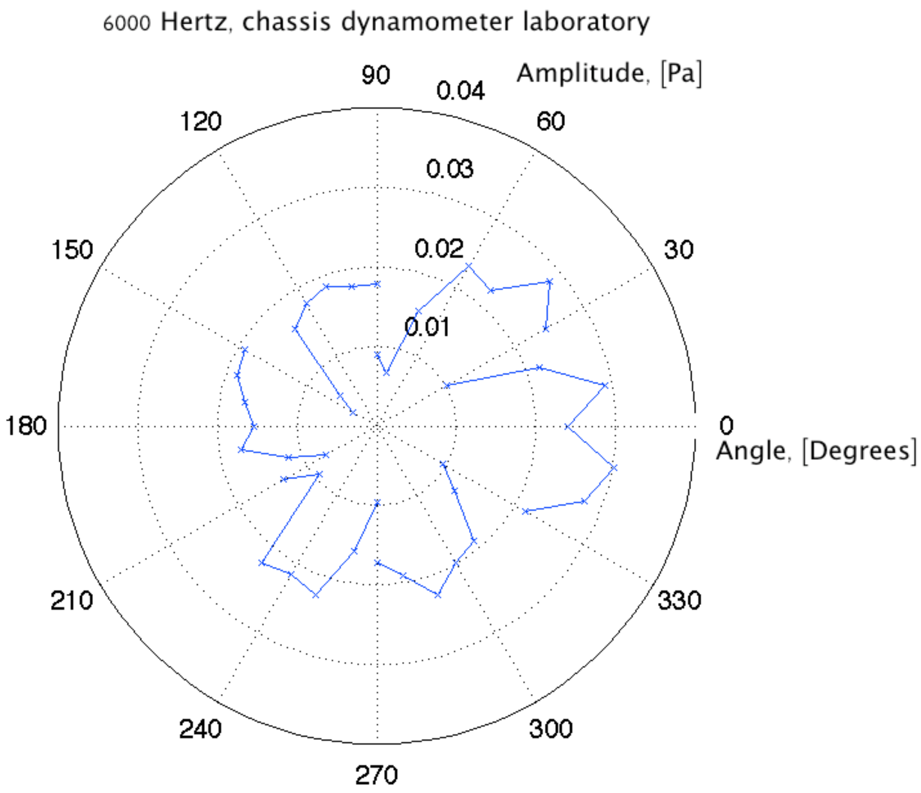

Figure A5.2 Sound radiation, at a frequency of 6000 Hertz, generated by a speaker facing to the right hand side of the plot, recorded in the chassis dynamometer laboratory

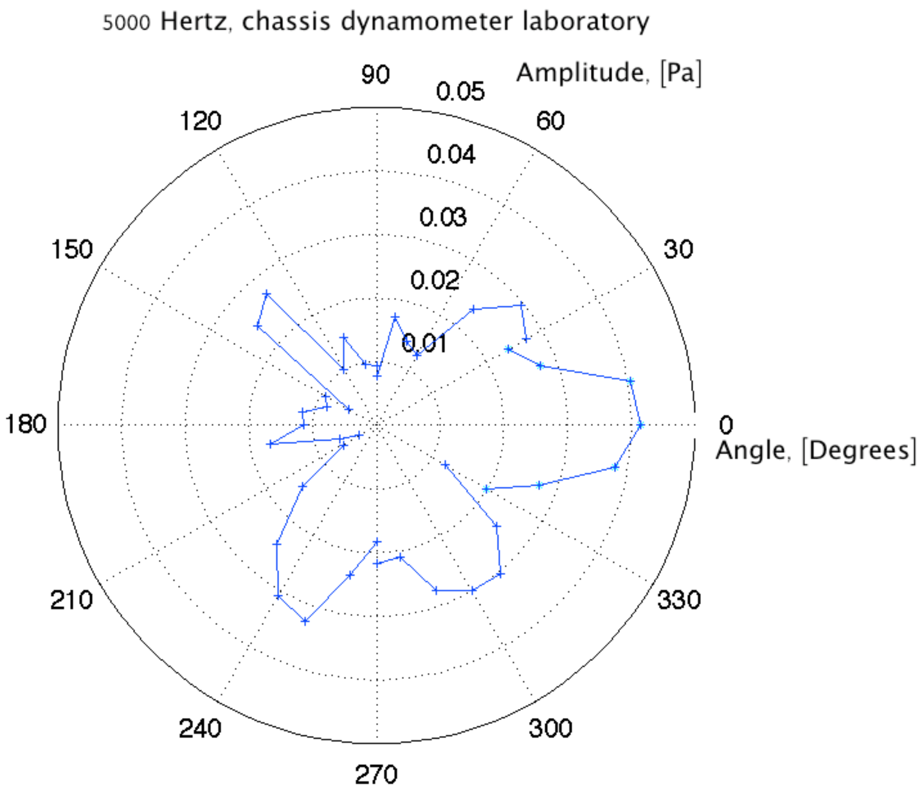

Figure A5.3 Sound radiation, at a frequency of 5000 Hertz, generated by a speaker facing to the right hand side of the plot, recorded in the chassis dynamometer laboratory

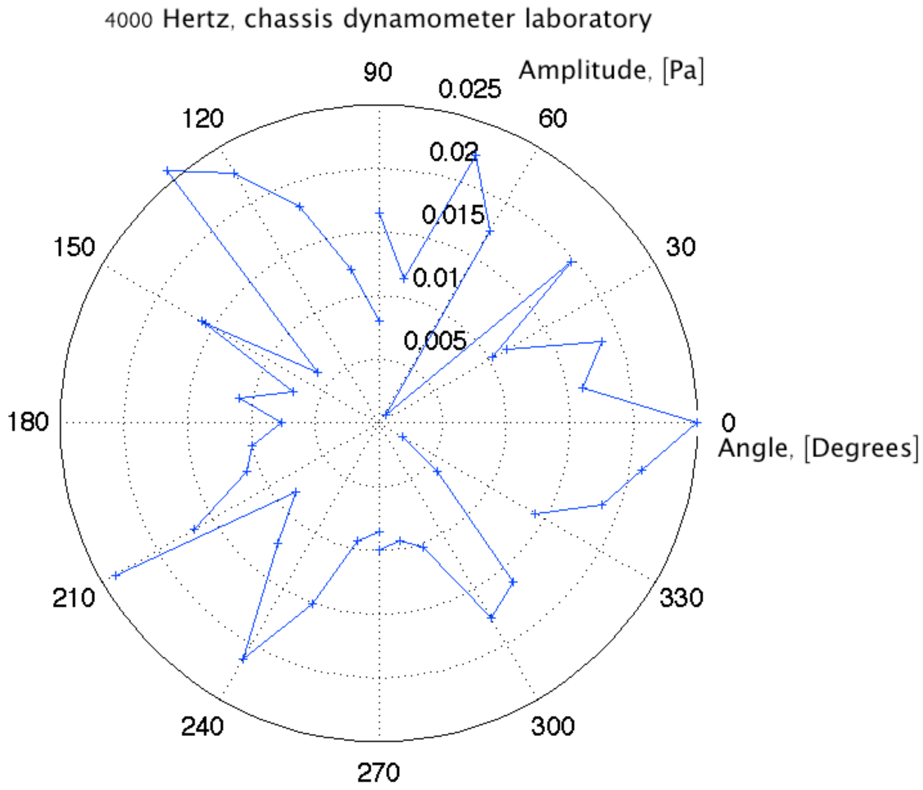

Figure A5.4 Sound radiation, at a frequency of 4000 Hertz, generated by a speaker facing to the right hand side of the plot, recorded in the chassis dynamometer laboratory

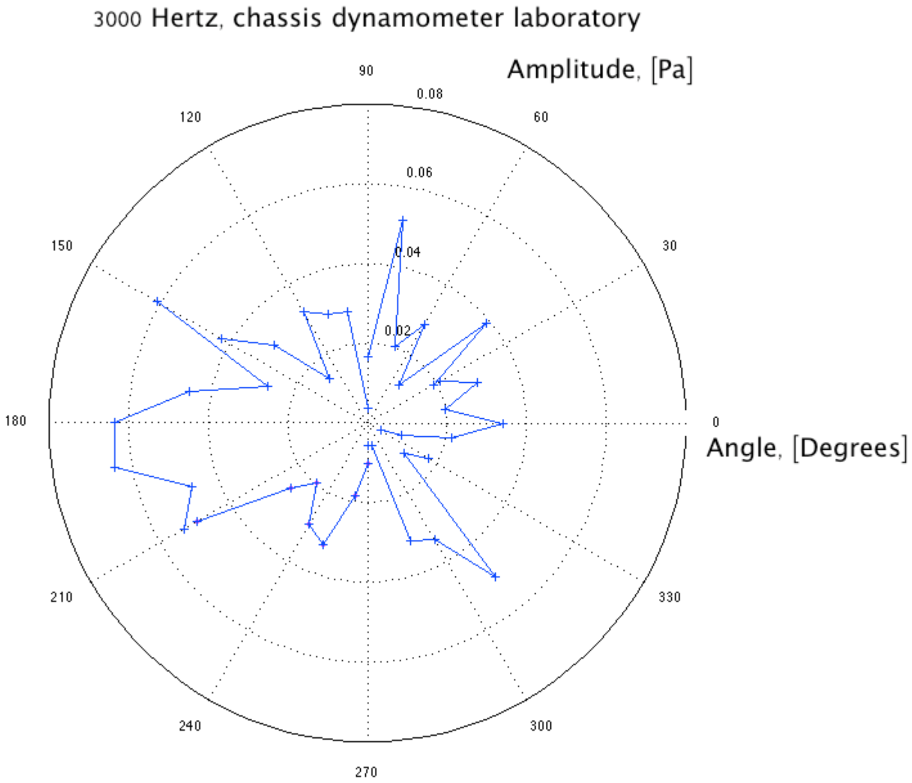

Figure A5.5 Sound radiation, at a frequency of 3000 Hertz, generated by a speaker facing to the right hand side of the plot, recorded in the chassis dynamometer laboratory

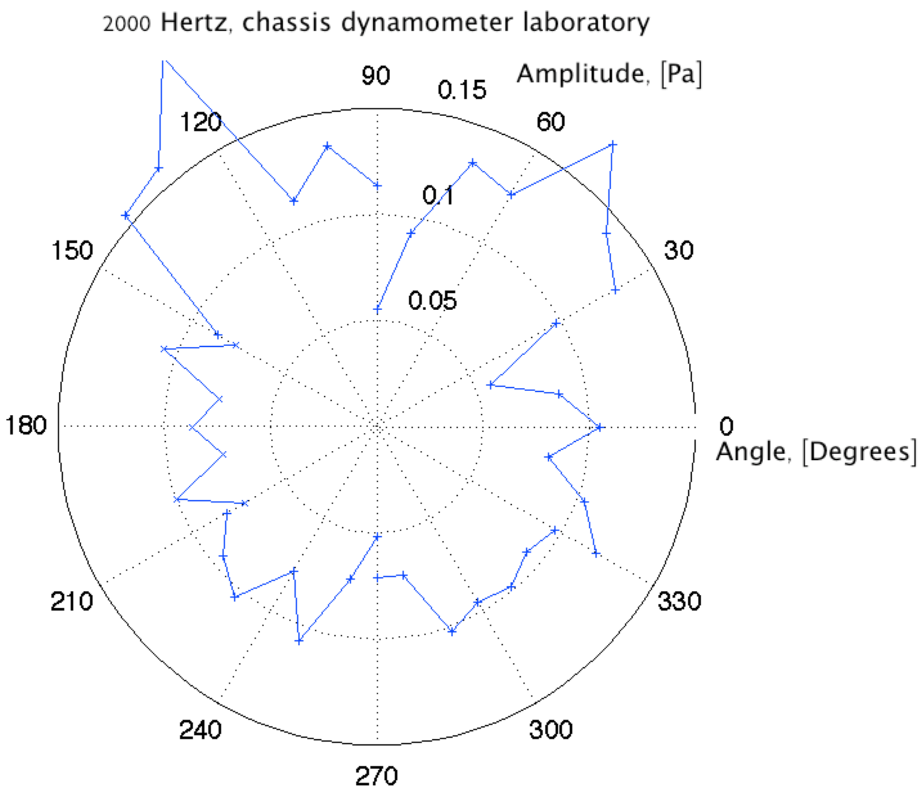

Figure A5.6 Sound radiation, at a frequency of 2000 Hertz, generated by a speaker facing to the right hand side of the plot, recorded in the chassis dynamometer laboratory

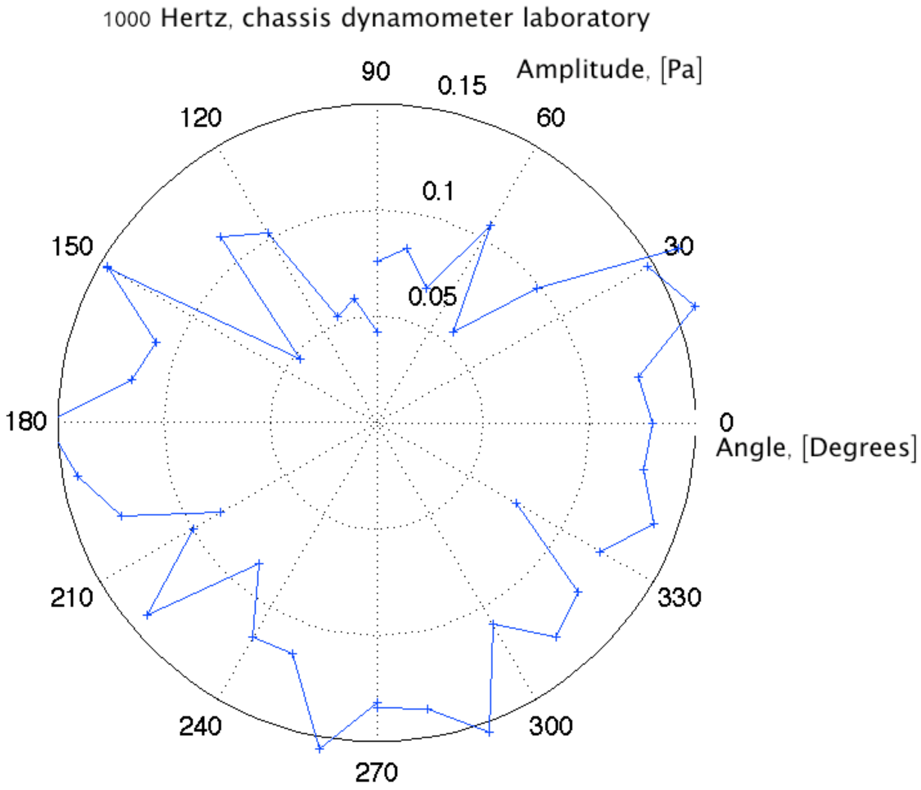

Figure A5.7 Sound radiation, at a frequency of 1000 Hertz, generated by a speaker facing to the right hand side of the plot, recorded in the chassis dynamometer laboratory

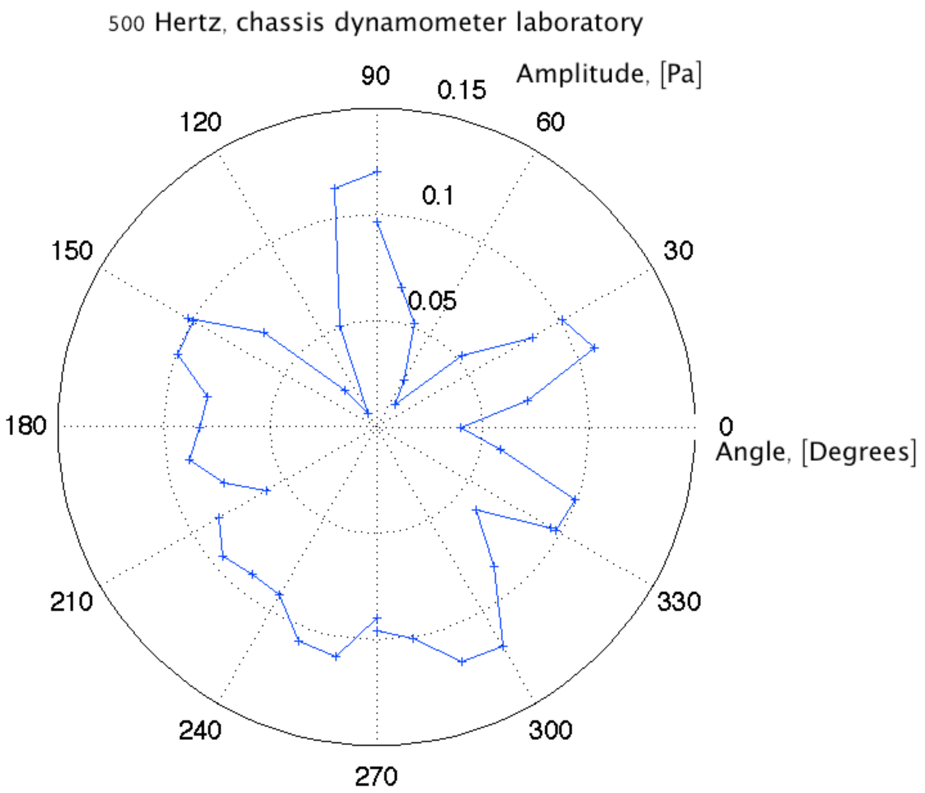

Figure A5.8 Sound radiation, at a frequency of 500 Hertz, generated by a speaker facing to the right hand side of the plot, recorded in the chassis dynamometer laboratory

A6. Displaced volume estimation

To investigate into the air volume that is displaced from the cavity measurements were done to identify the length of the contact patch. The tyre tread was coated with a thin layer of water and then carefully placed on the chassis dynamometer drum. At that time the drum was covered with a sheet of paper as shown in Figure A6.1. On this sheet of paper a footprint was generated by the tyre that had the average length of 17.5 mm. This value of the stationary measurement could also be the assumed length of the contact patch also during driving conditions. There might be a slight change in contact patch length when the tyre is moving especially at high speed when the contact patch should be shorter. However, the speeds used during the experiments are of low nature, thus, the change in contact patch length is assumed to be negligible.

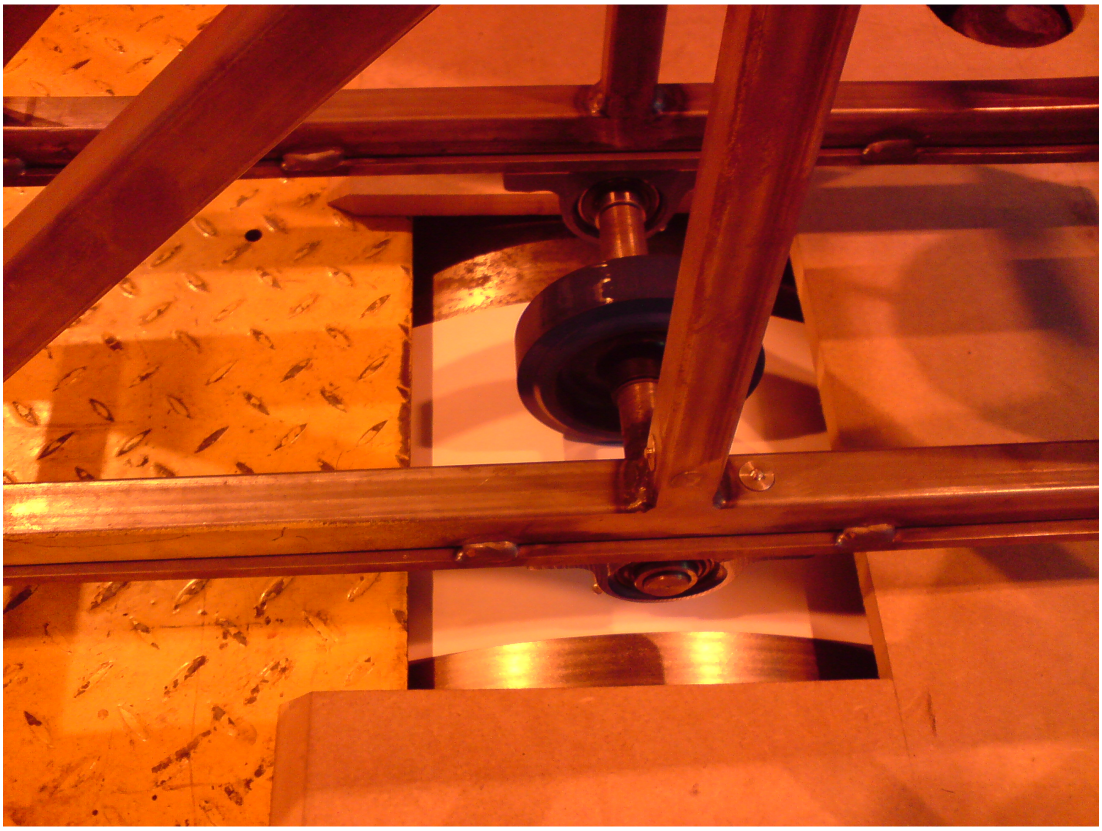

Figure A6.1 Photograph of the stationary contact patch measurement with the loaded tyre on the chassis dynamometer, white paper in place to get a footprint of the contact patch

Figure A6.2 overleaf shows the illustration of the calculated volume change estimation for a contact patch of length *C*. Fist the height *h* needs to be calculated. This is done with a trigonometry definition for the triangle with the sides *r*, *h* and *C/2*, defined as

$$r^2 = (r-h)^2 + \left(\frac{C}{2}\right)^2 . \tag{A6.1}$$

The roots of this quadratic function in Equation (A6.1) in dependence of the variable *h* are defined as

$$h = r \pm \sqrt{r^2 - \left(\frac{C}{2}\right)^2} . \tag{A6.2}$$

For the values of *r* and *C* named in Table A6.1 the height *h* results in 0.6308 mm. In comparison to the tyre rubber coating thickness of 15 mm this is about 4.2 %. Thus, the volume change of every cavity in this tyre is assumed to be in the region of 4.2 % as well. Obviously there is going to be a slightly larger contact patch resulting in a higher volume change, for tyres equipped with large cavities. For those tyres a lot of rubber is missing when the cavity is in touch with the drum of the chassis dynamometer, which could results in a bigger compression and thus bigger volume change. However, again this is just a reference value to get an idea about the approximate volume fluctuations for the solid rubber tyres at the contact area.

	r	*C*	*h*
Dimension, [mm]	61	17.5	0.6308

Table A6.1 Contact patch dimensions and resulting difference in tyre radius

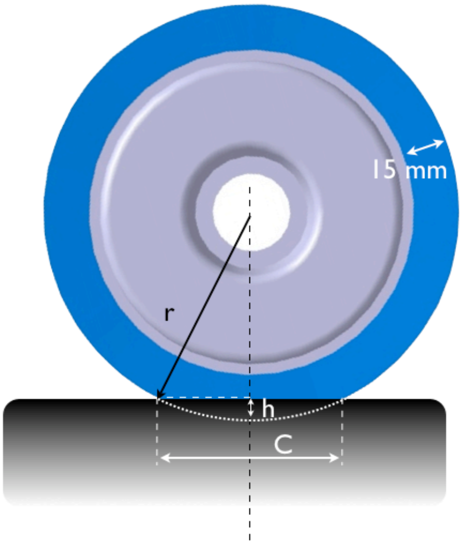

Figure A6.2 Illustration of the tyre deformation at the contact patch

A7. Unloaded tyre

The rig designed for this Thesis also had the option of changing the load of the tyre running on the chassis dynamometer. During the experiments it was found that the more load applied the more sound was generated at the leading and trailing edges. Thus, in the main body of the thesis only the results of the loaded tyre are shown. In this section the results of the unloaded tyre are presented but the only difference is the amplitude of the signal not the frequency.

The normal weight of the rig was about 13.5 kg in addition to that another 20 kg of extra weights could be added to the rig. With an assumed centre of equilibrium of the rig at 30 % of the actual length L_R the load on the tyre can be calculated according to the illustration in Figure A7.1.

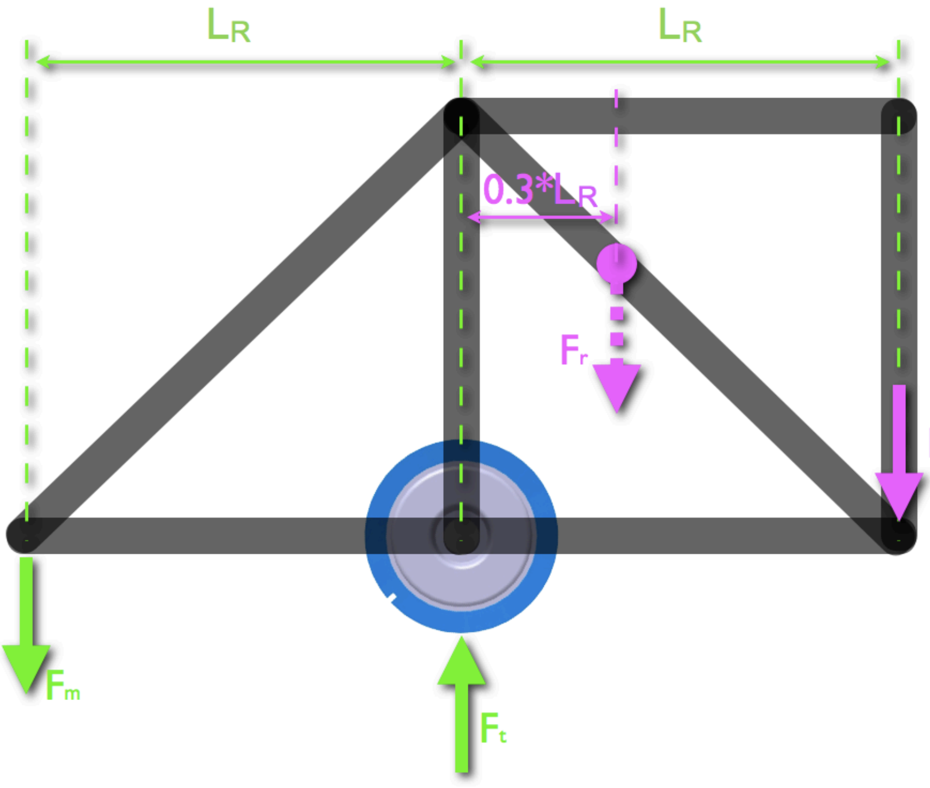

Figure A7.1 Schematic view of static forces at the tyre and rig construction

The resulting moment equilibrium around the point where the rig is fixed (F_m=0) can be expressed as

$$L_R \cdot F_t \approx 1.3 \cdot L_R \cdot F_r + 2 \cdot L_R \cdot F_w , \tag{A7.1}$$

which can be reduced to

$$F_t \approx 1.3 \cdot F_r + 2 \cdot F_w = 564.6\ N. \tag{A7.2}$$

This results in a load of about 57.6 kg that is resting on the tyre. Without the additional weight on the rig the factor F_w in Equation (A7.1) becomes zero. Then the load on the tyre is approximately 17.6 kg, which is equivalent to a reduction of 70 %.

A comparison of the recordings of the tyre equipped with the 'large cavity' with load and without load is shown in the next figures. Here only the measurements at a speed of 41 km/h are presented as reference, measurements with other velocities and types of cavities have been conducted and similar results have been obtained.

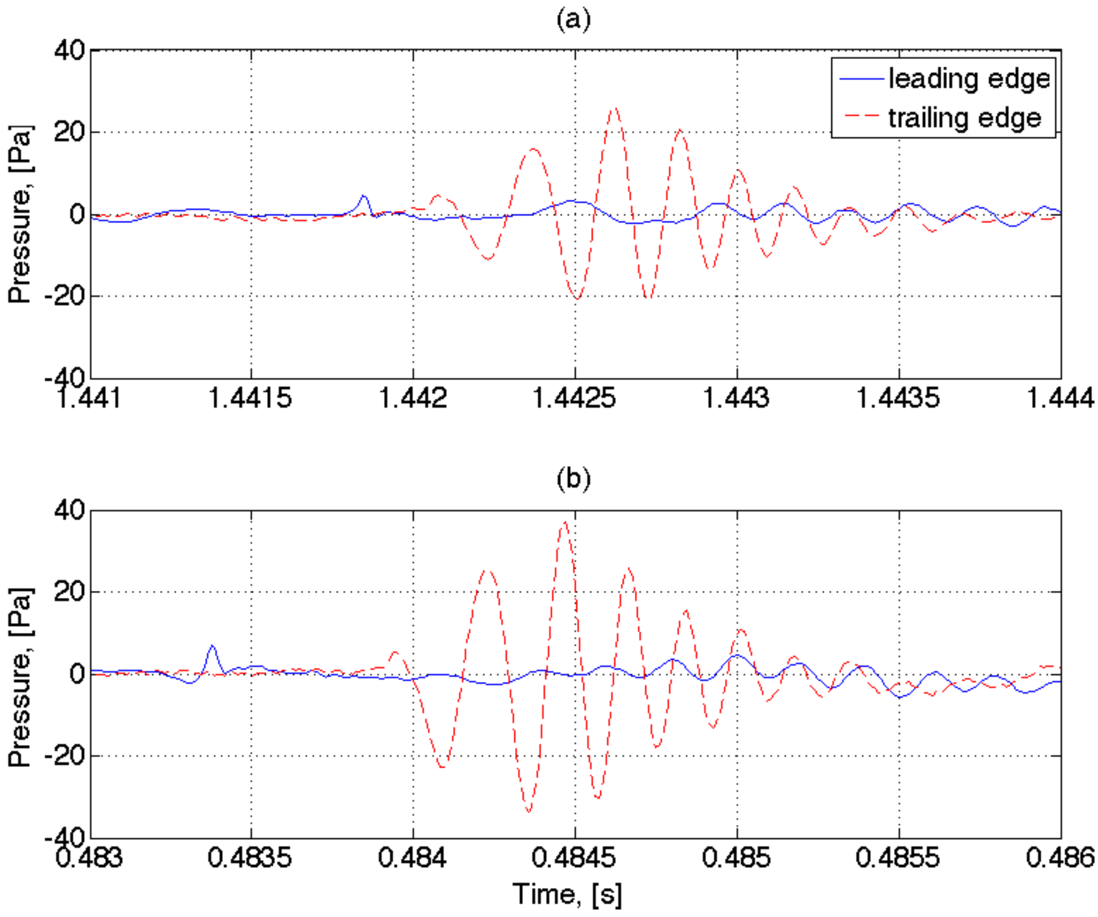

Figure A7.2 Example recordings leading and trailing edge overlaid: (a) tyre with no additional load; and (b) tyre with additional load

Figure A7.2 shows an instance of a leading and trailing edge recording for the loaded and unloaded tyre with the ‘large cavity’. Both signal amplitudes, at the leading (blue) and at the trailing edge (red) are dependent on the load of the tyre. A higher load results in signal of higher pressure amplitude as it can be seen when Figure A7.2a (unloaded) is compared to Figure A7.2b (loaded). In addition to that the contact patch length is influenced by the load as well.

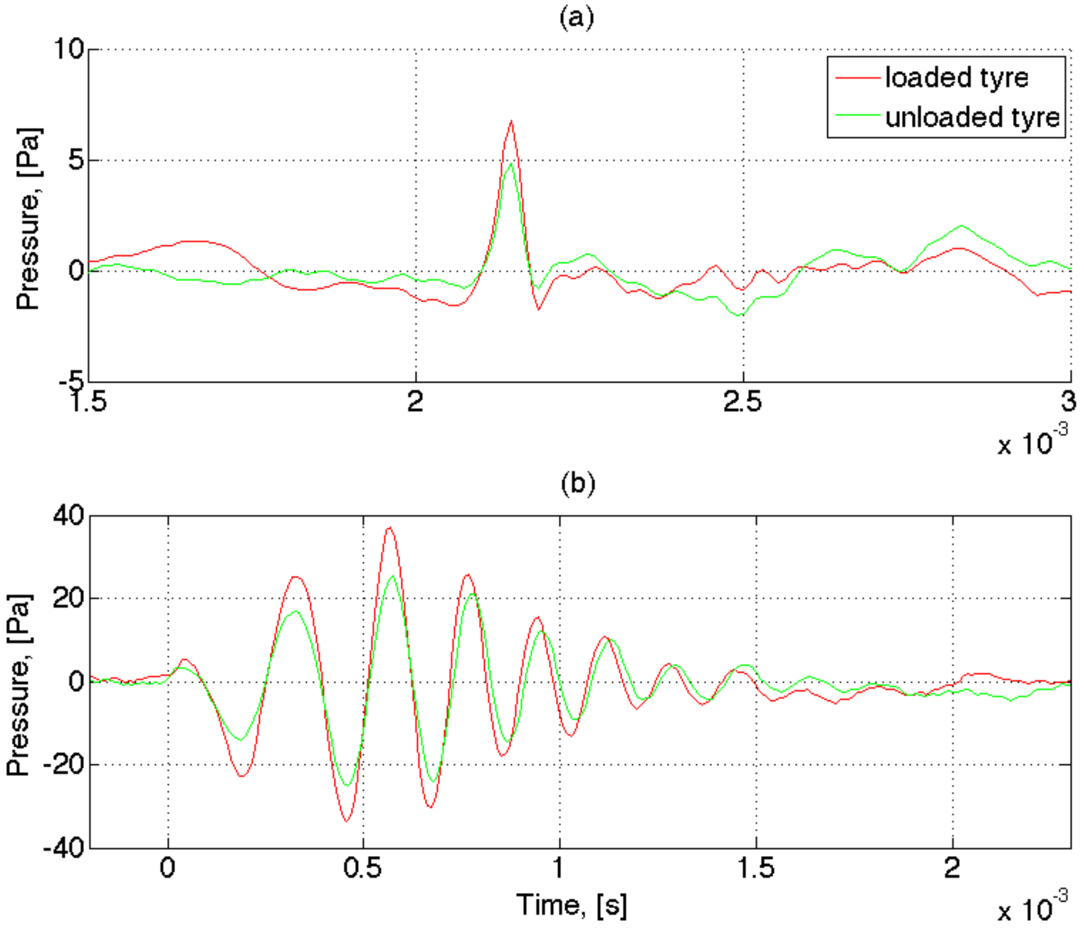

Figure A7.3 Direct comparison of example event at: (a) the leading edge; and (b) the trailing edge for the loaded (red) and the unloaded tyre (green)

Figure A7.3 shows a direct comparison of the example signals from Figure A7.2. The figure is separated into the leading edge example recordings at the top and trailing edge example recordings at the bottom. The green line is the recording for the loaded tyre used through this Thesis and the red line is the recoding from the unloaded tyre. For both, leading and trailing edge, only the amplitude is different not the length of the signal nor the frequencies of the oscillations. Thus, the air generated noise radiation at to contact patch of a tyre equipped with a cavity is proportional to the load of the tyre and so the volume of air which is rushing out and back into the cavity.

A8. Air resonant radiation amplitude

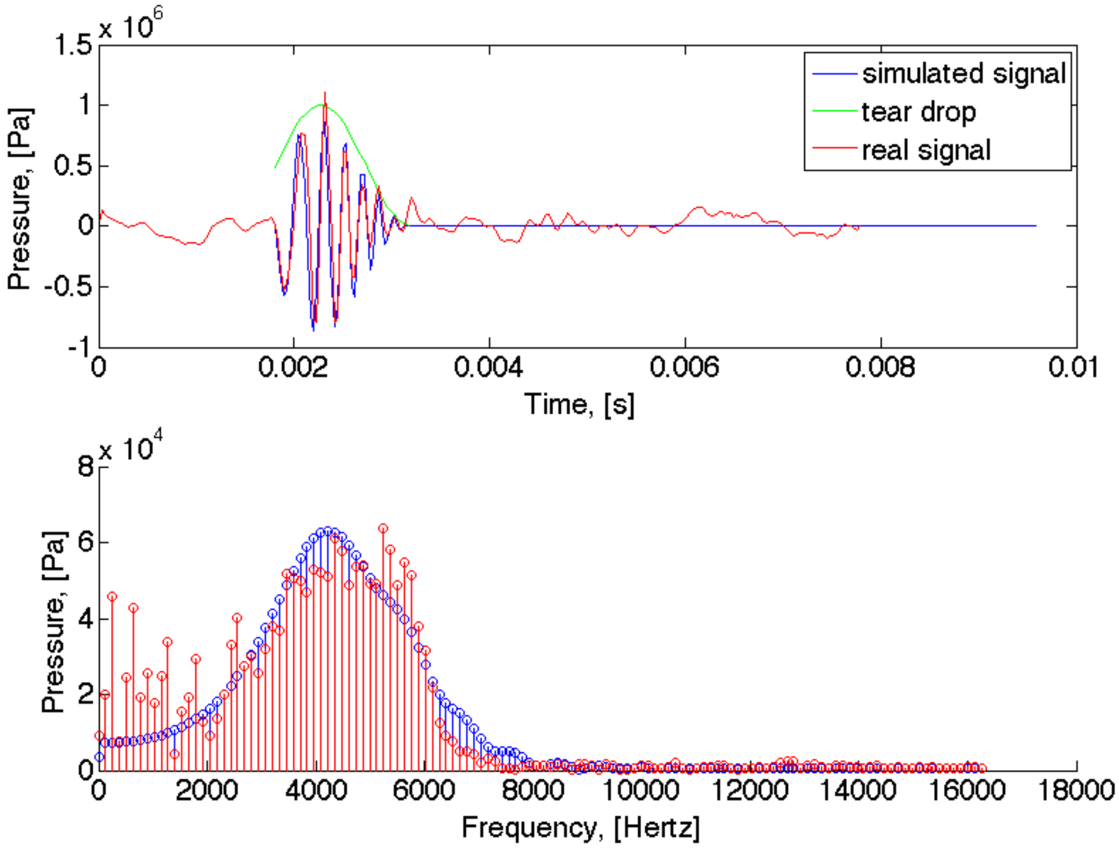

Figure A8.1 Direct comparison of example event at (a) the trailing edge and simulated signal; and (b) the frequency content of measured (red) and simulated trailing edge signal (blue)

Nilsson's model previously explained, only deals with the frequencies generated at the trailing edge signal of a tyre. Neither the air resonant radiation model cannot predict maximum amplitude nor the shape. A sinusoidal signal with frequencies modulation in the range of the frequencies obtained by Nilsson’s model is built and compared to the signal of the tyre with the ‘large cavity’. A teardrop function is used to simulate the shape of the signal as shown in Figure A8.1a. Even the frequency content of both signals show a similar result as shown in Figure A8.1b.

However, a mathematical explanation for the amplitude behaviour cannot be found, the duration of the signal is hard to investigate from the measurements. Even with the damping part of Equation (A3.11) attempts have been made to approach the measured amplitude behaviour but this was not successful. Thus, a simulation of the whole trailing edge signal cannot be found during this research despite of the large number of experiments conducted.